The Presenilin-1-PEN-2 complex, the minimal catalytic subunit of the γ-secretase

--Isolation and characterization of the tetrameric PS1-PEN-2 complex in *E.coli*

Inaugural-Dissertation

zur Erlangung des Doktorgrades
der Mathematisch-Naturwissenschaftlichen Fakultät

der Heinrich-Heine-Universität Düsseldorf

vorgelegt von

Chengcheng Tao

aus Chongqing, China

Hamburg, April 2022

aus dem Institut für Physikalische Biologie

der Heinrich-Heine-Universität Düsseldorf

Gedruckt mit der Genehmigung der
Mathematisch-Naturwissenschaftlichen Fakultät der

Heinrich-Heine-Universität Düsseldorf

Referent: Prof. Dr. Jörg Labahn

Korreferent: Prof. Dr. Henrike Heise

Tag der mündlichen Prüfung: 23.06.2022

Table of Contents

IV

List of Figures

x

List of Tables

XI

1. Introduction

Alzheimer's disease

More than 55 million people worldwide are living with dementia, with nearly 10 million new cases added each year, according to a WHO fact sheet on the 2nd of September and Alzheimer's disease (AD) is the most common form of dementia and may cause 60-70% of cases. Alzheimer's disease, a neurodegenerative and prominent protein-conformational disorder, leads to a progressive cognitive loss of brain function and further contributes to dysfunctional neurosynapses [1–3]. As shown in Figure 1.1, AD can be classified as familial type (FAD) and sporadic type (SAD), or as early-onset type (EOAD) and late-onset type (LOAD) [4], FAD is similar to EOAD which occurs in about 5% to 6% of people with Alzheimer's disease but develop symptoms before the age of 65 and is caused by autosomal dominant mutations in three different proteins: Amyloid Precursor Protein (APP) Presenilin-1 (PS1) and Presenilin-2 (PS2) [5]. SAD is predominantly LOAD, of which the majority of AD patients are diagnosed as LOAD, defined by the age of onset of 65 years or older. Although the contribution of genetics in SAD is not as straightforward as in FAD, the presence of a heritable factor has been recognized [6]
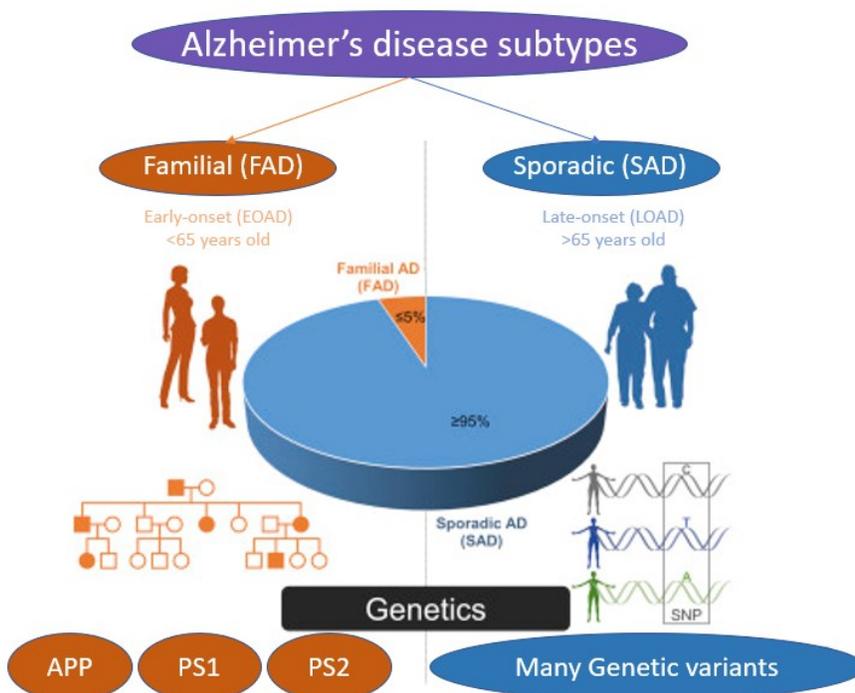
Figure 1.1 Subtypes and their genetics of Alzheimer's disease. (picture adapted from [6])

Schematic diagrams of the two main types of AD. 5% of AD is EOAD, which usually occurs in patients under 65 years of age and is caused by autosomal dominant mutations in APP, PSEN1 and PSEN2, while 95% of AD patients are over 65 years old and diagnosed with LOAD

1

Alzheimer's disease is named after German psychiatrist and pathologist Alois Alzheimer who reported distinctive plaques and neurofibrillary tangles in the histology of the brain, which are thought to be responsible for the onset of AD [7]. Different symptoms are distinguished in various stages of AD and are shown in Figure 1.2 A. Mild memory loss and prominent language impairment are the first symptoms that appear in the early stages of AD and are referred to as mild cognitive impairment (MCI) [8–10]. In the middle stages of AD, increased memory loss and confusion are diagnosed, as well as loss of reading and writing skills, while complex movements become less coordinated over time, contributing to the risk of falls [11,12]. In the final stage, known as the severe stage, severe cognitive impairment and loss of basic psychomotor skills mean that independent living is no longer possible and requires assistance with daily living. [13,14]. The brains of AD patients usually show significant atrophy, with widening of the sulci and reduction of the cerebral gyri. [15]. The insoluble Aβ plaques, located outside neurons, are composed of Aβ peptides, which are formed by sequential cleavage APP by β-secretase and γ-secretase [16,17]. Aβ plays a critical role in inducing and regulating reactive oxygen species (ROS) production which leads to oxidative stress, mitochondrial dysfunction, and neuronal damage or death in the pathophysiology of Alzheimer's disease [18–21]. Neurofibrillary tangles (NFTs), another hallmark of AD, are the clusters of hyperphosphorylated tau protein polymers [22]. Both Aβ peptides and the accumulation of NFTs lead to neuronal dysfunction with subsequent death [23,24] (Figure 1.2 B).
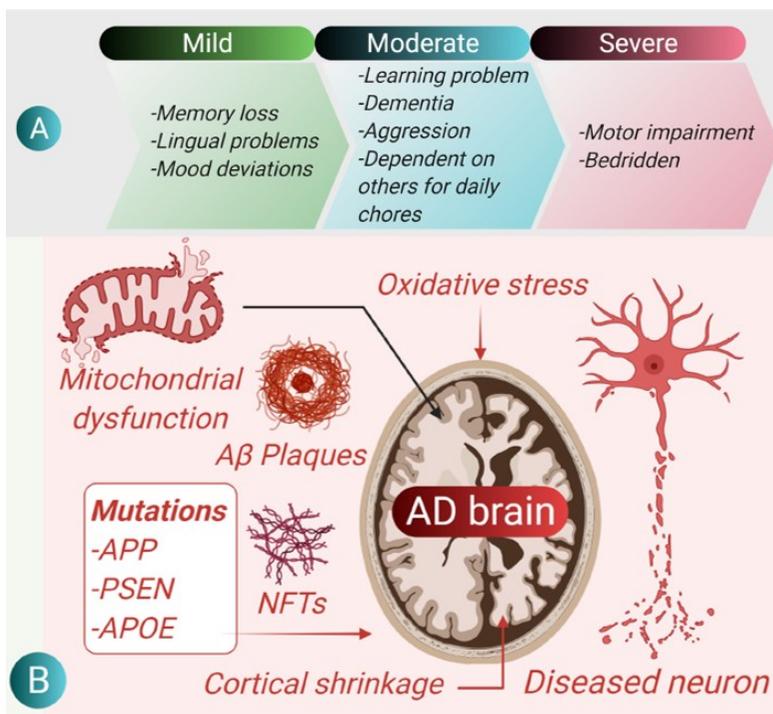
Figure 1.2 Alzheimer's disease and its pathogenesis (adapted from [3])

(A) Symptoms of different stages of AD. (B) Characteristics and causative factors of Alzheimer's disease

There are two main hypotheses of AD, one is the tau hypothesis. Tau protein is a microtubule-associated protein that plays an essential role in maintaining the stability of microtubules assembly [25]. Tau proteins contain 2-3 moles of phosphate per mole in a normal brain, while at least three times more are observed in AD brain, due to that, tau is abnormally hyperphosphorylated. In this altered state, hyperphosphorylated tau proteins aggregate into paired helical filaments (PHFs), leading to the formation of NFTs, which is a histopathological hallmark of AD and cause neuronal dysfunction and death [26–28] (Figure 1.3).

Another hypothesis of AD is the amyloid hypothesis, also known as the amyloid cascade hypothesis or the Aβ hypothesis, this has been the dominant explanation for the pathogenesis of AD for the past two decades [23,29–31]. APP is cleaved by β-secretase (BACE1) and subsequently by γ-secretase, which causes various Aβ peptides to be re-released. Aβ40 and Aβ42, containing 40 or 42 amino acids respectively, are the primary ingredients of accumulated Aβ [32]. The formation of Aβ amyloid fibrils is induced by an increase in the level of Aβ 42, which is more hydrophobic than Aβ 40, or the ratios of Aβ 42 to Aβ 40 [33,34]. Aβ amyloid fibrils progress to senile plaques, which cause neurotoxicity and induce tau pathology, resulting in neuronal cell death and neurodegeneration [35,36] (Figure 1.3). As mentioned in Figure 1.3, the γ-secretase complex plays a significant role in producing toxic Aβ peptides, therefore it has become an essential spotlight in AD and is considered a potential therapeutic target for the treatment of AD. [37].
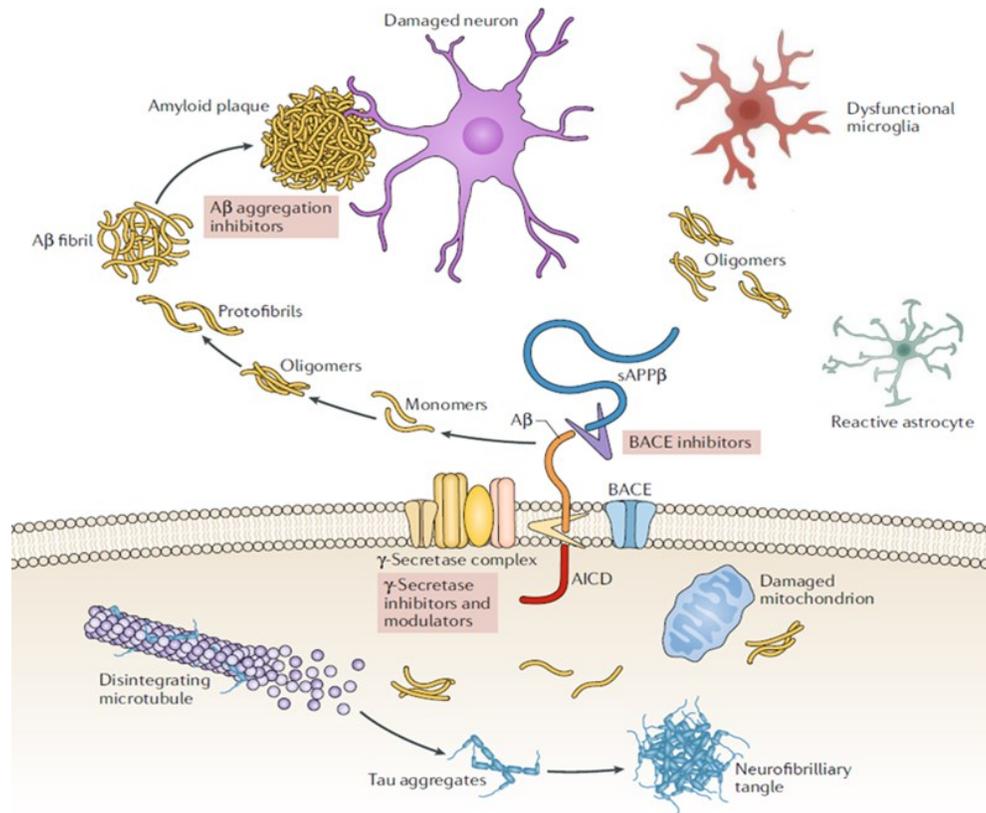
Figure 1.3 Schematic diagram of the amyloid hypothesis and the tau hypothesis (picture adapted from [38])

Aβ peptides are released by successive cleavage of β-secretase and γ-secretase of APP. Aβ peptides then form Aβ fibers and develop amyloid plaques, leading to neuronal damage. Hyperphosphorylated tau proteins dissociate from microtubules and then aggregate, leading to the formation of neurofibrillary tangles.

Assembly and function of γ-secretase

γ-secretase is a high molecular weight intramembrane aspartyl protease consisting of four subunits: Presenilin (PS), Presenilin Enhancer 2 (PEN-2), Nicastrin (NCT) and Anterior Pharynx Defective 1 (APH-1) [39–41]. In addition to the mentioned substrate APP-c99, γ-secretase cleaves more than 90 type I transmembrane proteins in the transmembrane domain as well [42] (Figure 1.4).

Presenilins (PSs) are multi transmembrane (TM) aspartyl proteases that are the catalytic units of γ-secretase. There are two isoforms of Presenilins, Presenilin-1(PS1) and Presenilin-2 (PS2), which are highly conserved and with an identical sequence of 67%[43]. The N-terminus of PSs are hydrophilic and flexible in the cytosol, while the C terminus sticks out into the lumen or

extracellular space [44,45]. Two conserved aspartate residues in TM6 (D257 in PS1 and D263 in PS2) and TM7 (D385 in PS1 and D366 in PS2) are reported as the active sites of γ-secretase [46,47]. PS full length is the inactive zymogens but undergoes endoproteolysis when integrated with PEN-2 and forms heterodimer of 28-35 kDa N-terminal fragment (NTF) and 18-20 kDa C-terminal fragment (CTF) and activates γ-secretase complex [48–50]. To date, more than 300 mutations in PS1 and more than 80 mutations in PS2 have been reported. Missense mutations in PS1 are the most common cause of EOAD as they can alter the Aβ species, whereas missense mutations in PS2 are a rare cause of EOAD, that's why PSs are considered the therapeutic targets for the treatment of AD (www.alzforum.org) [51,52]. Besides the influence of the Amyloidogenic pathway, PSs also exhibit additional non-catalytic roles in cellular signaling processes, including protein trafficking and degradation, calcium homeostasis and apoptosis [53–55].

PEN-2 was identified via Genetics and Enhancer Screens in *C. elegans* and is the smallest component of γ-secretase with two TMs, which is necessary for endoproteolysis of PS-FL into PS-NTF/CTF heterodimer and for the activation of γ-secretase [56–59]. It has been proved by the recovery of PS1 fragments when transient overexpression of PEN-2 in PEN-2 deficient cells, while knock-down of PEN-2 by RNA interference leads to the decrease of PS1 fragments and the stable PS1 holoprotein (holoPS) in PS1/APH-1/NCT complex [60]. Meanwhile, reconstitution of PS1 and PEN-2 protein into liposomes facilitates the endoproteolysis of PS1-FL into PS1 NTF and CTF, indicating that PEN-2 is sufficient for the activation of PS [61]. To answer the question of whether PEN-2 is necessary for γ-secretase activity or whether PEN-2-induced PS endoproteolysis is the only condition under which active γ-secretase can occur, the endoproteolysis-deficient mutant PS1-delE9 was expressed in PEN-2-deficient cells, forming a PS1-delE9/APH-1/NCT trimeric complex but showed no activity. This result implies that PEN-2 may regulate γ-secretase activity through multiple levels [62]. However, several studies prove that PEN-2 is dispensable for endoproteolysis of PS-FL but is essential for stabilizing the PS-NTF/CTF heterodimer [63–65]. TMD1 of PEN-2 is reported to interact with TMD4 of PS1, and its cytosolic region loop is located in a water-containing cavity and close to the CTF of PS1 [62,66,67]. Furthermore, knock-down of PEN-2 induces a p53-dependent apoptotic pathway and leads to neuronal loss, suggesting that PEN-2 promotes neuronal cell survival and protects from apoptosis in vivo [68,69].

In addition to PEN-2, which has been reported to act as a stabilizer of the PS-NTF/CTF heterodimer, another subunit, APH-1, is considered as a stabilizer of γ-secretase [70]. APH-1 is a ~29kDa protein

5

with seven TMs and forms a stable subcomplex when interacting with NCT [71–73]. Two isoforms APH-1a and APH-1b have been reported in humans and additional APH-1c in rodents which is the duplication of APH-1b and arranged in tandem with APH-1b on the chromosome [74–76]. APH-1a contributes to the shorter Aβ peptides formations while APH-1b and APH-1c lead to the production of longer peptides. APH-1S, the short form, and APH-1L, the long form, are the alternative splicing of APH-1a and with C-terminal sequence variations. Taking the expressions of different isoforms of APH-1 combined with PS1 or PS2 into account, at least six different γ-secretase complex compositions have been proved [58,77]. Mutation on Gly^{122} in APH-1 disrupts the interactions between APH-1 and NCT and reduces the γ-secretase complex. Moreover, disrupted transmembrane GXXXG motif with G122D and L123D mutations present lower expression levels than APH-1 wild type. That proves the conserved GXXXG motif in TM4 of APH-1 is essential for γ-secretase complex assembly and activation [78,79].

Nicastrin, which provides a scaffold for the γ-secretase complex when it forms a stable sub-complex with APH-1, is the biggest component of γ-secretase and contains a large extracellular domain (ECD), a short C-terminus and a single transmembrane domain in between [80]. NCT with deletion of residues 312–340 inhibits the substrates binding to γ-secretase and suppresses the protease activation. Meanwhile, mutation of Glutamic acid at 333 does not affect the endoproteolysis of Presenilin but significantly inhibits intramembrane cleavage of substrates. Those results prove that NCT plays an important role in the substrate recognition of γ-secretase [81,82]. Dr. Kun Yu from our group has successfully expressed and purified human NCT alone with the proper folding from *E. coli* cells and investigated the formations and initial sub-complex of NCT and APP-C99 by pull-down assay, confirming that NCT participants as the substrates recognizer [83]. However, generally it is accepted that NCT acts as the substrate recognizer, but there are some controversies. Mutation of Glu332 in mice, which is homologous to Glu333 in humans, inhibited the assembly of the γ-secretase complex but not the activity. Meanwhile, γ-secretase activity can be detected in NCT-deficient mice, proving that the PS1/PEN-2/APH-1a trimeric complex existed γ-secretase activity but was unstable. Those results indicate that NCT is essential for the assembly of γ-secretase but not the recognition of substrates [84,85]. In addition to this, a depigmented phenotype is observed in a Nicastrin-deficient zebrafish model which could be inhibited by Tyrosinase inhibitors, indicating that deficiency of NCT would induce Tyrosinase-dependent depigmentation and skin inflammation [86]. Furthermore, deficiency of NCT in mice

oligodendrocytes would lead to the hypomyelination in central nervous system, therefore altering dopamine signaling and contributing to the abnormal phenotypes, which could result in schizophrenia with compulsive behavior [87].

The order of assembly of those four components has been illustrated by the knock-down or knock-out of individual components in cell cultures [88]. Before assembling into a stable and active complex, all four subunits are synthesized in the ER. During the assembly process, any protein that does not form a more stable complex is rapidly degraded mainly through the proteasome. After synthesis, NCT is quickly N-glycosylated in the ER and forms the partially glycosylated immature NCT (imNCT) [89–92]. Assembly starts from APH-1, which has been reported to first interact with imNCT to form a stable subcomplex with a 1:1 ratio and a molecular weight of approximately 140 kDa [73]. The stable APH-1 and imNCT heterodimer bind PS holoprotein in ER and facilitate APH-1/imNCT/holoPS heterotrimer prior to the involvement of PEN-2 [70]. At last, PEN-2 combines with APH-1/imNCT/holoPS sub-complex in the ER through highly compact binding to the TMD4 of PS and form a very transient complex APH-1/imNCT/holoPS/PEN-2 [93,94]. The incorporation of PEN-2 rapidly facilitates the endoproteolysis of holoPS into PS NTF and CTF and contributes to the existence of the γ-secretase complex from the ER to the Golgi, the place where NCT is heavily N-glycosylated and can fully mature before trafficking to other locations. The final stable and active complex APH-1/mNCT/PS-NTF/PS1-CTF/PEN-2 moves to the plasma membrane [67,95–97]
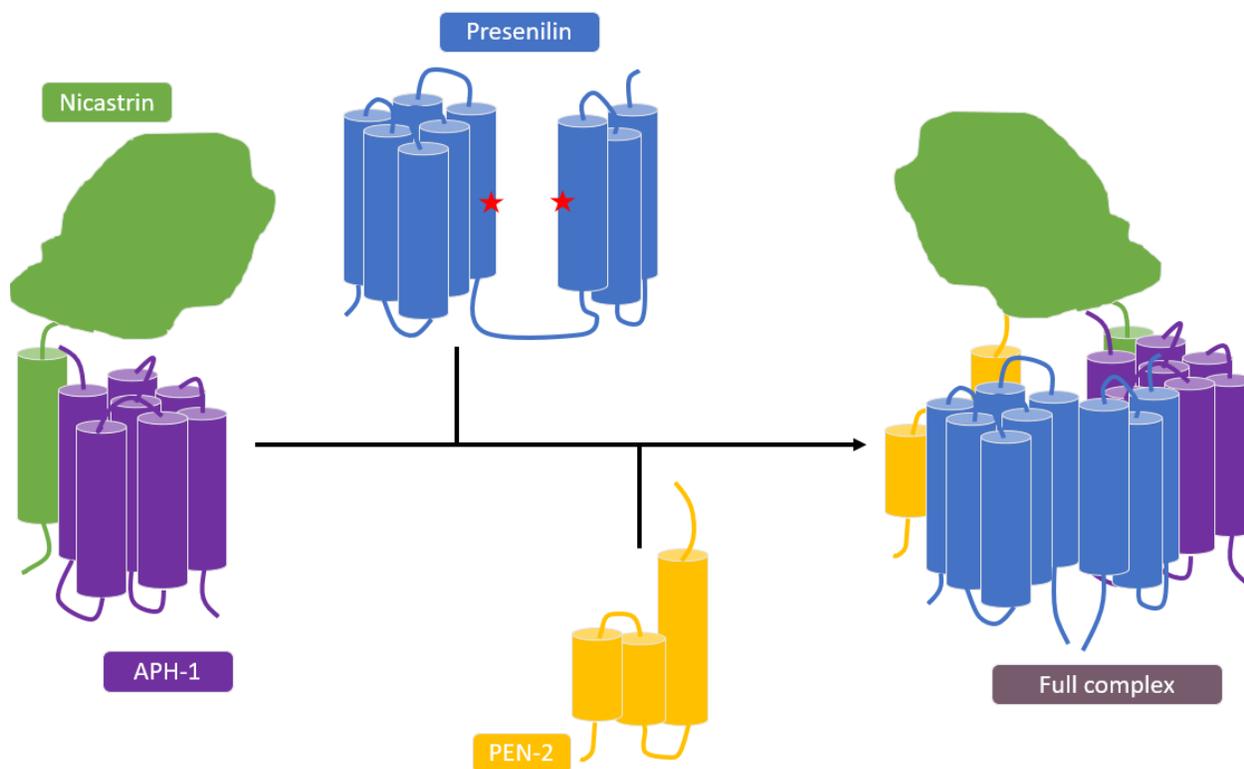
Figure 1.4 The assembly of γ-secretase (picture adapted from[58])

Nicastrin and APH-1 first interact to form a dimeric subcomplex. Full-length Presenilin is then incorporated into the Nicastrin and APH-1 complexes to form a trimeric complex. When PEN-2 is incorporated into the complex, Presenilin undergoes endoproteolysis, generates an N-terminal fragment and a C-terminal fragment, and activates the γ-secretase complex.

Structural research of γ-secretase

Structural characterization of γ-secretase complexes is vital for the understanding of recognizing and processing of substrates. However, the structural characterization of γ-secretase has lagged far behind its functional studies over the past two decades due to the enormous challenges of the expression and purification of intact γ-secretase complexes. [37,98].

There were only several electron microscopy (EM) structures of γ-secretase complex with a maximum resolution of 12 Å before 2014 [99–104]. A flat heart-shaped structure model occupied a volume of 560 Å × 320 Å × 240 Å was revealed using negative stain electron microscopy at the resolution of 48 Å and existed C2 symmetry [101]. Meanwhile, a model of the spherical structure with a resolution of 20 Å shows a large, cylindrical inner chamber with a diameter of 120 Å and 20-40 Å wide and 20 Å pores at the top and bottom, which can release lysis products into the subcellular

compartment [99]. Based on this structure, an improved 12 Å globular structure was determined with dimensions of 80 Å × 90 Å × 85 Å, provided a 1:1:1:1 stoichiometry of the four subunits and revealed several extracellular side domains, three low-density cavities which are solvent accessible, and a potential substrate-binding surface groove in the transmembrane region [102]. Furthermore, another globular structure of the γ-secretase complex has been reported with an 18 Å resolution, which illustrates a cup-like shape and a water-accessible internal chamber. This research also provides a trimeric pre-activation sub-complex structure containing NCT, APH-1, and PS and demonstrates that the binding of PEN-2 modifies the structure of the active site during the maturation of the complex [103].

Besides the early globular models, recent bi-lobed shapes have been proved to be the native states of γ-secretase complexes. The first bi-lobed shape structure has been determined with 17 Å resolution containing a larger base with a volume of 93 Å × 93 Å × 60 Å and a separate, smaller head with a volume of 65 Å × 60 Å × 55 Å [100]. More recently, due to the tremendous advances in cryo-EM, the first high-resolution structure of the γ-secretase complex with 4.5 Å resolution has been reported by the research group of Yigong Shi's group at Tsinghua University and Sjors H.W. Scheres' group at the MRC Laboratory of Molecular Biology, illustrating a horseshoe-shaped structure of 19 TMDs and a large ECD from NCT [105]. But the resolution is not sufficient to detect the details of the γ-secretase complex due to the lack of side-chain features of TMDs, which prevents the assignment of four components [106–108]. In the same year, Yigong Shi's group demonstrated the crystal structure of NCT from *Dictyostelium purpureum* with a resolution of 1.95 Å resolution, which is the first γ-secretase subunit atomic-resolution structure and showed a large top lobe responsible for recognition of substrates and a small bottom lobe in ECD of NCT [109]. The crystal structure of the Presenilin homolog (PSH) from the archaeon *Methanoculleus marisnigr*i JR1 revealed two catalytic residues in TMD6 and TMD7, and two potential substrate entry pathways [110]. Based on those models, the ambiguity of TMDs assignment of γ-secretase is resolved that NCT interacts with APH-1 and PS-CTF located at the thick end of horseshoe shape while PEN-2 and PS-NTF are located in the thin end of horseshoe shape [105,109–111] In 2015, Yigong Shi's group fused T4 lysozyme in the C-terminus of PS1 and obtained the 3D structure of the γ-secretase complex at 4.32 Å resolution in the presence of digitonin, revealing that a 20 TMDs model of γ-secretase complex where PEN-2 showed 3 TMDs, two of which traverse the membrane only from the inner half of the cell [112]. The same year, they reported another atomic structure at 3.4 Å overall

9

resolution, demonstrated the unambiguous assignment of the TMDs, including a highly flexible TMD2 of PS1, which could be functional as the gate of substrate trafficking, and revealed that the active sites are located on the convex side of the horseshoe-shaped TMD alignment (Figure 1.5 upper panel) [113]. Furthermore, they introduced the dipeptidic inhibitor *N*-[*N*-(3,5-difluorophenacetyl)-L-alanyl]-*S*-phenylglycine *t*-butyl ester (DAPT), which could significantly reduce the conformational mobility of TMD2 and TMD6 of PS1, and obtained the 3D structure of γ-secretase complex at 4.3 Å resolution [114]. This DAPT-bound structure clearly shows the cavity in which TMD2, TMD3 and TMD5-TMD7 are bound and will help to understand how substrates enter the transmembrane domain [114]. Based on the DAPT bound γ-secretase complex structure, two new structures reported from the Shi laboratory present the first detailed complexes structures of γ-secretase and substrates at high-resolution, providing substantial insight into properties of substrate recognition by γ-secretase [115–117].

Protein complex   Bound with Notch   Bound with APPC
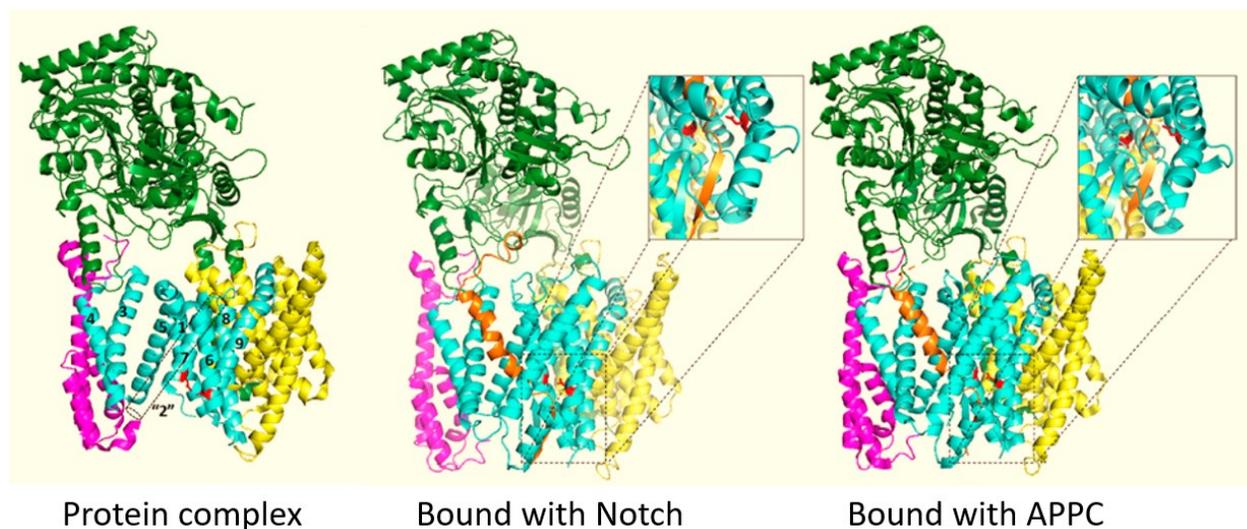
Figure 1.5 Overall structure of human γ-secretase (picture adapted from [107])

The first detailed 3D structure of the human γ-secretase complex (left). γ-secretase complex bound to substrate Notch (middle) and γ-secretase complex bound to substrate APP-C99 (right). NCT is marked with green color. PEN-2 is marked with pink color. PS1 is marked with cyan color, and APH-1 is marked with yellow color.

Aim of this study

As the γ-secretase processes a broad range of type I substrates, abnormal cleavage of Notch is associated with cancer, and abnormal cleavage of amyloid precursor proteins leads to Alzheimer's disease. Several high-resolution structures of human γ-secretase and the complexes of γ-secretase and its substrates have been detected, but the understanding of its structure and mechanism in the native environment is still a critical open question and a significant challenge, which is due to the difficulties of expression and purification of intact γ-secretase sub-complexes.

This project aimed mainly at the assembly and isolation of γ-secretase sub-complexes in both detergents environment and native environment for structure and activity analysis. To achieve the aims, several objectives were defined as follows:

Expression or co-expression and purification of γ-secretase subunits in detergent or detergent-free conditions:

Dr. Kun Yu, a previous Ph.D. student, successfully established the expression and purification of wild type γ-secretase subunits NCT, PEN-2 and PSs in *E. coli*. She also obtained high yield monomeric proteins from Fos-14 solubilization. As APH-1 protein is essential for the stability of the γ-secretase complex, our plan was to first stably express the APH-1 protein in E. coli, which is known to degrade during expression and purification. In order to facilitate the subsequent reconstitution, we planned to fuse the γ-secretase subunits with an expression tag to increase the protein solubility or make the protein water-soluble to remove the influences of Fos-14 detergent. Furthermore, I planned to co-express γ-secretase subunits in the Duet vector in *E.coli* and solubilize by different detergents or directly solubilize by the membrane solubilizing polymers like SMA or DIBMA to form γ-secretase complex or sub-complexes.

Reconstitution of detergent-solubilized or detergent-free γ-secretase subunits into the lipidic environment:

Although several high-resolution structures of the γ-secretase complex have been detected, how the γ-secretase complex behaves in its native environment is still less known. After isolation of γ-secretase subunits, sub-complexes or complex from detergent solubilization or detergent-free, we

planned to reconstitute these proteins into nanodiscs or liposomes to obtain the active γ-secretase sub-complexes or complex.

Function assay and biophysical characterization of γ-secretase proteins

The isolated proteins in both detergents or lipidic environments were planned to further activity assay. Biophysical characterization was designed to carry out by MS/MS experiment to identify the purified proteins and CD-spectroscopy for the secondary and tertiary structures. The stability of the γ-secretase proteins was scheduled to be monitored by thermal denaturation experiments

2. Materials and methods

2.1 Instruments and materials

Table 2.1 Instruments used

Instruments	Company
Benchtop centrifuge 5417R	Eppendorf
Benchtop centrifuge Sigma 1-14K	Sigma
Superspeed Centrifuge Sorvall LYNX 6000	Thermo Scientific
NanoDrop™ 2000 Spectrophotometer	Thermo Scientific
Ultracentrifugation OPTIMA XPN 90	Beckman Coulter
Cell disrupter EmulsiFlex-C3	Avestin, Inc.
Akta Explorer	GE Healthcare Life Science
T100 Thermal cycler	Bio-Rad
Bio-rad mini sub cell GT	Bio-Rad
Bio-rad mini protein tetra cell	Bio-Rad
Trans-Blot Turbo Transfer System	Bio-Rad
ChemiDoc MP Imaging System	Bio-Rad
AVIV Model 425	AVIV
UNITRON plus Incubator Shaker	INFORS AG
Tecan plate reader Spark 20M	Tecan
Monolith NT.115	NanoTemper
T80 UV-VIS Spectrophotometer	PG Instruments Limited

Table 2.2 Materials used

Materials	Company
BenchMark Protein Ladder	Thermo Scientific
FastDigest restriction enzyme	Thermo Scientific
T4 DNA ligase	Thermo Scientific
GeneRuler DNA ladder	Thermo Scientific
GeneJET Plasmid Miniprep Kit	Thermo Scientific
GeneJET Gel Extraction Kit	Thermo Scientific
Zeba Spin Desalting Columns	Thermo Scientific
Phusion Hot Start II DNA Polymerase	Thermo Scientific
Detergents (Fos-14, DDM)	Cube Biotech
Polymers (SMA, DIBMA)	Cube Biotech
Affinity resin (Ni-NTA resin, Rho1D4 Agarose)	Cube Biotech
Rho1D4 peptide	Cube Biotech
Detergents (CHAPSO, LMNG)	Anatrace
Lipids	Anatrace
PD-10 desalting column	GE Healthcare Life Science
PVDF membrane	GE Healthcare Life Science
Size-exclusion chromatography columns	GE Healthcare Life Science
Nanosep MF and NAB Centrifugal Devices	Pall Laboratory

Pre-stained Protein Marker	Jena Bioscience
Protein Labeling Kit RED-NHS 2nd Generation	NanoTemper
Monolith NT.115 Premium Capillaries	NanoTemper

All chemicals are purchased from Carl Roth and AppliChem.

2.2 Materials for bacterial culture

Table 2.3 Bacterial strains

Strains	Genotype
Top10	F- mcrA Δ(mrr-hsdRMS-mcrBC) φ80lacZΔM15 ΔlacX74 nupG recA1 araD139 Δ(ara-leu)7697 galE15 galK16 rpsL(StrR) endA1 λ-
BL21 (DE3)	F– ompT gal dcm lon hsdSB(rB–mB–) λ(DE3 [lacI lacUV5-T7p07 ind1 sam7 nin5]) [malB+]K-12(λS)
C43(DE3)	F– ompT gal dcm hsdSB(rB-mB-)(DE3)

The genotypes of the strains are obtained from https://openwetware.org/wiki/E._coli_genotypes.

Table 2.4 Expression vectors

Vectors	Inducer	Resistance	DNA inserted
pET-15b	IPTG	Ampicillin	(i) Presenilin-1 and its mutants (ii)MBP construct expressed in cytoplasm
pET-21b	IPTG	Ampicillin	MBP-APPC
pET-28a	IPTG	Kanamycin	(i) MSP1D1 (ii) FleB-APH1

pET-11a	IPTG	Ampicillin	Protein fused with nGFP
pQE2	IPTG	Kanamycin	(i) Presenilin-2 (ii) His-PEN-2
pMRBAD	Arabinose	Kanamycin	Protein fused with cGFP
pMAL-P4X	IPTG	Ampicillin	MBP construct expressed in periplasm
pETDuet-1	IPTG	Ampicillin	Co-expressed PS1 and PEN-2

All expression vectors are purchased from Addgene.

Table 2.5 Medium for bacterial culture

	Compositions
lysogeny broth (LB)	Yeast extract (5 g/l) Tryptone (10 g/l) Sodium chloride (10 g/l)
Super Optimal Broth (SOB)	2% w/v tryptone 0.5% w/v Yeast extract 10mM NaCl 2.5mM KCl add 10mM $MgCl_2$ and 10mM $MgSO_4$ before use
Terrific Broth (TB)	Bacto-tryptone (12 g/l) Yeast extract (24 g/l) Glycerol (5 g/l) Add 100ml KPi buffer (0.72 M K_2HPO_4 and 0.17 M KH_2PO_4) to 900ml medium before use

All mediums are dissolved in Milli-Q water and autoclaved at 121°C for 20 minutes.

2.3 Buffers

Table 2.6 Buffers for gel electrophoresis

Buffers	Compositions
Agarose gel running buffer (50X TAE)	2M Tris-base 1 M acetic acid 50 mM EDTA pH:8.0
SDS-Sample buffer (5X)	62 mM Tris, 2 % (w/v) SDS 5 % (v/v) β-Mercaptoethanol 20%(w/v) Glycerol 0.2 % (w/v) Bromophenol blue
SDS-PAGE running buffer	25 mM Tris 192 mM Glycine 0.1 % (w/v) SDS%
Blue silver staining solution	10% Phosphoric acid 10% Ammonium sulfate 1.2g/L Coomassie G-250 20% (v/v) Methanol
Transfer Buffer for Western blot	39 mM Glycine 48 mM Tris base 20% (v/v) Methanol
TBS buffer	20 mM Tris base pH 7.6 137 mM NaCl
TBS-T buffer	TBS buffer with 0.1% (w/v) Tween 20
Blocking buffer	TBS-T buffer with 5% (w/v) non-fat milk

Table 2.7 sodium dodecyl sulphate–polyacrylamide gel electrophoresis (SDS-PAGE)

	10% resolving gel (20ml)	12% resolving gel (20ml)	15% resolving gel (20ml)	5% stacking gel (5ml)
H$_2$O	7.9 ml	6.6 ml	4.6 ml	3.4 ml
30% Acrylamide	6.7 ml	8.0 ml	10.0 ml	0.83 ml

1.5 M Tris, pH8.8	5.0 ml	5.0 ml	5.0 ml	-
1 M Tris, pH 6.8	-	-	-	0.63 ml
10 % SDS	0.2 ml	0.2 ml	0.2 ml	0.05 ml
10 % Ammonium Persulfate	0.2 ml	0.2 ml	0.2 ml	0.05 ml
TEMED	8 µl	8 µl	8 µl	5 µl
0.5% Trichloroethanol (TCE) (optional)	0.1 ml	0.1 ml	0.1 ml	-

Table 2.8 Buffers for purification

Buffers	Compositions
Sucrose Buffer for Osmotic shock	50 mM HEPES, 20% Sucrose, 1 mM EDTA, pH 7.9.
Lysis Buffer	20 mM HEPES, 10% Glycerol, PH 7.4, 1 mg/ml Lysozyme, 5 mg/20 g DNase I, 1uM E64, 1uM Pepstatin A, 1uM Leupeptin, 1mM AEBSF, 1mM PMSF, 1mM Benzamindine
Solubilization buffer (For detergent solubilization)	20 mM HEPES, pH 7.4, 300 mM NaCl, 10 % Glycerol, 1 % FC 14 or 0.5% DDM or 1% CHAPSO, 1 mM PMSF (optional), 1 mM TCEP (optional)
Solubilization buffer (For DIBMA solubilization)	20mM HEPES, pH 7.4, 200mM NaCl, 5% DIBMA polymers
Ni-NTA washing buffer I	20mM HEPES, pH 7.4, 10% glycerol, 1% Fos-14 or 0.5% DDM or 1% CHAPSO, 300mM NaCl, 1mM TCEP (optional), 15mM Imidazole
Ni-NTA washing buffer II	20mM HEPES, pH 7.4, 10% glycerol, 3CMC Fos-14 or 3CMC DDM or 0.5% CHAOSO, 500mM NaCl, 1mM TCEP (optional), 15mM Imidazole

Ni-NTA washing buffer III	20mM HEPES, pH 7.4, 10% glycerol, 3CMC Fos-14 or 3CMC DDM or 0.5% CHAOSO, 1M NaCl, 1mM TCEP (optional), 15mM Imidazole
Ni-NTA elution buffer	20mM HEPES, pH 7.4, 10% glycerol, 3CMC Fos-14 or 3CMC DDM or 0.5% CHAOSO, 150mM NaCl, 1mM TCEP (optional), 500mM Imidazole
Rho tag resin washing buffer	20mM HEPES, pH 7.4, 10% glycerol, 3CMC Fos-14 or 3CMC DDM or 0.5% CHAOSO, 150mM NaCl
Rho tag resin elution buffer	20mM HEPES, pH 7.4, 10% glycerol, 3CMC Fos-14 or 3CMC DDM or 0.5% CHAOSO, 150mM NaCl 1mM Rho peptide
SEC buffer (for detergents solubilization)	20mM HEPES, pH 7.4, 10% glycerol, 3CMC Fos-14 or 3CMC DDM or 0.5% CHAOSO, 150mM NaCl, 1mM TCEP (optional)
SEC buffer (For Nanodiscs)	20mM HEPES, 150mM NaCl, 5% glycerol, pH:7.4

Table 2.9 Buffers for characterazation

Buffers	Compositions
Buffer for CD	5mM NaPi, 50mM NaF, 0.02% DDM, (0.002% CHS), ph:7.4
Activity assay buffer I	20mM HEPES, 150mM NaCl, 5mM $CaCl_2$, 5mM $MgCl_2$, pH:7, and 0.25% CHAPSO
Activity assay buffer II	20mM HEPES, 150mM NaCl, 5mM $CaCl_2$, 5mM $MgCl_2$, pH:7.4, and 0.25% CHAPSO or 0.05% DDM or 0.05% Fos-14
Activity assay buffer III	20mM HEPES, 150mM NaCl, 2mM EDTA, pH: 7.4, and 0.25% CHAPSO or 0.05% DDM or 0.05% Fos-14
Activity assay buffer IV	20mM HEPES, 150mM NaCl pH: 7.4, and 0.25% CHAPSO or 0.02% DDM

2.4 Cloning

Molecular cloning is a kind of experiment in molecular biology to assemble recombinant DNA molecules by polymerase chain reaction (PCR), invented in 1983 by American biochemist Kary Mullis[118,119]. Ligation Independent Cloning (LIC) is a technique developed in the 1990s and allows to insert the gene of interest into the selected vector by restriction enzyme digestion and ligation[120,121]. Site-directed mutagenesis is one of the most important techniques to introduce mutations (substitutions, deletions and insertions.) into DNA sequences[122]. In this work, the primers of full-length DNA sequences were designed on the online primer design software from Thermo Fisher, and the primers of mutations were designed on the online software NEBaseChanger from New England BioLabs (see Appendix I: DNA and protein sequences and Appendix II: Primers). All primers were synthesized from BioTeZ Berlin-Buch GmbH, Germany and resuspended in ddH$_2$O to the final concentration of 50 µM. The PCR reactions were set up as follow:

Table 2.10 PCR reactions

Components	20 µL reaction	Final concentration
5X Phusion HF Buffer	4 µL	1X
10 mM dNTPs	0.4 µl	200 µM
Forward primer	0.2 µl	0.5 µM
Reverse primer	0.2 µl	0.5 µM
Template DNA	1 µl	5 ng
DMSO	0.6 µl	6%
Phusion Hot Start II DNA Polymerase	0.2 µl	0.02 U/µL
H2O	Up to 20 µl	

The PCR experiment was performed with the gradient annealing temperatures from 55 °C to 72 °C and the extension time of the amplicon was set to 15 seconds per 1 kb according to the manual of Phusion Hot Start II DNA Polymerase.

Table 2.11 PCR program

Steps	Temperature	Duration	No. of cycles
Initial denaturation	98 °C	30s	1
Denaturation	98 °C	10s	
Annealing	55-72°C	30s	30
Extension	72°C	15s per kb	
Final extension	72°C	5 mins	1

The PCR product was further purified on 1% agarose gel with a voltage of 120V for 30mins. The corresponding bands were cut and extracted by using GeneJET Gel Extraction Kit from Thermo Fisher. The concentration of DNA was measured according to the absorption at 260 nm. For Ligation Independent Cloning, the purified PCR product and selected vector were digested by relative restriction enzymes at 37 °C for 30 mins, purified by 1% agarose gel, and further extracted by Gel Extraction Kit. The purified insert and vector DNA were ligated together with the molar ratio of 3:1 by using the rapid ligation kit under 22 °C for 30 mins.

For Site-directed mutagenesis, the template DNA needs to be digested by the enzyme DpnI under 37 °C for one hour to avoid template DNA contamination. After purified by 1% agarose gel and extracted by Gel Extraction Kit, 5'-end phosphorylations of linear DNA were performed by Thermo Fisher T4 polynucleotide kinase, which catalyzes the transfer of gamma phosphate from ATP to 5'-end of DNA or RNA[123]. Self-ligation of linear DNA was performed directly after 5'-end phosphorylation by using the rapid ligation kit under16 °C overnight.

The mentioned reactions are listed below:

Table 2.12 Restriction enzyme digestion reaction

Components	50 μL reaction
10X FastDigest Green Buffer	5 μl
DNA	1 μg
FastDigest enzyme I	1 μl
FastDigest enzyme II	1 μl
Nuclease-free water	Up to 50 μl

Table 2.13 DpnI digestion

Components	40 μL reaction
10X Reaction Buffer	4 μl
DNA	30 μl
DpnI	1 μl
Nuclease-free water	Up to 40 μl

Table 2.14 reaction of phosphorylation of DNA

Components	50 μL reaction
10x reaction buffer A for T4 Polynucleotide Kinase	4 μl
DNA (from DpnI digestion)	40 μl
10mM ATP	4 μl
T4 Polynucleotide Kinase	2 μl

Table 2.15 Ligation reaction

Components	20 μL reaction
10X Ligase Reaction Buffer	2 μl
Vector DNA (For LIC)	70 μg
Insert DNA (For LIC)	3 times molar ratio to vector DNA
Linear (For self-ligation)	70 ng
T4 DNA Ligase	0.2 μl
Nuclease-free water	Up to 20 μl

The ligation products were then incubated with Top10 competent cells for 15mins and followed by 90s heat shock under 42 °C. After the mixture was incubated on ice for two mins for recovery, 900 μl LB medium was added to the mixture and incubated under 37 °C for 1 hour with 400 rpm shaking. After incubation under 37 °C, the mixture was centrifuged under 3000 xg for 1min and the supernatant was discarded until 200μl remained. The rest was pipetted to the agar LB-medium plate with the corresponding antibiotic and incubated at 37 °C overnight.

Several colonies were picked individually into 5 ml LB liquid medium and grew at 37 °C with 180 rpm shaking overnight. The bacteria cultures were harvested under 8000 rpm at room temperature and the plasmids were extracted by using the GeneJET Plasmid Miniprep Kit. The correct plasmids need to be checked by relative restriction enzymes double digestion and confirmed by DNA sequencing from Microsynth company prior to using them for protein expression.

2.5 *In vivo* expression and purification

Once confirmed by DNA sequencing, the plasmid was then transformed into expression strains with the same procedure as mentioned above. All colonies were picked from the agar plate and inoculated in 50ml TB medium with relative antibiotics and 2% glucose, controlling basal

expression in the pET system[124]. The pre-culture was incubated at 37 °C with 250rpm shaking till the OD reached 5.0. The pre-culture was diluted 100 times into TB medium with corresponding antibiotics and incubated at 30 °C with 180 rpm shaking. The final concentration of 0.4mM IPTG was added into each flask for induction when the OD_{600} was 0.3-0.5 and incubated at 16 °C with 120 rpm shaking overnight.

The cells were harvested at 5000rpm for 30min after overnight incubation. Osmotic shock was performed after harvesting the cells. *E.coli* cells can produce highly specific metal chelators and metallophores under stress conditions when over-expressed recombination proteins. Thus, removing periplasmic fractions could improve the yield of His-tagged recombination proteins through the increased binding capacity of His-tag to the affinity column. [125,126]. Cell pellets were re-suspended in sucrose buffer with a ratio of 5 ml per gram cell pellet and homogenized by Glass Porter before pelleting down at 8,500 ×g centrifugation for 40 min at 4 °C. The supernatant was discarded, and the pellets were re-suspended in 5mM MgSO4 buffer. The mixture was then incubated on ice for 10 min and centrifuged at 4500 × g for 20 min at 4 °C.

Cells were then re-suspended in lysis buffer with the ratio of 10ml per gram cell pellet combined with the protease inhibitor cocktail and incubated in cold-room with 300 rpm speed stirring for 1 hour. The French press was used to open cells for at least 3 rounds with a pressure between 10,000-15,000 psi. 150 mM NaCl and 10 mM EDTA were added after the cells were open, and the inclusion body was pelleted down by 9000 xg centrifugation. Membrane fractions were collected under 150,000 xg ultracentrifugations and solubilized with the corresponding detergents at 4 °C overnight for further purification or stored in 30% glycerol buffer in -80 freezer.

Ultracentrifugation was performed after overnight solubilization to remove the insoluble part and solubilized fractions were mixed with the Affinity chromatography resin. In this work, recombination proteins were purified with relative affinity tags: His-tag and Rho-tag.

The polyhistidine tag is a purification tag for efficient protein purification originally invented in 1988, which is based on the interaction between the tag fused to the protein of interest and a novel metal chelate adsorbent[127,128]. For His-tagged protein purifications, solubilized fractions were mixed with the Immobilized Metal Affinity Chromatography (IMAC) and incubated at 4 °C for at least 3 hours with 10mM Imidazole added, which could decrease the unspecific binding of impurities[129]. Three wash steps were performed, including the first wash step with high detergent

concentration, the second wash step with higher salt concentration, and the last wash step with even higher salt concentration and higher imidazole concentration. The target proteins were eluted under 500mM of Imidazole and concentrated to a certain amount for further purification by size-exclusion chromatography (SEC).

Rho-tag, also known as the Rho1D4 tag discovered in 1984, is an epitope tag original from bovine rhodopsin's C-terminal end, containing nine amino acids TETSQVAPA[130,131]. Unlike IMAC, the highly specific binding between the Rho-tag and the Rho1D4 antibody could avoid many impurities and increase the purity in protein purification. For Rho-tag purification, Solubilized parts were mixed with Rho-tag resin and incubated at 4 °C overnight, and the resin was washed with plenty of Rho-tag SEC buffer until the absorption at 280nm to 0. The target proteins were eluted with an excessive amount of Rho1D4 peptide for several rounds and each round contained at least 200 µM peptide until all target proteins were eluted. The eluted proteins were mixed and concentrated to a certain amount for further SEC purifications.

Size-exclusion chromatography (SEC), known as gel filtration, could separate proteins in their molecular sizes and some cases the molecular weight (MW)[132,133] Separation occurs when molecules of various sizes are incorporated or excluded from the pores in the matrix. Small molecules spread into the pores and their flows in the column are delayed according to their size, while large molecules remain out of the pores and are eluted in the void volume of the column. Thus, molecules are separated according to their size as they pass through the column and are eluted in decreasing order of MW [134–136]. In this work, several SEC columns were applied according to the molecular weight fractionation range, including Superose 6 Increase 10/300 GL, Superdex 200 Increase 10/300 GL, Superdex 200 10/300 GL and HiLoad 16/600 Superdex 200 pg. The SEC column calibrations were performed by Gel Filtration Markers Kit from SIGMA, using the standard protein molecular weights 29,000-700,000 Da. All protein samples need to be filtered by through a 0.22 µm filter before loading on the chromatography. The protein concentration of the elution fractions from SEC was determined by monitoring 280 nm absorption using a Nanodrop.
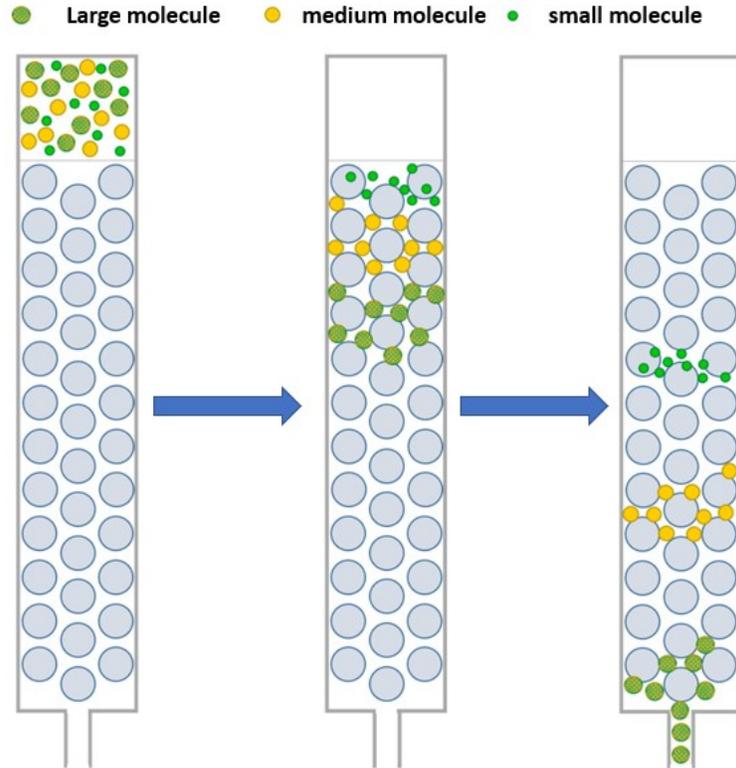
Figure 2.1 Principle of size-exclusion chromatography (picture adapted from[132])

Separation occurs when molecules of various sizes are incorporated or excluded from the pores in the matrix. Small molecules spread into the pores and their flows in the column are delayed according to their size, while large molecules remain out of the pores and are eluted in the void volume of the column. Thus, molecules are separated according to their size as they pass through the column and are eluted in decreasing order of MW

2.6 Protein reconstitution

In general, membrane proteins appear to be delipidated due to solubilization from the native membrane by detergents[137]. Integral membrane proteins maintain their functional activities by being associated with the lipids molecules in membranes and the interactions could be affected by the composition of lipids bilayers[138–140]. Thus, several model membranes were developed to restore the native-like environment, such as amphipathic polymers (also known as Amphipols), membrane scaffolding proteins (MSP) nanodiscs and lipid vesicles[141–143].

Amphipols are a new type of surfactant that can deal with membrane proteins in detergent-free solutions in water, just as they do with soluble proteins[144]. Amphipols adsorb to the hydrophobic

26

transmembrane surface of membrane proteins due to their hydrophobic moieties and maintain the water solubility of the resulting complexes due to their hydrophilic moieties. To reconstitute membrane proteins into amphipols, the SEC purified proteins were mixed with a different molar ratio of amphipol A8-35 polymers in the presence or absence of lipids. The detergents were removed by Bio-beads SM-2 Resin at room temperature 2hours for the first and second rounds and in cold room overnight for the last round. Considering that the proteins were solubilized by Fos-14 detergents, the excess amount of Bio-beads was used to absorb the detergent in each round. Ultracentrifugation of 100,000 xg was performed to remove the precipitation from the reconstitution process.

MSP nanodiscs are a non-covalent combination of phospholipids and genetically engineered membrane scaffold proteins based on the human serum apolipoprotein A-I sequence[145]. As shown in Figure 2.2, the phospholipids are bound together as a bilayer structural domain, while the two molecules of MSP molecules surround the edges of the disc structure in a belt-like pattern, where one MSP covers the hydrophobic alkyl group of each leaflet[146,147]. And the size of an MSP nanodisc can range between 7 - 17 nm, which is determined by the used membrane scaffolding protein[148]. In order to reconstitute membrane proteins into MSP nanodiscs, the specific molar ratio of target proteins to MSPs and lipids needs to be calculated based on the size of the target proteins and the ratio of MSPs to lipids can be checked through the literature. Before mixing with MSPs, the selected phospholipids are required to be hydrated and solubilized in NaCholate buffer and incubated at a particular temperature, which should be slightly higher than the transition temperature of the phospholipids. The solubilized lipids are then mixed with the specific MSP and target protein and incubated at room temperature or 4°C for 1 hour, depending on the lipid used. The assembly procedure was happened during Bio-beads SM-2 abosorption. Absorption was performed with an excess of Bio-beads for at least 3 rounds, the first and second rounds at room temperature for 2 hours and the last round in a cold room overnight. The suspension of bio-beads and MSP nanodiscs was filtered with a 0.45 μm membrane filter, and nanodiscs containing the target protein required a further purification step (purification by affinity chromotography or size exclusion chromotography) to separate the empty nanodiscs.
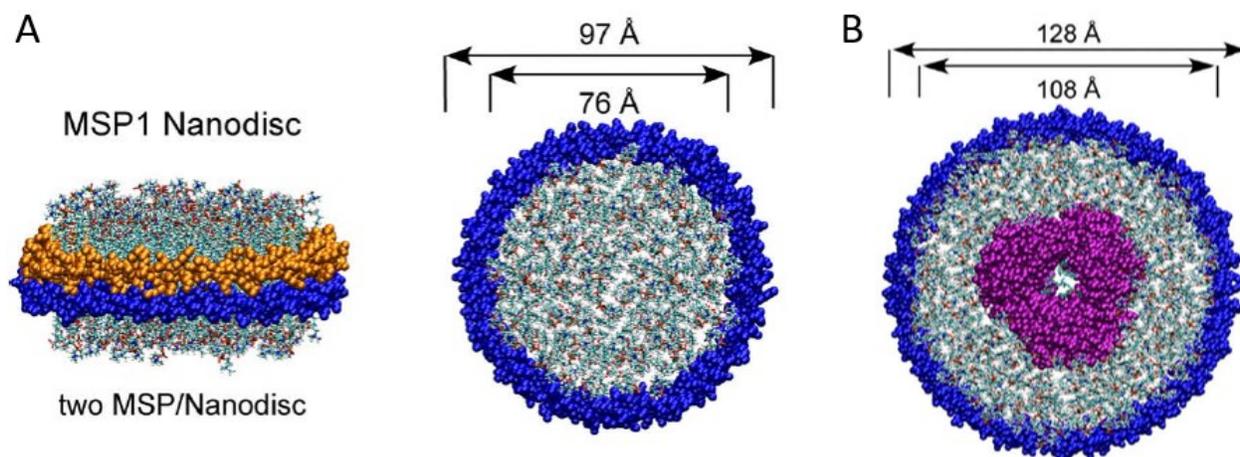
Figure 2.2 The MSP nanodiscs (picture adapted from [149])

(A) Composition of MSP1D1 and phospholipid in empty MSP nanodiscs and two MSPs are colored with different colors. (B) Illustration of MSP1E3, phospholipid and Bacteriorhodopsin trimer complex. The sizes of the distinct MSPs nanodiscs are marked.

Liposomes are compact artificial vesicular systems consisting of one or multiple phospholipid bilayers with polar groups of phospholipids oriented in the internal and external aqueous phases[150,151]. The necessity of reconstitution is that many membrane proteins can exhibit their full activity when properly oriented and inserted into the lipid bilayer[152,153]. Phospholipid mixture was dried by the freeze dryer to remove the chloroform and resuspended in hydration buffer to a final concentration of 20 mg/ml. The suspension was then hydrated at a particular temperature slightly above the transition temperature of the lipids for 1 hour. A minimum of three cycles of freezing and thawing steps are performed: freezing in liquid nitrogen, holding at -80°C for 10 minutes, and thawing in a water bath at a specific temperature for 10 minutes. After the freezing and thawing steps, the lipids are extruded more than 10 times at the correct temperature through a polycarbonate filter of the desired size until the solution becomes clear. The prepared liposomes were diluted to 4mg/ml, destabilized by the detergents CHAPSO or DDM to the saturation point of liposomes and detergents[154], and mixed with the target protein in a protein: lipids molar ratio of 1:50. The mixture was incubated in cold-room overnight with end over rotation. The detergents were removed by treatments with Bio-beads SM-2 Resin at room temperature for 2 hours for the first and second rounds and in the cold room overnight for the last round. The empty liposomes were removed by sucrose gradient ultracentrifugations with gradient sucrose concentrations 40%, 37.0%, 32.5%,

29.5%, 21.0%, 17.2%, 13.4%, 9.0. The reconstituted proteoliposomes were mixed with 80% sucrose buffer and layered at the bottom of the tubes. Other sucrose buffer percentages were carefully layered into the tubes from high to low concentrations. The ultracentrifugation was performed using SW 32 Ti Swinging-Bucket Rotor with 100,000 xg at 4 °C for 16 hours. The proteo-liposomes were collected for further experiments.

2.7 Protein identification and Characterization

Spectroscopic protein quantification

Protein concentrations were determined in different ways: by UV-VIS, Bradford assay or BCA assay. UV-VIS or NanoDrop Spectrophotometers determined purified protein concentrations within a range from 330nm -200nm based on the Tryptophan and Tyrosine residues absorbed at 280 nm[155], and the concentrations of purified proteins were calculated according to the Beer-Lambert law [156]:

$$c = \frac{A_{280nm}}{\varepsilon_{280nm} * d}$$

Where c stands for the molar concentrations and A_{280nm} refers to the 280nm absorption, while $\varepsilon 280nm$ is the molar attenuation coefficient. The specific extinction coefficient and protein molecular weight were evaluated on the online Expasy ProtParam tool (https://web.expasy.org/protparam/)[157].

Bradford assay was performed to measure the total protein concentration when solubilized with DIBMA or SMA polymers. Bradford assay is a rapid and accurate spectroscopic analytical procedure to measure the concentrations based on the absorbance shift from 465 to 595 nm of Coomassie brilliant blue G-250[158–160]. The standard curve was generated by adding 2 µl of gradient concentrations of bovine serum albumin (BSA) to 998 µl of Bradford solution to make the final BSA concentration 2/5/8 mg/ml. The unknown protein suspensions of 2 µl were also added to 998 µl Bradford solutions, and all mixtures were incubated at room temperature for 10 minutes. Absorbance was measured at 595 nm with a Tecan plate reader, and the concentration of unknown protein suspensions was calculated according to the standard curve.

It is known that detergents affect the Bradford assay, so the concentration of detergent-solubilized proteins is examined by the Bicinchoninic acid (BCA) assay. The BCA assay was invented by Paul K. Smith in 1985 and is based on the chelation of Bicinchoninic acid with Cu^{1+} ions, which are released by the biuret reaction of peptide bonds with Cu^{2+}, and produce a purple complex with an absorption wavelength of 562 nm[161,162]. The standard curve was created with the gradient BSA concentration of 0, 0.5, 1, 2.5, 5, 10, 20, 40, 200 µg/ml. The protein solutions were mixed with the working reagent with the same volume ratio as preparing the samples for the standard curve. The samples were incubated at 60 °C for 1hour with 600 rpm shaking and the hot lid of the instrument needs to be set. Absorbance was measured at 562 nm with a Tecan plate reader, and the concentration of unknown protein suspensions was calculated according to the standard curve.

SDS-PAGE and Western blot

Sodium dodecyl sulfate-polyacrylamide gel electrophoresis (SDS-PAGE) was first developed by Ulrich K. Laemmli and is a commonly used method for separating proteins based on molecular weight[163,164]. Protein samples were mixed with 5X SDS-Sample buffer and incubated under 46 °C for 30 minutes to allow SDS to bind in the hydrophobic region and complete denaturation. The prepared samples were loaded on the different percentages of SDS-PAGE gel according to the target protein molecular weight and ran with 80V voltage for stacking gel first and then 120V voltage for the resolving gel until the dye front ran out of the gel.

The tryptophans in proteins react with some compounds and produce fluorescence in the visible range when incorporated with 2,2,2-Trichloroethanol (TCE) and allow to detect of the SDS-PAGE gel under UV light[165,166]. Gels were also stained with Blue silver staining solution after collecting the fluorescence detected images and incubated at room temperature overnight with 120rpm shaking. The background of stained gels was destained by Milli-Q water or 5% acetic acid solutions.

The western blot is a widely used method to identify specific proteins in samples or crude lysate[167]. After separating by SDS-PAGE, proteins were transferred to the PVDF membrane from the gels via electrophoresis with the standard program on Trans-Blot Turbo Transfer System from Bio-Rad. Blocking of non-specific binding is achieved by depositing the membrane in 5% non-fat dry milk dissolved in TBS-T buffer at room temperature for 1 hour. Primary antibody diluted in TBS-T

buffer was incubated with the membrane at room temperature for an hour or overnight at 4°C. The membranes were washed afterward with two times TBS-T buffer at room temperature for 10 minutes each round and one-time TBS buffer for at least 10 minutes. His-tag detection can be done without secondary antibodies involved. For Flag-tag or Rho-tag western blot, secondary antibodies will be performed in the same procedures as primary antibodies. The enzyme horseradish peroxidase (HRP)was conjugated to the primary antibody of His-tag or secondary antibody of Rho-tag of Flag-tag and catalyzed the oxidation of luminol in the presence of H_2O_2 [168]. The signal was detected via Chemiluminescent detection on ChemiDoc MP Imaging System.

Mass spectrometry identification

The stained protein bands were cut and sent to EMBL- Heidelberg Proteomics Core Facility. The protein identification was performed with in-gel in-gel trypsin digestion followed by LC-MS/MS on a Dionex Ultmate 3000 HPLC coupled to an Orbitrap Fusion Lumos System.

Circular Dichroism spectroscopy

Circular Dichroism (CD) is an absorption spectroscopy method based on the different absorption of left and right circularly polarized light and used to investigate the protein structure and folding property[169]. Peptide bonds in proteins are optically active and the ellipticity they exhibit changes based on the local conformation of the molecule[170]. Secondary structures of proteins can be analyzed using the far-UV (190-250 nm) region of light. The ordered α -helices, β -sheets, β -turn, and random coil conformations all have characteristic spectra (Figure 2.3) and are the basis for protein secondary structure analysis[171,172].
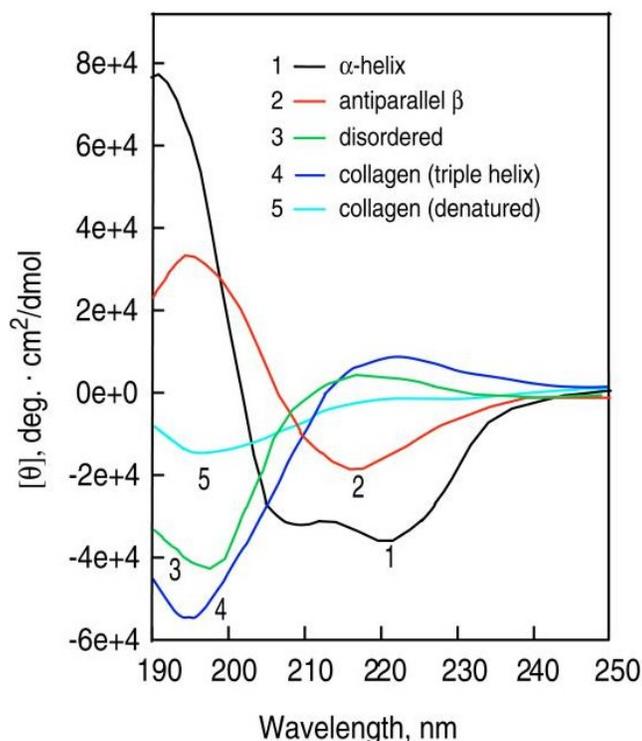
Figure 2.3 CD spectra of polypeptides and proteins with representative secondary structures. (picture adapted from [173])

The α-helical proteins have negative bands at 222 nm and 208 nm and positive bands at 193 nm, meanwhile, proteins with well-defined anti-parallel β-pleated sheets present negative bands at 218 nm and positive bands at 195 nm, while disordered proteins show a low ellipticity above 210 nm and negative bands near 195 nm.

CD measurements were carried out using an Aviv CD425 spectrometer. Usually, CD spectra are normalized to the mean residue ellipticity using the following equation for comparison[174],

$$[\theta]_{mrw,\lambda} = \frac{MRW * \theta}{10d * c}$$

Where [θ]mrw,λ is the mean residue ellipticity which has the units of deg×cm^2×$dmol^{-1}$, MRW stands for the mean residue weight and is calculated by the following equation. The θ is the observed ellipticity (degrees), d is the path length in unit centimeters and c is the protein concentration in units of a milligram per milliliter.

$$MRW = \frac{molecular\ weight}{number\ of\ residues - 1}$$

Secondary structure evaluation was investigated by Deconvolutions of obtained CD data performed on the online server DichroWeb (http://dichroweb.cryst.bbk.ac.uk/html/home.shtml) with the CDSSTR analysis program and Reference set SMP180, which is mainly for membrane proteins[175–177].

To perform the CD measurements, the NaCl needs to be exchanged to their NaF by Zeba Spin Desalting Columns due to the strong absorption of chloride iron at a wavelength less than 195 nm. As the accurate concentration of the protein is essential for a CD measurement, BCA assay was used to determine the protein concentrations. All CD spectra measurements were performed at 4 °C and temperature scans were performed from 4 °C to 98 °C at a heating rate of 2 °C per round with an averaging time of 9 seconds.

Fluorescence spectroscopy

Jablonski diagrams are commonly utilized in fluorescence spectroscopy to describe the excited states of molecules and the radiative and non-radiative transitions that may occur between them[178]. There are 3 steps in the generation of fluorescence, which are detailed in the Jablonski diagram (Figure 2.4 A). Following light absorption, the fluorophore is excited to some higher vibrational level of S1 or S2 depending on conformational changes, collisional quenching, and other processes, after which the fluorescence emission returns to the excited vibrational state at the S0 level[179,180]. The aromatic amino acids Tryptophan (Trp), Tyrosine (Pyr) and Phenylalanine (Phe) are intrinsic sources of fluorescence for proteins (Figure 2.4 B). The indole group of tryptophan residues is the most critical UV absorption and emission source in proteins. In contrast, tyrosine, similar to tryptophan, has a narrower distribution in the wavelength range. The emission of tryptophan is highly sensitive to its local environment and is therefore commonly reported as a reporter group for conformational changes in proteins. Unfolding and denaturation of proteins may alter the microenvironment of Trp, leading to a decrease in fluorescence intensity and red-shift of the emission spectrum[180].

The experiments of fluorescence spectroscopy were performed by using AVIV Model 425 spectrometer. An excitation wavelength of 295 nm was used while the range of emission spectra

was collected from 450 nm to 260 nm. Thermal denaturation experiments were performed from 4 °C to 98 °C with a heating rate of 2 ºC per minute and an averaging time of 1 second.
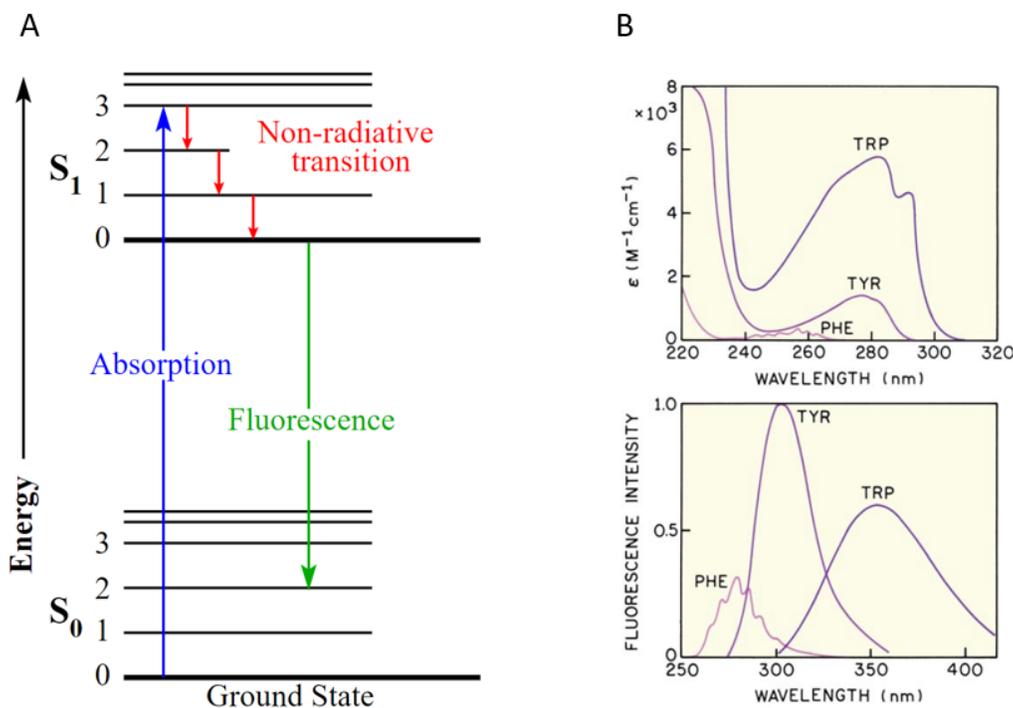
Figure 2.4 Illustration of Jablonski diagrams and absorption and emission spectra of the fluorescent amino acids (picture adapted from[179,180])

(A)Jablonski diagram including vibrational levels for absorbance, non-radiative decay, and fluorescence. (B) Absorption (upper panel) and emission (lower panel) spectra of fluorescent amino acids in water at pH 7.0.

Microscale thermophoresis

Microscale thermophoresis (MST) is on the rise as a sensitive approach allowing the evaluation of biomolecular interactions and used to investigate the interactions between a wide range of binding partners of various molecular sizes: protein-protein, antibody-antigen, protein-DNA, protein-RNA interactions[181–183]. As shown in Figure 2.5, the high sensitivity of detecting MST requires fluorescent labeling of the protein of interest and the sample is loaded on a glass capillary without much sample volume. An infrared laser heats a specific spot and results in a temperature gradient that leads to thermophoresis of the labeled molecule, which is observed by the reduction of fluorescence in the heated region. Due to the binding-induced changes in size, charge and hydration

shell, the thermophoresis of proteins is usually quite different from the thermophoresis of protein-ligand complexes[184].

MST analysis was performed using NanoTemper Monolith NT.115 (NanoTemper, GmbH). Purified complexes of PS1-WT and PEN-2 or PS1-DDAA and PEN-2 were labeled with the dye using the NanoTemper Protein Labeling Kit RED-NHS 2nd Generation. The labeling procedure was performed at room temperature for 20minutes. 25 nM of the labeled complex was incubated with different ligands containing gradient concentrations and loaded into Monolith NT.115 Premium Capillaries. Measurements were performed at 20 °C by using 20-40% LED power and medium IR-laser power.
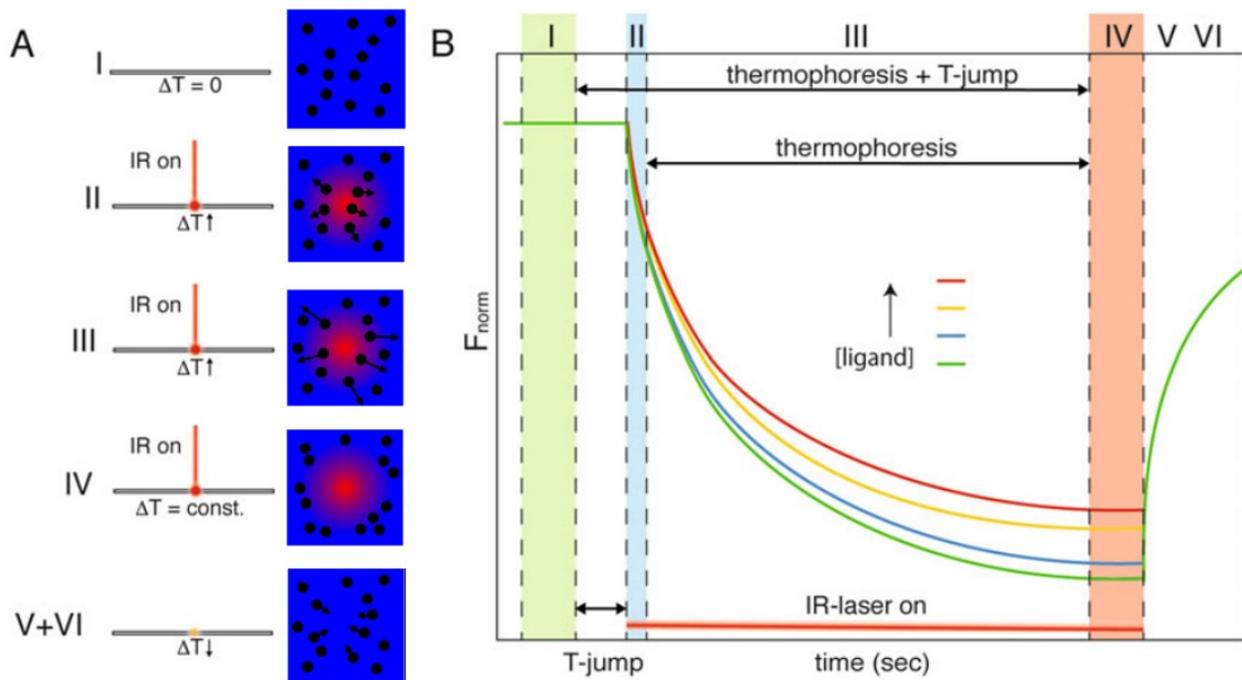
Figure 2.5 Principle of Microscale thermophoresis (picture adapted from [185])

Illustrations of the (A) MST experiment and (B) MST time trace. Phase I refers to the equilibrium state before Phase II, which shows the started laser irradiation. During thermophoresis (Phase III), the particles move in or out of the heated volume and reach the steady-state (Phase IV) when thermal diffusion is balanced with mass distribution. The particle concentration is re-equilibrated when the laser is turned off (Phase V+VI).

Plate reader spectrophotometer

Plate readers are instruments used to detect biological, chemical or physical events in samples in microplates. The most commonly used microplate format is 96-well, which allows screening of sample conditions in a short period of time[186–188]. 96 Well Black/Clear Bottom Plates were used to screen the conditions of the activity assay. The excitation wavelength was set to 355nm and the emission wavelength was assigned to a single wavelength of 440 nm or the range of 400-480nm. For kinetic collection, the plates were shaken in a plate reader at 300 rpm and the fluorescence signal was collected every 10 min.

2.8 Activity assay

The activity assay was performed with different substrates: MBP-APPC, APP-C99 and the fluorogenic γ-Secretase substrate. Activity assay of MBP-APPC or APP-C99 was performed with Activity assay buffer IV where the protein concentration was around 0.15 mg/ml and the concentration of the substrate 0.5 mg/ml. The mixture was incubated under 37 ºC for 16 hours and the signal was detected on SDS-PAGE or Tricine Protein Gels according to the bands shift. The activity assay of the fluorogenic γ-Secretase substrate was performed according to the literature[189]. Purified complexes or the cell membranes with or without PS1-PEN-2 complex were mixed with 10µM of the fluorogenic γ-Secretase substrate. The mixtures were incubated at 37 ºC in the Tecan plate readers and the signals were collected at the emission wavelength of 440 nm with 355nm excitation wavelength.

3. Results

3.1 Fos-14 purified sub-units reconstitution

In this work, I reconstituted different Fos-14 solubilized γ-Secretase sub-units into lipidic environments.

3.1.1 Mechanism of autoinhibitory of Presenilin-1

Presenilin is a zymogen that undergoes proteolysis when associated with PEN-2, forming PS1-NTF/CTF heterodimers. As shown in Figure3.1 and Table3.1, we introduced a thrombin site into Presenilin-1 after Methionine (M) 298 to make a PS1-thrombin construct that can manually generate PS1-NTF and PS1-CTF after thrombin protease cleavage. Another construct, PS1-thrombin-E321, was created by introducing a thrombin cleavage site after Glutamic acid (E) at position 321, after the autoinhibitory loop exon 9. Methionine (M) at position 292 is reported to activate Presenilin-1 alone when mutated into Aspartic acid (D). We created a construct PS1-M292D-thrombin to combine an M292D mutation with a thrombin cleavage site after Methionine at position 298. PS1-DDAA double mutation is mutated from the catalytic amino acids Aspartic acid (D) at positions 257 and 385 into Alanine (A). All Presenilin-1 constructs have an additional thrombin protease cleavage site between the N-terminal His-tag and the protein sequence.

Table 3.1 Constructs of Presenilin-1 wild type and mutations

Protein	Constructs Details	Numbers of Thrombin cleavage site
PS1-WT	His-tag+thrombin+Presenilin-1	1
PS1-DDAA	His-tag+thrombin+Presenilin-1 with DDAA mutation	1

PS1-thrombin	His-tag+thrombin+Presenilin-1 with thrombin after M298	2
PS1-thrombin-E321	His-tag+thrombin+Presenilin-1 with thrombin after E321	2
PS1-M292D-thrombin	His-tag+thrombin+Presenilin-1 with thrombin after M298 and M292D mutation	2
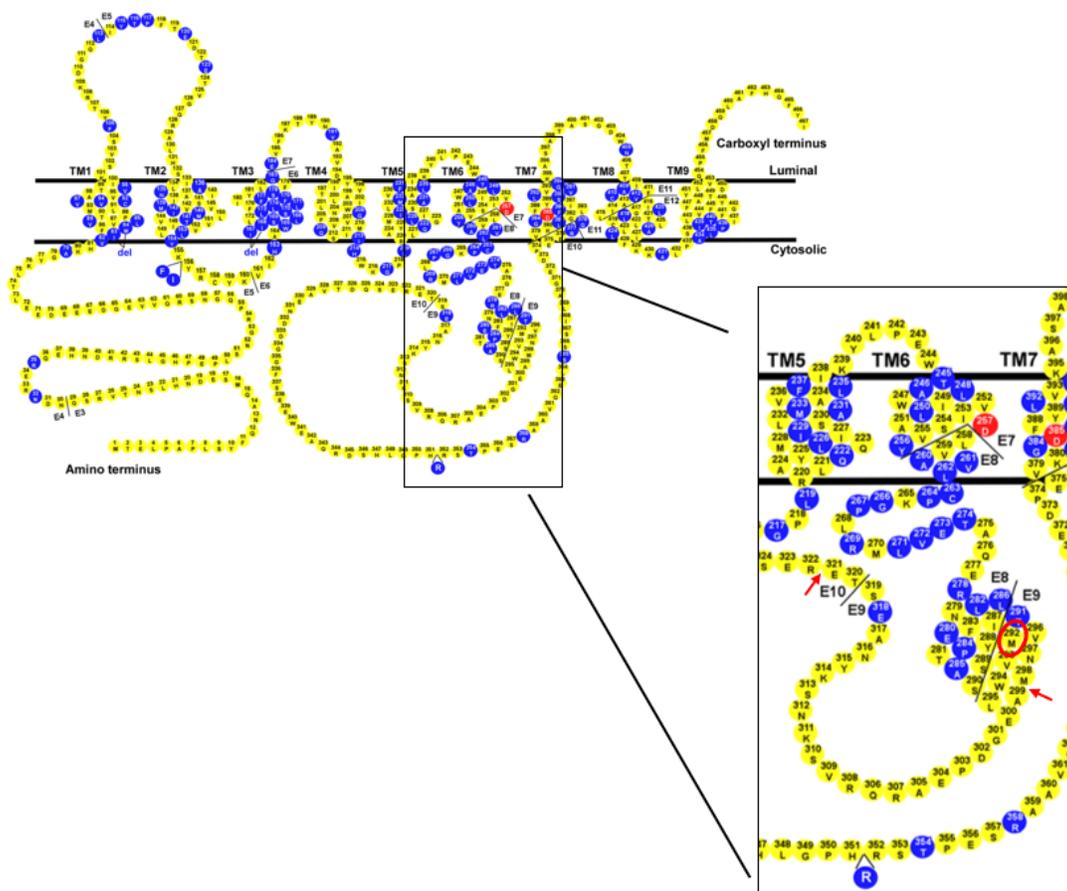
Figure 3.1 Design of Presenilin-1 mutations

Different mutations were made by point mutations or insertion. Red arrows indicate that where we introduced the thrombin protease cleavage site separately. The red circle indicates the point mutations site. The two red buttons showed the catalytic sites of Presenilin-1, where we mutated into Alanine.

All constructs have two cleavage sites for thrombin: the first site is after the his-tag and allows the release of a 1.5 kDa peptide from the protein sequence. The other one is in the middle of the protein sequence and allows the manual generation of the N-terminal and C-terminal fragments of the Presenilin-1. As shown in Figure 3.2, after thrombin protease treatment, the bands on SDS-PAGE were slightly shifted. No difference was observed between the proteins alone and those mixed with thrombin protease cleavage reaction buffer, indicating that only the his-tags of PS1-DDAA, PS1-WT and PS1-thrombin were removed. But the thrombin cleavage site after M298 was not accessible to thrombin protease, suggesting that the auto-inhibitory loop exon 9 of PS1 is highly hydrophobic and is blocked between TM6 and TM7, thus hindering substrate processing.
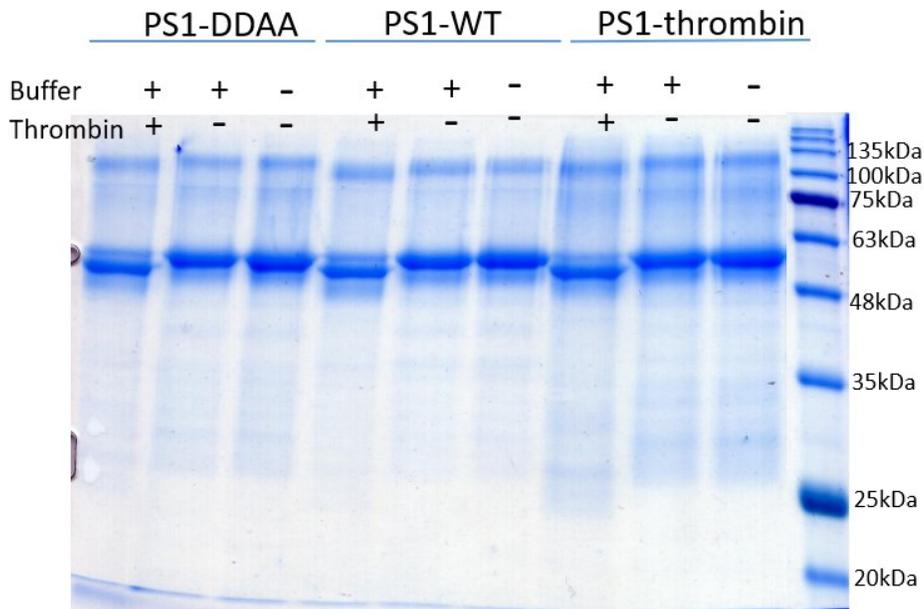
Figure 3.2 Thrombin cleavage of Presenilin-1 WT and its mutations

Presenilin-1 WT, DDAA, and thrombin mutation were cleaved by thrombin protease. Reactions without thrombin protease and proteins alone as the negative control.

To confirm the autoinhibitory loop exon 9, I proceeded with thrombin protein cleavage using PS1-thrombin-E321 and PS1-M292D-thrombin. As shown in Figure 3.3, a slight shift was observed in the PS1-M292D-thrombin sample. Only the N-terminal thrombin site was cleaved in PS1-M292D-thrombin, indicating that exon 9 of the autoinhibitory loop is still blocked at the active site of Presenilin and is not accessed by thrombin protease. Several bands of the PS1-thrombin-E321 sample, representing the full length of PS1, NTF and CTF, were detected on SDS-PAGE and confirmed by Western blot. This suggests that only exon 9 of the autoinhibitory loop is highly hydrophobic and acts as a steric constraint on the processing of the substrate. Some weak signals were still detected on the Western blot. Considering that excess thrombin protease was used, the his-tags appeared to be not completely accessible to thrombin protease.
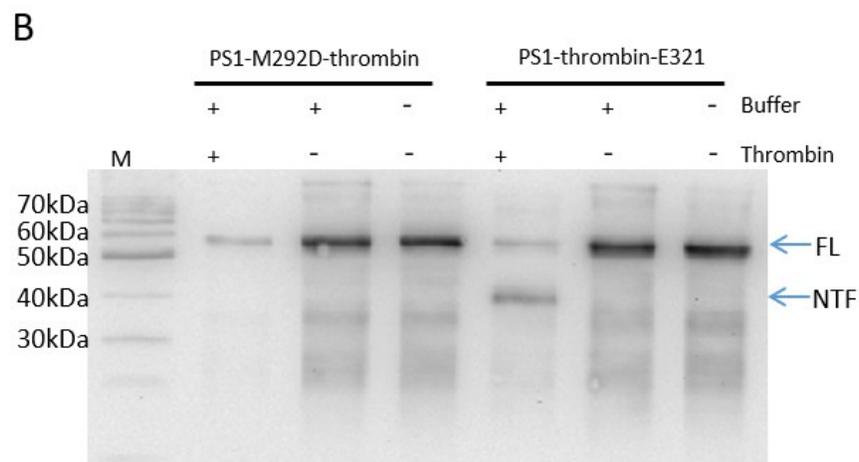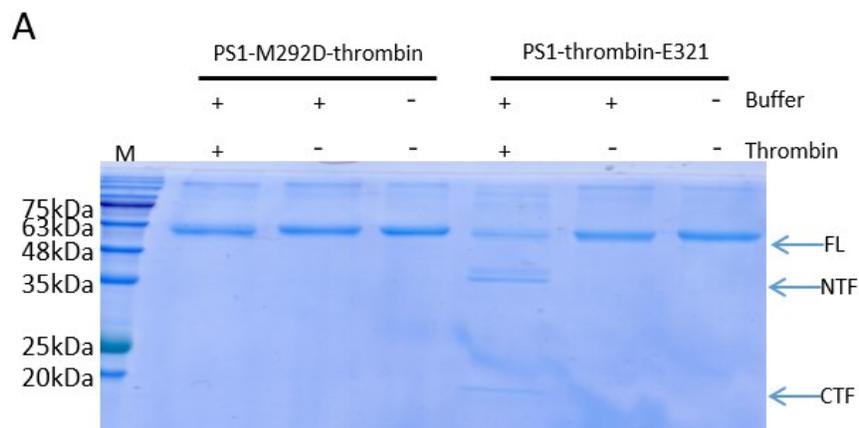
Figure 3.3 Thrombin cleavage of Presenilin-1 mutations

PS1-M292D-thrombin and PS1-thrombin-E321 were cleaved by thrombin protease. Reactions without thrombin protease and proteins alone as the negative control. (A) Blue silver stained SDS-PAGE of cleaved Presenilin-1 mutations. (B) Anti-His-tags western blot of cleaved Presenilin-1 mutations. M: protein marker

MBP-APPC (plasmid obtained from Yigong Shi[190]) was considered to be the soluble protein, which can be purified without detergent and used as a γ-secretase substrate. MBP-APPC protein was made with an MBP expression tag followed by a thrombin protease cleavage site fused in the N-terminus of APP-C99 protein, while a His-tag with right histidines in the C-terminus. The red part indicates the transmembrane domain of APP-C99. The potential cleavage sites were marked by yellow arrows with different protein products names described (Figure 3.4A). MBP-APPC was expressed in BL21 (DE3) and induced at an OD of 0.6. Cells were harvested after incubation at 20°C for 5 h with 100 rpm shaking and opened with cell disruptor. The supernatant after 100,000xg was passed through Amylose resin (Cube biotech) 5 times, which was subsequently washed with Column buffer (20mM Tris-HCl, pH:7.4, 200mM NaCl, 1mM EDTA). MBP-APPC was eluted with the Column buffer in the presence of 10 mM maltose. As shown in Figure 3.4 B and D, samples were obtained from every purification step and analyzed by SDS-PAGE. The flow-through lanes showed that most of the target protein was not bound to the resin, probably because of a low affinity. Although some of the MBP-APPC was washed off during the washing steps, a sufficient amount of protein for further experiments was eluted with 10mM maltose. Blue silver stained SDS-PAGE showed the high purity of MBP-APPC, indicating the suitability for the activity assay (Figure 3.4C).
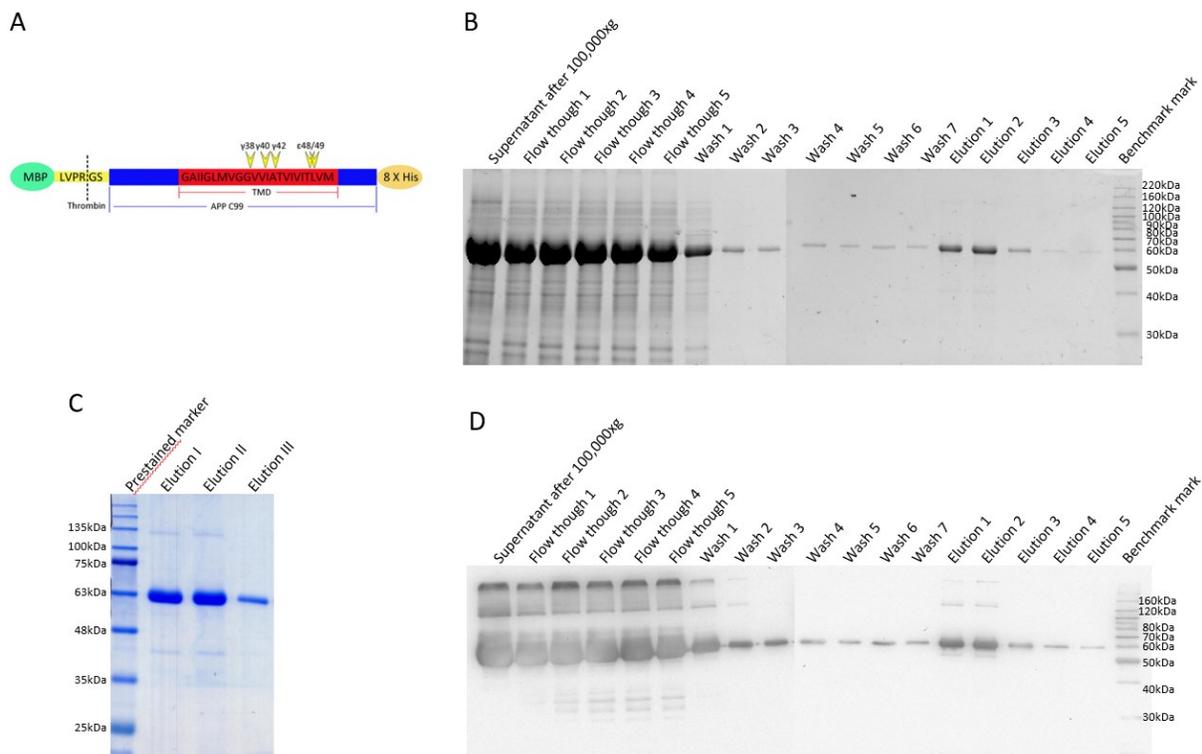
Figure 3.4 Purification of γ-secretase substrate MBP-APPC

Purification of MBP-APPC protein for γ-secretase activity assay. (A) A schematic diagram of the APP C99 substrate (adopted from [190]). MBP expression tag was fused in the N-terminus of APP-C99 protein with a thrombin cleavage site in between and a His-tag with eight histidine residues in the C-terminus. The transmembrane domain of APP-C99 was labeled by red color and the potential cleavage sites were marked by yellow arrows with the different protein products names. (B) Intrinsic tryptophan fluorescence detection of the purification steps of MBP-APPC. (C) Blue stained SDS-PAGE of the Elution of MBP-APPC proteins. (D) His-tag Western blot of purification steps of MBP-APPC.

Fos-14 solubilized PS1-WT and mutations were used to measure the activity with detergent-free purified MBP-APPC. Besides the original buffer condition of Fos-14 containing with pH 7.4, the buffer conditions for the other proteins were exchanged on the concentrator for PBS buffer containing DDM at pH 7.4 or 5.1. Presenilin-1 WT or mutations were mixed with the substrate separately and incubated at 37 °C overnight. As shown in Figure 3.5, MBP-APPC was cleaved by thrombin protease (lane 11) proving that MBP-APPC is a suitable construct. No differences were observed after overnight incubation at 37°C (lanes 15 & 16) implying that MBP-APPC is stable at high temperatures. An additional band was observed in the PS1-M292D-thrombin sample under Fos-14 conditions (lanes 3&13) but not under DDM conditions (lanes 6&9), suggesting that it may

be a degradation band that entered the flow through during the buffer exchange. Unfortunately, no cleaved product was observed for the samples in Fos-14, while the DDM sample in both pH conditions also showed no activities compared to the MBP-APPC control.
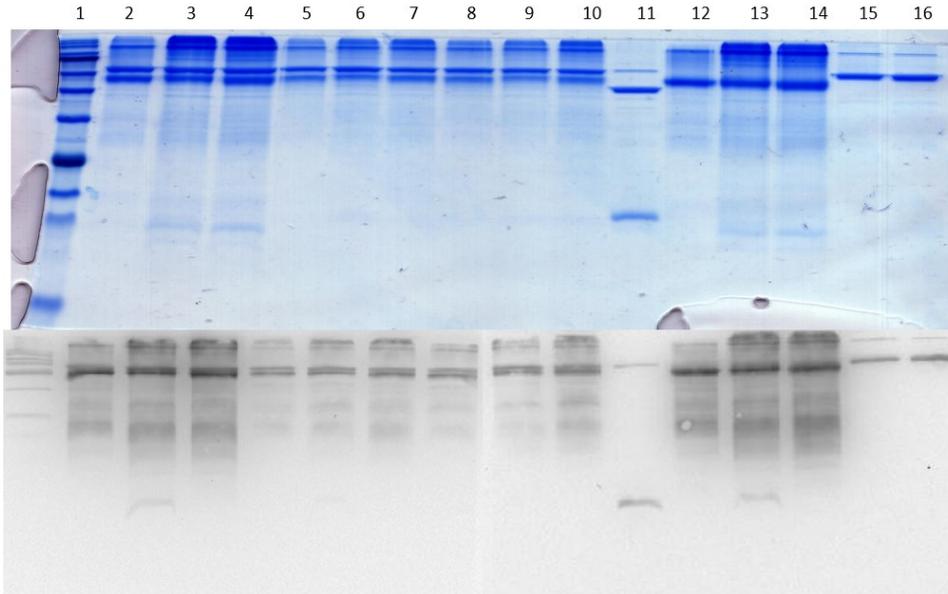
Figure 3.5 Activity assay of Fos-14 solubilized Presenilin-1 wild type and mutations with the substrate MBP-APPC

Activity assay of Presenilin-1 WT and its mutations were performed with the substrate MBP-APPC under two different detergents conditions. Upper part: Blue stained SDS-PAGE of activity assay. Lower part: Western blot of activity assay. 1: Marker, 2: PS1-WT in Fos-14+substrate, 3: PS1-M292-thrombin in Fos-14+substrate, 4: PS1-thrombin-E321 in Fos-14+substrate, 5: PS1-WT in PBS and DDM+substrate, 6: PS1-M292-thrombin in PBS and DDM+substrate, 7: PS1-thrombin-E321 in PBS and DDM+substrate, 2-7 has all pH 7.4, 8-10 is the same order and conditions as 5-6 but the pH of 5.1, 11: MBP-APPC99+thrombin protease, 12: PS1-WT control, 13: PS1-m292d-thrombin control, 14: PS1-thrombin-E321 control, 15: MBP-APPC99 after 37 °C, 16: MBP-APPC99 control at 4 °C.

After isolation of the substrate, I could proceed to the γ-secretase activity assay at pH 7.4 or 5.1 with the thrombin cleaved PS1-thrombin-E321 which was supposedly activated by cleavage into PS1-NTF and PS1-CTF. For the activation, the protein was mixed with thrombin protease and incubated at 30°C for 4 h. The activity of thrombin protease was inhibited with 1 mM PMSF. I performed the activity assay for PS1-M292D-thrombin with PS1-WT as the control because the Presenilin-1 M292D mutation was reported to be active without endoproteolysis[61]. To measure the

activities, Presenilin-1 WT, M292Dmutation, and the thrombin treated PS1-thrombin-E321 were each mixed with detergent-free purified MBP-APPC and incubated at 37 °C overnight. As shown in Figure 3.6, thrombin protease treated PS1-thrombin-E321 displayed the presenilin-1 N-terminal fragment and C-terminal fragment (lanes 5&12) and no thrombin protease cleaved MBP-APPC was found, indicated that thrombin protease successfully cleaved PS1-thrombin-E321 and was inhibited by PMSF, which won't influence the downstream experiment. No cleavage products were observed, indicating that no activity was detected. Possible reasons are that harsh detergents are involved or that the substrate forms oligomers that prevent activity.
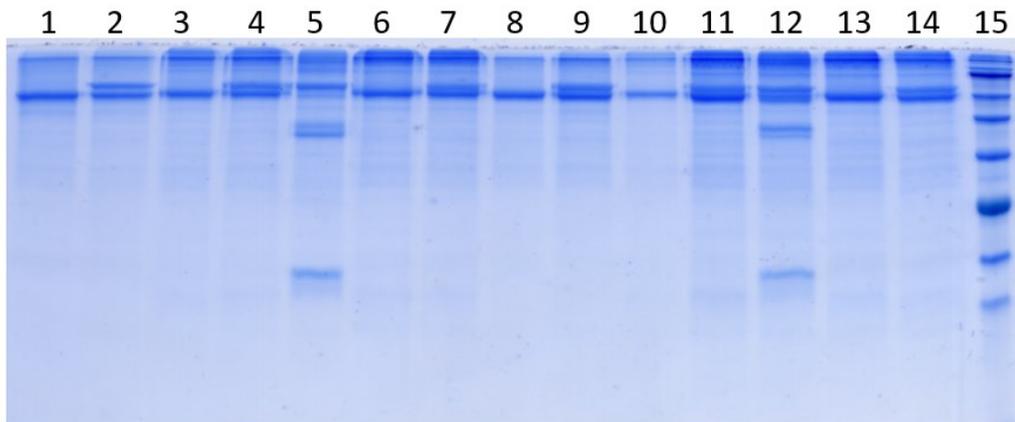
Figure 3.6 Activity assay of thrombin protease treated Fos-14 solubilized Presenilin-1 wild type and mutations with the substrate MBP-APPC

Activity assay of Thrombin protease treated Presenilin-1 WT and its mutations were performed with the substrate under two different detergents conditions. 1: PS1-WT control, 2: PS1-WT+MBP-APPC99, 3: PS1-Thrombin-E321 control, 4: PS1-thrombin-E321+MBP-APPC99, 5: PS1-thrombin-E321+MBP-APPC99+thrombin protease, 6: PS1-M292D-thrombin control, 7: PS1-M292D-Thrombin+MBP-APPC99. 8-14 were the same sample orders as 1-7 but pH at 5.1 instead of 7.4. 15: Prestained marker.

3.1.2 Reconstitution of Presenilin-1 mutations into MSP1D1 nanodiscs

To assemble γ-secretase into nanodiscs, I tried first to reconstitute a single subunit into membrane scaffold protein (MSP) nanodiscs. First, we reconstituted Fos-14 solubilized PS1-M292D-thrombin into MSP1D1 nanodiscs with DMPC lipids to optimize the reconstitution conditions of a single subunit into MSP nanodiscs. 48.41μg PS1-M292D-thrombin with the final concentration of 0.2μg/μl was applied together with 400μg MSP1D1 protein and 1mg DPMC lipids at the final

molar ratio of the target protein to MSP1D1 to lipids 1:19:1607. DMPC lipids were hydrated in 100mM NaCholate buffer at 37 °C for 20 minutes and finally mixed with MSP1D1 proteins and PS1-M292D-thrombin. The mixture was incubated at room temperature for 2 hours for assembly. SM-2 bio-beads from Bio-rad were used to absorb the detergents, 150mg bio-beads were used in total, 50mg for each of three rounds. The first two rounds were incubated at room temperature for 1 hour each, and the last round in the cold room overnight. As seen in Figure 3.7A, we observed expected two peaks after reconstitution into MSP nanodiscs and purification by size exclusion chromatography: the first peak for the protein-nanodiscs, and a second for the empty nanodiscs. PS1-M292-thrombin nanodisc complex was eluted at 14.5ml with a molecular weight of 120kDa. The his-tag signal around 50kDa in western blot confirmed PS1-M292D-thrombin while MSP1D1 protein showed a his-tag negative signal. The strongest signal appeared in SEC profile and SDS-PAGE for fraction b6, indicating that the first peak of SEC is the reconstituted PS1-M292D-thrombin nanodiscs (Figure 3.7B). To confirm the successful reconstitution, the first peak of SEC was pooled and purified by Ni-NTA affinity overnight at 4 °C. As shown in Figure 3.7C, only MSP protein was detected in the Ni-NTA FT sample, which shows that all PS1-M292D-thrombin nanodisc complex was bound to the Ni-NTA resin, whereas empty nanodiscs separated from PS1-M292D-thrombin nanodiscs. Some weak bands of PS1-M292D-thrombin and MSP proteins on SDS-PAGE in the wash step were also observed. 500mM imidazole concentration was used to elute the PS1-M292D-thrombin DMPC nanodiscs. I detected both the PS1-M292D-thrombin and MSP protein on SDS-PAGE in the elution sample. Since MSP proteins have no His-tag, free MSP protein and nanodisc without PS1 have already been removed in the Ni-NTA flow through. The MSP protein eluted from Ni-NTA with PS1-M292D-thrombin indicates that PS1-M292D-thrombin has successfully integrated into MSP1D1-DMPC nanodisc.
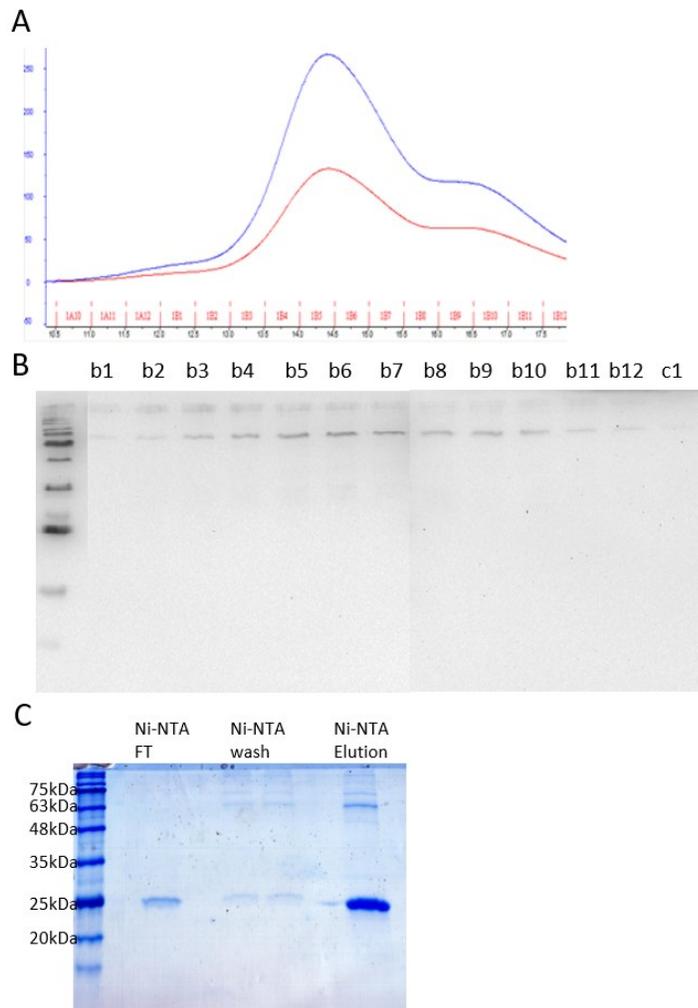
Figure 3.7 Reconstitution of PS1-M292D-thrombin into MSP1D1 DMPC nanodiscs

SEC profile and SDS-PAGE of reconstitution of PS1-M292D-thrombin into nanodiscs. (A) SEC profile of reconstituted PS1-M292D-thrombin nanodiscs. (B) Anti-His-tags western blot of the SEC fractions of reconstituted PS1-M292D-thrombin nanodiscs. (C) Blue silver stained SDS-PAGE of purification step of PS1-M292D-thrombin DMPC nanodiscs. FT: flow through

3.1.3 Reconstitution of PEN-2 into MSP1D1 nanodiscs

Second, I reconstituted Fos-14 solubilized PEN-2 into MSP1D1 DMPC nanodiscs., 28μg PEN-2 protein with a final concentration of 0.127μg/μl was combined with 888μg MSP1D1 protein and 2.2mg DPMC lipids at the final molar ratio of the target protein to MSP1D1 to lipids 1:20:1621. DMPC lipids were hydrated in a hydration buffer containing 100mM NaCholate at 37 °C for 20 minutes and finally mixed with MSP1D1 proteins and PEN-2. The mixture was incubated at 30 °C for 2 hours for assembly. Detergents were absorbed by the SM-2 bio-beads from Bio-rad. Each round used 50 mg of Bio-beads for a total of three rounds. The first two rounds were performed at room temperature for 1hour each, while the last round was incubated in cold room overnight. Figure

3.5A shows the SEC file of reconstituted PEN-2 nanodiscs, only a single peak was detected, probably because the difference in molecular weight between the PEN-2 nanodisc complex and the nanodiscs without PEN-2 was too small to be separated by SEC. SDS-PAGE of SEC fractions were shown in Figure 3.8B, and the red arrow demonstrates the MSP1D1 protein bands, where fraction b5 gives the highest intensity. The red triangle indicates the PEN-2 bands, but unfortunately, due to the low intensity of PEN-2, we can barely see the band on SDS-PAGE. Anti His-tag western blot was performed to detect the PEN-2 signal (Figure 3.8C). We observed monomers of PEN-2 at the bottom of the PAGE, as well as some oligomers, which have been proved to be concentration-dependent on the protein itself. Based on the PEN-2 signal on the Western blot, SEC fraction b5 also showed the highest intensity, consistent with the performance of the MSP1D1 protein in SDS-PAGE in Figure 3.8B. Given that all of the detergents have been completely absorbed and there is no detergent at all in the SEC buffer, PEN-2 can be detected after SEC purification, illustrating that PEN-2 has successfully reconstituted into MSP1D1 DMPC nanodiscs. The higher intensity of MSP on SDS-PAGE compared to PEN-2 also suggests that there are some empty MSP nanodiscs that are unable to separate from MSP nanodiscs carrying PEN-2 protein.
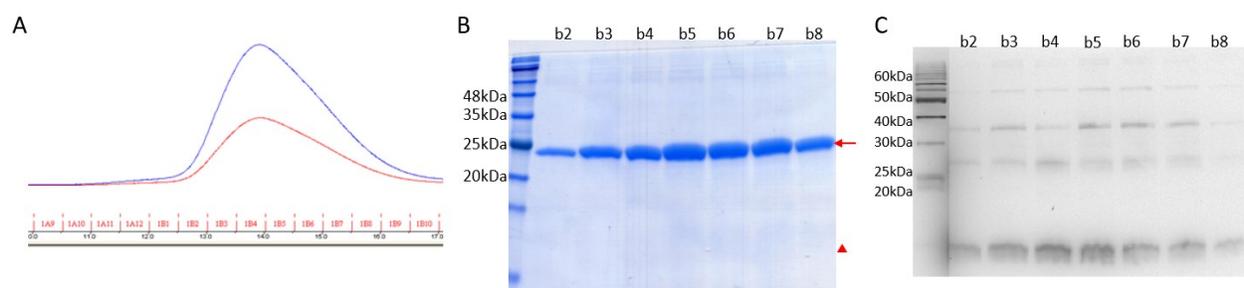
Figure 3.8 Reconstitution of PEN-2 into MSP1D1 DMPC nanodiscs

SEC profile and SDS-PAGE of reconstitution of PEN-2 into nanodiscs. (A) SEC profile of reconstituted PEN-2 MSP1D1 nanodiscs. (B) Blue silver stained SDS-PAGE of SEC fractions. The red arrow demonstrates the MSP1D1 protein bands, the red triangle indicates the PEN-2 bands (C) Anti-His-tags western blot of the SEC fractions of reconstituted PEN-2 nanodiscs.

3.1.4 Reconstitution of PS2-WT into Amphipols

Amphipols are novel surfactants that make it possible to treat membrane proteins in detergent-free aqueous solutions, just as soluble proteins are treated. Here we reconstituted the Presenilin-2 wild

type (PS2-WT) into Amphipols in a 200 µl reaction in the presence or absence of Brain Extract Total lipids with different protein to amphipol ratios. SEC-purified Fos-14-solubilized PS2-WT monomer peaks were used to reconstitute into amphipols at 1:2, 1:5 and 1:10 ratios. Brain Extract Total lipids were used with the molar ratio of protein to lipids 1:10. Bio-beads were employed to absorb the detergent (330mg per round) in 3 rounds. Precipitated fractions were removed by 100,000xg ultracentrifugation. When amphipols were missing, most of the PS2-WT protein precipitated or was absorbed after bio-beads uptake and was undetectable in the supernatant, and only a small fraction was observed in the pellet, indicating that the bio-beads successfully absorbed all the detergent. In the presence of amphipols, all PS2-WT proteins were displayed in the supernatant after ultracentrifugation, suggesting that all the proteins were successfully reconstituted into amphipols (Figure 3.9A, B). Two bands were found for the supernatant and identified as the dimer and monomer of PS2-WT. The dimer bands showed much higher intensity than monomer bands on SDS-PAGE (Figure 3.9 A) which indicated that PS2-WT formed an SDS resistant dimer. The higher abundance of monomeric bands exhibited in samples containing lipids also suggested that lipids may help prevent dimer formation.
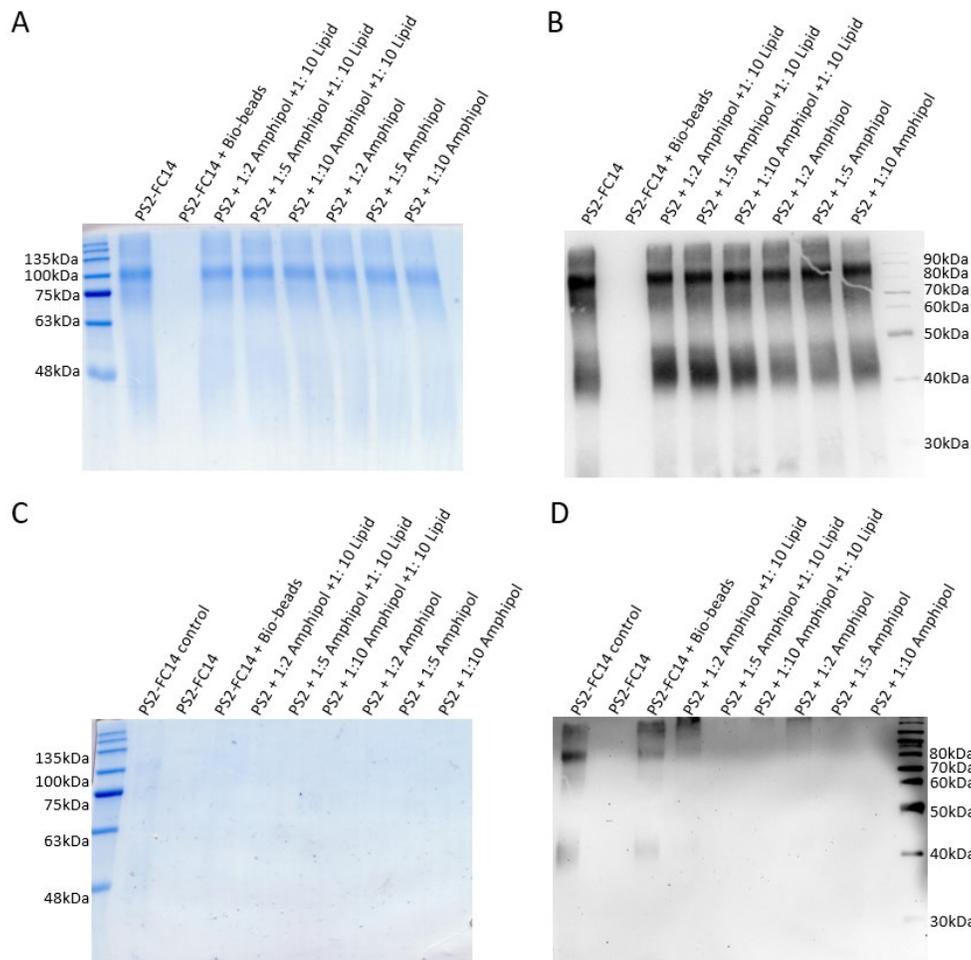
Figure 3.9 Reconstitution of PS2-WT into Amphipols

Amphipol A8-35 was used to the reconstitution of Presenilin-2 WT in the presence or absence of Brain Extract Total lipids and with different protein to amphipol ratios. Blue silver stained SDS-PAGE (A) and Western blot (B) of the supernatant of reconstituted PS2-WT after 100,000xg ultracentrifugation. Blue silver stained SDS-PAGE (C) and Western blot (D) of the pellet of reconstituted PS2-WT after 100,000xg ultracentrifugation.

3.1.5 Reconstitution of γ-Secretase sub-units into Liposomes

Given some of the drawbacks of reconstitution into nanodiscs or amphipols, I next attempted to reconstitute γ-secretase subunits into liposomes. To assemble γ-secretase into lipidic environments, we reconstituted the Fos-14 solubilized γ-secretase sub-units into liposomes that contain 65% EggPC, 25% Brain Extract Total and 10% cholesterol with a liposome diameter of 100nm. The PS1-WT and PEN-2 proteins were reconstituted together into liposomes in a 300 µl reaction, while

49

the PS1-WT or the PS1-delE9 protein alone served as control. Because I used more detergents in the case of liposomes, the detergents removal procedure was adopted to one round of 3 hours at room temperature and two rounds of 16 hours in the cold room using SM-2 bio-beads. For each round, 200mg bio-beads were used. Sucrose gradient centrifugation was performed with gradient sucrose concentrations 37.0%, 32.5%, 29.5%, 21.0%, 17.2%, 13.4%, 9.0% and at 100,000xg for 16 hours. As shown in Figure 3.10 A, most liposomes were observed on the top of the centrifuge tubes after the sucrose cushion, and several layers were noticed in the PS1+PEN-2 sample. Western blot anti His-tag shows that the target proteins were in the liposome layers. No protein was observed in the bottom part of the sucrose cushion or the empty liposomes, suggesting that the target proteins did not precipitate during reconstitution and were successfully integrated into liposomes (Figure 3.10B). A fluorescent γ-secretase substrate was used to measure the activity of γ-secretase, which includes the N-terminal fluorescent molecule NMA and the transmembrane domain of the amyloid β-peptide precursor protein sequence followed by an internally quenched fluorescent peptide Dnp. Dnp will be released from the substrate once the substrate is cleaved and NMA can be excited at the wavelength 355 nm and emitted at the wavelength 440 nm (Figure 3.10C). The activity was assayed with 30μM of the substrate at a protein concentration of 0.45μM. The reactions were incubated at 37 °C overnight, followed by 100,000xg centrifugation for 1 hour. The fluorescence signal was measured using circular dichroism (CD) with an excitation wavelength of 355 nm and an emission scan from 400-480 nm. Proteoliposomes containing PS1-WT alone or empty liposomes showed similar emission profiles, while proteoliposomes carrying PS1-delE9 or PS1-WT/PEN-2 complexes exhibited more activity than those containing PS1-WT alone. According to the emission curves, proteoliposomes carrying PS1-delE9 showed 7% more activity and proteoliposomes containing PS1-PEN-2 complexes showed 15% more activity than the control (Figure 3.10 D).
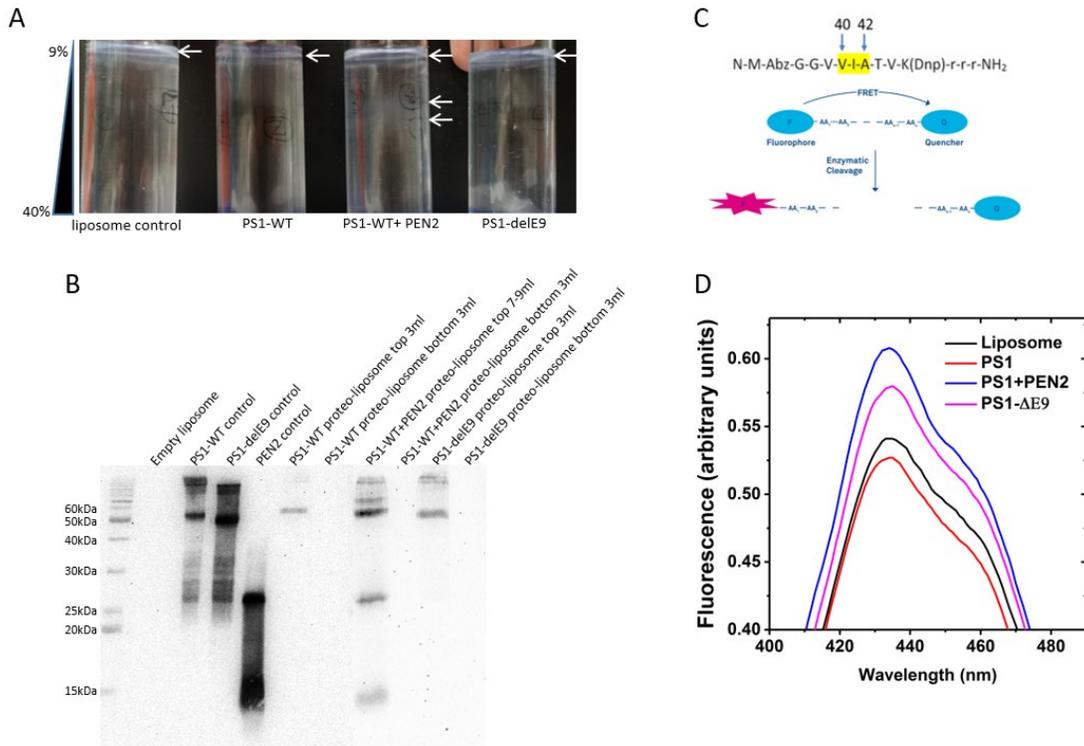
Figure 3.10 Reconstitution of γ-secretase sub-units into liposomes.

Reconstitution of γ-secretase sub-units into liposomes containing 65% EggPC, 25% Brain Extract Total, 10% cholesterol and purification by sucrose gradient centrifuge. Activity assay was performed by cleaving the fluorogenic γ-secretase substrate. (A) Liposomes after sucrose gradient centrifugation. The number on the left of the picture shows the gradient of sucrose concentration, and arrows indicate the positions of liposomes. (B) Western blot anti His-tag of different sucrose cushion fractions. The number of the volume on the picture indicates the volume from the top of the tube down. (C) Schematic diagram of fluorogenic γ-secretase substrate. (D) *In vitro* activity was measured by using fluorogenic γ-secretase substrates, and the fluorescence signal was measured by a CD instrument with an excitation wavelength of 355 nm and the emission scan wavelength collected from 400 nm to 480 nm.

3.2 Solubility tag fused sub-units reconstitution

Maltose binding protein (MBP) is a common protein expression tag, as it is known to significantly increase the solubility of many proteins. Here, I have tagged the γ-secretase subunits with the MBP tag, allowing the protein to be detergent-free and to be readily reconstituted into liposomes.

3.2.1 Expression of MBP-construct in periplasm

First, I cloned all γ-secretase subunits into the pMAL-p4x vector, which expresses MBP-fused proteins in the periplasm. MBP-PS1 was expressed in BL21(DE3), induced by 1 mM IPTG at an OD of 0.6 and shaken at 16 °C, 100 rpm for 16 hours. Cells were harvested at 5000xg, resuspended in lysis buffer and then opened with a cell disrupter. Membrane fractions were collected with 100,000xg ultra-centrifugations. Most of the MBP-PS1 protein was observed in membrane fractions. At the same time, a small amount was present in the supernatant fraction after ultracentrifugation. A molecular weight shift of ~43 kDa occurred between MBP-PS1 and PS1-WT, which is consistent with the molecular weight of the MBP tag (Figure 3.11A). Although some degradations happened in the supernatant, I still can detect the MBP-PS1 full-length in the supernatant. The supernatant was bound to Ni-indigo resin and incubated in the cold room on a roller overnight. The protein was washed with wash buffer to remove the contaminants and eluted with 500mM imidazole. Unfortunately, MBP-PS1 was degraded to fragments of ~75kDa and ~25kDa, indicating that MBP-PS1 is unstable in detergent-free purification or that this type of MBP tag leads to degradation.
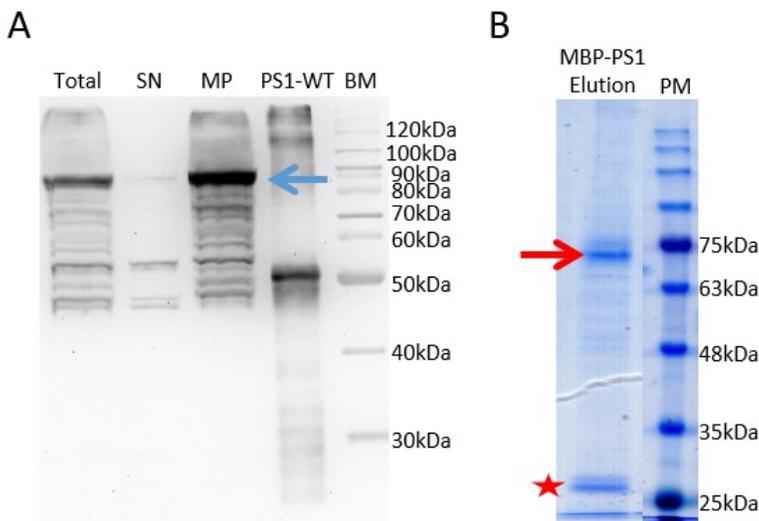
Figure 3.11 Opening of MBP-PS1 and purification with detergent-free

Expression and purification of MBP-PS1 in pMAL-p4x vector. (A) Western blot anti His-tag of lysate of MBP-PS1 from pMAL-p4x vector, PS1-WT was loaded as control. (B) Blue silver stained SDS-PAGE of the MBP-PS1 elution from Ni-NTA. The red arrow and star indicate the degradation bands of MBP-PS1. Total: cells after opening. SN: supernatant after 100,000xg ultracentrifugation. MP: Membrane pellet. BM: benchmark ladder. PM: pre-stained ladder.

I also tested the expression of other MBP-tagged constructs. Here we expressed MBP-PS2, MBP-PEN-2 and MBP-NCT in BL21 (DE3). After overnight expression under induction with 1mM IPTG at an OD of 0.6, cells were also opened with a cell disruptor and membrane pellets were collected by ultracentrifugation at 100,000xg. Based on the Western blot images (Figure 3.12), a full-length MBP-PS2 with a theoretical molecular weight of 96.8 kDa was not detected in both supernatant and membrane fractions, but a band of about 45 kDa was detected. We do not know if this is due to lack of expression or if the protein was degraded during expression. MBP-PEN-2 shows full-length bands of 70 kDa in both the supernatant and membrane fractions, compared to a theoretical molecular weight of 60 kDa which are labeled with red stars. MBP-NCT also showed the full-length protein which were marked by red arrows in both fractions. Compared to the theoretical molecular weight of 122.8 kDa, MBP-NCT showed an experimental molecular weight below 120kDa. In both MBP-PEN-2 and MBP-NCT, I observed heavy degradation bands in both the supernatant and the membrane fractions. Those indicated that expression of MBP tagged γ-secretase in the periplasm is not stable.
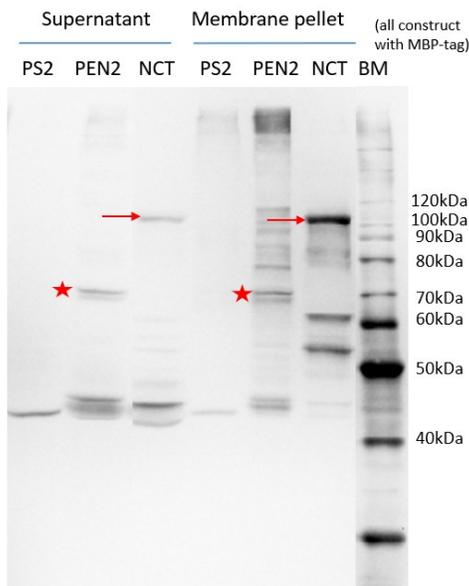
Figure 3.12 Expression test of different γ-secretase sub-units fused with MBP tags

Western blot anti His-tag of expression of different MBP-constructs. MBP-PS2, MBP-PEN-2 and MBP-NCT were expressed in pMAL-p4x vector in BL21 (DE3). The red arrows indicate the MBP-NCT full length, and the red stars indicate the MBP-PEN-2 full length.

3.2.2 Expression of MBP-construct in cytoplasm

Here we used a homemade MBP-vector by Dr. Oliver H. Weiergräber from Forschungszentrum Jülich IBI-7, which leads to cytoplasmic expression. MBP-PS1 was first expressed in BL21 (DE3) and induced with 0.1 mM IPTG at an induction OD of 0.6. Cells were harvested 4 h after induction and opened with a cell disruptor. Inclusion bodies were removed by centrifugation at 9,000xg and membrane fractions were collected under ultracentrifugation at 150,000xg. As shown in Figure 3.13, most of the MBP-PS1 protein is in the membrane fraction, with some of it accumulating in the inclusion bodies, indicating that the MBP tag may cause incorrect folding of the protein. Full-length MBP-PS1 was also detected in the supernatant after ultracentrifugation, implying that the MBP tag also increased the solubility of Presenilin-1. Less degradation was observed compared to MBP-PS1 expressed in periplasm, which was used in further experiments.
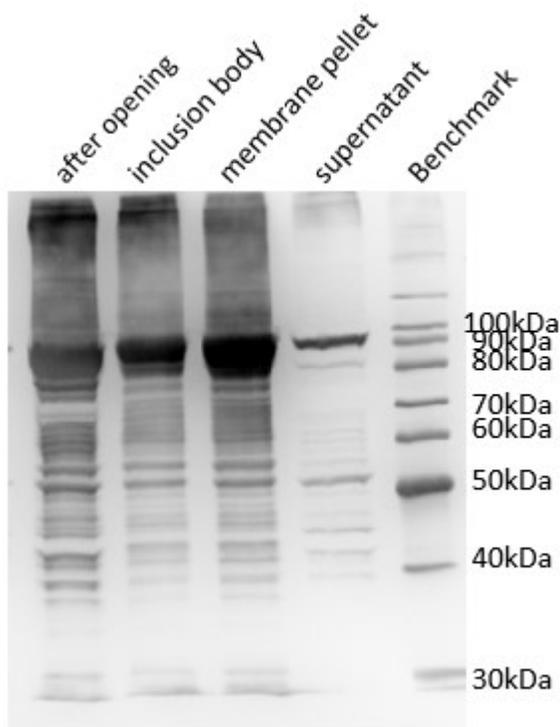
Figure 3.13 opening of MBP-PS1

Western blot anti His-tag of opening of MBP-PS1 which is expressed in BL21(DE3) and located in cytoplasm membrane.

Next, I expressed MBP, MBP-PEN-2, and MBP-APH-1 separately in BL21(DE3) under the same induction conditions as MBP-PS1. The supernatant of each sample was combined with Ni-indigo resin after ultracentrifugation at 150,000xg and rotated overnight in a cold room. The matrix was washed with excess wash buffer until the 280 absorption was 0 and eluted with 500 mM imidazole.

MBP showed a fat smear band in the eluted samples in the western blot, while MBP-PS1 and MBP-PEN-2 showed clear bands for full length protein. The shift in molecular weight was consistent with the size of the fusion protein. MBP-APH-1 appeared as the full-length protein and form of degradation band. Although degradation bands were observed for MBP-PS1 and MBP-PEN-2, the most abundant bands were still full-length proteins. All fused proteins showed the SDS resistant dimer on the western blot (Figure 3.14). Compared to MBP-PEN-2 expressed in periplasm, cytoplasm located MBP-PEN-2 showed the correct molecular weight of MBP-PEN-2 of 59.4kDa, suggesting that the MBP-PEN-2 protein may be folded correctly.
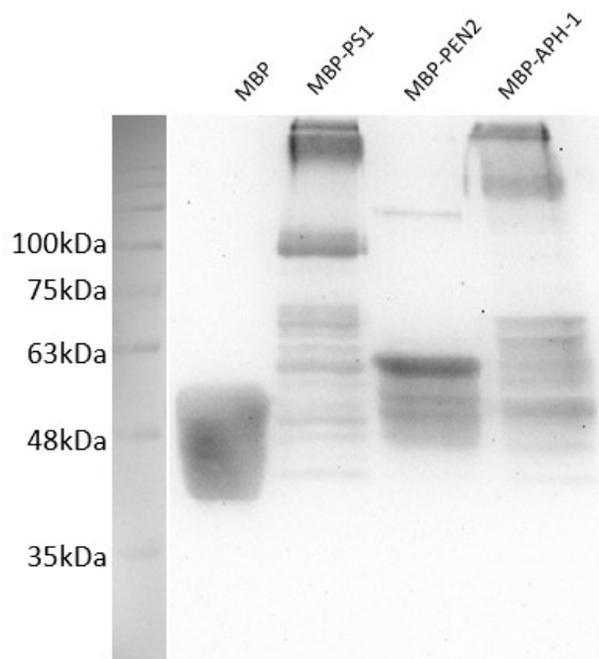
Figure 3.14 Detergent-free purification of MBP-constructs

Western blot anti His-tag of detergent-free purification of MBP-constructs. All fused constructs showed the right molecular shift of fused proteins compared to MBP alone.

To assemble PS1 and PEN-2 into liposomes, dialysis was performed to remove imidazole from MBP-PS1 and MBP-PEN-2 elutions and to switch to a buffer condition of 20 mM HEPES, 150 mM NaCl. MBP-PS1 was concentrated to 0.1 mg/ml while MBP-PEN-2 was concentrated to 0.05 mg/ml concentration. 1 ml of MBP-PS1 was mixed with 1 ml of MBP-PEN-2 in combination with 1 ml DMPC liposomes at a concentration of 2 mg/ml which were destabilized by DDM (1:1 molar ratio) to allow protein insertion. Under the same conditions, the same amount of MBP-PS1 or MBP-PEN-2 was also mixed with liposomes separately, and the empty liposomes were used as a control. The detergents removal procedure was adopted for one round of 3 hours at room

temperature and two rounds of 16 hours in the cold room using SM-2 bio-beads. For each round, 200mg bio-beads were used. Sucrose gradient centrifugation was performed with gradient sucrose concentrations 37.0%, 32.5%, 29.5%, 21.0%, 17.2%, 13.4%, 9.0% and at 100,000xg for 16 hours. As shown in Figure 3.15A, liposomes layers were observed in the middle of the centrifuge tubes after the sucrose cushion. The empty liposomes layer (Tube no.4) is higher than the other 3 tubes, indicating that the density of empty liposomes are smaller than proteoliposomes, proving that proteins were successfully reconstituted into liposomes. MBP-PS1 liposomes (tube 2) showed two layers, probably due to the separation of empty liposomes from proteoliposomes. We collect different fractions from the top of the centrifuge tube in a volume of 3 ml each to determine the location of the proteins. If the proteins were not incorporated into the liposomes, they should be present at the top of the tube or precipitated at the bottom. Western blotting showed that all proteins were in the liposome layer and no proteins were detected either at the top or bottom of the centrifuge tubes, which also indicated that all proteins were successfully integrated into the liposomes (Figure 3.15B). Both MBP-PS1 and MBP-PEN-2 are detected in the liposome layer, which can be formed in complex or incorporated into liposomes alone. Compared to control samples of MBP-PS1 and MBP-PEN-2 labeled with AD or BD, we lost most of the protein during reconstitution into liposomes, probably occurring at the time of detergent uptake by Bio-beads. Only full-length proteins were observed in the recombinant samples, suggesting that the degraded fraction of the protein may have not integrated into the liposomes due to the absence of transmembrane domain or incorrect folding.
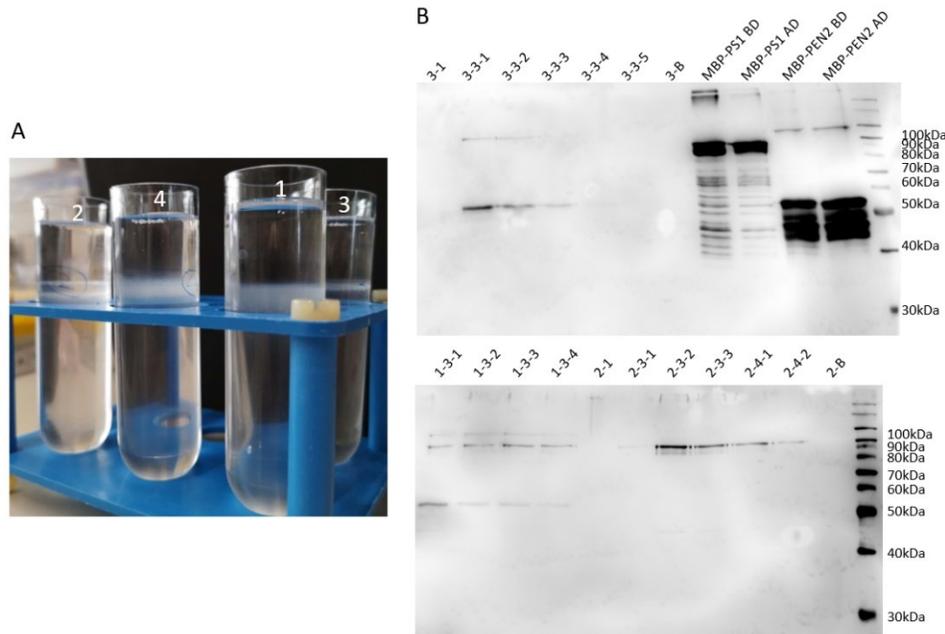
Figure 3.15 Reconstitution of MBP-PS1 and MBP-PEN-2 into DMPC liposomes

Reconstitution of MBP-PS1 and MBP-PEN-2 into DMPC liposomes. Empty liposomes were used as the negative control. (A) Sucrose gradient ultracentrifugations of proteo-liposomes. 1: MBP-PS1 + MBP-PEN-2. 2: MBP-PS1.3: MBP-PEN-2. 4: empty liposomes. (B) Western blot of different sucrose cushion fractions. Number in the beginning: 1) MBP-PS1 + MBP-PEN-2, 2) MBP-PS1, 3) MBP-PEN-2, 4) empty liposomes. Number in the middle: 1) 1st 3cm from the top, 3) 3rd 3cm from the top, B) bottom part of the centrifuge tube. Numbers at last indicate the sample number. BD: before dialysis. AD: after dialysis.

Reconstitution of membrane proteins into liposomes requires the detergent-destabilized liposomes which allows the insertion of membrane protein into liposomes[143]. Considering the use of detergent in liposomes preparation, I tested the MBP-PS1 and MBP-PEN-2 with CHAPSO solubilization from membrane fraction. MBP-PS1 and MBP-PEN-2 were solubilized by 2% CHAPSO individually and incubated with rotations in cold room overnight. Insoluble parts were separated by 150,000xg ultracentrifugations and solubilized by 8M urea buffer in the presence of 2% SDS at room temperature overnight. Although both MBP-PS1 and MBP-PEN-2 were reasonably soluble by 2% CHAPSO, MBP-PS1 also showed a degradation band, while MBP-PEN-2 showed a double band.
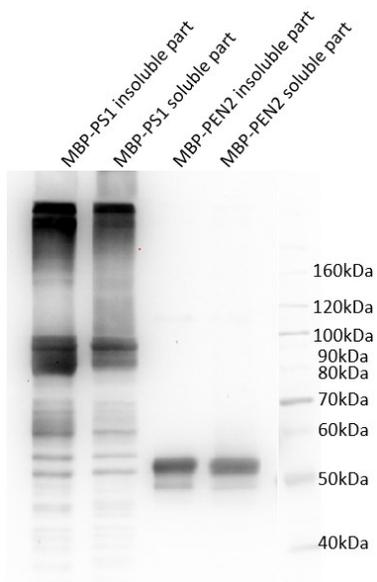
Figure 3.16 Detergent solubilization test of MBP-PS1 and MBP-PEN-2

MBP-PS1 and MBP-PEN-2 membrane pellet was solubilized by 2% CHAPSO and incubated in cold room with rotations overnight followed by 150,000xg to separate the insoluble part.

3.3 Expression of APH-1 protein in *E.coli*

APH-1 is one of the subunits of γ-secretase, which has seven transmembrane structural domains and plays a role in the stability of the γ-secretase complex. Here, we attempted to stably express and purify APH-1 in E. coli under different conditions.

3.3.1 Expression of His-APH-1 in *E.coli*

First, we tested the expression of His-APH-1 in different E.coli strains in the presence or absence of cholesterol. E Coli strains BL21 (DE3) and C43 (DE3) were used to test the expression level of APH-1 at 16 or 30 °C in the absence or presence of cholesterol. As listed in Table 3.2, half a gram of cell was obtained in BL21(DE3) at 16 °C overnight expression in 50ml cell cultures and but there is no significant difference between samples with or without cholesterol. Expressions of BL21 (DE3) Cells at 30°C still grew after induction and yielded 3g cells in 50ml. Cell amount was normalized and loaded on western blot. Sharp bands were observed in 16 °C samples and weak bands were detected in 30 °C samples (Figure 3.17A), indicating that APH-1 can be expressed at low temperatures after induction but is unstable at 30°C. There was no significant difference between the samples with or without cholesterol. I next tested the expression level of APH-1 in C43 (DE3) in the presence or absence of cholesterol at 16 and 30 °C overnight expression. We obtained 0.9g cells at 16°C, while 0.5g cells were collected at 30°C expression (Table 3.2). Western blot signal showed a slight band expression of APH-1 (Figure 3.17B), but there was a significant difference in expression with or without cholesterol involvement, with APH-1 being expressed only in the presence of cholesterol.

Table 3.2 Expression conditions of His-APH-1

Strains	Cholesterol	Temperature (°C)	Pellet in 50 ml culture
DE3	-	16	0.5g
DE3	+	16	0.5g
DE3	-	30	3g
DE3	+	30	3g

C43	-	16	0.9g
C43	+	16	0.9g
C43	-	30	0.5g
C43	+	30	0.5g
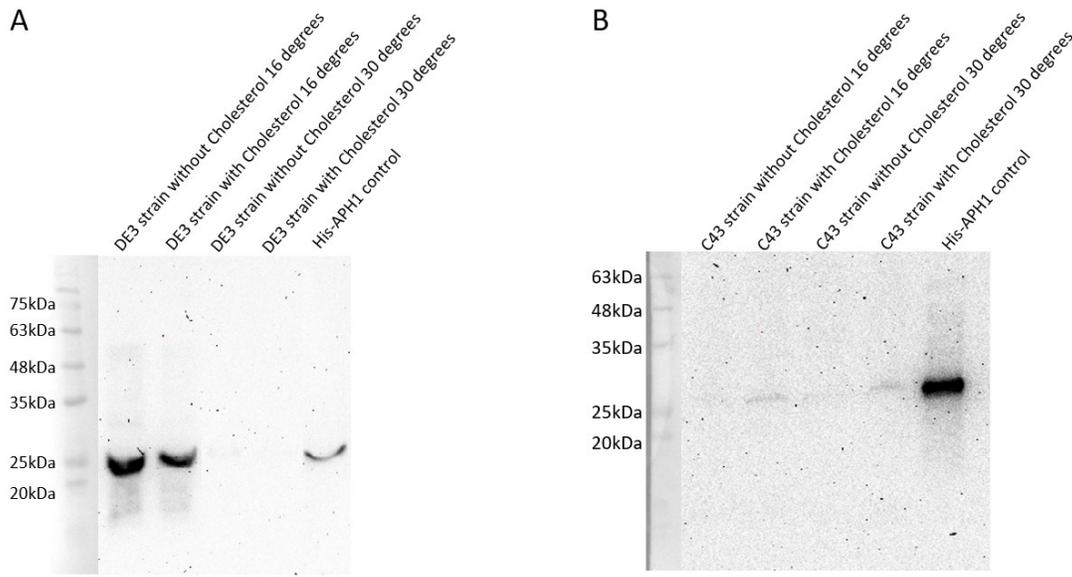
Figure 3.17 Expression of His-APH-1 in *E.coli*

His-APH-1 was expressed in BL21(DE3) or C43(DE3) strains in the presence or absence of cholesterol with different temperatures. (A) Western blot anti His-tag of expression of His-APH-1 in BL21(DE3) at 16 or 30 °C. (B) Western blot anti His-tag of expression of His-APH-1 in C43(DE3) at 16 or 30 °C.

3.3.2 Expression of APH-1 with MBP tags

Expression of fusion proteins, such as Maltose-Binding Protein (MBP) fusions, can improve the solubility of the expressed protein in E. coli and make it soluble. Here we fused an MBP tag at the N-terminal end of APH-1, while two His tags were fused in the sequence: at the N-terminus of the sequence and between the MBP tag and the APH-1 protein, and expressed in BL21 (DE3). MBP-APH-1 cells were induced at the OD of 0.4 and incubated with 100 rpm shaking overnight at 16 °C. After cell opening, membrane fractions were pelleted down at 150,000 xg ultracentrifugation. As shown in Figure 3.18A, two bands were observed in the supernatant sample on Anti his-tag western

blot, the upper one supposedly being the full length of MBP-APH-1 and the other possibly a degradation band. Most of the protein was detected in the membrane pellet and no degradation was observed, suggesting that lipids are essential for stabilizing APH-1 proteins. MBP-APH-1 membrane pellets were solubilized with Fos-14 in the presence or absence of cholesteryl hemisuccinate tris salt (CHS) and purified by Ni-NTA affinity chromatography. Individual bands were observed on SDS-PAGE for different samples, but there were no significant differences between the protein bands for different solubilization conditions. (Figure 3.18B). MBP-APH-1 has a theoretical molecular weight of 76 kDa, but it migrates faster than expected, with an experimental molecular weight of approximately 68 kDa on SDS-PAGE. It is not uncommon for membrane proteins that protein runs aberrantly on SDS-PAGE.
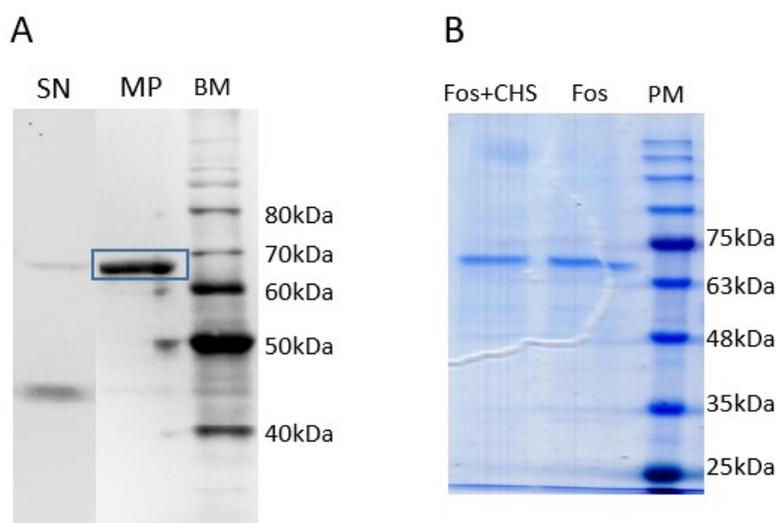
Figure 3.18 Expression and purification of MBP-APH-1

MBP-APH-1 was expressed in BL21(DE3) cells and opened by cell disrupter. Membrane fractions were precipitated with 150,000xg and solubilized by Fos-14 alone or combined with CHS. (A) Western blot of MBP-APH-1 after collection of membrane fractions. SN: Supernatant after 150,000xg. MP: membrane pellet after 150,000xg. BM: BenchMark Ladder. (B) Blue silver stained SDS-PAGE of purified MBP-APH-1. PM: Prestained ladder.

3.3.3 Expression of APH-1 with FleBt tags

In order to compare the different solubility tags, the Yersinia-derived truncated flagellin FleB (FleBt, residues 54 to 332) produced by Prof. Michael Kolbe's group has been chosen as the solubility tag. FleBt-APH-1, which has the theoretical molecular weight of 61.5 kDa, has a FleBt tag at the N-terminus of APH-1 and two his tags in the sequence, one at the N-terminus of the sequence and the other one between the FleBt tag and APH-1 protein. Both MBP-APH-1 and FleBt-APH-1 were expressed with the same conditions: induced at the OD 0.4 and incubated with 100 rpm shaking at 16 °C overnight. The same cell amount was obtained after overnight expressions. Cells were resuspended with 10ml lysis buffer per gram cells and opened with cell disrupter. Inclusion bodies were removed by centrifugation at 9,000 x g and membrane pellets were collected by ultracentrifugation at 150,000 x g. Most of the MBP-APH-1 is in the inclusion bodies. At the same time, a small proportion of the protein is embedded in the membrane fractions and even less is soluble and remains in the supernatant after ultracentrifugation at 150,000xg. FleBt-APH-1 showed a lower expression level compared to MBP-APH-1 protein according to the lysates. FleBt-APH-1 showed more protein embedded in the membrane fraction and less protein in the inclusion bodies than MBP-APH-1, suggesting that the FleBt tag contributes to the correct folding of APH-1 proteins. By contrast, more proteins accumulated in inclusion bodies when expressed with MBP-tag, indicating that MBP tags were not efficient in the solubilization of APH-1 proteins. Meanwhile, A reasonable part of proteins still stayed in the supernatant, implying that the FleBt tag was more effective in increasing protein solubility (Figure 3.19).
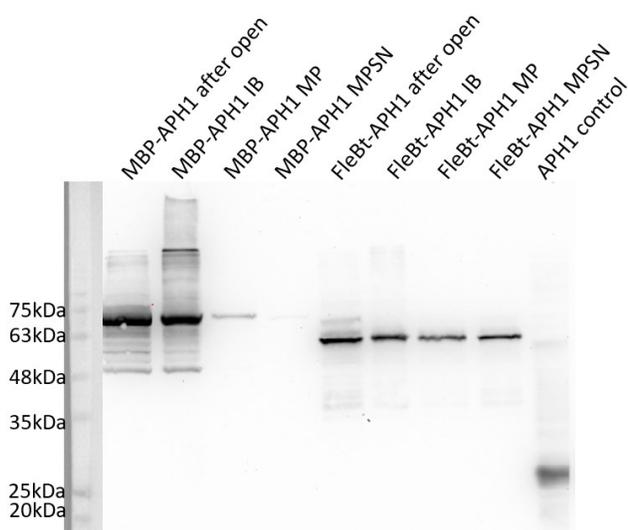
Figure 3.19 Opening procedure of fused APH-1

APH-1 protein was expressed in BL21(DE3) cells after fusion with MBP-tag or FleBt-tag. Cells were resuspended with lysis buffer, opened with a cell disrupter, and then the inclusion bodies were removed with 9,000xg and membrane fractions were precipitated with 150,000xg. IB: inclusion body. MP: membrane pellet after 150,000 xg. MPSN: supernatant after 150,000xg.

3.3.4 Detergent screening of fused-APH-1 proteins

Given the thoughts that the potential incorrect folding of fused-APH-1 in the supernatant after 150,000xg ultracentrifugation, different detergents were tested to solubilize the membrane fractions. 2% CHAPSO, 1% LMNG and 1% DDM were used to solubilize, while 1% Fos-14 was considered as the control that solubilized all membrane pellets. As shown in the western blot in Figure 3.20, there was no significant difference in the solubilization of FleBt-APH-1 by any of the four detergents. However, only Fos-14 was able to dissolve most of MBP-APH-1 from the membrane, while the other three detergents did not dissolve well, suggesting that FleBt tags can increase the solubility of APH-1 proteins.
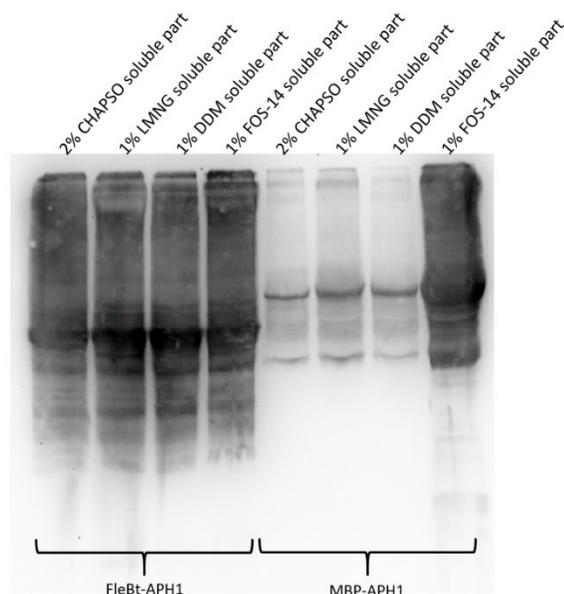
Figure 3.20 Detergent screening of fused APH-1 proteins

Western blot of detergent screening of fused APH-1 proteins. Four different detergents with different percentages were used to solubilize the fused APH-1 protein.

3.3.5 Purification of FleBt-APH-1

First, I solubilized FleBt-APH-1 with 2% CHAPSO and incubated it in cold room overnight. According to the SDS-PAGE and anti His-tag western blot (Figure 3.21), Three main bands were detected on western blot which indicates that FleBt-APH-1 forms SDS resistant dimer and oligomers. No target protein was detected in any of the washing steps of the Western blot, and no protein was detected at all in washes II and III on the blue silver-stained SDS-PAGE, suggesting that all impurities should have been washed away. FleBt-APH-1 was then eluted with 250Mm and

500 mM imidazole. FleBt-APH-1 was eluted at a concentration of 250 mM imidazole, but two major impurities were also observed. A small amount of protein was eluted with 500 mM imidazole but was barely visible on the blue-stained SDS-PAGE.
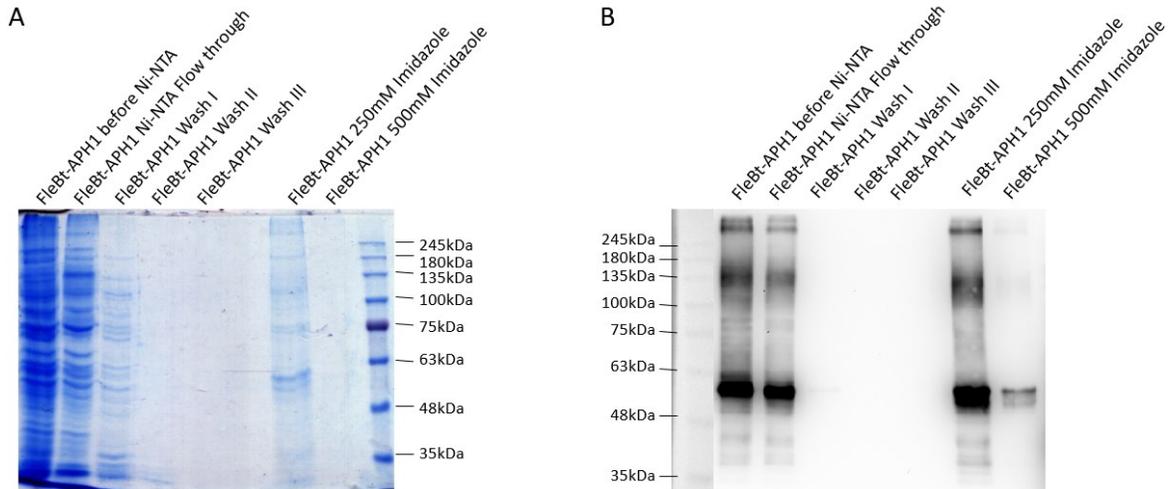
Figure 3.21 Purification of FleBt-APH-1 with CHAPSO

Purification steps of CAHPSO solubilized FleBt-APH-1. (A) Blue sliver stained SDS-PAGE of purification steps of FleBt-APH-1. (B) Western blot anti His-tag of purification steps of FleBt-APH-1.

Next, I dissolved FleBt-APH-1 with DDM in the presence or absence of cholesterol hemisuccinate tris salt (CHS) and FleBt-APH-1 with 1% DDM with or without 0.1% CHS and incubated the mixture overnight in a cold room with stirring. The proteins were purified with a Ni-NTA affinity column and followed by Size exclusion chromatography. Two prominent peaks were observed after SEC, representing an oligomer peak and a dimer peak. A shift occurred for the second peak between the two samples due to the involvement of CHS (Figure 3.22A). We observed some degradation bands on both blue-stained SDS-PAGE and Western blot, probably because the lysis and purification time was too long, indicating that FleBt-APH-1 is not very stable. Nevertheless, we isolated the monomer of FleBt-APH-1 from the second peak. In the absence of CHS, a potential degradation band of 30 kDa was detected in the second peak, which was located below the monomer band, but not in the sample containing CHS. No Western blot signal was detected for the degradation band, indicating that it could be C-terminal APH-1 degradation or a contaminant (Figure 3.22B).
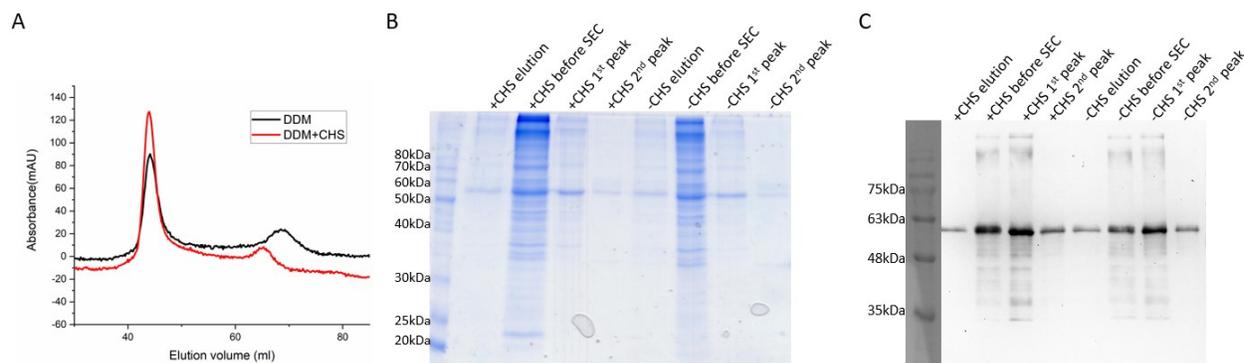
Figure 3.22 Purification of FleBt-APH-1 with DDM

FleBt-APH-1 was solubilized with 1% DDM in the presence or absence of 0.1% CHS and purified by Ni-NTA affinity column followed by Size exclusion chromatography using Superdex 200 10/600 GL column. (A) SEC profile of FleBt-APH-1. Solid black line indicates the DDM solubilized FleBt-APH-1. Solid red line indicates the DDM solubilized FleBt-APH-1 in the presence of CHS. (B) Blue silver stained SDS-PAGE of FleBt-APH-1 elution and SEC peak fractions. (C) Western blot anti His-tag of FleBt-APH-1 elution and SEC peak fractions. +CHS means with CHS while -CHS is without CHS.

To identify the FleBt-APH-1, the major band was processed by in-gel trypsin digestion followed by LC-MS/MS on a Dionex Ultmate 3000 HPLC coupled with an Orbitrap Fusion Lumos System. The entire sequence of FleBt-APH-1 with matched peptides was shown in Figure 3.23, which is labeled with red color. 50% coverage was matched to the whole sequence with sequence spectral matches of 433 and a total score of 4096. Although most of the matching peptides were identified as the FleBt tag, several peptides were matched the APH-1 proteins. Unfortunately, we could not identify the transmembrane domains of APH-1. As the C-terminus of APH-1 is identified, we can confirm that we isolated the full-length of FleBt-APH-1.

MGSSHHHHHHSSGLVPRGSHMTSNINGLTVAARNANDGISLSQTAEGALGEINNNLQRVRDLTVQAQNSSNSASDID
SIQSEVNQRMEEINRVTKQTDFNGIKVLDNRTKTDSSYDFQVGSKDNEQISIAIGASSGWNLATANADGTSSDTVNTYA
FTKKAALDTAQTDYDTANTAYLAAVKSGVAGDITTTKATLDGKNTALATAVKDATAVNEAVNGKVRTVAAKGFDVLNG
TVAADGKATGTTPLADIDKALKAVDTQRSVLGASQNRFESTITNLNNTVNNLTSARGGASMHHHHHHHHHHAIEGRG
AAVFFGCTFVAFGPAFALFLITVAGDPLRVIILVAGAFFWLVSLLLASVVWFILVHVTDRSDARLQYGLLIFGAAVSVLLQE
VFRFAYYKLLKKADEGLASLSEDGRSPISIRQMAYVSGLSFGIISGVFSVINILADALGPGVVGIHGDSPYYFLTSAFLTAAIIL
LHTFWGVVFFDACERRRYWALGLVVGSHLLTSGLTFLNPWYEASLLPIYAVTVSMGLWAFITAGGSLRSIQRSLLCRRQE
DSRVMVYSALRIPPED

Figure 3.23 Peptide identification of DDM solubilized FleBt-APH-1 by LC-MS/MS

The entire protein sequence of FleBt-APH-1 is shown. Matched peptides are marked in red and transmembrane domains are underlined.

3.4 Isolation of Presenilin-1 and PEN-2 complex

3.4.1 Detection of PS1 and PEN-2 interactions *in vivo*

To confirm the interaction of Presenilin-1 and PEN-2, Split-superpositive GFP was introduced as a fast, efficient, and robust method to identify and study protein-protein interactions *in vivo*. Split-superpositive GFP reassembly is a fast, efficient, and robust method for detecting protein-protein interactions *in vivo*[191]. Here, we labeled the N-terminal end of Presenilin-1 with nGFP to generate nGFP-PS1 construct which has a molecular weight of 73.1 kDa. At the same time, we fused cGFP to the N-terminal or C-terminal end of PEN-2 to generate cGFP-PEN-2 or PEN-2-cGFP constructs with molecular weight of 23.8 kDa or 22.8 kDa. Split GFP labeled PS1 and PEN-2 were co-expressed in BL21 (DE3) and induced by 1mM IPTG and 0.2% (L)-arabinose at the OD: 0.4. After 16 hours of incubation at 18°C, cells were harvested at a 5000xg centrifugation and GFP fluorescence was measured at 488nm excitation wavelength using Bio-rad's ChemiDoc MP Imager. Split GFP fused high-affinity antiparallel leucine zipper peptides were used as the positive control but showed extremely high fluorescence signal compared to the fluorescence signal of Split GFP labeled PS1 and PEN-2 interaction. This situation contributes to the undetectable GFP signals of PS1 and PEN-2 interaction (Figure 3.24A). Split GFP labeled PS1 and PEN-2 showed the GFP fluorescence when detected against the negative control with no GFP expressed, indicating that the labeled PS1 and PEN-2 interacted with each other and the Split GFP fragments formed full length of GFP (Figure 3.24B). To confirm the proper folding of the split GFP labeled PS1 and PEN-2, the inclusion body was removed by 10,000 xg centrifugation after the cells being opened by cell disrupter, while the membrane pellet was separated by 100,000xg ultracentrifugation. Membrane fractions showed the GFP fluorescence signals (Figure 3.24C), indicating that split GFP labeled PS1 and PEN-2 have successfully embedded in cell membranes and interacted with each other.

A — (cell pellet with positive control)

B — (cell pellet with negative control)

C — (membrane pellet with negative control)
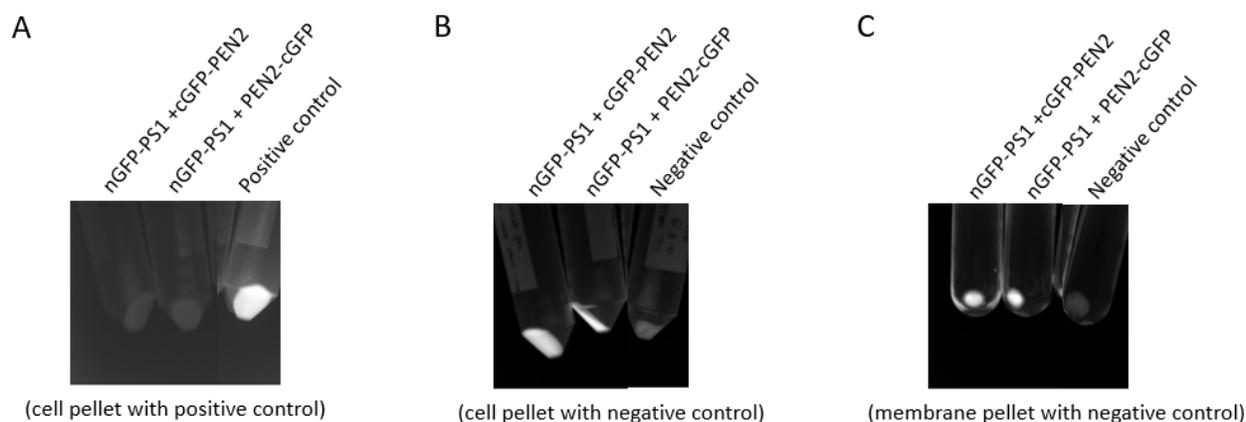
Figure 3.24 *In vivo* expression of split GFP fused PS1 and PEN-2

In vivo co-expression of split-GFP fused PS1 or PEN-2 and protein-protein interaction was detected by fluorescence excitation of 488 nm. Cells after expression were harvested and measured with the excitation wavelength of 488 nm by using ChemiDoc MP Imager from Bio-rad. (A) high-affinity antiparallel leucine zipper peptides were fused to Split GFP as the positive control. (B) The cells without any fluorescence protein were used as the negative control. (C) Cell membranes were pelleted with 100,000xg ultracentrifugation.

To confirm the expression of co-expressed split GFP labeled PS1 and PEN-2, we took samples after the cells being opened and loaded on SDS-PAGE. Individually expressed split GFP labeled GFP were also examined. All nGFP-PS1 protein were expressed by 16 hours incubation, both individually and together. A 20 kDa band was observed which indicated that nGFP-PS1 may be partially degraded during expression. Compared to PS1-WT control, a ~18kDa shift was observed also fits the molecular weight of the GFP N-terminal fragment (Figure 3.25A).

Interestingly, the cGFP labeled PEN-2 showed a significant difference between the co-expressed sample and the individually expressed one. Both cGFP-PEN-2 and PEN-2-cGFP were detected when co-expressed but barely observed when expressed alone (Figure 3.25A&B). Given that nGFP labeled and cGFP labeled proteins were induced by different inducers, and cGFP labeled PEN-2 can be expressed together with nGFP-PS1, it was expected that the cGFP labeled PEN-2 could be expressed but appeared to be unstable in the absence of nGFP-PS1. Overall, nGFP-PS1 formed with cGFP-tagged PEN-2 complete GFP indicated by the increase of GFP fluorescence, showing that we could co-express and isolate the PS1 and PEN-2 complex from *E. coli*.
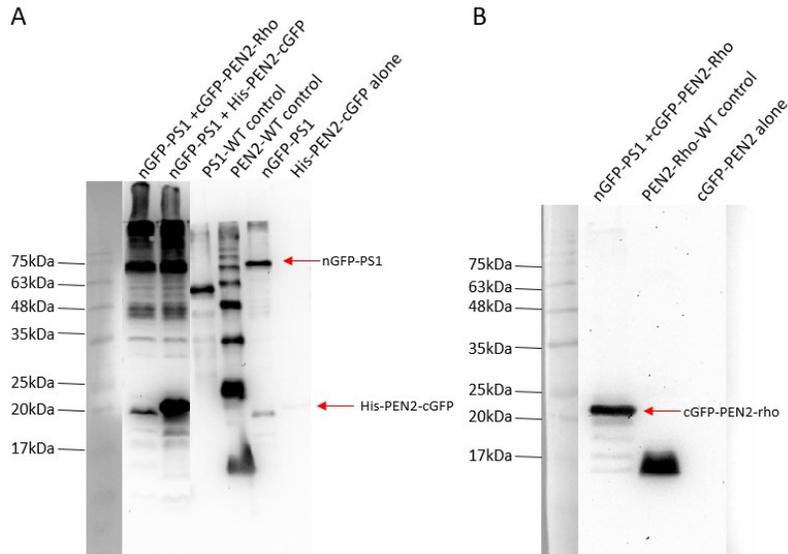
Figure 3.25 Western blot of expression of split GFP fused PS1 and PEN-2

Split GFP labeled PS1 and PEN-2 were expressed individually or co-expressed in BL21(DE3) with overnight incubations under 18 °C. Cells were opened with cell disrupter before being loaded on SDS-PAGE. (A) Anti His-tag western blot image. His-PS1-WT and His-PEN-2-WT protein alone were used as the control. The nGFP-PS1 full length and His-PEN-2-cGFP were labeled with the red arrows. (B) Anti Rho-tag western blot image. PEN-2-Rho protein was used as the control. The cGFP-PEN-2-rho was labeled with the red arrow.

3.4.2 Isolation of PS1-PEN-2 complex with DIBMA solubilization

The pETDuet-01 vector was used to co-express His-Presenilin-1 and His-PEN-2 together in *E.coli*. Proteins were co-expressed in BL21(DE3) with 0.4 mM IPTG induced at OD 0.4 and incubated with 120 rpm shaking overnight at 16 °C. Cells were harvested under 5,000xg and opened with cell disrupter. After removing the inclusion bodies by centrifugation at 10,000xg, the membrane fractions were collected by ultracentrifugation at 150,000xg and resuspended in HEPES buffer to a concentration of 50mg/ml. The membrane fractions were solubilized by 5% (w/w) DIBMA polymers to obtain the DIBMA-lipid-protein complex and keep the target protein in a native lipidic environment. DIBMA solubilizations were performed at three different temperatures (4°C, 25°C, 37°C) and incubated for 16 hours with high-speed shaking on a benchtop thermal shaker. Fos-14 detergents solubilization were used as a positive control.

After overnight solubilization, insoluble pellets were separated by 150,000xg ultracentrifugation. The presence of DIBMA polymers and lipids led to the smearing of protein bands on SDS-PAGE, Therefore Methanol/chloroform protein precipitation was carried out to separate proteins from DIBMA polymers and lipids. The precipitates were solubilized by 8M urea buffers containing 2% SDS before loading to the SDS-PAGE. As shown in the western blot and SDS-PAGE, DIBMA polymers solubilizations were more effective at higher temperatures (37 °C) where most of the target proteins were solubilized. But most of the proteins in the pellet couldn't be solubilized. In contrast, half of the proteins can be solubilized when incubated at 25 °C. As the positive control, co-expressed His-Presenilin-1 and His-PEN-2 were totally solubilized by Fos-14 (Figure 3.26).

DIBMA-solubilized PS1 and PEN-2 were then bound to the Ni-NTA affinity column and washed with sufficient HEPES buffer until no protein was detected at 280 nm absorption. DIBMA-solubilized PS1 and PEN-2 can be eluted with a gradient of imidazole at concentrations from 50 mM to 250 mM. A small amount of PEN-2 was eluted after 300 mM imidazole, and no PS1 was found in the last two elutions, implying that some un-complexed PEN-2 was present.

To test the solubility of DIBMA polymers, different DIBMA polymer concentrations (1.2%, 2.5% and 5%) and membrane concentrations (25 or 40 mg/ml) were used to examine the solubility of co-expressed His-Presenilin-1 and His-PEN-2 with DIBMA polymers at room temperature. In 25mg/ml membrane concentrations, 5% (w/w) DIBMA showed the highest solubilization while 1.2% DIBMA presented the lowest solubilization as expected, indicating that the increase in solubility is proportional to the ratios of DIBMA to cell membranes. Membranes at a 40 mg/ml concentration were also solubilized by 2% DIBMA but with lower efficiency (Figure 3.26 C&D).

The supernatant after ultracentrifugations was bound to Ni-INDIGO affinity column without dilution and fewer target proteins were detected in the Ni-INDIGO flow through on fluorescence excited SDS-PAGE, demonstrating that most of the target proteins were sufficiently bound to the resin which implies that the proteins which were not attached to the resin were improperly folded (Figure 3.26 E). After washing with more volumes of washing buffer, proteins were eluted with 500 mM imidazole. Both PS1 and PEN-2 were observed on the SDS-PAGE and labeled with the blue arrow or star. Compared to the previous purification, the purity of this batch of purification has improved (Figure 3.26 F).
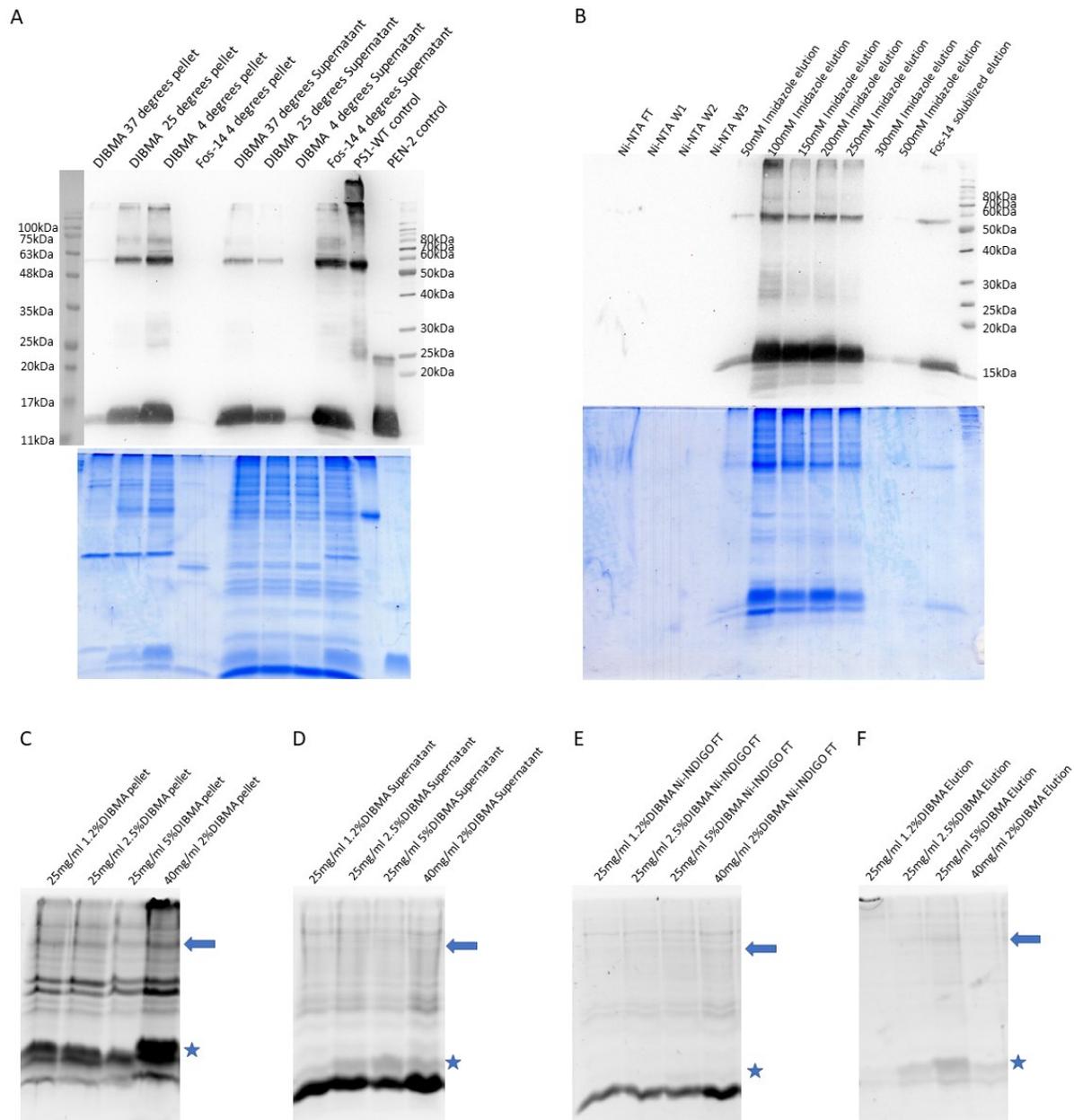
Figure 3.26 Solubilization and purification of co-expressed PS1 and PEN-2.

A&B: PS1 and PEN-2 membranes were solubilized with 5% DIBMA at different temperatures at a concentration of 25 mg/ml. (A) Solubilization at different temperatures. solubilization of Fos-14 at 4 °C was used as a positive control for solubilization, while PS1-WT and PEN-2-WT alone were used to identify PS1 and PEN-2. (B) Purification steps of DIBMA-solubilized PS1 and PEN-2. Gradient concentrations of imidazole were used for elution. Co-expressed PS1 and PEN-2 solubilized with Fos-14 were used as positive controls. Upper part: western blot image. Lower part: Blue silver stained SDS-PAGE. C-F: Different DIBMA concentrations were used to solubilize the membranes of co-expressed PS1 and PEN-2 with a membrane concentration of 25mg/ml. 40mg/ml membrane pellet was also tested with 2% DIBMA

concentration. Intrinsic fluorescence of the pellet (C) and the supernatant (D) were detected under UV light in Bio-rad ChemiDoc. Purification of DIBMA solubilized PS1 and PEN-2 by using Ni-INDIGO affinity column. Intrinsic fluorescence of the Ni-INDIGO resin flow through (E) and the elution (F) was also detected under UV. The blue arrows mark the PS1 proteins, while the blue stars indicate the PEN-2 proteins.

Upscale purification was performed with the solubilization condition of 5% (w/w) DIBMA combined with 25mg/ml membrane concentrations and overnight shaking at 25 °C. The same purification procedures were utilized with the test experiment mentioned above.

Thrombin protease digestion was performed prior to high concentration imidazole elution to remove the His-tag from Presenilin-1. The resin was incubated with excess thrombin protease with up-and-down rotations at room temperature. Protein elution was concentrated to 500μl and loaded on the Superdex 200 increase column on Size Exclusion Chromatography column for further purification. A peak of ~574 kDa was identified but with a wide range (Figure 3.27A).

As shown in the blue-stained SDS-PAGE (Figure 3.27B) and Western blot anti His-tag (Figure 3.27C), some proteins went to the Ni-INDIGO flow through before thrombin treatment, which could be the inproperly folded proteins. After thrombin protease cleavage, two bands in flow-through showed slight shift compared to the elution samples, which fits the molecular weight shift of His-tag removal. Taking into account that only His-Presenilin-1 has a thrombin cleavage site, while PEN-2 does not, these two bands can be considered as PS1. The lower band showed the same molecular weight as Presenilin-1 WT which proved to be the full length of PS1-WT. The upper band could be an unknown conformation of PS1. No PEN-2 protein and His-tag signal were detected in the thrombin cleavage flow-through, which means that all PEN-2 protein is still bound to the resin. After purification by size-exclusion chromatography, fractions were collected separately for B3-B5, while fractions B6-C4 were pooled together.
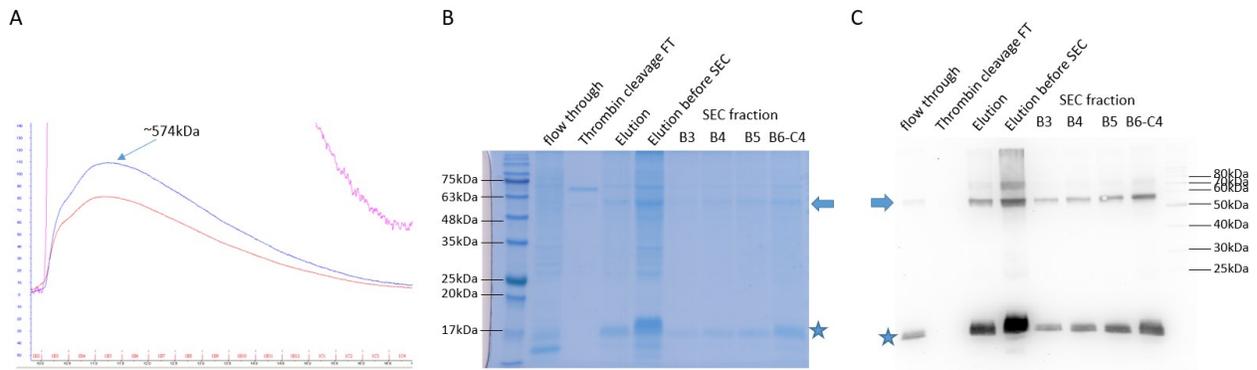
Figure 3.27 SEC profile, blue-stained SDS-PAGE and western blot of purification of DIBMA solubilized PS1 and PEN-2.

Purification of DIBMA solubilized PS1 and PEN-2 including thrombin protease cleavage. (A) SEC profile of purified DIBMA-protein complex. Blue stained SDS-PAGE (B) and Western blot (C) of purification of DIBMA-protein complex. The blue arrows mark the PS1 proteins, while the blue stars indicate the PEN-2 proteins. FT: flow through. SEC: Size Exclusion Chromatography.

To isolate PS1 and PEN-2 from DIBMA-solubilized PS1, thrombin protease cleavage was performed to eliminate the His-tag from SEC-purified Presenilin-1 WT, which was then re-bound with the Ni-NTA to separate the free PS1. No cleaved PS1 was observed in the Ni-NTA flow-through (Figure 3.28 A&B "DIBMA PS1 and PEN-2 thrombin FT" lane), suggesting that no uncomplexed PS1 after purifications. Only Pen-2 proteins were detected in both elutions on Western blot, while PS1 was identified before thrombin treatment, indicating that all His-tag had been removed from PS1. SDS-PAGE showed that cleaved PS1 was presented in elution I and II with a slight shift compared to His-PS1, which also confirmed the removal of the His-tag and proved that PS1 interacted with PEN-2. Although we detected only low abundance bands of PS1 with the His-tag removed, we could still confirm the complex formation of PS1 and PEN-2 in the DIBMA-lipid environment.
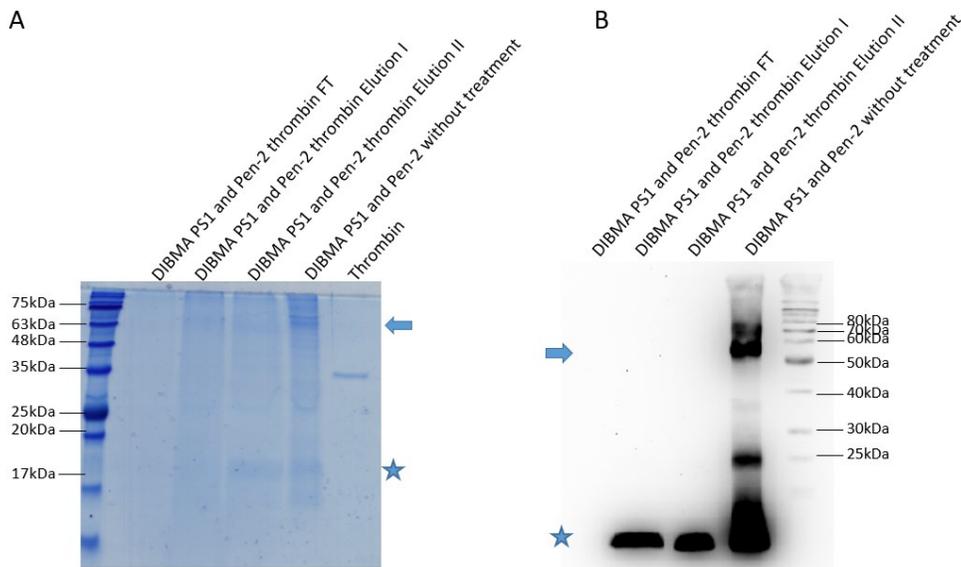
Figure 3.28 Isolation of DIBMA-protein complex after thrombin treatment.

Isolation of DIBMA solubilized PS1 and PEN-2 complex after thrombin protease treatment. Blue stained SDS-PAGE (A) and western blot (B) of purification steps after thrombin protease treatment. The blue arrows and marked PS1 proteins, while the blue stars indicated the PEN-2 proteins.

After the PS1-PEN-2 complex has been proven to be formed, I performed the activity assay for DIBMA-lipids-protein complex against MBP-APPC. Different SEC fractions, soluble fractions after DIBMA solubilization and cell membrane were used for activity assay. MBP-APPC of 40 µg was incubated with different PS1 and PEN-2 complexes at 22 °C overnight with 600rpm shaking using a benchtop thermal shaker. Methanol/chloroform protein precipitation was carried out to precipitate the mixture with DIBMA polymers involved and the precipitations were dissolved by 8M urea buffer containing 2% SDS. To detect the potential cleavage products which are smaller than 10kDa, Tris-Tricine Precast Gels from Bio-rad company were utilized. As shown in Figure 3.29, SEC purified DIBMALP PS1 and PEN-2 displayed poorly defined protein bands on western blot and the DIBMA PS1 and PEN-2 control was not detected in both SDS-PAGE and western blot. The soluble part after DIBMA solubilization and cell membrane exhibited the PS1 and PEN-2 signals on both SDS-PAGE and Western blot. There is no activity observed on both SDS-PAGE and western blot.
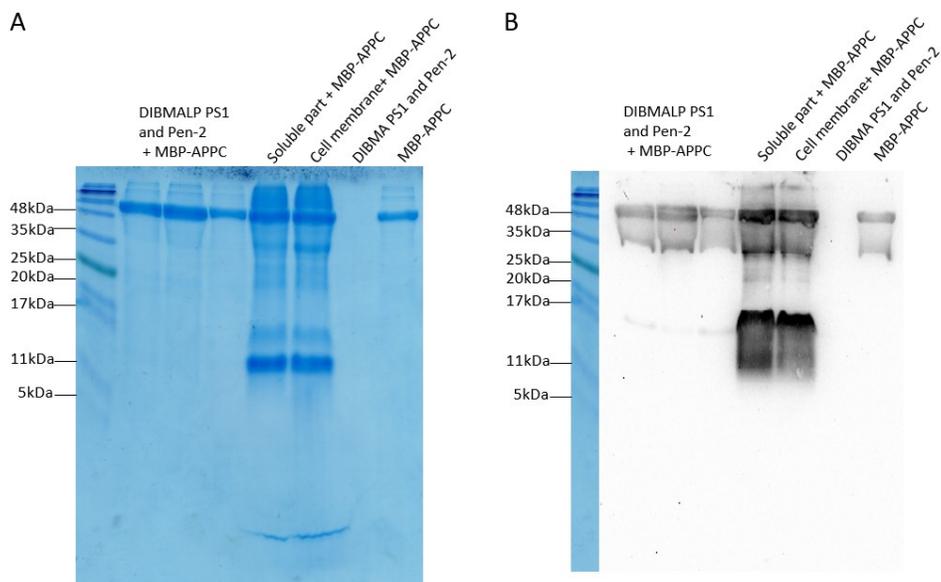
Figure 3.29 Activity assay of DIBMALP PS1 and PEN-2 with MBP-APPC substrate

The activity of SEC fractions B3-B5, cell membrane and soluble fraction after ultracentrifugation was determined by the substrate MBP-APPC. Blue stained (A) and western blot (B) Tricine–SDS-PAGE of activity assay of DIBMALP PS1 and PEN-2.

I also performed the activity assay with gradient substrate concentrations in case that the oligomerization of high concentrations of substrates. Pooled DIBMALP PS1 and PEN-2 complexes after SEC were incubated with a gradient of substrate from 50 µg to 200 µg at 22 °C overnight with 600rpm shaking using a benchtop thermal shaker. The proper controls were used to detect if DIBMALP PS1 and PEN-2 complex was unstable. As shown in blue stained tris-tricine (Figure 3.30), the activity of PS1 and PEN-2 remained undetected. Weak bands were observed in DIBMA PS1 and PEN-2 after being incubated at 22°C. The proteins incubated at 22 °C showed lower stability compared to untreated DIBMA PS1 and PEN-2 complex, indicating that purified DIBMALP PS1 and PEN-2 were unstable under prolonged incubation at room temperature. The same tags in both PS1 and PEN-2 caused more steps to obtain the complex, which could prolong the duration of experiments and lead the instability protein complexes.
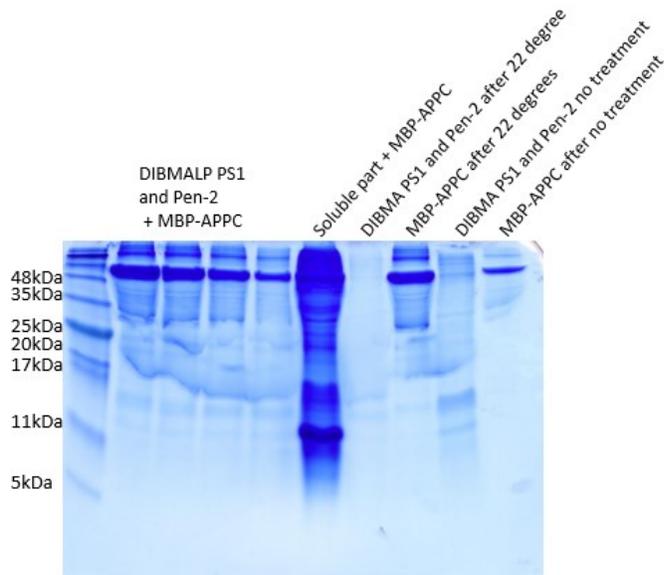
Figure 3.30 Activity assay of DIBMALP PS1 and PEN-2 with MBP-APPC substrate under room temperature

Blue stained Tricine–SDS-PAGE of activity assay of DIBMALP PS1 and PEN-2 with different substrate concentrations. Individual DIBMALP PS1 and PEN-2 or MBP-APPC were treated under the same conditions as the control.

3.4.3 Isolation of PS1-PEN-2 complex with detergents solubilization

For further experiments, I made a new construct which was consisting of His-PS1-PEN-2-rho instead of His-PEN-2. His-PS1 and PEN-2-rho construct was expressed in BL21(DE3) strain with overnight expression at 16 °C. Cells were harvested under 5,000 xg centrifuge and resuspended with lysis buffer. Cells were opened with cell disrupter while membrane pellet was collected by 150,000 ultracentrifugations. Western blot (Figure 3.31) showed all opening steps of His-PS1 and PEN-2-rho by using different antibodies. Monomeric bands of His-PS1 and PEN-2-rho were observed on both Western blot images, indicating that His-PS1 and PEN-2-rho can be well co-expressed. There was no significant difference between the cells before and after opening, which means that all cells were correctly opened. Weak bands were detected in the inclusion bodies, implying that a small part of PS1 and PEN-2 proteins were improperly folded. Almost all target proteins were embedded in the membrane. There was no protein efflux in the supernatant after ultracentrifugation, confirming that His-PS1 and PEN-2-rho can be well co-expressed and correctly folded.
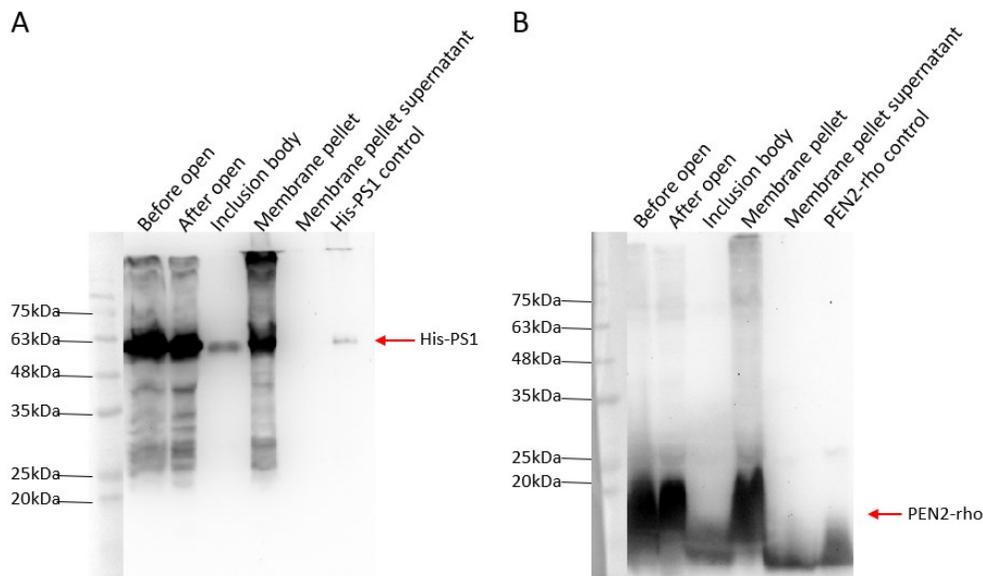
Figure 3.31 Opening of co-expressed His-PS1 and PEN-2-rho

Western blot of opening procedures of co-expressed His-PS1 and PEN-2-rho. Samples were normalized and loaded on SDS-PAGE for His-tag (A) or Rho-tag (B) detections.

The membrane fractions were collected with 150mg/ml concentrations stock and the solubilizations were performed with 1:2 dilutions. SMA and DIBMA polymers were used to solubilize the PS1-PEN-2 complexes in the lipid environment, while detergents were also used for solubilization. Here, we chose SMA polymer with a styrene to maleic anhydride ratio of 2.3:1, which is the most commonly used SMA. DIBMA polymers and two modified DIBMA polymers, which are less charged and compatible with high concentrations of cations, were also tested here. The SMA and DIBMA polymers were utilized with 2.5% (w/w) polymer concentration combined with 75 mg/ml membrane concentrations and the mixtures were incubated at 4 °C with end-over-end rotations overnight. In addition to the solubilization by SMA and DIBMA polymers, CHAPSO, DDM and Fos-14 were also used in various ratios (w/w) for solubilization and the mixtures were incubated in cold-room overnight. Insoluble pellets after 150,000xg ultracentrifugations were displayed in Figure 3.32 A, almost nothing was left in the 1% Fos-14 solubilization tube, while a tiny particle was existed in the 0.5% Fos-14 solubilization tube. Solubilization by 1% CHAPSO or 0.5% DDM resulted in a small amount of residue after ultracentrifugation and little reduction in polymer solubilization was observed, suggesting that the detergents showed higher efficiency in

His-PS1 and PEN-2-rho solubilization. Due to the small number of membrane particles used, I was not able to properly measure the weight of the membrane particles before and after solubilization.

Bradford assay was performed to measure the total amount of solubilized proteins. Since polymers are sensitive to acidic environments, I precipitated all proteins which were solubilized by polymers by using a Methanol/chloroform protein precipitation method. I hypothesized that 1% Fos-14 overnight solubilization would solubilize all proteins from the membrane fractions. As shown in Figure 3.32 B and Table 3.3, The solubilization by 0.5% Fos-14 showed a high solubilization efficiency and solubilized 95.34% of the protein compared to 1% Fos-14 solubilization. Simultaneously, the solubilization by 1% CHAPSO or 0.5% DDM exhibited solubilization efficiency of 25% or 33% to 1% Fos-14 solubilization.

Compared to 1% Fos-14 solubilization, it appeared that only a small fraction of membrane pellets can be solubilized by SMA polymers, which showed a maximum solubilization efficiency of 12.69%. Only 6% of proteins can be solubilized from membrane fractions by DIBMA solubilization.
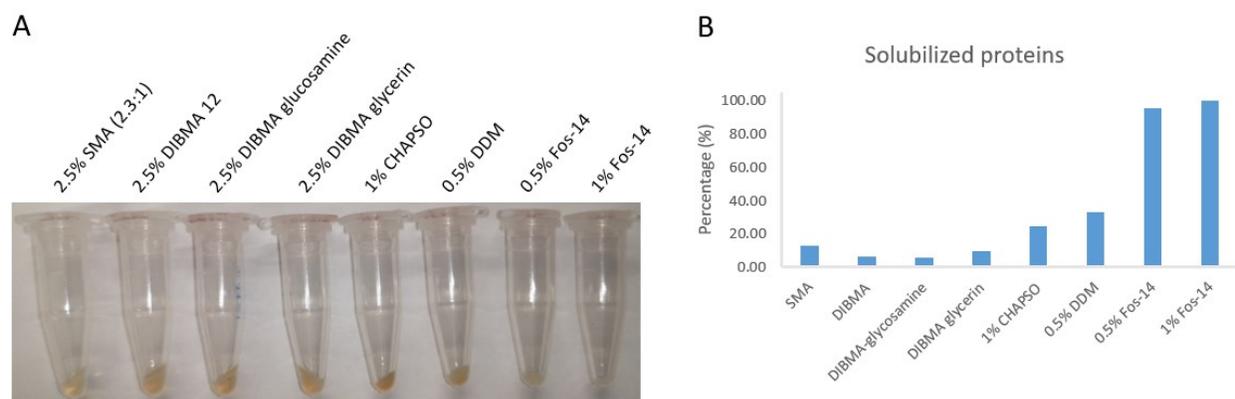
Figure 3.32 Solubilization of His-PS1 and PEN-2-rho

Solubilization of His-PS1 and PEN-2-rho with different polymers or detergents. SMA and different DIBMA polymers were used with the concentration of 2.5%. At the same time, CHAPSO, DDM and Fos-14 under different concentrations were performed. (A) Insoluble parts of solubilization after ultracentrifugation. (B) Percentages of different solubilizers on the solubilization of His-PS1 and PEN-2-rho and 1% Fos-14 solubilized protein was considered as 100%.

Table 3.3 Percentages of different solubilizers on the solubilization of His-PS1 and PEN-2-rho

Solubilizers	Percentage (%)
SMA	12.69
DIBMA	6.60
DIBMA-glycosamine	5.59
DIBMA glycerin	10.00
1% CHAPSO	24.99
0.5% DDM	32.97
0.5% Fos-14	95.34
1% Fos-14	100.00

Since the Bradford assay only displayed the total protein dissolved from the membrane fraction, I detected the target protein signals on SDS-PAGE and Western blot. The intrinsic tryptophan fluorescence signal was detected under UV light in Bio-rad ChemiDoc, and the PEN-2-rho protein was clearly shown on SDS-PAGE with the correct molecular weight (Figure 3.33 A). Meanwhile, His-PS1 protein was also observed on anti-His-tagged Western blot, but we could not observe it clearly on SDS-PAGE as PEN-2-rho behaved on fluorescence-detectable PAGE because of the weak bands (Figure 3.33 B). Therefore, we can conclude that the expression level of the PEN-2-rho protein was higher than the His-PS1 protein when co-expressed.

In polymers solubilization, most of the PEN-2-rho proteins were accumulated in membrane fractions after ultracentrifugation and were barely visible in the supernatant. The same situation was observed on the anti-His Western blot, where the His-PS1 protein was hardly seen in the supernatant. In combination with the Bradford assay, SMA and DIBMA polymers performed poorly solubilizations on His-PS1-PEN-2-rho protein complexes.

Fos-14 detergent solubilization appeared the highest solubilization efficiency. Most of the target proteins were solubilized in the supernatant and a small fraction of the proteins were retained in the membrane. After solubilization by CHAPSO and DDM, more than half of His-PS1 and PEN-2-rho proteins were stacked in the membrane fraction, but 1/3 of the protein was solubilized. Even though CHAPSO and DDM detergents cannot solubilize as well as Fos-14 detergents, they showed the suitability for isolation of His-PS1-PEN-2-rho protein complexes.
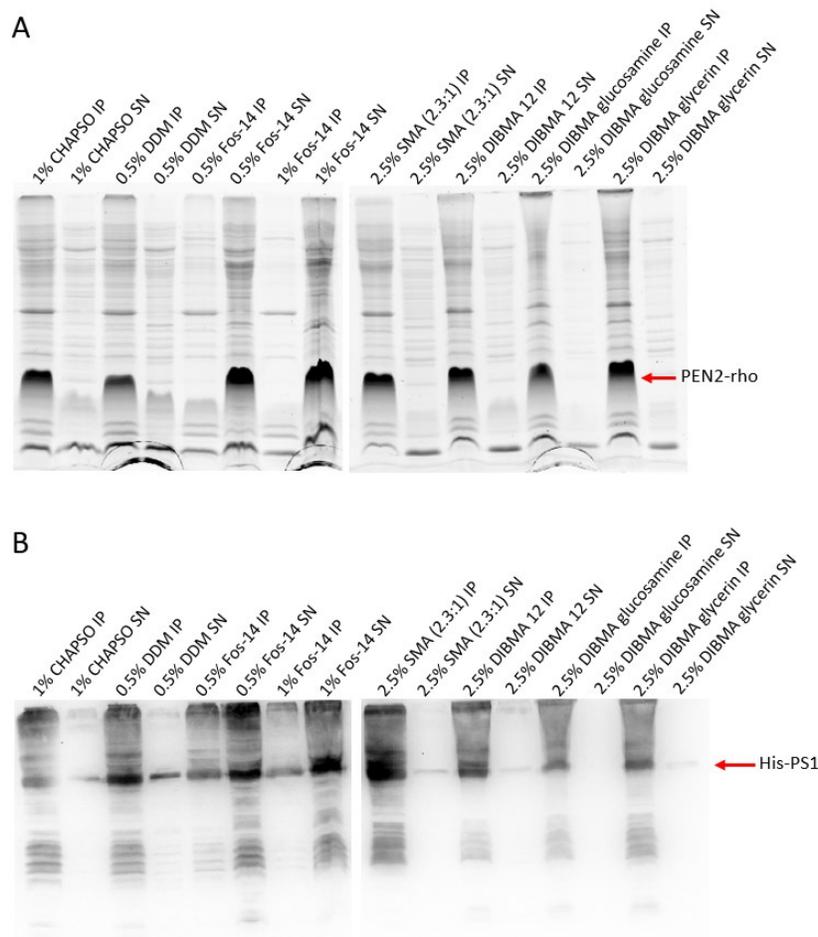
Figure 3.33 SDS-PAGE and Western blot of solubilization of His-PS1 and PEN-2-rho under different polymers or detergents.

SDS-PAGE fluorescence detection of intrinsic tryptophan signal (A) and Western blot anti His-tag (B) of His-PS1 and PEN-2-rho proteins after solubilization. PEN-2-rho and His-PS1 are marked with red arrows and their respective names. IP: insoluble pellet after solubilization. SN: supernatant after 150,000xg ultracentrifugation.

Afterwards, I purified His-PS1 and PEN-2-rho in different detergents to isolate His-PS1-PEN-2-rho protein complexes. Different detergents solubilized His-PS1 and PEN-2-rho proteins were purified with respective detergents. The concentrations in the purification buffers were 0.5% CHAPSO, 3CMC DDM or 3CMC Fos-14. I performed purifications with the Ni-NTA affinity column, which could not bind PEN-2-rho protein. Given that PEN-2-rho protein does not contain a His-tag and can not interact with nickel, PEN-2-rho proteins were detected on blue-stained SDS-PAGE from all purified batches (Figure 3.34 A), demonstrating that the PEN-2-rho protein and the His-PS1 protein interacted with each other and successfully formed complex. Western blots against different antibodies were performed to confirm that the proteins were correct. In all batches purified, monomeric bands of the His-PS1 protein were observed on Western blot with anti-His-tag (Figure 3.34 B right panel), while the PEN-2-rho protein was detected as monomeric and oligomeric bands by Western blot with anti-Rho-tag (Figure 3.34 B left panel). Our previous experiments observed concentration-dependent oligomers of the PEN-2 protein on SDS-PAGE (Figure 3.34B right His-PEN-2 control), so I can conclude that the same is true for oligomers and dimers of the PEN-2-rho protein.
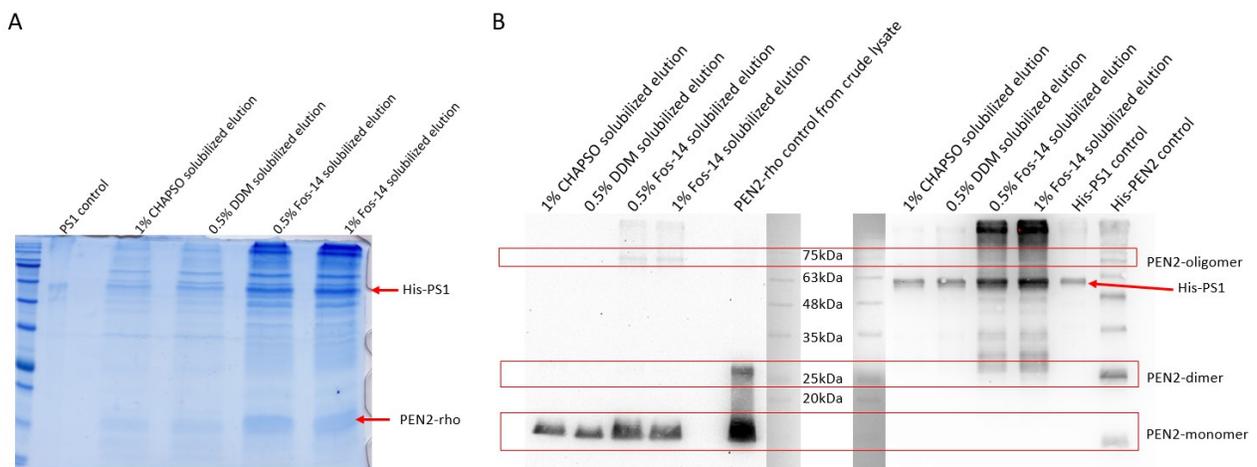
Figure 3.34 Purification of His-PS1 and PEN-2-rho with different detergents

His-PS1 and PEN-2-rho were solubilized by different detergents (1% CHAPSO, 0.5% DDM, 0.5% Fos-14 and 1%Fos-14) and purified with respective detergents. Blue stained SDS-PAGE (A) and Western blot anti His-tag (B, right panel) or anti Rho-tag (B, Left panel). Protein monomer bands were marked with red arrows with respective names. The red boxes indicated the different states of PEN-2-rho

Since I confirmed the formation of His-PS1 and PEN-2-rho protein, I performed large-scale purification of His-PS1-PEN-2-rho complexes under different detergents conditions. First, I processed a large-scale purification of CHAPSO-solubilized His-PS1-PEN-2-rho protein complex with all buffers containing 0.5% CHAPSO. The proteins were bound to a Ni-NTA affinity column and stirred overnight. The affinity column was washed by using different salt concentrations in the washing steps and the flow-through was monitored at wavelength 280 nm until the absorption peak dropped to 0. The protein complex was eluted by 500mM imidazole and loaded on Size Exclusion Chromatography for further purification. Four peaks were monitored on the SEC with the calculated molecular weight of 1285, 323,72, 45 kDa and a dead volume peak was shown (Figure 3.35 A). All SEC fractions contained the PEN-2-rho protein on SDS-PAGE which indicated that the His-PS1-PEN-2-rho complex was formed (Figure 3.35 B). The last two peaks showed higher absorption at 260 nm than at 280 nm, which implied that they contained DNA impurities. The higher 260 nm absorption in the 323 kDa peak appeared to be influenced by the 72kDa peak. The protein bands were barely visible in the C8 and C9 fractions, which appeared to be the residues from the 323 kDa peak. PS1-NTF and CTF were not detected on SDS-PAGE, which could be the influence of the high degree of CHAPSO-induced aggregation.
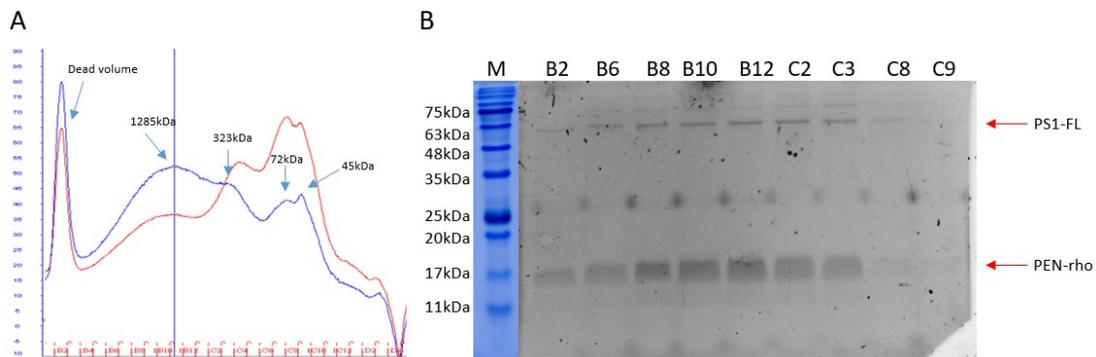
Figure 3.35 Purification of CHAPSO solubilized His-PS1 and PEN-2-rho with His-tag purification

1% CHAPSO solubilized His-PS1 and PEN-2-rho protein complex was purified by a buffer containing 0.5% CHAPSO. SEC profile (A) and fluorescence detected SDS-PAGE (B) of purified His-PS1-PEN-2-rho complex. The calculated molecular weight of each peak is marked with a blue arrow. The red arrows indicate the His-PS1 protein full-length and the PEN-2-rho protein.

Second, I purified the Fos-14-solubilized His-PS1-PEN-2-rho protein complex by using buffers containing 3CMC Fos-14. Three peaks were observed on the SEC curve and labeled with molecular weights of 1037, 273, 93 kDa and a dead volume peak was shown (Figure 3.36 A). SDS-PAGE showed that all SEC fractions contained His-PS1 and PEN-2-rho, indicating that Fos-14-solubilized His-PS1 and PEN-2-rho protein also formed complexes (Figure 3.36 B). The peak at 93 kDa was consistent with dimer complexes of His-PS1 and PEN-2-rho with Fos-14 micelles but was difficult to separate from the peak at 273 kDa. Two main peaks with the molecular weight of 1037 and 273 kDa showed the oligomer and tetramer of the His-PS1-PEN-2-rho protein complexes with high purity of proteins. These results could confirm the complex formation of the His-PS1-PEN-2-rho protein complex. No PS1-NTF and CTF were detected on SDS-PAGE, indicating that the oligomerization states interfered with the self-activation of the PS1 protein. Meanwhile, it is known that Fos-14 detergents may lead to membrane protein destabilization and unfolding, Fos-14 also could interfere with the self-activation of the PS1 protein.
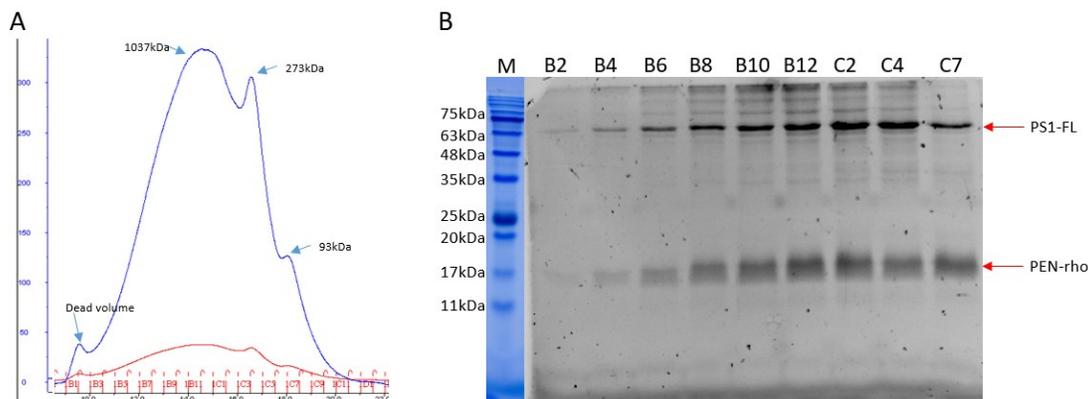
Figure 3.36 Purification of Fos-14 solubilized His-PS1 and PEN-2-rho with His-tag purification

The His-PS1-PEN-2-rho protein complex with 0.5% Fos-14 solubilization were purified by a buffer containing 3CMC Fos-14. SEC profile (A) and fluorescence detected SDS-PAGE (B) of purified His-PS1-PEN-2-rho complex. The calculated molecular weight of each peak is marked with a blue arrow. The red arrows indicate the His-PS1 full-length and PEN-2-rho.

The last, the DDM solubilized His-PS1-PEN-2-rho protein complex was purified by using the buffers containing 3CMC DDM. After purified by Ni-NTA affinity column and then size exclusion

chromatography, Two prominent peaks were displayed with the respective molecular weight of 548, 167 kDa and a dead volume peak was shown (Figure 3.37 A). SDS-PAGE image demonstrated that all peaks contained the His-PS1 and PEN-2-rho proteins, indicating the formation of PS1-PEN-2 complexes (Figure 3.37 B). Interestingly, the bands at 35kDa and 18kDa on SDS-PAGE from the fractions of C3-C9 were shown on SDS-PAGE. It is known that the PEN-2 protein enhances the endoproteolysis of Presenilin through interaction with Presenilin and produces heterodimers of the N-terminal and C-terminal fragments of Presenilin, Both bands on SDS-PAGE also corresponded to the molecular weights of PS1-NTF and PS1-CTF, suggesting that, the His-PS1 and PEN-2-rho proteins were correctly interacted and contributed to the endoproteolysis of PS-1 in the case of DDM solubilization. Fraction C5 was used for the Blue native PAGE to determine the correct molecular weight of the His-PS1-PEN-2-rho complex. We observed a main band slightly above the 146 kDa marker band on the blue native PAGE, and three weak bands barely visible below (Figure 3.37 C). The main band was consistent with the calculated molecular weight of C5, and the other three bands may be residues from other fractions. To confirm the N-terminal and C-terminal fragments of PS1, we performed LC-MS/MS to identify the peptides from the bands on SDS-PAGE. The red peptides were identified from the PS1-NTF band, while two peptides were from the PS1-CTF band and are labeled blue. Some NTF peptides were identified from the PS1-CTF band, indicating the interactions of NTF and CTF.
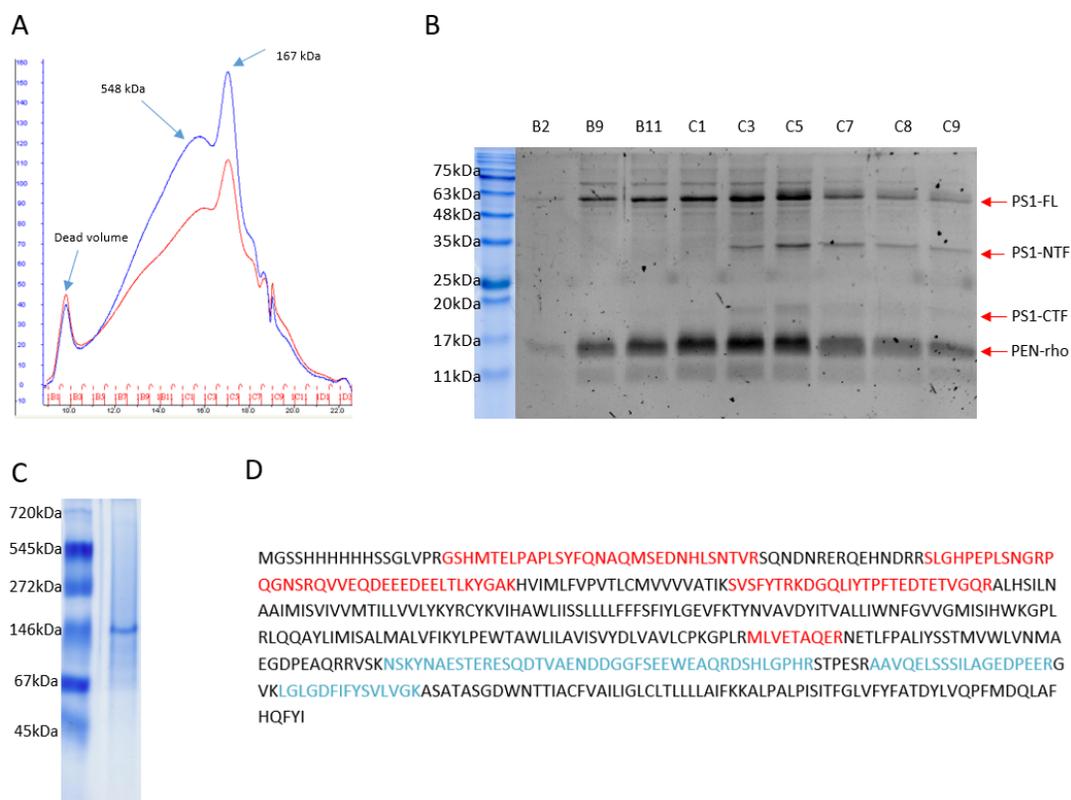
Figure 3.37 Purification of DDM solubilized His-PS1 and PEN-2-rho with His-tag purification

His-PS1 and PEN-2-rho under 0.5% DDM solubilization were purified by a buffer containing 3CMC DDM. SEC profile (A) and fluorescence detected SDS-PAGE (B) of purified His-PS1-PEN-2-rho complex. The calculated molecular weight of each peak is marked with a blue arrow. The red arrows indicate the His-PS1 full-length and PEN-2-rho and the potential PS1-NTF and PS1-CTF. (C) Blue Native PAGE of the C5 fraction of His-PS1 and PEN-2-rho from SEC. (D) Peptide identification of PS1 fragments by LC-MS/MS, peptides that matched PS1-NTF were labeled in red, and the blue color indicates the peptides that correspond to PS1-CTF.

In addition to His-tag purification with different detergents, I also purified the His-PS1-PEN-2-rho protein complex by a Rho-tag affinity column. The DDM-solubilized His-PS1-PEN-2-rho protein complex was incubated with Rho-tag resin overnight at 4°C with stirring and the resin was washed with sufficient washing buffer containing 3 cmc DDM until the absorption at wavelength 280 nm dropped to 0. The protein was eluted by 200 µM of Rho1D4 peptide and the elution process was also monitored at a wavelength of 280 nm. After further purification by size exclusion chromatography, two main peaks and a tiny dead volume peak appeared (Figure 3.38 A). Blue stained SDS-PAGE showed both the monomeric His-PS1 and PEN-2-rho proteins (Figure 3.38 B),

suggesting that His-PS1 interacted with PEN-2-rho and formed a complex. As shown from the blue-stained SDS-PAGE, the His-PS1 protein showed the highest abundance in fraction C2 and the PEN-2-rho protein showed the highest abundance in fraction C6. The peak shift on blue-stained SDS-PAGE indicated the right peak was the uncomplexed PEN-2-rho protein. This was also consistent with the result that the expression level of the PEN-2-rho protein was higher than the His-PS1 protein when co-expressed.
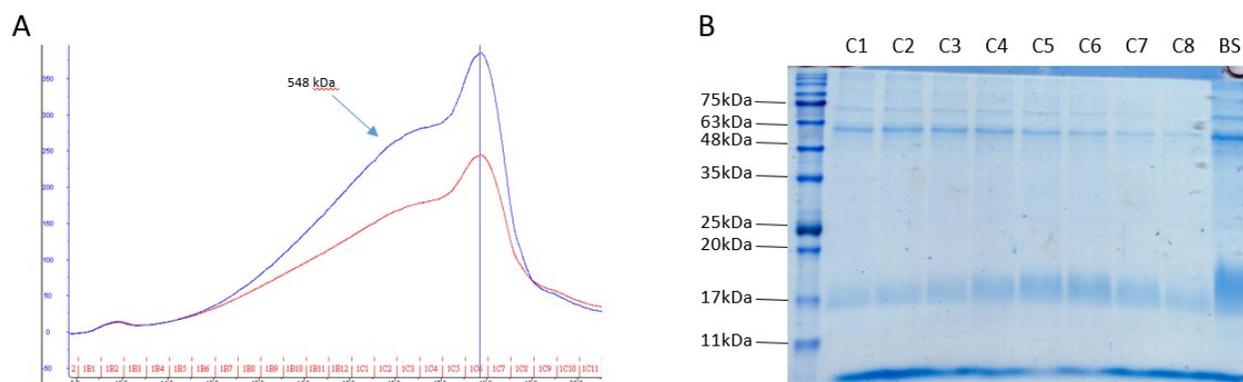
Figure 3.38 Purification of DDM solubilized His-PS1 and PEN-2-rho with Rho-tag purification

Purification of DDM solubilized His-PS1 and PEN-2-rho by Rho-tag resin only. (A) SEC profile of purification by Rho-tag resin. (B) Blue stained SDS-PAGE of SEC fractions. BS: before SEC sample. The calculated molecular weight of the peak is marked with a blue arrow

Next, I performed the purification for the individually expressed His-PS1 or PEN-2-rho protein. The His-PS1 or PEN-2-rho protein was expressed individually in BL21(DE3) and the cells were opened by cell disruptor. Inclusion bodies were removed by 9000xg ultracentrifugation while membrane fractions were harvested at 100,000xg. Same solubilization conditions were used as His-PS1 and PEN-2-rho co-expressed membrane fractions. As shown on the Western blot (Figure 3.39), a small portion of the protein was stacked in the inclusion bodies on both the His-PS1 and PEN-2-rho protein samples, indicating some proteins were incorrectly folded. The solubility of 0.5% DDM on the His-PS1 showed the same efficiency on co-expressed His-PS1 and PEN-2-rho membranes. But only a small amount of the PEN-2-rho protein was solubilized by 0.5% DDM, which was

barely visible on the Western blot for Rho tag detection, suggesting that the solubility of DDM on the PEN-2-rho protein increased when the complex was formed.
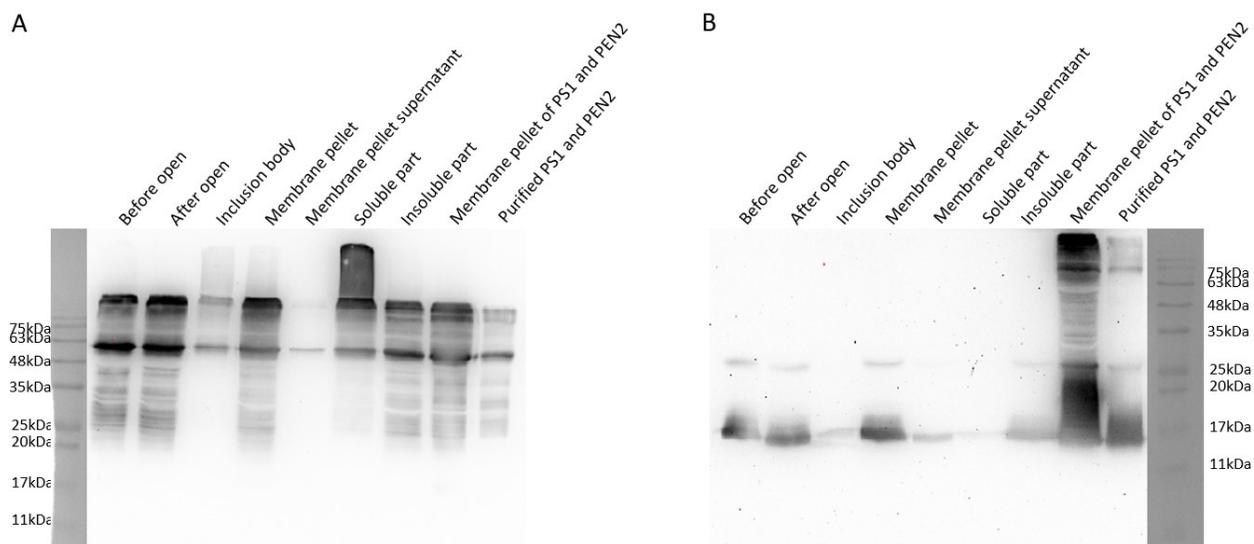
Figure 3.39 Opening procedures of single expressed His-PS1 or PEN-2-rho

The single expressed His-PS1 or PEN-2-rho was opened by a cell disruptor and the membrane fractions were collected by ultracentrifugation at 100,000xg. Membrane fractions were dissolved with 0.5% DDM and purified with the buffer containing 3 cmc of DDM. Purified His-PS1-PEN-2-rho complexes were loaded onto SDS-PAGE as positive controls. Western blots of anti-His-tag (A) or Rho-tag (B) are shown here.

The elutions of individually expressed His-PS1 or PEN-2-rho protein were further purified by Size Exclusion Chromatography. Two Peaks were observed on the SEC curve of the PEN-2-rho protein (Figure 3.40 A) and identified as the PEN-2 rho protein oligomers and monomers (Figure 3.40 B). Due to the dead volume of the SEC column, a peak on the left side of the His-PS1 protein curve was considered to be a large oligomer of the His-PS1 protein, while two main peaks were also shown on the SEC curve. Both main peaks contained the His-PS1 protein, but the NTF and CTF bands of PS1 were also slightly showed in the second peak (Figure 3.40 C&D).
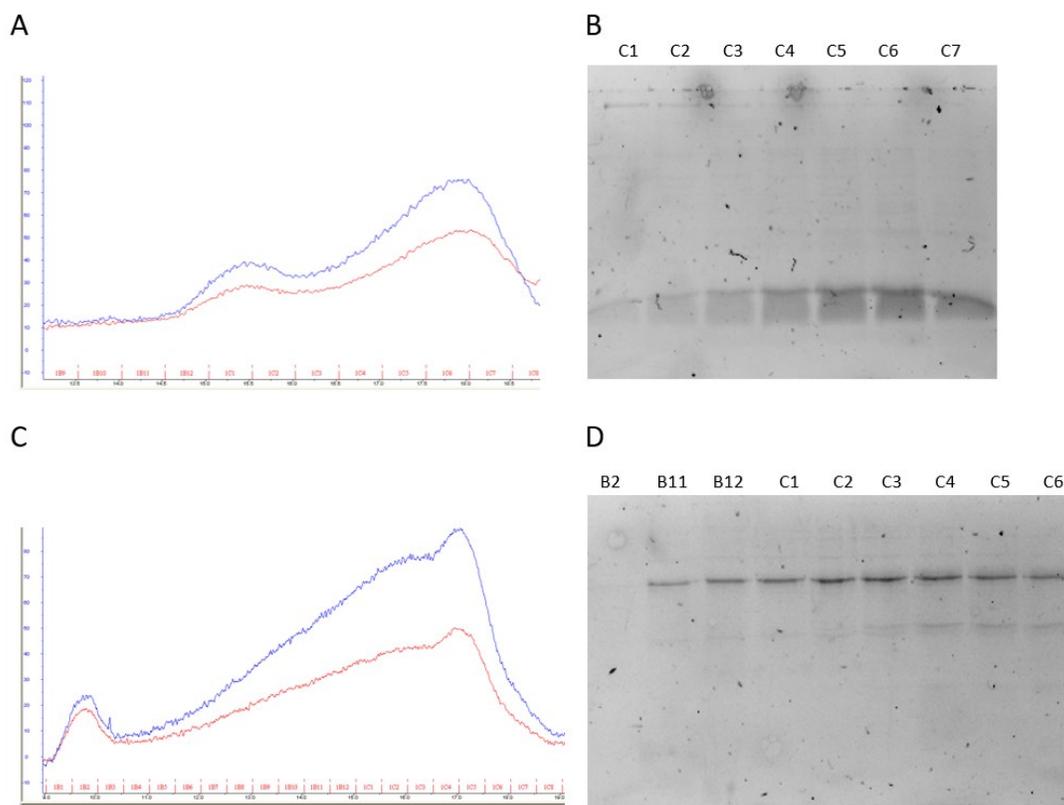
Figure 3.40 Purification of DDM solubilized single expressed His-PS1 or PEN-2-rho

Individually expressed His-PS1 or PEN-2-rho were eluted from the respective affinity column and further purified by Size Exclusion Chromatography. SEC profile (A&C) and the SDS-PAGE of SEC fractions (B&D) were shown.

To further confirm the formation of the complexes, I overlayed the SEC curves from different purification batches (Figure 3.41). The second peak of His-PS1 and PEN-2-rho after rho-tag purifications (pink curve) showed the same elution volume as the second peak of PEN-2-rho alone (black curve) which was consistent with the previous result that the amount of PEN-2 exceeds that of the complex and the right peak is the PEN-2-rho protein alone. The His-PS1 protein alone (blue curve) and the PEN-2-rho and His-PS1 proteins after His-tag purification (red curve) exhibited similar curves with a significant shift compared to the peak of PEN-2-rho, indicating the formation of complexes. No difference was observed between the His-PS1 protein alone and the PEN-2-rho and His-PS1 protein complex with His-tag purification, which was appeared to be the resolution errors of the SEC column. To obtain high resolution, I loaded the His-PS1-PEN-2 protein complexes or the His-PS1 protein alone onto a Superdex 200 increase column, and the two major

88

peaks were separated from each other, with a new peak appearing in the middle which could be the transition phase. The right peak of the complex curve (black peak) showed a slight left shift compared to the right peak of the His-PS1 protein alone (red curve), proving that the His-PS1-PEN-2-rho protein complex was formed.
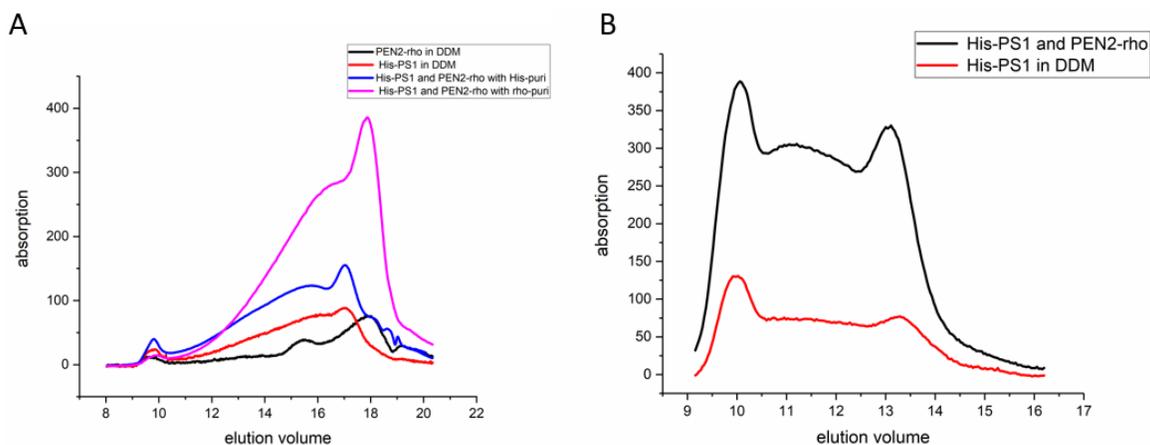
Figure 3.41 Overlay of SEC profiles of different purification batches.

(A) Overlay of different purifications batches of single expressed or co-expressed proteins with Superose 6 increase column. Black curve: PEN-2-rho alone in DDM. Red curve: His-PS1 alone in DDM. Blue curve: His-PS1-PEN-2-rho complexes with His-tag purifications. Pink curve: His-PS1-PEN-2-rho complexes with Rho-tag purifications. (B)Overlay of the SEC peaks of His-PS1-PEN-2-rho complexes from His-tag purification (black curve) and His-PS1 alone (rea curve) after Superdex 200 increase column.

Next, I performed a two-step purification of the His-PS1-PEN-2-rho protein complex, which was first with the His-tag purification and followed by the Rho-tag purification. Due to the high concentration of imidazole after His-tag purification, the elution after His-tag purification was dialyzed to remove imidazole and was further bound to the Rho-tag resin. After eluting from Rho-tag resin by 200 μM concentrations of Rho1D4 peptides, sample qualities were checked on SDS-PAGE before being loaded on SEC. As shown in SDS-PAGE (Figure 3.42 A&B), the PS1-full-length and the PEN-2-rho proteins were detected in both elution I and elution II with high purity and a broad peak was shown on the SEC profile with the calculated molecular weight of 616kDa, which was close to the molecular weight of the oligomer peak when purified using His-tag or Rho-tag, indicating that this peak was consistent with our previous observation of the oligomer peak. Only the oligomer peak was observed in this case, suggesting that the tetramer complex could exist

with a different protein conformation and contained the inaccessible Rho-tag. The oligomer peak was then used for Blue native PAGE (Figure 3.42 C) and a band above the 545kDa marker band was detected, proving that the oligomer peak had a molecular weight of around 600 kDa. SDS-PAGE image (Figure 3.42 D) showed that all fractions from SEC contained both the His-PS1 and PEN-2-rho proteins with high purities.
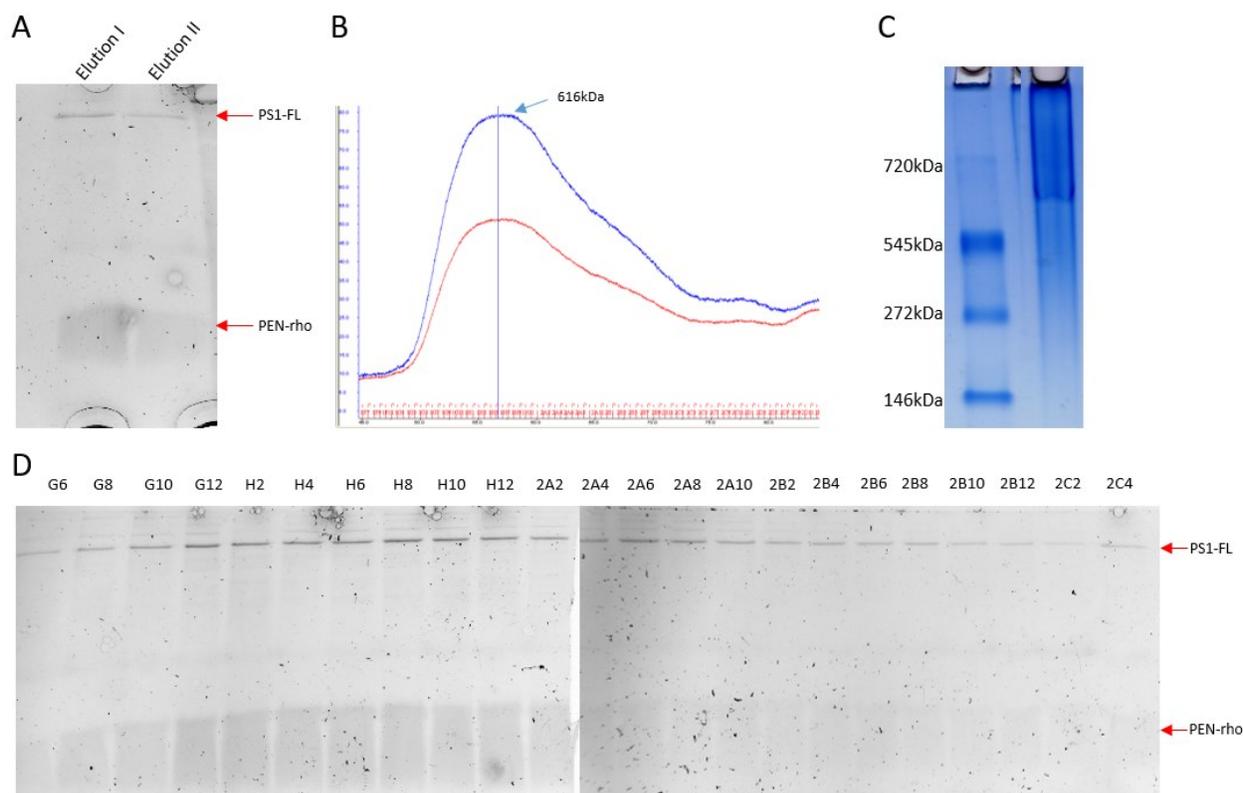
Figure 3.42 Two-step purification of His-PS1 and PEN-2-rho, first with His tag and subsequently with Rho tag.

His-PS1-PEN-2-rho complex was first purified by His-tag and followed by Rho-tag. (A)SDS-PAGE of the elutions after His-tag and Rho-tag purifications. PS1-full-length and PEN-2-rho were marked with red arrows. (B) SEC profile of two-steps purified His-PS1 and PEN-2-rho. The molecular weight of the main peak was marked with a blue arrow. (C) Blue native PAGE of the main peak of His-PS1 and PEN-2-rho after two-step purification. (D) Fluorescence detected SDS-PAGE of SEC fractions.

We mutated the catalytic aspartic acid at positions 257 and 385 to alanine, which was used here as a negative control. The PS1-DDAA mutation was cloned into the His-PS1 and PEN-2-rho construct

90

to replace His-PS1 to obtain the His-PS1-DDAA and PEN-2-rho construct. His-PS1-DDAA and PEN-2-rho protein complexes were purified with His-tag using the same procedures with the His-PS1 and PEN-2-rho protein performed. As shown in SDS-PAGE, I did not observe differences between the DDAA complex and the WT complex, and the PS1-NTF or CTF fragments were displayed in the DDAA complex (Figure 3.43). The identical SEC profiles were observed in the DDAA and WT complexes, indicating that the DDAA mutation didn't significantly change the conformation of the Presenilin-1 and PEN-2 complexes.
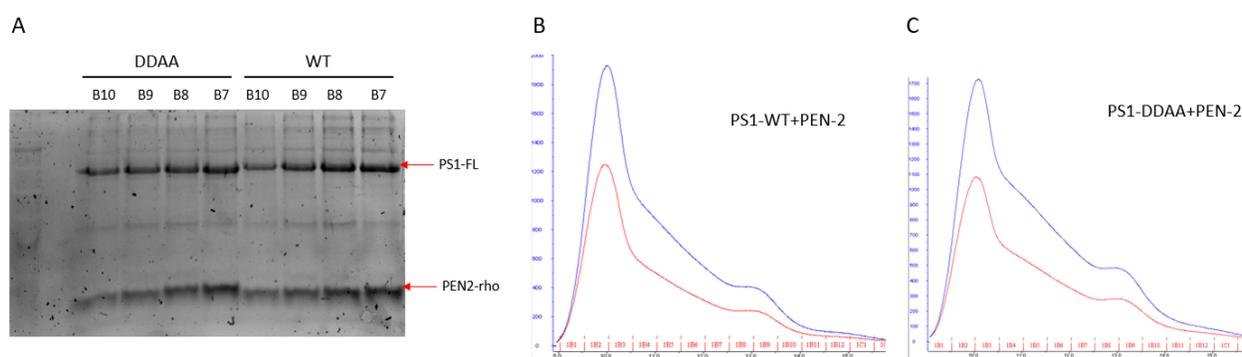
Figure 3.43 Comparison of PS1-WT complex and PS1-DDAA mutation complex.

His-PS1-DDAA mutation and PEN-2-rho complex were purified under the sample procedures as His-PS1 and PEN-2-rho. (A) Fluorescence detected SDS-PAGE of purified DDAA mutations and WT SEC fractions. PS1 full-length and PEN-2-rho were marked by red arrows. Size Exclusion Chromatography was used for further purification of WT complex (B) and DDAA complex (C).

To determine the ratio of the PS1 and the PEN-2 proteins in the complex, I calculated the protein molar concentration by the protein band intensity of the PS1-PEN-2 protein complexes. The gradient amounts of the Fos-14 purified PS1 or PEN-2 protein were used as standards to measure the ratio of PS1-PEN-2 complexes in different states. The intensity of the complex bands was measured by the Software Image Lab from Bio-Rad Laboratories. The purified PS1 or PEN-2 protein with gradients of 1-3 μg were used as standard curves (Figure 3.44) and the intensity of the bands displayed on SDS-PAGE for the target proteins was quantified. Based on the volumes we loaded on SDS-PAGE, I calculated the molar concentrations of each component in the different state complexes (Table 3.4). The oligomeric state with a molecular weight of 600 kDa contains 71.3 nM His-PS1 protein and 418.06 nM PEN-2-rho protein, indicating the ratio of PS1 to PEN-2

in the oligomeric state was 1:6, which may include 5 His-PS1 protein molecules and 30 PEN-2-rho protein molecules. The tetramer peak of the PS1-WT and PEN-2 protein complexes or the PS1-DDAA and PEN-2-rho protein complex after His-tag purification showed a similar ratio of 1:1. I quantified that 809.43 nM PS1-WT bound with 1176.8 nM PEN-2, while 906.65 nM PS1-DDAA interacted with 970.04 nM PEN-2. The ratio in both cases was less than 1:1 because of the formation of NTF and CTF fragments. The PS1-WT and PEN-2 protein complex showed a lower rate than the PS1-DDAA and PEN-2 protein complex, suggesting that PS1-WT interacted with PEN-2 and produced more NTF and CTF fragments than the DDAA protein complex.
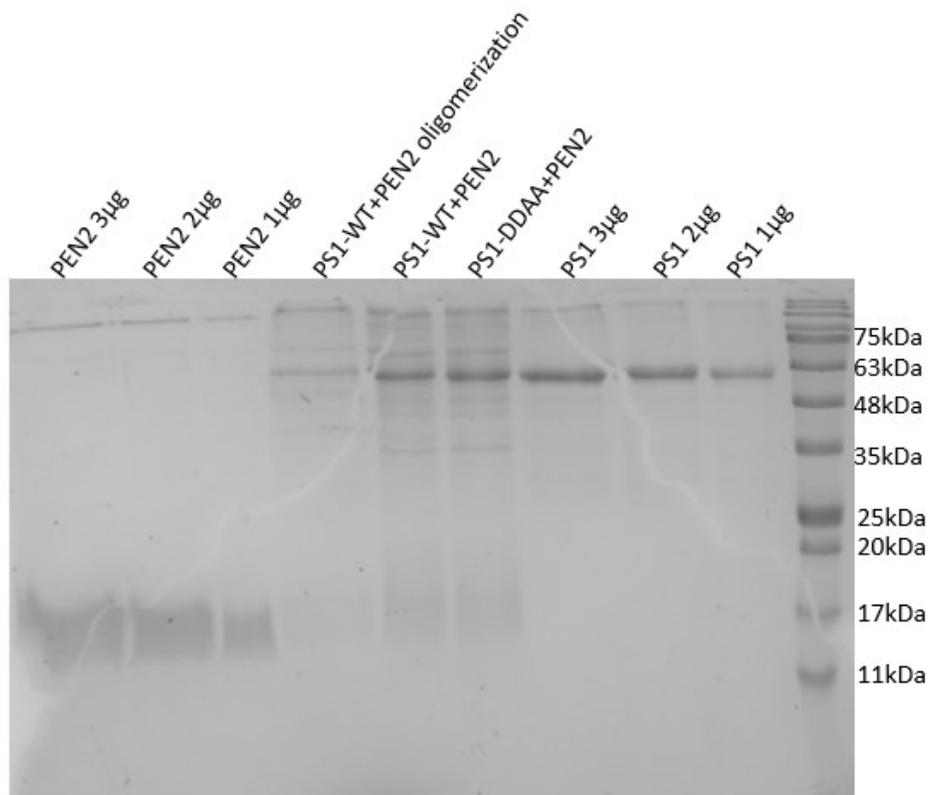
Figure 3.44 SDS-PAGE of quantification of PS1 and PEN-2 ratio in complex

The ratio of the Presenilin-1 and PEN-2 proteins in the complex was calculated from the intensity of the protein bands on SDS-PAGE. Gradient Fos-14 purified Presenilin-1 and PEN-2 monomers were used as the standards.

Table 3.4 Calculated molar concentration of each component in PS1-PEN-2 complex

	PS1 (nM)	PEN-2 (nM)
PS1-WT+PEN-2 oligomerization	71.3	418.06
PS1-WT+PEN-2	809.43	1176.8
PS1-DDAA+PEN-2	906.65	970.04

Cholesterol is a crucial component of eukaryotic cell membranes and plays a key role in membrane organization, fluidity, and function[192]. Many membrane proteins and important membrane activities, including those involved in signal transduction, have been identified in cholesterol-rich lipid rafts[138]. In addition to the effects of cholesterol on membrane structure and function, interactions between membrane proteins and cholesterol have been reported. Here I included the Cholesteryl Hemisuccinate Tris Salt (CHS), which had a ratio of 1:10 (w/w) to DDM concentration, in both solubilization and purifications. The purification of His-PS1 and PEN-2-rho in the presence of CHS was performed on a Ni-NTA affinity column followed by size-exclusion chromatography. Three peaks were shown on the SEC profile and all peaks contained both the His-PS1 and PEN-2-rho proteins as we expected (Figure 3.45).
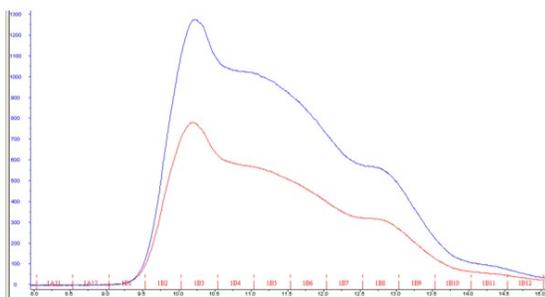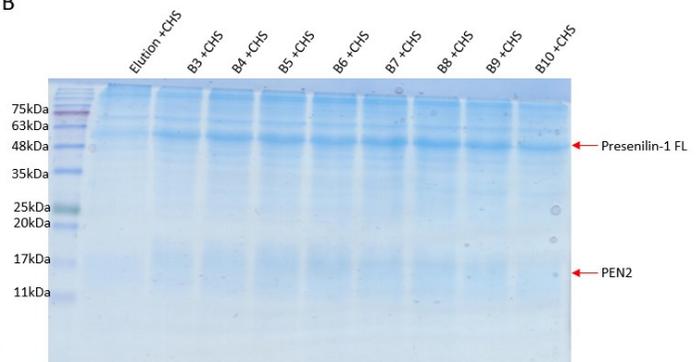
Figure 3.45 purification of His-PS1 and PEN-2-rho with DDM in the presence of CHS

The His-PS1 and PEN-2-rho proteins were purified with 3 cmc DDM in the presence of CHS. (A) SEC profile of purified the His-PS1 and PEN-2-rho proteins in DDM and CHS buffer. (B) Blue stained SDS-PAGE of SEC fractions.

For comparison with the solubilization and purification of the His-PS1 and PEN-2-rho protein complex in the absence of CHS, I overlaid the SEC profiles and loaded the solubilization steps and SEC fractions onto the same SDS-PAGE. Even though the SEC curves of the His-PS1-PEN-2-rho protein complex in the presence or absence of CHS showed similar profiles, there were still significant differences between the curves (Figure 3.46 A). The second peak showed almost the same intensity in both curves, the oligomeric state was significantly reduced when cholesterol is involved, indicating that cholesterol interacted with the His-PS1-PEN-2-rho protein complexes and helped to prevent the oligomerization. As shown in Western blot (Figure 3.46B&C), more protein was solubilized from the membrane when cholesterol was involved compared to previous solubilization in the absence of CHS, suggesting that cholesterol increased the solubility on the His-PS1-PEN-2-rho protein complexes. The tetramer peaks in both situations were checked and no difference was found in the western blot, implying that the cholesterol didn't affect the conformations of the complexes.
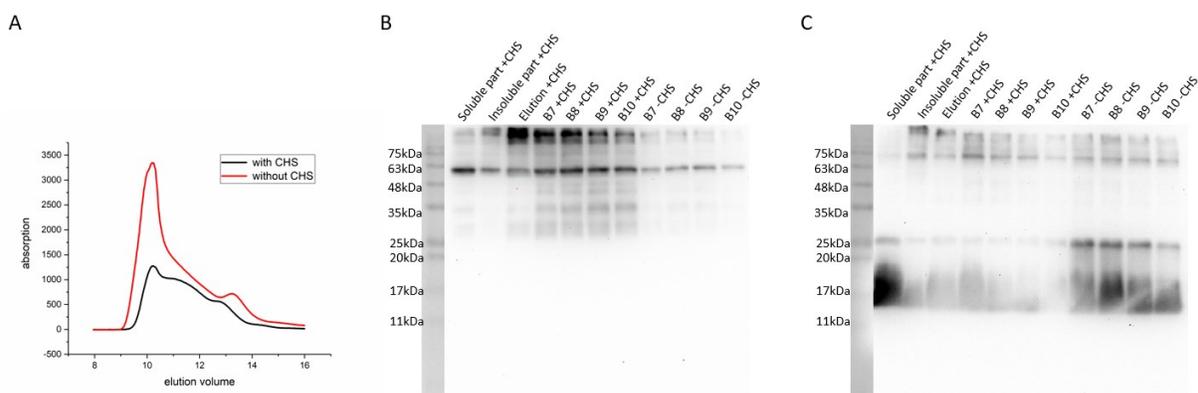
Figure 3.46 Comparison of purification of His-PS1 and PEN-2-rho in the presence or absence of CHS

Comparison of the His-PS1-PEN-2-rho protein complexes in the presence or absence of CHS under DDM purification. (A) Overlay of the SEC profiles of the His-PS1-PEN-2-rho protein complex purifications in

the presence or absence of CHS. The red curve indicates the purification without CHS, while the black curve shows the purification with CHS.

Liposomes containing 65% egg PC, 25% total brain extract and 10% cholesterol were prepared by 100 nm membrane extrusion. The His-PS1-PEN-2-rho protein tetramer complex was reconstituted into liposomes and the protein buffers were used as the negative control. Reconstitution steps were performed by Bio-Beads absorption and the empty liposomes were removed by sucrose gradient ultracentrifugations with the sucrose gradient of 37.0%, 32.5%, 29.5%, 21.0%, 17.2%, 13.4%, and 9.0%. Empty liposomes stayed on the top while the proteo-liposomes presented lower than empty liposomes (Figure 3.47 A). Western blot image showed the His-PS1 and PEN-2-rho protein signals in the proteo-liposomes layer but not at the bottom, indicating that the proteins were not precipitated and successfully reconstituted into liposomes (Figure 3.47 B).
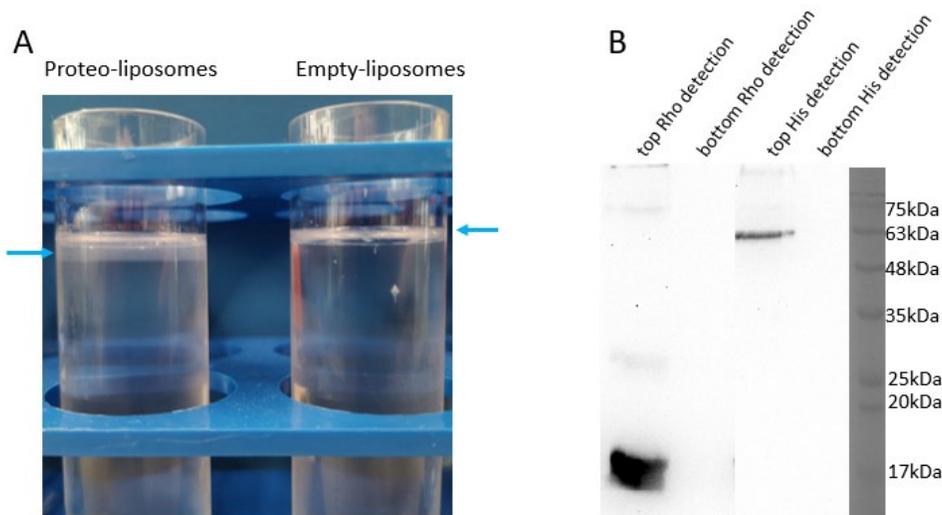
Figure 3.47 Reconstitution of the His-PS1-PEN-2-rho complex into liposomes.

The His-PS1-PEN-2-rho protein complex was reconstituted into liposomes containing 65% EggPC, 25% Brain Extract Total and 10% Cholesterol. (A) Sucrose gradient with concentrations of 37.0%, 32.5%, 29.5%, 21.0%, 17.2%, 13.4%, and 9.0% were performed. The blue arrows indicated the liposome layer after ultracentrifugation. (B) Western blot of proteo-liposomes under different antibody detections.

The activity of the purified proteo-liposomes was measured with a fluorescent γ-secretase substrate. The reactions were incubated at 37 °C overnight and followed by 100,000xg centrifugation for 1 hour. Western blot showed protein bands in proteoliposomes after 37°C, indicating that proteoliposomes were stable during incubation at 37°C (Figure 3.48 A). Empty liposomes and hydration buffer showed no signal in both the His-tag and the Rho-tag detection, confirming that no contamination was in the control experiments. Activity assay was measured before and after ultracentrifugations by Tecan plate reader with 355nm excitation wavelength and the emission spectrum was collected from the wavelength of 400nm to 480nm. Similar emission curves were shown in the before and after ultracentrifugation samples. There was no signal detected in the hydration buffer, while empty liposomes showed fluorescence signals. The proteo-liposomes exhibited a 30% higher fluorescence signal than the empty liposomes, indicating that the recombinant His-PS1-PEN-2-rho protein complexes are active. Even though we detected an active signal in the recombinant His-PS1-PEN-2-rho protein complexes, the signal was too low because of the high dilution at the time of reconstitution.
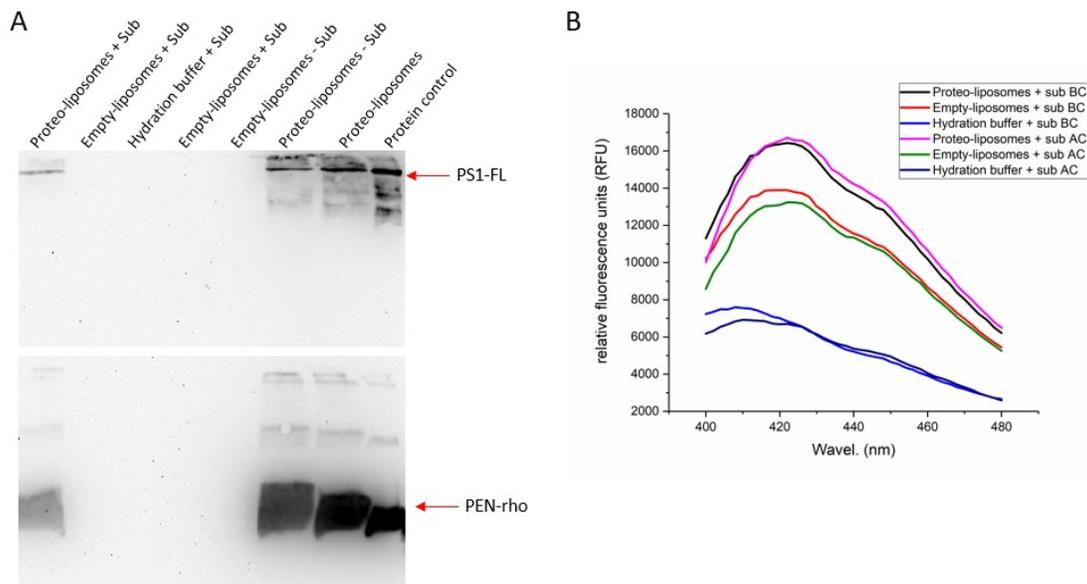
Figure 3.48 Activity assay of His-PS1-PEN-2-rho complexes

Reconstituted His-PS1-PEN-2-rho complexes proteo-liposomes were incubated with Fluorogenic γ-Secretase Substrate overnight at 37 °C. (A) Western blots of proteo-liposomes after 37 °C incubations. Upper part: His-tag detection. Lower part: Rho-tag detection. (B) *In vitro* activity was measured by using fluorogenic γ-secretase substrates, and the fluorescence signal was measured by a Tecan plate reader with an excitation wavelength of 355 nm and the emission scan wavelength collected from 400 nm to 480 nm. BC: before centrifugation. AC

As we only detected low activity in His-PS1-PEN-2-rho proteo-liposomes, here we performed the activity assay directly in the membrane fractions or the soluble parts after solubilizations. CHAPSO and DDM solubilized membrane fractions and the membranes without solubilization were performed and those fractions without substrates were used as the negative control. The fluorescence signal after 37°C incubations were measured by a Tecan plate reader with 355nm wavelength excitations and collected the emission wavelength was from 380nm to 490nm. As shown in Figure 3.49, Both membranes and solubilized fractions exhibited high activity signals while the fraction without substrate showed no activity due to the absence of absorption at 430 nm. The membrane fraction showed high absorbance at 390 nm, indicating that the membrane fraction exhibits high scattering when measuring the absorbance. The high absorbance in the CHAPSO and DDM solubilized fractions suggested that the detergent-solubilized His-PS1 and PEN-2-rho protein may exhibit the γ-secretase activities.
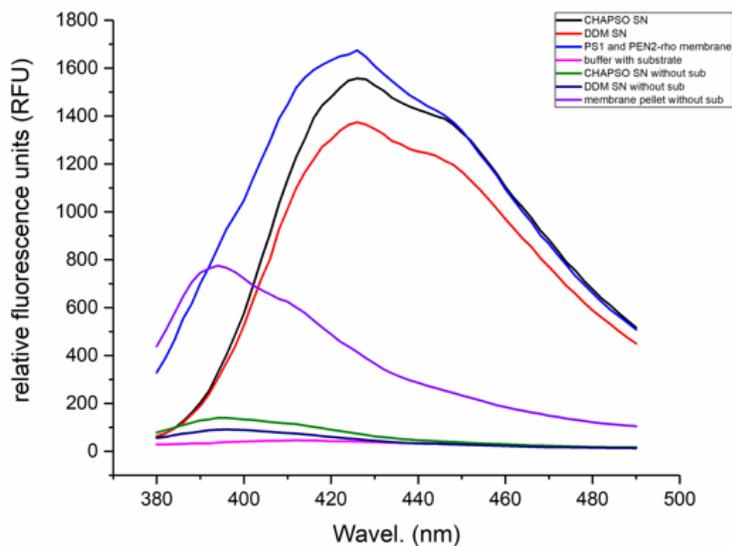
Figure 3.49 *In vitro* activity of different solubilized His-PS1-PEN-2-rho complexes

The activity of different fractions of the His-PS1-PEN-2-rho protein complexes was measured with fluorogenic γ-secretase substrates. His-PS1-PEN-2-rho membranes and the soluble part of solubilized membranes were used and those fractions without substrates were performed as the negative control.

Next, I measured the activity assay with the DDM purified His-PS1-PEN-2-rho protein tetramer. The SEC purified His-PS1-PEN-2-rho tetramers were mixed directly with 10 μM of fluorescent substrate to measure activity, and one replicate was performed. The SEC buffer was also measured with fluorescence substrates as a negative control to see whether there were any contaminants in the SEC buffer. The His-PS1-PEN-2-rho protein tetramers showed much higher activity than the

SEC buffer with substrates at the emission of 430nm (Figure 3.50). SEC buffer and the purified His-PS1-PEN-2-rho protein tetramers without substrates showed no emissions at 430nm. That indicated the purified His-PS1-PEN-2-rho tetramers existed qualitative activity.
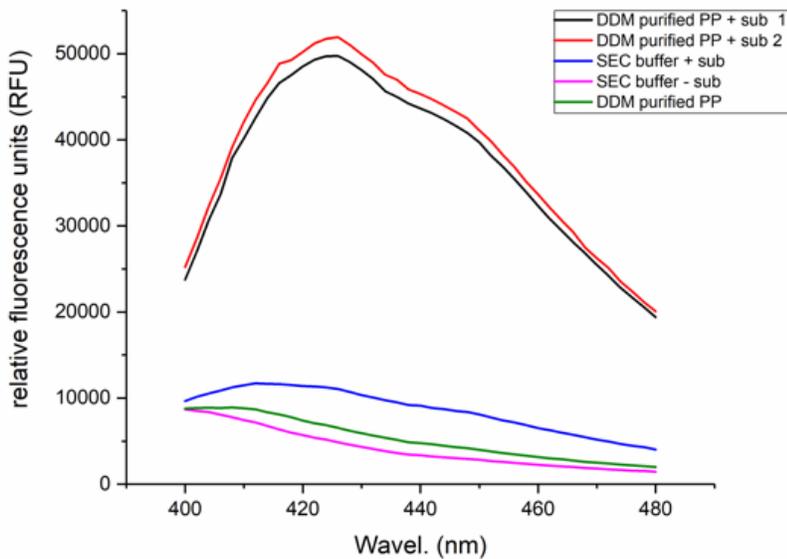
Figure 3.50 Activity assay of purified His-PS1-PEN-2-rho tetramer complexes

Purified His-PS1-PEN-2-rho tetramer complexes have measured the activity with the Fluorogenic γ-Secretase Substrate and one replicate was performed. SEC buffer was used as negative control while the purified protein was engaged without substrates to observe scattering. +sub means with substrates while -sub is without substrates. PP indicates His-PS1-PEN-2-rho complexes.

γ-Secretase inhibitor L-685,458 was used to inhibit the cleavage of the fluorescence substrates by the His-PS1-PEN-2-rho protein complex. The γ-secretase inhibitor was dissolved in DMSO and incubated in an ultrasonic bath to homogenize. L-685,458 was utilized in a gradient from 1 µM to 40 µM with a constant substrate concentration of 10 µM. The mixture was incubated at 37°C for 16 h. The fluorescence signal was measured with a Tecan plate reader at an excitation wavelength of 355 nm and an emission scan was collected from the wavelength of 400 nm to 480 nm. As shown in Figure 3.51 A, all controls which didn't contain substrate showed no fluorescence at all, indicating that only the Fluorogenic substrates can influence the fluorescence signals but not other components. Almost no fluorescence signal was detected in the SEC buffer containing the substrate, indicating that there were no interferers in the SEC buffer that affected the fluorescence signal. High fluorescence signals were detected in all His-PS1-PEN-2-rho tetramer complex and substrates mixtures, suggesting that the substrates were cleaved when incubated with the proteins. Figure 3.51

B showed the activity of each reaction by detecting the percentage of cleavage of the substrate and the reaction without DMSO or GSI was considered as 100% cleavage. But we didn't see significant differences between those curves with different concentrations of γ-secretase inhibitor and the DMSO control, suggesting that until 40 µM could not inhibit the cleavage of the substrates by the His-PS1-PEN-2-rho protein tetramer complex because of the tetramer state of the His-PS1 and PEN-2-rho protein, which could block the binding of the proteins and the inhibitors.
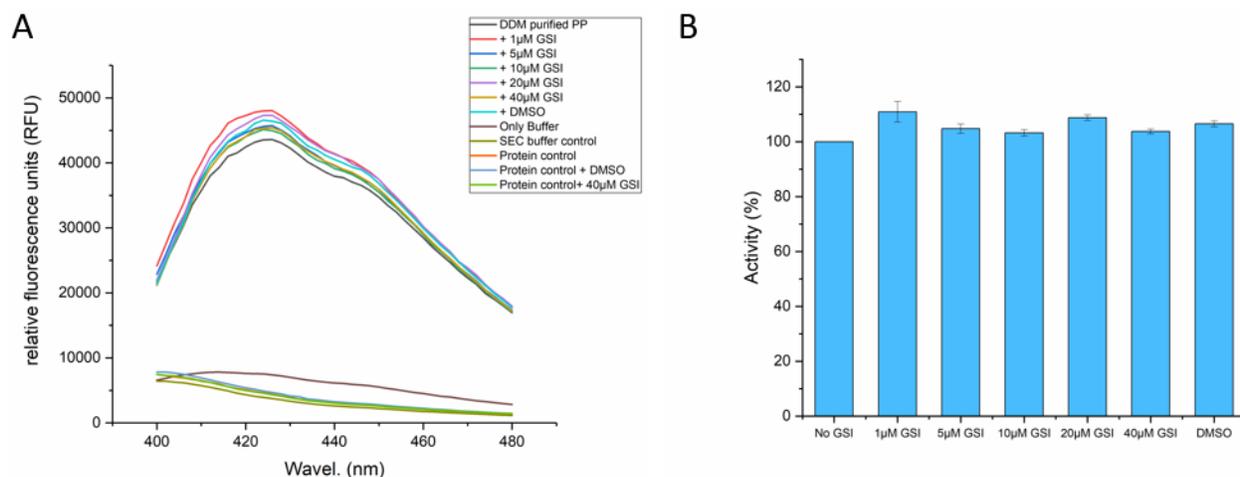
Figure 3.51 Activity assay of His-PS1-PEN-2-rho tetramer complexes with γ-secretase inhibitor L-685,458.

The γ-secretase inhibitor L-685,458 was used in a concentration gradient from 1 to 40 µM and DMSO was used as a control as it was used to solubilize the substrate. A: Fluorescence signal of substrate cleavage after 16 hours incubated. B: Activity of PP proteins expressed by the percentage of the cleaved substrates. All curves labeled with "control" mean no substrates were involved in the reactions. SEC buffer was also engaged as the negative control. PP: His-PS1-PEN-2-rho complexes. GSI: γ-secretase inhibitor

Since I did not see any inhibition of lysis at low concentrations of L-685,458, another γ-secretase inhibitor, III-31C, was used at concentrations of 5, 50, and 500 µM. L-685,458 was also used at 500 µM to check the inhibition. The reaction without inhibitors showed the highest fluorescence signal after 37 °C incubation overnight. The DMSO concentration in all involved samples was normalized to the concentration involved in the 500 µM inhibitor. As shown in Figure 3.52, the reaction with DMSO shows a 20% lower fluorescence signal compared to the reaction that contained only the protein complex and the substrate, implying that DMSO interfered with the

cleavage of substrates by the protein complex. The reactions containing 5 µM or 50 µM III-31C showed similar curves to the reaction with DMSO, indicating that low concentrations of inhibitor could not inhibit the cleavage of the substrate due to the tetrameric states of the complex. Both reactions containing 500 µM L-685,458 and III-31C demonstrated a significant decrease of 15-30% in fluorescence signal, suggesting that high concentration inhibitors influenced the cleavage of substrates. All collected fluorescence signals started from the same point, indicating that the differences in fluorescence signals were not due to the scattering by proteins. No significant fluorescence signal was detected in the SEC buffer containing substrates or in the reactions without substrates, demonstrating the absence of external contaminants which could affect the cleavage of substrates or signal detections.
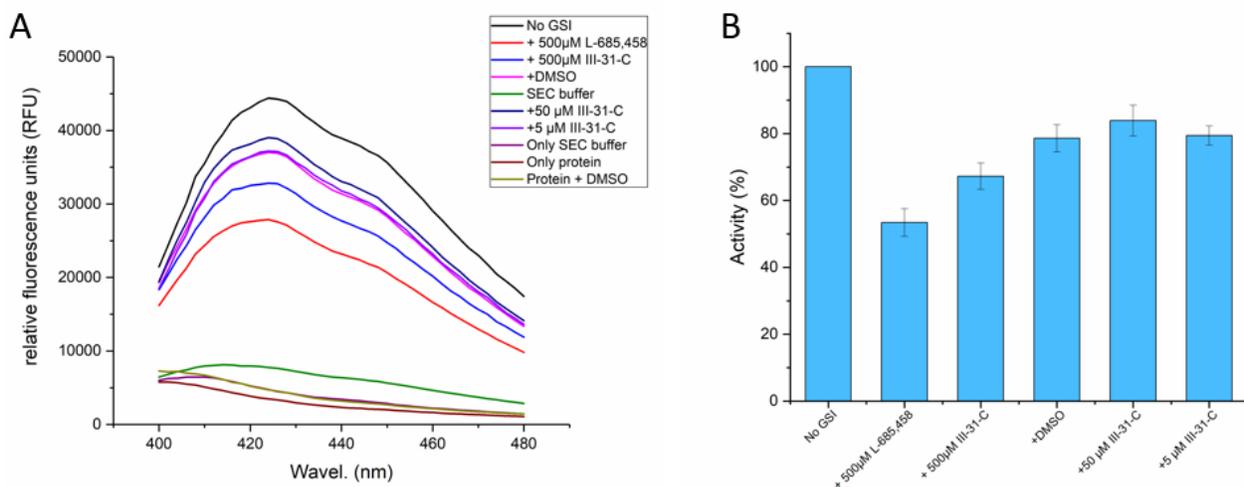
Figure 3.52 Activity assay of His-PS1-PEN-2-rho tetramer complexes with γ-secretase inhibitor III-31-C

The γ-secretase inhibitor III-31-C was used in a concentration gradient of 5, 50 and 500 µM and DMSO was used as a control as it was used to solubilize the substrate. SEC buffer was also engaged as the negative control. 500 µM of L-685,458 was also used in this experiment. A: Fluorescence signal of substrate cleavage after 16 hours incubated. B: Activity of PP proteins expressed by the percentage of the cleaved substrates. GSI: γ-secretase inhibitor

Cell membranes without Presenilin-1 and PEN-2 were used as a negative control, while the Proteinase K was used as the positive control because of the random cleavage of the substrates.

Cell membranes were incubated with the substrates in the presence or absence of EDTA at 37 °C. The fluorescence signals were measured every 1 hour using a Tecan plate reader. As shown in Figure 3.53, Proteinase K displayed a constant fluorescence signal at 440nm wavelength, indicating that Proteinase K demonstrated a high efficiency to cleave the substrates from the beginning and was sufficient as a positive control to show that all substrates are cleaved. No fluorescence signal was detected at the beginning in all other reactions, suggesting that the cleavage of the substrates in the cell membranes was not as fast as with Proteinase K. It also proved that the fluorescence signal would not be influenced by the fluorescence scattering from cell membranes. After 1 h of incubation, cell membranes containing His-PS1-PEN-2-rho began to show fluorescent signals at 440 nm, while the other reactions did not show any fluorescent signal, suggesting that the substrates started to be cleaved by the proteins. After 5hours of incubation, cell membranes containing His-PS1-PEN-2-rho in the absence of EDTA displayed almost the same intensity as Proteinase K, suggesting that the substrates were totally cleaved by the proteins in the membrane. The fluorescence signal was significantly decreased in the reaction containing His-PS1-PEN-2-rho with EDTA, illustrating that EDTA inhibited the interaction between the protein and the substrate and interfered with the cleavage of substrates. Cell membranes without His-PS1 and PEN-2-rho produced fluorescent signals from 2 h, but lysis was slow, and only very weak fluorescent signals were present after 5 h of incubation in the presence or absence of EDTA. After 16 hours of incubations, the cell membrane containing His-PS1-PEN-2-rho showed 100% cleavage of substrates in the absence of EDTA, while 80% of substrates were cleaved in the presence of EDTA. The cell membrane without His-PS1-PEN-2-rho only produce less than 20% activity which appeared to be the endogenous intramembrane protease activity from the cell membranes.
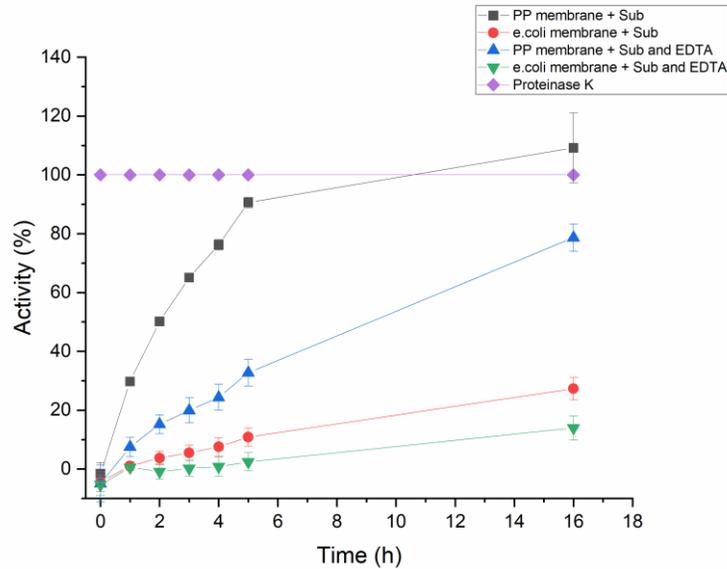
Figure 3.53 Activity assay of membrane fractions with and without His-PS1-PEN-2-rho expressed

Cell membranes of co-expressing His-PS1 and PEN-2-rho or not expressing PS1 and PEN-2 were measured the activity via fluorescence γ-secretase substrates. Two different buffer conditions were introduced while Proteinase K was used as the positive control, randomly cleaving the substrates. Cell membranes without substrates were performed to monitor the protein scattering. PP: His-PS1 and PEN-2-rho. +sub: with the substrate.

Different states of His-PS1-PEN-2-rho complexes (WT or DDAA mutant) have measured the activity with fluorogenic γ-secretase substrate (Figure 3.54). SEC fractions B2 which is the oligomeric states and B9 is the tetrameric states of the complexes. All protein amounts used here were normalized when incubated with the substrate. After overnight incubation at 37 °C, both tetramers of His-PS1-WT and PEN-2-rho complex and His-PS1-DDAA and PEN-2-rho complex showed high fluorescence signals, indicating that both the WT complexes and DDAA complexes possess potential γ-secretase activity, which was not I expected. The oligomeric state of both complexes showed a lower fluorescence signal than the tetrameric state, indicating that oligomeric state inhibited the activity.
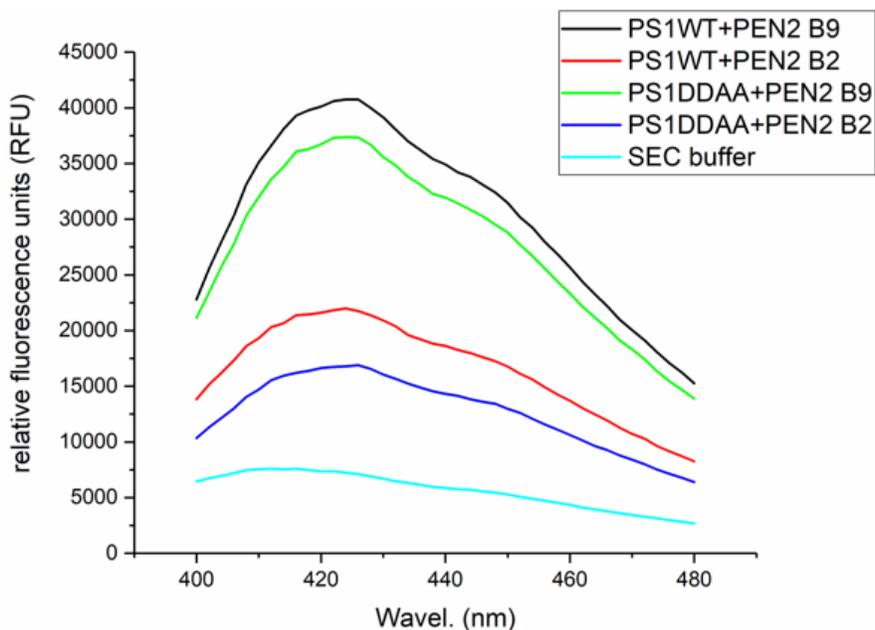
Figure 3.54 Activity assay of different states of His-PS1 (WT or DDAA mutation) and PEN-2-rho complexes

Activity assay of different states of His-PS1 WT or DDAA mutation and PEN-2-rho complexes. Protein amounts were normalized in every sample and mixed with 10 µM fluorescence substrates overnight. The emission wavelength was collected from 400 -480nm with 355nm excitation wavelength.

Due to the unexpected activity found for the DDAA mutant, it appeared to be contaminated in the purified samples. Therefore, common protease inhibitors are added to the reaction to determine conclusively whether contamination is present and what type of contamination is in place. General Cysteine protease inhibitor E-64 with the concentration of 10 µM, Aspartic protease inhibitor Pepstatin A (PepA) with the concentration of 1µM and 1mM Serine protease inhibitor AEBSF were used. Cell membrane without γ-secretase expressed was also used as the negative control. The amounts of cell membranes were normalized to the same concentration. Reactions were incubated on a Tecan plate reader at 37 °C for 16 hours. The signals at the wavelength 440nm were collected every 10 minutes and plotted. As shown in Figure 3.55 A and B, membranes with expressed His-PS1-PEN-2-rho complexes (WT or DDAA mutation) with E-64 and PepA showed similar profiles as the reactions without protease inhibitors which indicated that E-64 and PepA don't inhibit the reactions. However, AEBSF demonstrated a significant decrease when added to the reactions, suggesting that a serine protease may be participating in the reaction. The negative

control (Figure 3.55C) also showed a similar ratio but lower signals than WT or DDAA mutation, which may be due to the lower expression of membrane proteins in the cells. Interestingly, the lower signals in AEBSF reactions indicated that the contamination may come from proteins expressed by *E. coli*. The reaction of DDAA mutation reached equilibrium after 6h incubation while the reaction of WT got the equilibrium after 8h incubation. Figure 3.55 D&E showed the specific activity of His-PS1-PEN-2-rho complex in cell membranes. After 16 hours of incubations, 10μM substrates were 100% cleaved by both cell membranes with WT or DDAA mutant, while AEBSF inhibits 20% of cleavage. Cell membranes with DDAA mutants demonstrated a 0.025 U/L specific protein activity whereas cell membranes with WT gave a specific activity of 0.02 U/L. AEBSF inhibited all 3 reactions, indicating the serine protease contaminations existed. PepA protease inhibitor inhibited 25% of specific activity of cell membranes with WT protein but not in DDAA mutant, suggesting that His-PS1-WT and PEN-2-rho complex may exist γ-secretase activity in the *E.coli* cell membranes.
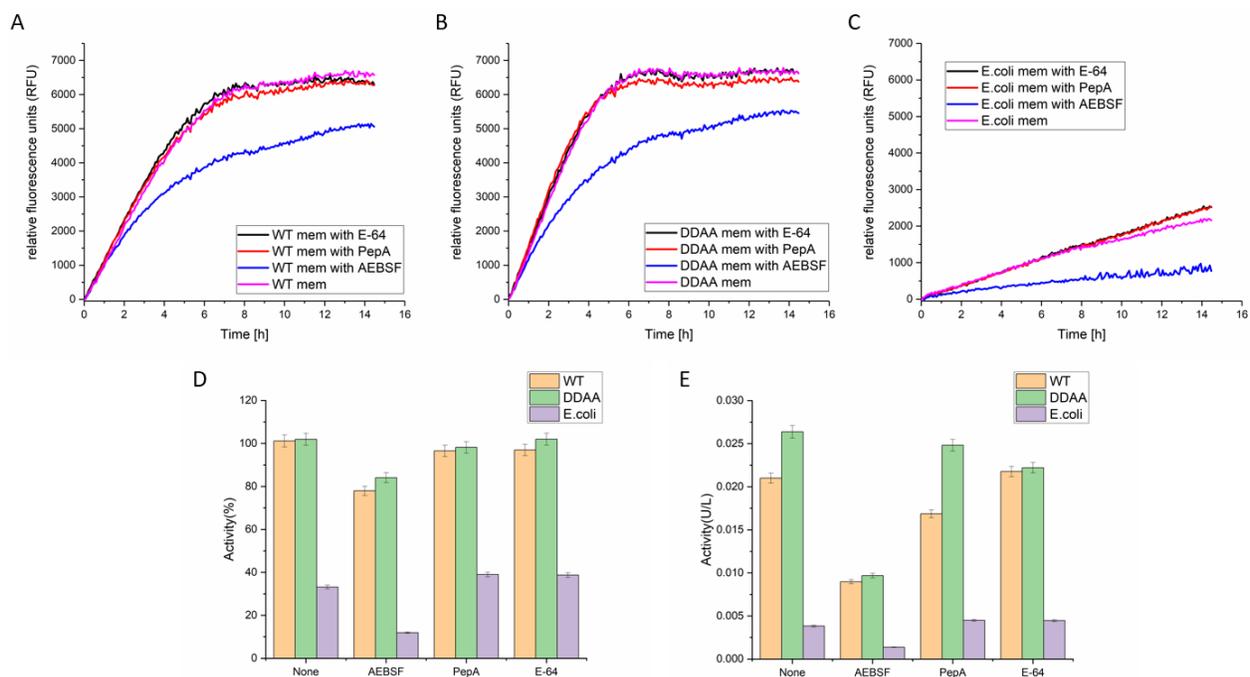
Figure 3.55 Activity assay of cell membranes with different common inhibitors

Activity assay of cell membranes with or without expressed His-PS1 (WT or DDAA mutation) and PEN-2-rho complexes in the presence or absence of common protease inhibitors. (A) Cell membrane containing His-PS1-WT and PEN-2-rho complex with or without common protease inhibitors. (B) Cell membrane

containing His-PS1-DDAA and PEN-2-rho complex with or without common protease inhibitors. (C) Cell membrane without γ-secretase in the presence or absence of common protease inhibitors. (D) Specific enzyme activity in cell membranes in the presence or absence of His-PS1-WT and PEN-2-rho complex with 10μM substrates. (E) The activity of cell membranes with or without His-PS1-WT and PEN-2-rho complex expressed by the percentage of the cleaved substrates.

The activity assay of purified His-PS1 (WT or DDAA mutation) and PEN-2-rho complexes with different common protease inhibitors were also performed and protein amounts were normalized. The plotted signals of WT (Figure 3.56A) and DDAA mutation (Figure 3.56B) demonstrated reactions similar to those in the membranes. Reactions involving AEBSF showed lower signals than the others. E-64 and PepA displayed only a slight decrease compared to the response without inhibitors. The WT reactions showed higher signals than the DDAA mutation, which may indicate that WT presented higher activity than the DDAA mutation. As with the reaction in the membrane, there was a significant inhibition of the reaction by AEBSF, but not by PepA, suggesting that there may be contamination by serine proteases and that the protein complexes may be inactive. The reactions inhibited by AEBSF reached equilibrium after 12h incubations, indicating the AEBSF inhibited the contamination activity or the binding to the proteins. A 50% cleavage was observed in WT protein with the specific activity of 1.2E-4 U/mg, while the DDAA mutant showed 32% substrate cleavage with the specific activity of 8.3E-5 U/mg. AEBSF inhibited more than 50% of substrates cleavage and yielded 7E-5 U/mg specific activity of WT and 3.2E-5 U/mg specific activity of DDAA. The initial velocities were calculated based on the fluorescence changes in first two hours (Figure 3.56 C). WT proteins demonstrated an initial velocity of approximately 6 nM/min while DDAA proteins illustrated an initial velocity of 3.5 nM/min. Protease inhibitors E-64 and Pep A didn't show significant inhibition of the activity but the serine protease inhibitor AEBSF exhibited strongly inhibition of the activities. The differences of WT protein and DDAA mutant were also shown in the graphs (Figure 3.56 D&E purple columns), indicating that WT protein existed significantly higher activity than DDAA mutant.
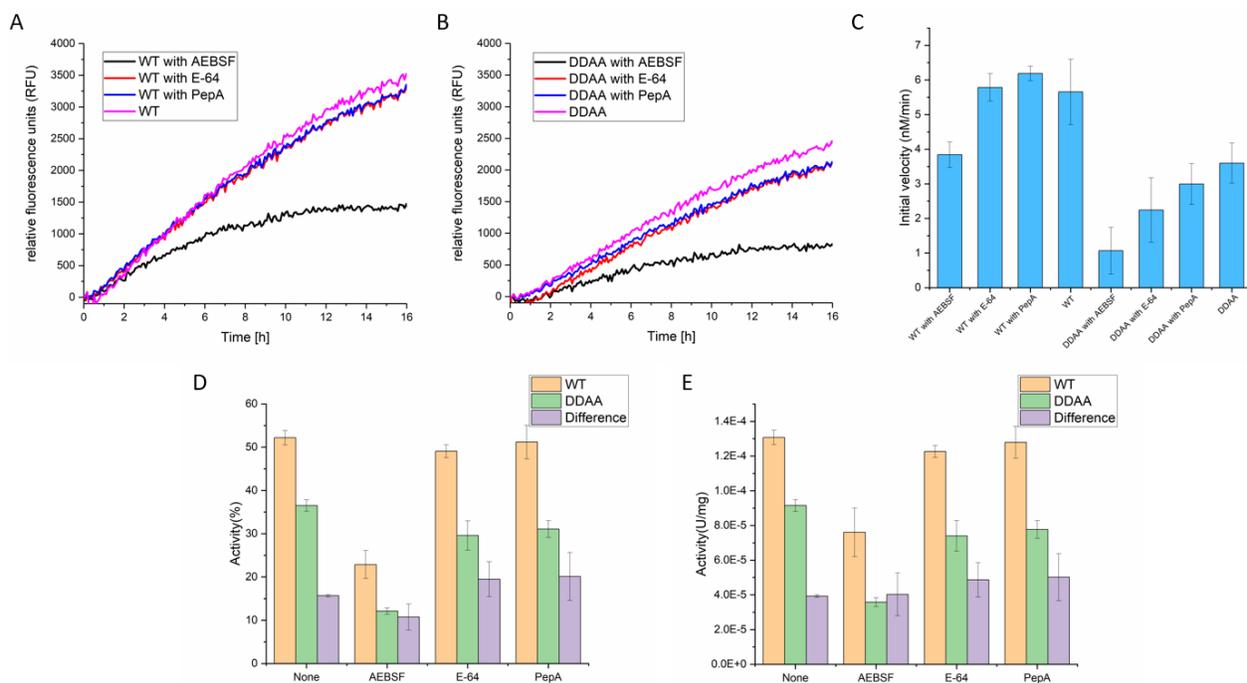
Figure 3.56 Activity assay of purified His-PS1 (WT or DDAA mutation) and PEN-2-rho complexes with different common inhibitors

Activity assay of purified PS1-PEN-2 complexes in the presence or absence of common protease inhibitors. (A) Purified His-PS1-WT and PEN-2-rho complex with or without common protease inhibitors. (B) Purified His-PS1-WT and PEN-2-rho complex with or without common protease inhibitors. (C) The initial velocity of reactions was determined by the fluorescence change in first two hours. (D) The activity of purified His-PS1-WT and PEN-2-rho complex (WT or DDAA mutant) expressed by the percentage of the cleaved substrates. (E) Specific enzyme activity in purified His-PS1-WT and PEN-2-rho complex (WT or DDAA mutant) with 10μM substrates. The difference between WT and DDAA also indicated in the graph C&D.

The far-UV CD and fluorescence spectra were measured for His-PS1 (WT or DDAA mutation) and PEN-2-rho. Temperature scanning from 4°C to 98 °C was measured with the increment of 2 °C and the selected data of several temperature points were plotted and shown in Figure 3.57. In far-UV CD spectra, the negative signals constantly decrease during temperature increases. The complete loss of α-helices happened after 60 °C. The fluorescence signal at the excitation wavelength of 295 nm rose during the temperature increase in the absence of cholesterol, while the emission peaks reduced, suggesting that thermally induced protein aggregation caused protein denaturation. Interestingly, the emission peak was decreased upon heating, but the 90° light scattering peak at a wavelength of 295 nm was slightly reduced, suggesting that thermally induced protein aggregation did not occur when cholesterol was involved. The emission peak of WT protein complexes without

cholesterol demonstrated a maximum at 326nm. When cholesterol was added, a blue shift of 2nm displayed in WT protein complexes indicated that more hydrophobic regions were buried in a hydrophobic environment. No peak maximum shift was detected after thermal denaturation in these two samples. The DDAA mutation illustrated a blue shift of 1nm compared to the cholesterol-free WT protein complex and a red shift from 325nm to 331nm during thermal denaturation, reflecting that the hydrophobic region of the protein is exposed to the solution and the differences in tertiary structure.
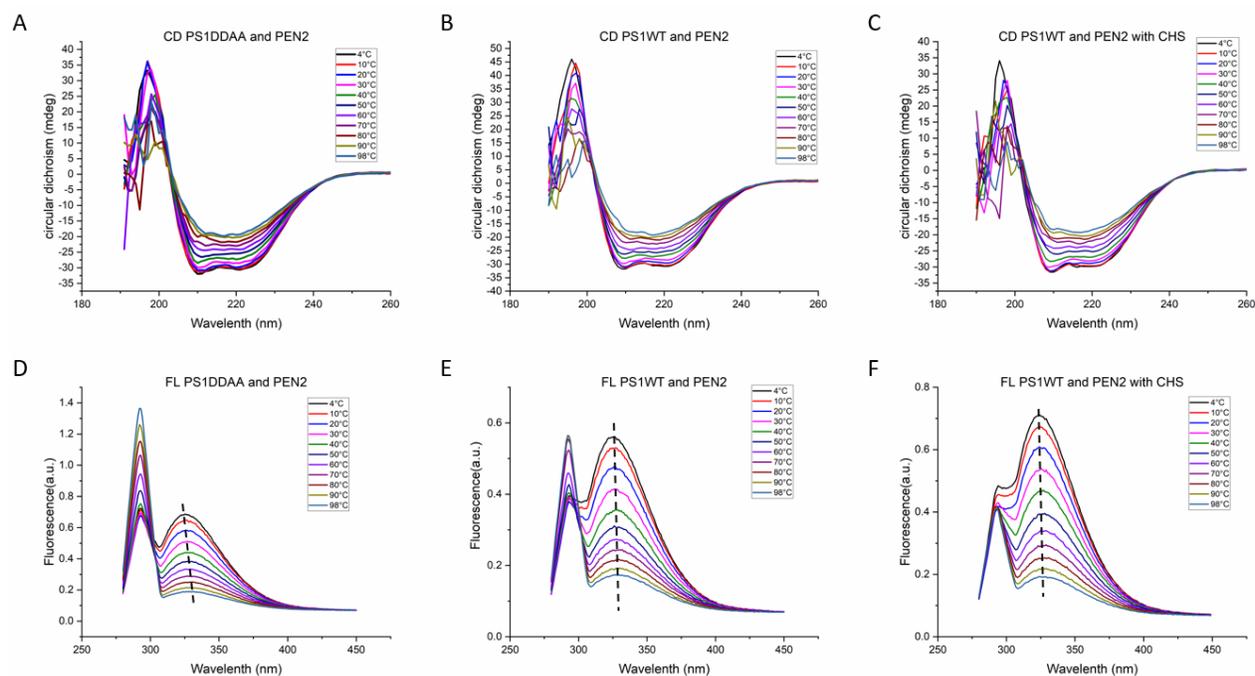
Figure 3.57 Far-UV CD and fluorescence spectra of His-PS1 (WT or DDAA mutation) and PEN-2-rho complexes.

Temperature scanning of His-PS1 (WT or DDAA mutation) and PEN-2-rho complexes from 4°C to 98 °C by Circular Dichroism Spectroscopy (A-C) and Fluorescence Spectroscopy(D-F). only spectra recorded at 4, 10, 20, 30, 40, 50, 60, 70, 80, 90, 98°C are presented.

CD deconvolutions were performed for all temperature scanning data and the α-helixes (Figure 3.58 A-C) or β- sheets (Figure 3.58 D-F) were plotted. The regular α-helices (helix 1) of all 3 protein complexes were significantly reduced starting from 55°C to 60°C, resulting in a decline in

the total helices. The total β-sheets content of all 3 protein complexes exhibited irregular fluctuations upon the decrease of the α-sheet.
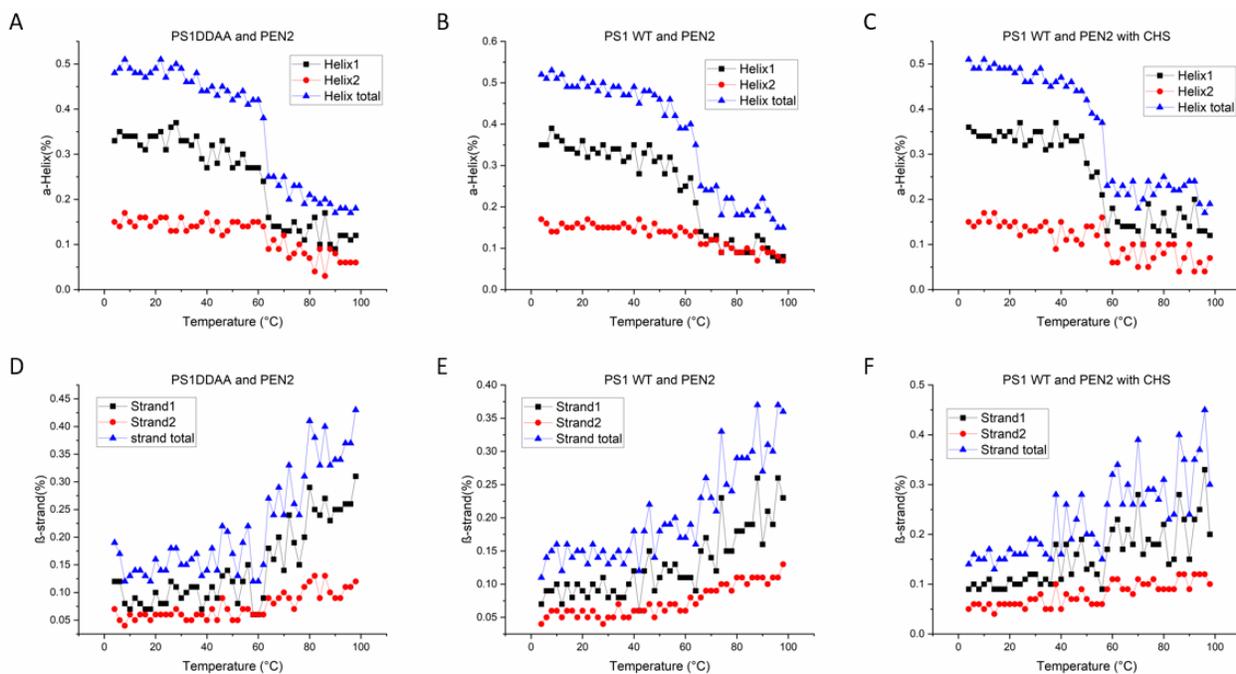
Figure 3.58 CD deconvolutions of His-PS1 (WT or DDAA mutation) and PEN-2-rho complexes.

CD deconvolutions of temperature scanning of His-PS1 (WT or DDAA mutation) and PEN-2-rho complexes from 4°C to 98 °C. The percentages of α-helices (A-C) and β-sheets (D-F) are recorded and plotted. Helix 1 or Strand 1 represents regular α-helices or β-sheets, while Helix 2 or Strand 1 refers to distorted α-helixes or β-sheets.

Deconvolutions of far-UV CD data obtained at 4°C before temperature scanning or cooling back to 4°C after finishing temperature scanning were analyzed by the online software DichroWeb . The secondary structures were shown in Table 3.5. His-PS1-PEN-2-rho complexes (WT or DDAA mutation) contain 49% α-helix which fits the predicted secondary structures where 226 residues in 487 amino acids of Presenilin-1 and 73 residues in 114 amino acids of PEN-2. Those indicated that the obtained complexes exhibited correct folding and no remarkable difference in secondary structures between WT and DDAA. The PS1-WT and PEN-2-rho complexes showed a 2% higher total α-helix content in the presence of cholesterol. Approximately 15% total β-sheets content was

obtained for all 3 samples. No significant differences between His-PS1 (WT or DDAA mutation) and PEN-2-rho complexes was observed. The PS1-WT and PEN-2-rho complexes exhibited a significant decrease of α-helices and an increase in β-sheets when cooling back to 4 °C after temperature scanning, while DDAA mutations display partial refolding upon cooling to 4°C after temperature scanning. The unordered structure was found to be increased by 12% points in DDAA during denaturation, compared to 16% points for WT in the absence of cholesterol and 19% in the presence of cholesterol.

Table 3.5 Deconvolutions of His-PS1 (WT or DDAA mutation) and PEN-2-rho complexes

	Helix1	Helix2	Strand1	Strand2	Turns	Unordered	Total	Helix total	Strand total
DDAA before macro	33%	16%	9%	6%	10%	25%	99%	49%	15%
DDAA after macro	19%	15%	11%	7%	12%	37%	101%	34%	18%
WT before macro	34%	15%	10%	6%	13%	22%	100%	49%	16%
WT after macro	13%	11%	14%	10%	13%	38%	99%	24%	24%
WT+CHS before macro	36%	15%	9%	5%	14%	20%	99%	51%	14%
WT+CHS after macro	12%	11%	16%	9%	13%	39%	100%	23%	25%

Before macro: samples were measured at 4°C before temperature scanning.
After macro: samples were measured at 4°C after temperature scanning.

All SEC fractions of His-PS1 (WT or DDAA mutation) and PEN-2-rho complexes were measured for far-UV CD and the deconvolutions were listed in Table 3.6. The α-helixes remain at around 50% in all SEC fractions from B9 to B2, while the β-sheets showed less than 5% differences in all fractions. Considering that the PEN-2 protein itself contains more than 70% of α-helices and that a higher PEN-

2 ratio occurs when the complexes form oligomers, the α-helices of the oligomers of the complex should theoretically be elevated. Due to the partial refolding happened in DDAA mutation but not in WT.

Table 3.6 Deconvolutions of each SEC fractions of His-PS1 (WT or DDAA mutation) and PEN-2-rho complexes

	Helix1	Helix2	Strand1	Strand2	Turns	Unordered	Total	Helix total	Strand total
WT B9	37%	13%	9%	9%	11%	21%	100%	50%	18%
WT B8	38%	12%	12%	8%	12%	18%	100%	50%	20%
WT B7	37%	15%	8%	7%	12%	21%	100%	52%	15%
WT B6	38%	13%	10%	8%	11%	20%	100%	51%	18%
WT B5	34%	14%	9%	7%	13%	23%	100%	48%	16%
WT B4	34%	13%	12%	7%	11%	24%	101%	47%	19%
WT B3	35%	14%	11%	6%	12%	22%	100%	49%	17%
WT B2	33%	15%	10%	7%	13%	23%	101%	48%	17%
DDAA B9	38%	12%	10%	10%	11%	21%	102%	50%	20%
DDAA B8	37%	13%	9%	8%	11%	21%	99%	50%	17%
DDAA B7	38%	14%	8%	8%	12%	22%	102%	52%	16%
DDAA B6	39%	12%	10%	9%	11%	19%	100%	51%	19%
DDAA B5	37%	12%	10%	8%	13%	21%	101%	49%	18%
DDAA B4	38%	12%	11%	9%	12%	19%	101%	50%	20%
DDAA B3	38%	12%	11%	8%	11%	20%	100%	50%	19%
DDAA B2	35%	15%	8%	7%	11%	23%	99%	50%	15%

The thermal stability of His-PS1 (WT or DDAA mutation) and PEN-2-rho complexes was calculated based on the far-UV CD signals at wavelength 208nm collected from the temperature scanning (Figure 3.59A) and the total α-helices which were collected from the heat-induced protein unfolding (Figure 3.59B). Both WT and DDAA protein complexes without cholesterol showed similar melting temperatures (Tm) slightly above 60 °C in both analyses. Superingly, there was a noticeable decrease in the Tm of the WT protein complex when cholesterol was involved and the Tms were observed at 56.3 or 54.4°C.
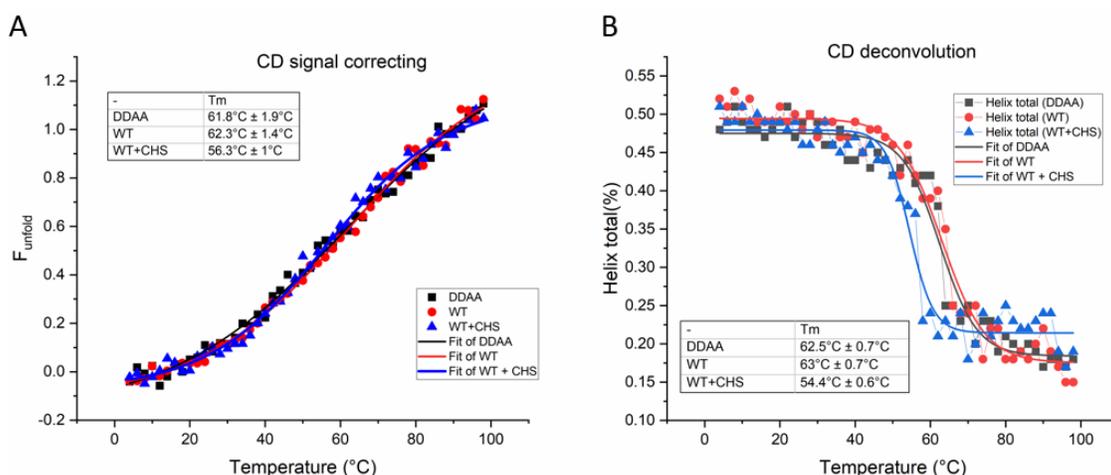
Figure 3.59 Thermal stability of His-PS1 (WT or DDAA mutation) and PEN-2-rho complexes.

(A)Thermal stability based on far-UV CD signals at wavelength 208nm of each temperature. (B) Thermal stability based on the total α-helices changes by deconvolutions of far-UV CD signals of each temperature.

The further assessment by MST experiments was performed to determine the interactions of the obtained protein complexes with the other two γ-secretase sub-units and the substrates. His-PS1 (WT or DDAA mutation) and PEN-2-rho complexes were labeled with NT647-NHS dye and titrated with serially diluted unlabeled ligands. According to the Capillary Type Check step, 20nM WT complexes and 25nM DDAA complexes were used and all ligands do not show any fluorescence signal, which didn't interfere with the measurements. All data analyses are based on the initial fluorescence signals but not MST signal due to the ligand-induced changes indicating a conformational change in protein binding to the ligand. It was also confirmed by SDS denaturation

test (data are not shown). Titrated to up to 10µM MBP-APPC (Figure 3.60A), WT complex was observed to have a dissociation constant (Kd) of 650nM ± 174.19 nM, whereas DDAA complexes showed a Kd of 216.13nM ± 36.275 nM. Both WT and DDAA displayed a high Kd of 2.3µM ± 1µM and 1.85µM ± 0.78µM when titrated with APP-C99 with the concentration up to 11µM (Figure 3.60C). Up to 12µM purified Nicastrin were titrated to labeled WT or DDAA complexes, resulting in a Kd of 783.44nM ± 179nM and 272.45nM ± 47.214nM (Figure 3.60B). FleBt-APH-1 with the highest concentration of 9.7µM exhibited the highest binding capacity with labeled WT and DDAA complexes with the Kd of 83.64nM ± 50nM and 33.155nM ± 10.48nM (Figure 3.60D).
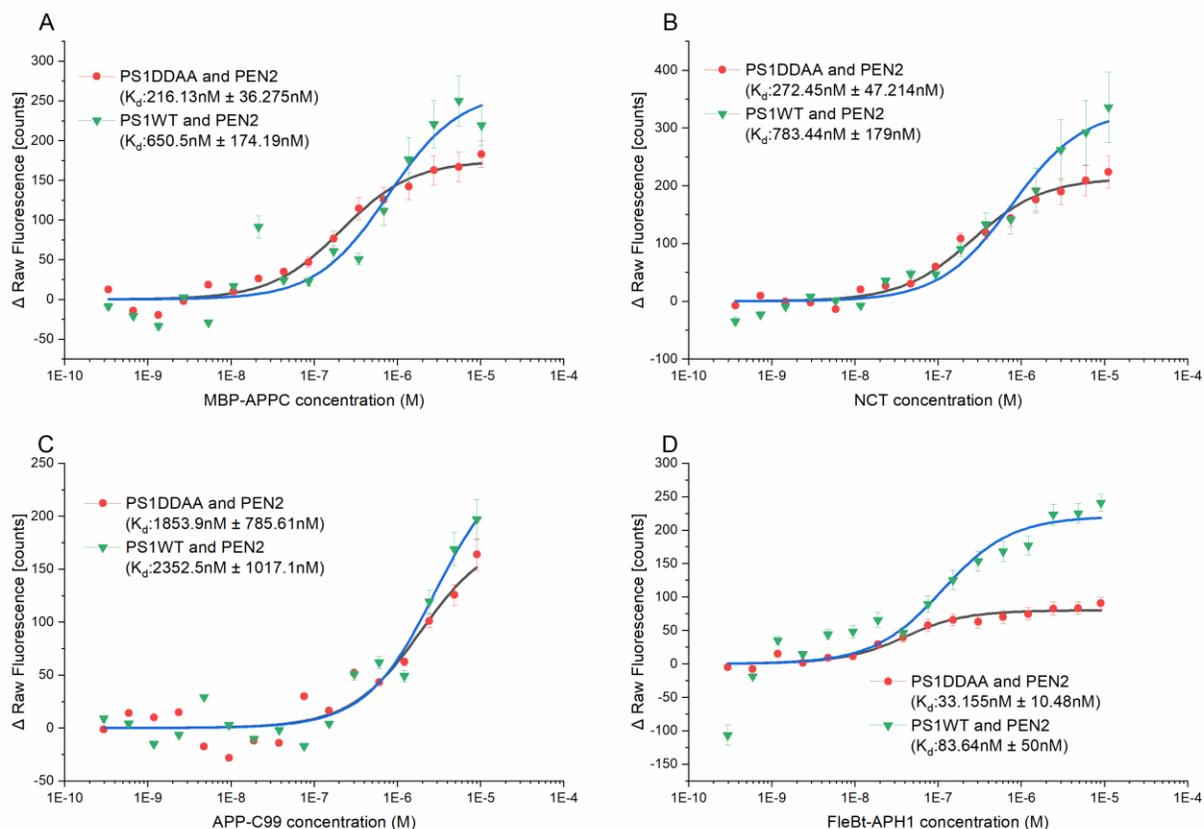
Figure 3.60 MST of His-PS1 (WT or DDAA mutation) and PEN-2-rho complexes with other γ-secretase subunits and substrates.

Microscale thermophoresis of DDM purified His-PS1 (WT or DDAA mutation) and PEN-2-rho complexes with 10µM γ-secretase substrates MBP-APPC (A) and 11µM APP-C99 (C) and the γ-secretase subunits Nicastrin (B) with 12 µM and FleBt-APH-1 (D) with 9.7 µM were also involved.

4. Discussion

Although there are plenty of studies on the activity and structural analysis of the γ-secretase, the mechanism of the assembly of the γ-secretase complex and the role of the complex in Alzheimer's disease are not very clear. Therefore, I isolated the PS1-PEN-2 complex, which is the minimal catalytic units of γ-secretase, from *E.coli* under various conditions including tag-solubilization, detergent solubilization and DIBMA solubilization. The obtained PS1-PEN-2 complex in detergent environment was used for secondary and tertiary structure analysis using CD spectrum. The specific γ-secretase activity of the complex was detected by the cleaved fluorogenic γ-secretase substrate.

4.1 Confirmation of the existence of co-expressed PS1-PEN-2 complexes *in vivo*

The interactions of the PS1 and PEN-2 proteins were detected *in vivo* by fusing with Split-superpositive GFP and measuring the fluorescence signal at the excitation wavelength of 488 nm. Positive signals confirmed the interaction of the PS1 and PEN-2 proteins *in vivo*, but surprisingly, both fusions of cGFP to the N-terminus and C-terminus of the PEN-2 protein showed interaction with nGFP-tagged PS1 (Figure 3.24). Although the PEN-2 protein was observed in multiple topologies[56,112,113,193], the C-terminus of PEN-2 is supposed to be exposed to the extracellular side whereas the N-terminus of PS1 should face to the opposite site of the membrane layers. The first atomic cryo-electron microscopy structure (PDB code: 5A63) shows that TM1 of PEN-2 enters the membrane halfway from the cytoplasm, which fits to the interactions between N-terminal fused cGFP to PEN-2 and N-terminal fused nGFP to PS1. The C-terminal domain of PEN-2 is essential for stabilizing the γ-secretase complex while the first TM is critical for the PEN-2 mediated endoproteolysis of PS1[66,91,194]. But the cGFP at the C-terminus of the PEN-2 showed interaction with the nGFP at the N-terminus of the PS1. This may be due to the elongation of the C-terminus of PEN-2 leading to a conformational change of PEN-2 in the complex with PS1 protein, though most likely it indicates that PS1 binds PEN-2 in both the possible orientations.

4.2 Isolation of co-expressed PS1-PEN-2 complexes

4.2.1 DIBMA-lipids-PS1-PEN-2 complex

The use of the diisobutylene maleic acid (DIBMA) copolymer is a specifically interesting approach to solubilize membrane proteins directly from membranes replacing the use of SMA polymers because, due to the aliphatic characters, it won't interfere with protein measurements in the far-UV range of the spectrum.[195,196] DIBMA polymers can solubilize membrane proteins as lipid complexes by forming large protein-lipids nanodiscs with varying sizes, which is superior to SMA-lipid-protein discs of constant size[197]. The *E. coli* rhomboid protease GlpG have been reported to be stable and functional in the lipid nanodisc when using DIBMA, indicating that DIBMA is a useful tool for membrane protein structural and functional analysis[198]. In my study, the His-Presenilin-1 and His-PEN-2 were successfully co-expressed and purified in a DIBMA solubilized form (Figure 3.26). After removing the His-tag from His-PS1 by thrombin protease cleavage and His-tag affinity chromatography purification, unlabeled PS1 was detected in the elution sample, indicating that the PS1 protein interacts and forms a complex with His-PEN-2 protein (Figure 3.28). SEC purification showed a 574kDa peak (Figure 3.27) and in DLS experiments displayed a ~19nm particle size which is consistent with the size of a DIBMA-lipid-protein complex according to literature [199,200]. No specific fragmentations into PS1-NTF and PS1-CTF were observed due to the oligomerizations of the complexes which prevents the endoproteolysis of PS1.

4.2.2 Detergents solubilized PS1-PEN-2 complexes

In order to separate the PS1-PEN-2 complexes easier, different purification tags were introduced to the two proteins. The His-PS1-PEN-2-rho proteins were successfully co-expressed in *E.coli* with a high expression level and only a small part of protein accumulated in the inclusion bodies (Figure 3.31). 1% CHAPSO solubilized 25% of total proteins and 33% were solubilized by 0.5% DDM from membrane fraction, whereas 1% Fos-14 could solubilize about 100% of the proteins (Figure 3.32 and Table 3.3).In comparison, SMA, DIBMA or modified DIBMA polymers could only solubilize less than 10% of the total proteins with the target proteins hardly detectable on Western blot, which may be due to size of the PS1-PEN-2complex. The complex formation was confirmed using affinity chromatography pull-down by detecting the PEN-2-rho protein in the elution after His-tag affinity chromatography purification, indicating that the PEN-2-rho protein was bound to

the His-PS1 protein (Figure 3.34). This interaction was confirmed *in vivo* by Split-superpositive GFP.

The CHAPSO solubilized PS1-PEN-2 complex displayed several peaks (Figure 3.35) after His-tag affinity chromatography purification followed by size exclusion chromatography with the molecular weights of 1285 and 323 kDa, which refers to a higher oligomer and a tetramer of the complex. No specific fragmentations were observed which may be due to the CHAPSO-induced aggregations. Fos-14 solubilized PS1-PEN-2 complexes showed several peaks with the molecular weight of 1037, 273 and 93 kDa (Figure 3.36), indicating a higher oligomer, a tetramer, and a dimer. The same situation occurred with Fos-14 solubilized protein complexes where no fragmentations of PS1 were observed, which may be due to (i) oligomerization states that interfered with self-activation or (ii) the Fos-14 detergent which lead to membrane protein destabilization and unfolding, thus the Fos-14 solubilized complex didn't show self-activation.

DDM-solubilized His-PS1-PEN-2-rho complexes yielded >5mg purified proteins per liter culture and displayed two major peaks in addition to the dead volume peak (Figure 3.37). They showed the molecular weights of 548 and167 kDa, which refers to a higher oligomer and a tetramer of the complex. Surprisingly, the fragmentation into PS1-NTF and PS1-CTF was observed on SDS-PAGE in this condition, showing that DDM different from Fos-14 allows the Presenilinase activity. The PS1-NTF was observed on the Western blot, showing that PEN-2 correctly interacts with PS1 and activates the PS1 protein endoproteolysis into NTF and CTF fragments. The native PAGE confirmed the His-PS1-PEN-2-rho protein complex and revealed a band above the 146kDa standard which fits the apparent molecular weight for the SEC fraction. LC-MS/MS identified the NTF and CTF fractions, confirming that the PS1 protein underwent specific endoproteolysis. The His-PS1 protein in the oligomerized complex didn't undergo endoproteolysis obviously because of steric hindrance, Confirming the earlier hypothesis that oligomerization prevents activation. The ratio of His-PS1 to PEN-2-rho in the two peaks was verified by measuring the abundance of the protein on SDS-PAGE (Figure 3.44 and Table 3.4). The ratios were found to be 1:6 for the oligomeric state and 1:1 for the tetrameric complex. The 1:1 ratio in tetrameric complex indicated that two presenilin-1 protein and two PEN-2 protein formed the tetramer complex. Interestingly, the crystal structure of a presenilin homologue (PSH), which is highly conserved to Presenilin-1 in γ-secretase, from archaeon Methanoculleus marisnigri JR1 expressed in *E.coli* demonstrated a tetrameric complex as well (PDB code: 4HYG) [110]. These suggest that the subcomplex likewise adopts a similar

tetrameric state to cover the hydrophobic region as it is found in the intact γ-secretase complex. The co-expressed His-PS1-PEN-2-rho protein complex with individual Rho-tag affinity chromatography purification showed two major peaks. The first one referred to the complex and the other one was the PEN-2-rho protein peak, indicating that the PEN-2-rho had a higher expression level than the His-PS1 protein when co-expressed. Double tag purifications were performed with His-tag affinity chromatography, followed with Rho-tag affinity chromatography, and exhibited a single peak with the molecular weight of 616kDa, which was confirmed by native PAGE (Figure 3.42). Unexpectedly, the tetramer complex didn't bind to the matrix during Rho-tag affinity chromatography purification, implying that the C-terminus of PEN-2-rho, where the rho-tag located, was inaccessible and hidden in the complexes: According to the structure of the γ-secretase complex, TM4 of PS1 packs against TM1 and TM3 of PEN-2 while TM8 and TM9 of PS1 extensively interact with APH-1 (Figure 4.1) [112,113]. My interpretation of the formation of tetramers is that in the absence of APH-1 and Nicastrin, the PS1-PEN-2 complex dimerizes by the interactions of the free hydrophobic surface. The involvement of cholesterol helps to decrease the formation of the oligomerization states, which is consistent with the literature regarding membrane proteins[192].
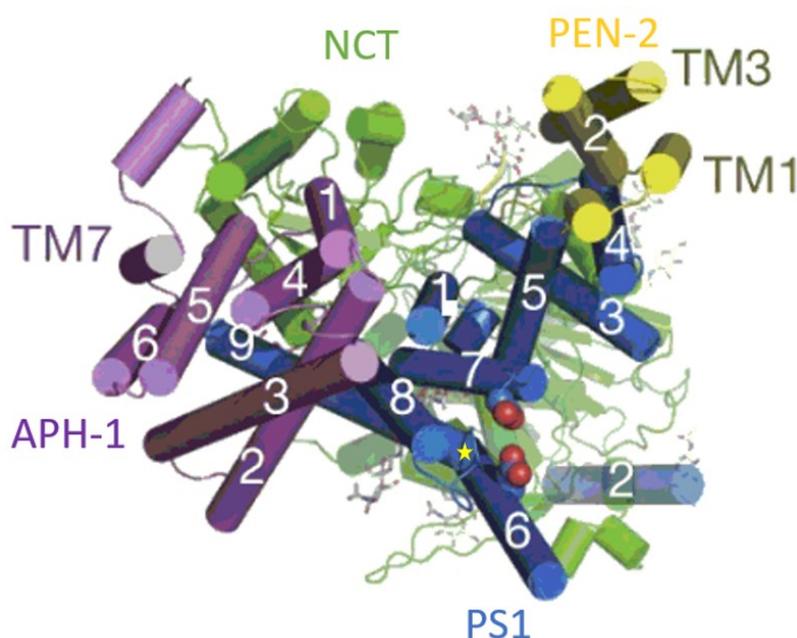
Figure 4.1 cryo-EM structure of γ-secretase complex (picture adapted from [113])

The cryo-EM structure of γ-secretase complex with respective TM labeled. APH-1 labeled with purple color. NCT marked with green color. PEN-2 labeled with yellow color and PS1 marked with blue color. The yellow star indicates the PAL motif in PS1.

4.3 Reconstitution of Fos-14 purified γ-secretase PSs and PEN-2 protein

It is known that detergents help to obtain large amounts of high-quality membrane proteins but also often lead to a loss of function of these proteins. Previous studies by Dr. Kun Yu showed that the Fos-14 detergent could prevent the interaction between the PS1 and the PEN-2 protein[201]. Amphipathic molecules and detergents contain both hydrophilic and hydrophobic regions that significantly affect the extractions and purifications, which often allows of the membrane proteins to be obtained in a good yield and quality. Though detergents can help producing large amounts of high-quality active γ-secretase, lipid components have proven to be essential for γ-secretase activity as well[202,203]. Previous studies in our laboratory showed successful expressions of γ-secretase sub-units *in vitro* into MSP nanodiscs. Here, I attempted to assemble γ-secretase sub-complexes in the lipidic environment and reconstitute the detergent-solubilized individual γ-secretase sub-unit Presenilin-1 or Presenilin-2 or PEN-2 into the native environment.

The Presenilin-1 mutant PS1-M292D-thrombin, which is supposed to be active without activation by endoproteolysis of the PS1 protein, was successfully reconstituted into MSP1D1 nanodiscs (Figure 3.7), as confirmed by co-elution of untagged MSP1D1 protein with Presenilin-1 protein by His-tag affinity chromatography. The Fos-14 purified PEN-2 protein was also successfully integrated into MSP1D1 nanodiscs based on the similar protein intensity distribution of PEN-2 and MSP1D1 on the Western blot and blue silver stained SDS-PAGE (Figure 3.8).

However, MSP nanodiscs exhibit well-defined dimensions and retain at least one internal lipid layer to form stable complexes with proteins resulting in a limit on the size of the insertable membrane proteins[204]. The PS1-PEN-2 proteins may face the problem of self-aggregations during bio-beads absorption, resulting in the inability of the protein complex to enter the naondiscs.

Meanwhile, oligomerizations of the PS1 or PEN-2 protein may also prevent proper complex formation.

Amphipols are amphipathic polymers that can possess a high affinity for the transmembrane regions, allowing the solubilization of membrane proteins in aqueous solutions in a detergent-free manner.[141]. They have been proven to be an important tool for EM investigations of the structure of membrane proteins. The first near-atomic resolution structure of human γ-secretase was obtained in amphipols[105,113]. Successful reconstitution of Presenilin-2 monomers into Amphipol polymers was confirmed by Western blot where the PS2s were detected in the presence of Amphipol polymers in the supernatant after bio-beads absorption but not in the pellet (Figure 3.9). Meanwhile, the PS2 protein was precipitated in the pellet in the absence of Amphipol polymers after bio-beads absorption, indicating the success of bio-bead absorption. The higher intensity of the monomeric bands observed on Western blot when lipids were involved suggests that lipids prevent the proteins from forming SDS-resistant oligomers.

Given the drawbacks of reconstitution of several proteins into nanodiscs or amphipols, liposomes would be the best choice for reconstitution due to the relatively large surface area of liposomes for the insertable membrane proteins [205]. To date, several studies have provided evidence that lipids are essential for γ-secretase activity. *E.coli* lipids do not support γ-secretase activity and have been proven to cause loss of function in the reconstitution of purified γ-secretase into *E.coli* lipid extracts. Therefore, apart from missing lipids, it should be the high content of PE in *E.coli* lipid extracts that abolishes activity[203]. PS1ΔE9 and other PS1 variants expressed in bacteria fused with the MBP tag were successfully reconstituted into liposomes and displayed the γ-secretase activity with a lipid mixture of egg PC: Total Brain Lipid Extract at a ratio of 70:30 (w/w)[61]. In addition, the lipidome associated with the γ-secretase complex is necessary for its integration and activation[206]. Therefore, the reconstitution of the single subunits PS1 and PEN-2 purified by Fos-14 detergent was considered to be essential. These proteins were successfully reconstituted into liposomes (Figure 3.10) with the lipids mentioned in the literature[61]. The proteins were confirmed to be in the liposome membrane by sucrose gradient ultracentrifugation. No fragmentations into PS1-NTF and PS1-CTF were observed on Western blot, indicating that Presenilin-1 didn't have Presenilinase activity during reconstitution. The probable reason might be that low CMC detergents like Fos-14 are harder to remove than high CMC detergents, therefore there might be some Fos-14 left after bio-beads absorption which prevents the interaction of PS1 and PEN-2.

4.4 Reconstitutions of MBP-tag fused PS1 and PEN-2 protein

Fos-14 is a known stringent detergent that may interfere with the protein structures and be hard to remove which may detrimental to reconstitution into polymers or liposomes[202]. The solubility problem in low concentrations of detergents can also be overcome, at least partially, by the use of a solubility tag. These tags have been used for a long time to increase the expression level and solubility of insoluble proteins. The MBP-tag has been applied in functional research of γ-secretase[61,207]. Here I labeled all γ-secretase subunits with the MBP-tag and tried to obtain the detergent-free γ-secretase subunits, which would be easier to be reconstituted into liposomes. I first cloned all sub-units individually into the pMAL-p4x vector purchased from NEB, which leads to the expression of the protein in the periplasm. Western blotting results showed that most of the protein accumulates in the membrane fraction and only a small fraction of the protein remains in solution (Figure 3.12). Although many MBP-fused membrane proteins are reported to be soluble, the γ-secretase subunits with MBP labeled still require a membrane environment to be stable. Moreover, all constructs exhibited heavy degradation, whether dissolved in the supernatant or buried in the membrane fractions, indicating that these constructs were not stable. Because of the lower expression levels observed in all constructs, it is unlikely that the degradation problem is due to protein aggregation.

No full-length MBP-PS1 was observed after detergent-free purification. a degradation into two distinct fragments of ~75kDa and ~25kDa, which are not the correct presenilinase activity products, indicated that MBP-PS1 expressed in the periplasm is unstable in the detergent-free condition or it acts as a specific Presenilinase with a changed cleavage site (Figure 3.11). In contrast, the MBP vector obtained from Dr. Oliver H. Weiergräber was used to express MBP-tag fused γ-secretase subunits into the cytoplasm. This vector combined with the mutation pair A215H/K219H should enhance MBP solubility and increased crystallizability [208]. Part of the MBP- fused PS1 was located in the inclusion bodies, indicating that the MBP tag is not sufficient to insure solubility of the protein. The full length MBP-PS1 and MBP-PEN-2 were obtained with detergent-free purification and yielded 2mg per liter cell culture for both fused proteins but several degradation bands were detected on the Western blot, indicating that MBP- mediated detergent-free membrane proteins are

not as stable as detergent purified (Figure 3.14).Therefore, the pH difference between periplasm and cytoplasm appears to be the likely cause for the different fragmentaions.

Partially purified full-length MBP-PS1 and MBP-PEN-2 were reconstituted into DMPC liposomes to test the interactions when MBP-labeled (Figure 3.15). The empty liposomes layer showed lower density than the proteoliposomes in the sucrose cushion, confirming the success of the reconstitution. No specific fragmentations into PS1-NTF and PS1-CTF were observed, indicating that MBP-PS1 didn't have Presenilinase activity. The possible reason could be that (i) MBP protein may interfere with the conformation of proteins, (ii) MBP-PEN-2 could not activate MBP-PS1 due to the incorrect folding of PEN-2 protein, (iii) Most proteins were lost during bio-beads absorption, which may prevent the interactions. or (iv) The main problem is the random orientation MBP-PS1 and MBP-PEN-2 insertion into liposomes, which reduces the proper interaction. Due to those potential problems, the MBP-tag fused γ-secretase subunits are not suit for assembly of γ-secretase complexes.

4.5 Overexpression of APH-1 in *E.coli*

APH-1 protein contains seven transmembrane domains and acts as the γ-secretase stabilizer[60,209]. It has been reported that APH-1 can be stably expressed in mammalian cells, though reports of isolation of the purified APH-1 protein are missing [71,75]. Thus, isolation of full-length APH-1 appeared to be an essential step to research the mechanism of how APH-1 stabilizes the γ-secretase complex or if it may be required to obtain activity. I successfully expressed the full-length APH-1 protein in both BL21 (DE3) and C43 (DE3) strains of *E. coli* (Figure 3.17), though the expression level was low in BL21 (DE3) and almost undetectable in C43 (DE3) strain. The previous Ph.D. student Dr. Kun Yu has already observed low expression level and instability of the APH-1 protein[201] . Interestingly, APH-1 can be expressed in C43 (DE3) only in the presence of cholesterol added to the medium, indicating that cholesterol helps the proper folding and stability of APH-1. I fused APH-1 with the MBP tag and obtained the stable full-length MBP-APH-1 from the membrane pellet which was solubilized by Fos-14, suggesting that the MBP tag increased the APH-1 expression level and stability. But most of the MBP-APH-1 protein located in inclusion bodies and only sparingly in the membrane fractions and supernatants, demonstrating that the MBP fusion tag is not sufficient for solubilization of MBP-APH-1

The Yersinia-derived truncated flagellin FleB (FleBt, residues 54 to 332) was used as a soluble tag for fusion with APH-1 protein as well [210] and showed slightly lower expression levels than the protein fused to MBP tag (Figure 3.19). Part of FleBt-APH-1 protein still accumulated in inclusion bodies, but some protein was found in the membrane fraction, illustrating that the FleBt tag contributes to the correct folding of APH-1 more than the MBP-tag. Most FleBt-APH-1 protein can be solubilized from the membrane by mild detergents as efficiently as by Fos-14 detergent which is different from the MBP-APH-1 case (Figure 3.20), suggesting that the FleBt tag efficiently increases the solubility. This is also reflected by the higher yield of detergent-free FleBt-APH-1 than MBP-APH-1 in the supernatant (Figure 3.19). Isolation of full-length FleBt-APH-1 was confirmed by LC-MS/MS (Figure 3.23). I observed that almost all the FleBt-APH-1 protein to be not degraded.

4.6 Biophysical characterization of the PS1-PEN-2 complexes

The primary structure of the PS1-PEN-2 complex was analyzed by LC-MS/MS and the secondary structure of the complex was determined by CD spectroscopy. The tertiary conformation of the complex was investigated by fluorescence spectroscopy and the quaternary structure of the complex was monitored on SEC. Fluorescence spectra showed a constant signal decrease of the emission peak and an increase in the excitation peak of WT or DDAA complexes in the absence of cholesterol during heating (Figure 3.57), demonstrating that the complexes faced thermally-induced protein aggregation caused by protein denaturation. In contrast to that, the excitation peak during thermal denaturation decreased slightly in the presence of cholesterol, implying the involvement of cholesterol prevented protein aggregation and reduced thereby scattering. The maximum emission wavelength varied from 324nm to 326 nm for all these samples and revealed that the tryptophan side chains are buried in a hydrophobic microenvironment. The DDAA mutant displayed a maximum emission shift from 325nm to 331nm during heating, demonstrating the exposure of tryptophan during thermal denaturation. No such shift was observed in WT complexes. There are 8 tryptophan residues in PS1 and 5 of them are in the hydrophobic regions: 1 in TM3, 1 in TM4, 2 in TM6 and 1 in the autoinhibitory loop. The observed maximum emission shift in the DDAA mutant suggests that the relevant TMs are moved during thermal denaturation and the autoinhibitory loop is exposed to the solvent. The differences in the maximum emission in WT or DDAA showed that there were different tertiary structures.

The TM2 of PS1 was claimed to be unobservable in the cryo-EM structures because of high flexibility, but to become ordered when PS1 with mutated catalytic residues was used or upon substrate binding [211,212],but TM2 does not contain a tryptophan residue. Therefore, a possible movement of TM2 cannot be linked to the observed changes in fluorescence.

Accessing the mutant for possible secondary structure, deconvolution of the far-UV CD spectra revealed 50% α-helical content in both WT and DDAA mutant complex (Figure 3.58 and Table 3.5), which is consistent with the resolved cryo-EM structures[105,113]. Previous studies in our laboratory showed 37% α-helical content in the Fos-14 purified single PS1 protein, which fits to the resolved structures[213]. However, the Fos-14 purified single PEN-2 protein showed 60% α-helical content [201] which was lower than 72% α-helical content in the resolved structure, which indicates that the conformation of PEN-2 is changed upon interaction with PS1 and that the here obtained His-PS1-PEN-2-rho protein complex is correctly folded.

Interestingly, the DDAA mutant showed a higher recovery rate than the WT complex after heating, probably due to slower speed of aggregation of DDAA than WT protein during thermal denaturation, which provides further evidence for different tertiary structures of WT and DDAA mutant. Deconvolutions of the far-UV CD spectra of all SEC fractions (Table 3.6) showed that the different complexes (oligomers) of PS1 and PEN-2 with stoichiometry of 1:1 to 1:6 are characterized by different fractions of α-helical structure, which indicates that either part of the PEN-2 or the PS1 lost α-helical structure.

The thermal stability of His-PS1 (WT or DDAA mutation) and PEN-2-rho protein complexes were calculated from far-UV CD spectra of thermal denaturation data by two different methods:

Table 4.1 Melting temperature of His-PS1 (WT or DDAA mutant) and PEN-2-rho complexes

	CD signal correcting	CD deconvolutions
DDAA	61.8°C ± 1.9°C	62.5°C ± 0.7°C
WT	62.3°C ± 1.4°C	63°C ± 0.7°C
WT + CHS	56.3°C ± 1°C	54.4°C ± 0.6°C

Similar melting temperatures were obtained for WT and DDAA, which is consistent with the deconvolution of the CD data, proving that WT and DDAA contained similar secondary structures. The addition of cholesterol resulted in a significant decrease in Tm. An increase in Tm is expected for cholesterol-protein complexes as well as for protein aggregation relative to the ligand-free complexes and monomers due to the binding energies. At the same time cholesterol reduced protein aggregation, as was also found during SEC and thermal denaturation. This indicates that the effect of cholesterol on protein de-aggregation is stronger than the effect of heat-induced protein aggregation.

4.7 Functionality of the PS1-PEN-2 complex

4.7.1 Activity assay

The previous Ph.D. student Dr. Kun Yu proved that the substrate APP-C99 expressed in *E.coli* has self-aggregation, which may inhibit or diminish the cleavage and overall complicates activity analysis. I attempted to measure the activity of the DIBMALP PS1-PEN-2 complexes by using the substrate MBP-APPC, which may prevent self-aggregation. But no cleaved product was observed on the PAGE (Figure 3.29 and Figure 3.30). The probable reasons that no activity was observed might be (i) The oligomerization states of the His-PS1 and His-PEN-2 protein complexes prevented the activity. (ii) No evidence has shown that PEN-2 interacted with PS1 in DIBMALP because no endoproteolysis of the PS1 protein was observed which is essential for γ-secretase activity. (iii) *E.coli* lipids have negative effects or do not support γ-secretase activity[203]. (iv) A eukaryotic expression system might be necessary to maintain the recombinant protein's correct folding and post-translational modification, thus leading to the extremely low activity of *E.coli* expressed γ-secretase sub-complex. Thus, the DIBMA solubilized PS1-PEN-2 complexes is not suitable for investigation of the function of PS1-PEN-2 complex.

The activity of the PS1 mutant PS1-thrombin-E321, which formed the NTF/CTF heterodimer after the autoinhibitory loop was cleaved, was also measured with MBP-APPC (Figure 3.6). But no activity was observed due to the presence of the harsh detergent Fos-14, indicating that enzymatic activity can be affected by detergent[214].

Considering the low activity of the *E.coli* expressed γ-secretase sub-complex, a highly sensitive fluorescent γ-secretase substrate was chosen to measure the activity[189]. Detergents solubilized membrane containing the His-PS1-PEN-2-rho protein complex, as well as the purified DDM solubilized complex, exhibited high activity when incubated with the fluorescent γ-secretase substrate (Figure 3.49 and Figure 3.50). The γ-secretase substrate is first recognized by the ectodomain of the NCT protein and stays in the substrate docking site which is formed by the NCT, PEN-2, and PS1-NTF protein in the complex [83,215]. Therefore, studying the catalytic PS1-PEN-2 complex, which lacks the complete docking site, can be the additional reason for the research of Alzheimer's disease. Before moving to the active site, the substrate needs to be recognized by the PAL motif in the C-terminus of PS1 (Figure 4.1 marked with the yellow star), which is located near the active site and essential for the γ-secretase activity[216–218]. The binding of the substrate after recognition by the PAL motif may trigger the alignment of the two conserved aspartate residues at the active site, resulting in catalysis[113]. It has been reported that the γ-secretase inhibitors (GSI) blocked the active site of γ-secretase or the substrate docking site [219–221]. Thus substrates were accumulated at the substrate docking site in the presence of GSI [215]. In my research, γ-secretase inhibitor III-31C and L-685,458, which can block the substrate docking site of γ-secretase, caused the inhibition of the γ-secretase activity at high concentrations. But no inhibition was observed at up to 50μM inhibitors, suggesting that the binding of GSI needs the involvement of the other two missing subunits, which complete the substrate docking site. I also observed a slight increase in activity in the presence of a low concentration of GSI (Figure 3.51), which is consistent with Gael Barthet's study that the γ-secretase inhibitors stabilize the complex and specifically increase Aβ levels by low concentrations of GSI [222]. Significant activity differences were observed between the membrane in the presence or absence of the overexpressed His-PS1-PEN-2-rho protein complex (Figure 3.53). The activity within the cell membrane fraction of the negative control without γ-secretase appeared to be an endogenous intramembrane presenilin-like protease activity in the cell membranes. EDTA showed inhibition of the activity, implying that cations are essential[223].

Presenilin is a zymogen of γ-secretase and undergoes endoproteolysis into the PS1-NTF -CTF heterodimer to activate γ-secretase activity [65,224]. It was suggested that the four components of γ-secretase are not only required for the stability of the γ-secretase complex but also constitute and regulate the Presenilinase activity, which is responsible for the endoproteolysis of Presenilins[225]. Unexpectedly, I observed a similar γ-secretase activity in the DDAA mutant, which was supposed

to be inactive (Figure 3.54), indicating either contaminants were present in the sample of the complex or residual activity of the DDAA mutant. At the same time, the fragmentations into PS1-NTF and PS1-CTF were found in DDAA mutant as well (Figure 3.43). Several publications suggested that the DDAA mutant γ-secretases expressed in eukaryotic cell are not completely inactive but retain residual activity[82,226,227]. In those works, mutated γ-secretase exhibited half of the activity compared to the WT using the fluorogenic substrate[82]. Also, the DDAA mutant complex showed self-activation, which implies the presenilinase activity, but no γ-secretase activity with regard to other substrates was found on PAGE, which provided evidence for two different activities[227]. Thus, I concluded that the Presenilinase activity and the γ-secretase activity observed in DDAA mutants could be both residual activities.

Inhibition by commonly used protease inhibitors showed the inhibition of γ-secretase activity by the serine protease inhibitor AEBSF but slight or no inhibition was observed by cysteine protease inhibitor E-64 and aspartic proteases pepstatin A (Figure 3.55 and Figure 3.56). Therefore, either a serine protease contamination existed in the preparation or AEBSF (Figure 4.2 A) inhibited the activity of the His-PS1-PEN-2-rho protein complex. Interestingly, the group of Nikolaos K. Robakis reported that Peptidyl aldehydes, which could inhibit both cysteine and serine proteases, inhibited the production of Aβ40 and Aβ42 by γ-secretase Meanwhile, the specific cysteine protease E-64 inhibited the production of Aβ40 but increased the production of Aβ42, suggesting that Aβ40 and Aβ42 are produced by different mechanisms[228]. Furthermore, the JLK isocoumarin inhibitors (Figure 4.2 B), which inhibit serine protease, have been proven to reduce the production of Aβ peptides markedly [229]. In addition, the peptide boronates, a series of reversible serine protease inhibitors, have been reported to lower the Aβ production[230]. Those findings imply that the γ-secretase is a multifunctional enzyme.

The group of Weiming Xia studied the endoproteolysis of Presenilin *in vitro* and screened the inhibition of γ-secretase activity by different types of protease inhibitors[231]. In their research, pepstatin A blocked the endoproteolysis of Presenilin but didn't interfere with the Aβ generation, which is consistent with our results that Pep A didn't inhibit or only slightly inhibit the activity of the purified protein complex or the cell membrane fraction. This suggests that the Presenilinase mediated by an aspartyl protease activity. They also demonstrated that the commonly used serine protease inhibitors Pefabloc could significantly reduce the fragmentations of Presenilin and the production of Aβ, while PMSF could decrease the creation of Aβ but doesn't affect the

endoproteolysis of Presenilin. Thereby, it has been clearly shown the serine protease inhibitors inhibit the activity of γ-secretase, though it has been identified as the aspartyl protease. Furthermore, the inhibition profiles also indicate that the Presenilinase activity is distinct from the γ -secretase activity [225,231–233]. Considering that we obtained high purity protein complexes, I conclude that therefore the serine protease inhibitor AEBSF indeed inhibits the γ-secretase activity like PMSF or Pefabloc and that the activity observed is not due to contaminants. In addition, the autoinhibitory loop of PS1, which blocks the active site and hinder the substrate processing, was proved to be highly hydrophobic (Figure 3.3). However, the Presenilinase activity was observed in the DDAA mutant complex (Figure 3.43) which may suggest that the two aspartic acids are not the only catalytic sites for the Presenilinase activity, but that another active site may exist and cleaves the PS1 protein. But given that the complex does not contain the complete docking site, it is unlikely that it is the Presillinase active site, most likely the different active sites are overlapping

A   B
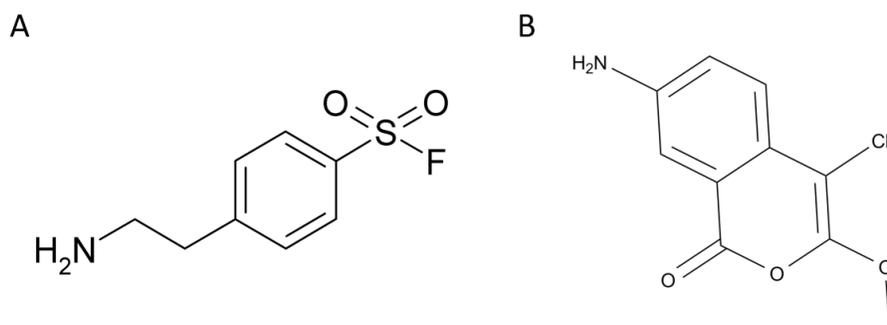
Figure 4.2 Chemical structures of inhibitors

The Chemical structures of (A) AEBSF protease inhibitor and (B) JLK isocoumarin inhibitor.

There were several studies that investigated the activities of γ-secretase from *E.coli*. Ahn, K. *et al.*reported that the bacterially synthesized, recombinant presenilin-1 ΔE9 mutant exhibited the γ-secretase activity after being reconstituted into liposomes but no specific activity was given[61]. Meanwhile, they showed that full-length PS1 underwent endoproteolysis and activated γ-secretase activity in the presence of PEN-2 but not in its absence, which implies that PS1-PEN-2 sub-complex is the minimal subunit for Presenilinase activity. Since there is no endogenous γ-secretase in *E.coli*, the Presenilinase activity observed when I co-expressed the PS1-PEN-2 complex

indicates that though the Presenilinase activity is distinct from the γ -secretase activity, it is still an activity of the γ -secretase (sub)-complex.

Shinoda, T. *et al.* expressed the T4L-PS1NTF•PS1CTF•Pen-2 complex *in vitro* (*E.coli* system) into liposomes and demonstrated the γ-secretase activity from Brij-78 or digitonin solubilizations. But unfortunately, no inactive mutant (negative control) was used in this research [234]. Takeo, K. *et al.* also found very low γ-secretase activity from unactivated uncleaved T4L-PS1 expressed *in vitro* (*E.coli* system) into liposomes without PEN-2 protein and reported a "relative" velocity of 0.3nM/min [235]. But there was also no negative control by an inactive mutant which would allow to address the problem of a potential *E.coli* protease contamination. Naing, S.-H. *et al.*performed the presenilin activity from a presenilin ortholog *Methanoculleus Marisnigri* microbial intramembrane aspartyl protease, which does not require other γ-secretase-like subunits, expressed by *E.coli* and found a maximum velocity of 15.9 ± 0.6 nM/min. No activity was observed for the DDAA mutant of this ortholog in their research[236]. In our research, I observed initial velocities of 5.6 ± 0.9 nM/min in the WT protein complex and 3.6 ± 0.6 nM/min in the DDAA mutant, which is higher than T4L-PS1 in liposomes but lower than the presenilin ortholog where it showed an initial velocity of ~10 nM/min with 10μM fluorescent γ-secretase substrates concentration.

Meanwhile, the differences in activity between the WT complex and the DDAA complex should be the lower estimate of the real γ-secretase activity, because the difference removes not only the activity of potential contaminant proteases but also the residual DDAA activity (Figure 3.56 D&E). The real γ-secretase activity of 4.0 E-5 U/mg in my experiments is lower than the DDAA residual activity of 8.3E-5 U/mg, which could also contain activity of a minor contaminant which has higher specific activity than the γ-secretase. There is no literature for the specific activity, therefore the effect of missing subunits or the influence of detergent cannot be estimated.

Table 4.2 Comparison of γ-secretase activity expressed in Bacteria

Author	Initial velocity	Protein concentration	Conditions
Koji Takeo [235]	0.3 nM/min	Not mentioned	(i) *In vitro* expression of T4L-PS1 in liposomes (ii) No PEN-2 involved

			(iii) No inactive mutant involved
Swe-Htet Naing [236]	~10 nM/min	500 nM	(i) a presenilin ortholog in DDM (ii) No PEN-2 involved (iii) No activity observed when active site mutated
My research	5.6 ± 0.9 nM/min (WT complex) 2.1 ± 0.4 nM/min (Real activity)	299 nM	(i) PS1-PEN-2 tetramer in DDM (ii) DDAA showed a initial velocity of 3.6 ± 0.6 nM/min

All reactions were incubated with 10μM fluorescent γ-secretase substrates.

The APP-C99 is cleaved by the γ-secretase activity and produce the toxic $A\beta_{40}$ and $A\beta_{42}$ peptides, which lead to Alzheimer's disease[237]. The inhibition profiles by Nikolaos K. Robakis implied that the production of $A\beta_{40}$ and $A\beta_{42}$ existed the distinct mechanisms, which would hint that there could be another active site overlapping with the known active site [228]. The autoinhibitory loop cleaved by Presenilinase activity is highly hydrophobic and blocks the active site where the substrate is cleaved, indicating that the Presenilinase active site overlaps with the γ-secretase active site. As there is no complete docking site in the PS1-PEN-2 complex, the substrate processing would be different from the intact γ-secretase. Although there is no real proof for the presence of a second active site in γ-secretase, the different mechanisms of the production of $A\beta_{40}$ and $A\beta_{42}$ may be mediated by the different activities of presenilinase and γ-secretase, which is very relevant to Alzheimer's disease.

The reasons that the obtained protein complexes exhibit low activity could be that: (i) The obtained PS1-PEN-2 protein complex behaves like the apoenzyme and needs the other two subunits to form the full complex with full activity. (ii) The PS1-PEN-2 protein complex needs the cofactors or activators like γ-secretase activating protein to fully activate the protein complex [238]. (iii) The obtained complexes showed no or low activities due to the detergents involved in sample preparation or missing essential lipids.

I conclude that the obtained Presenilin-1-PEN-2 protein complexes possess the γ-secretase activity whether the activity is low or high cannot be judged because no other specific activities were published.

4.7.2 Binding constant

The dissociation constant of the obtained WT or DDAA complexes to the substrates or the other sub-units was obtained by MST (Figure 3.60).

Table 4.3 dissociation constants of the complexes to substrates or other sub-units

	Wild type	DDAA mutant
MBP-APPC	650nM ± 174.19nM	216.13nM ± 36.275nM
APP-C99	2.3μM ± 1μm	1.85μM ± 0.78μM
Nicastrin	783.44nM ± 179nM	272.45nM ± 47.214nM
FleBt-APH-1	83.64nM ± 50nM	33.155nM ± 10.48nM

The different tertiary structures between WT and DDAA samples, which may be the main reason why DDAA exhibits a higher dissociation constant than WT in all binding experiments.

TM2 and 4 of APH-1 interact with TM8 and 9 of PS1 while the C-terminus of PS1 inserts into the cavity which is formed by TM2-6 of APH-1, indicating that the PS1 protein has strong interactions with APH-1 in the complexes[112]. In more detail, Leu30 of APH-1 is located on the Ala79 of TMD1 of PS1, while Thr164 is close to Tyr466 in the carboxy-terminus of PS1 protein (Figure 4.3) [239]. FleBt-APH-1 displayed the highest binding capacity with both the WT and DDAA protein complexes, which indicates that APH-1 is essential for stabilizing the complexes and is much closer to the PS1 protein in the complexes.
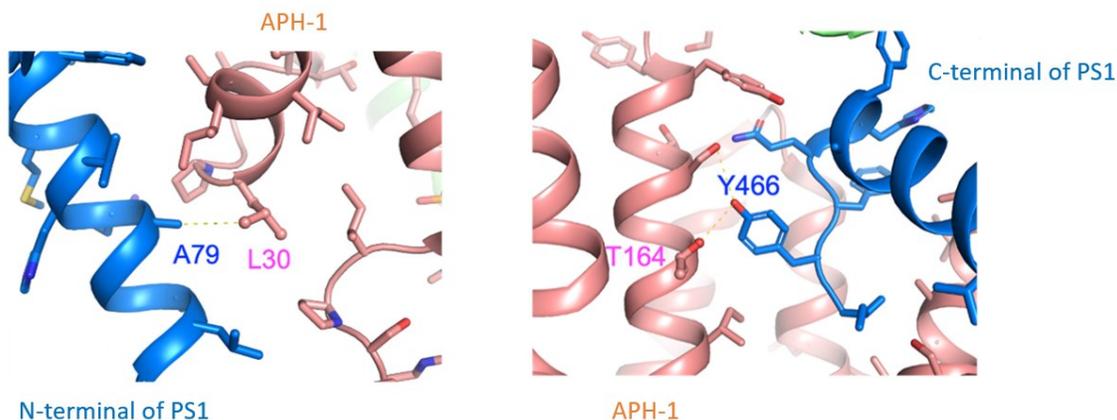
Figure 4.3 The interaction between APH-1 and PS1 (picture adapted from [239])

The cryo-EM structure showed that Leu30 and Thr164 of APH-1 the interactions with Ala79 and Tyr466 of PS1 respectively.

As a substrate recognizer, the unique TM of Nicastrin strongly interacts with the TM1,5,7 of APH-1 to form a stable subcomplex before the recruitment of PS1[74,95,112]. In the complexes, an α-helix and its surrounding structural elements in the ectodomain of Nicastrin interact with the C-terminus of Pen-2, whereas in the case of APH-1 a multitude of interactions can be seen with Presenilin-1. This could be the explanation for the lower binding constant of Nicastrin compare to the case of the FleBt-APH-1[83,113,240].

Interestingly, during the purification step, I observed that the C-terminus of PEN-2 is hidden in the complexes and inaccessible, which would further reduce the interaction between Nicastrin and PEN-2. Therefore, the interaction observed in the structure shows that the conformation of PEN-2 must change upon Nicastrin binding, which was confirmed by the initial fluorescence changes in MST experiments (Figure 3.60 B).

4.7.3 Assembly of γ-secretase

The order of assembly of intact γ-secretase complex have been reported to be that APH-1 interacts with Nicastrin and form the enzyme scaffold first. Next, full-length Presenilin is included. Finally, PEN-2 is recruited to the complex, which activates the γ-secretase activities[58].

The rational for assembly of γ-secretase in a different order starting with the minimal catalytic subcomplex PS1-PEN-2 was to study this complexs and possibly evaluate the role of APH-1 and Nicastrin in the catalytic mechanism. Therefore, I started with the 2:2-PS1-PEN-2 sub-complex.

Obtaining the complete γ-secretase from the minimal catalytic sub-complex would require the 3rd subunit to be APH-1 based on the lowest dissociation constant. The APH-1 protein shows strong interaction with C-terminus of the PS1 protein but has no direct interaction with PEN-2 according to the resolved cryo-EM structures[105,113]. This situation implies that one of the two Presenilin molecules will be substituted when the 3rd sub-unit APH-1 is incorporated into the sub-complex. After the addition of the last subunit Nicastrin, the single TM of Nicastrin should strongly interact with the TMs of APH-1 on the opposite site of PS1. At the same time, one PEN-2 protein molecule should be replaced when the ectodomain of Nicastrin interacts with the C-terminus of the other PEN-2 and the intact complex is formed.
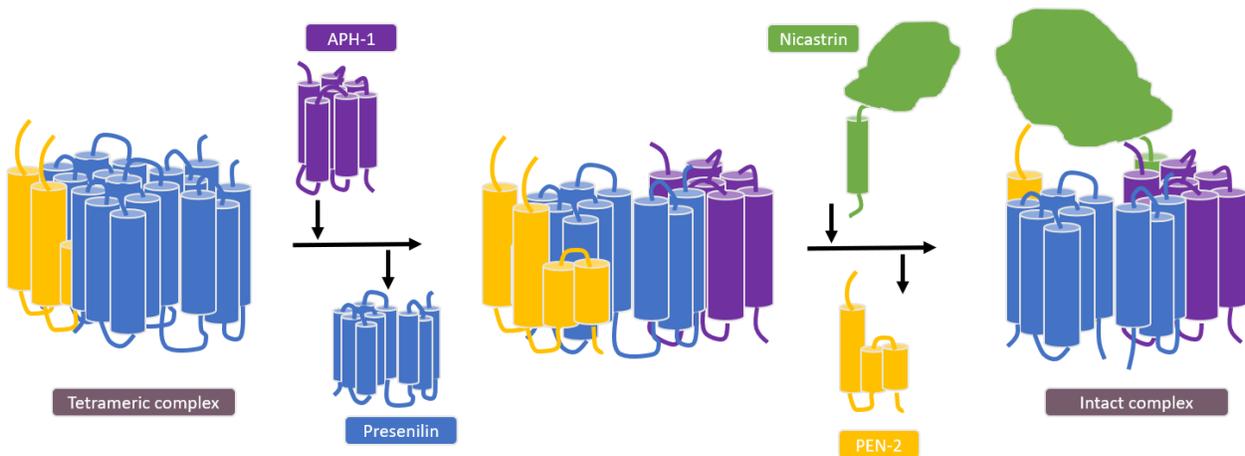
Figure 4.4 Model for the assembly of intact γ-secretase complex starting from PS1-PEN-2 sub-complex.

Model for the assembly of the intact γ-secretase complex starting from the PS1-PEN-2 tetrameric subcomplex. The APH-1 protein is added to tetrameric complex and one presenilin molecule is substituted. One of the two PEN-2 molecule is replaced when NCT is added to PS1-PEN-2-APH-1 complex and the intact complex is formed.

4.8 Conclusion

In order to obtain the γ-secretase (sub)-complex, I tried several methods to reconstitute the individual sub-units into a lipidic environment. MSP nanodiscs perform well in single protein reconstitution but are not suitable for the assembly of the γ-secretase due to the well-defined dimensions which leads to the inability to integrate the complex into nanodiscs. Liposomes are available with a large surface for insertion of large protein complexes but are not stable in the presence of the harsh detergent like Fos-14. Besides the influence on the stability of liposomes, Fos-14 also reduces the interactions between the PS1 and the PEN-2 proteins thus preventing the Presenilinase activity. MBP-tag contributes to the detergent-free purification of membrane proteins and reduces the detergent influence on liposomes stability. Although the MBP-fused PS1 and PEN-2 proteins were successfully reconstituted into liposomes, Presenilinase activity was not observed, showing that the MBP tag reduces protein interactions. In both cases, a major issue is the random orientation when reconstituting membrane proteins into liposomes, which can lead to incorrect assembly of the complexes.

The PS1-PEN-2 protein complex has been reported to be the minimal catalytic subunits of the γ-secretase, therefore I co-expressed the PS1-PEN-2 protein complex in *E.coli* cells and confirmed the interaction between the PS1 and the PEN-2 proteins by the assembly of fused split GFP *in vivo*. Ahn's study was restricted to a qualitative γ-secretase activity determination when reconstituting MBP-fused sub-units into liposomes[61]. Unlike his study, I successfully isolated the first PS1-PEN-2 tetramer complex from *E.coli* and showed the specific activity of γ-secretase by detecting the cleavage of the fluorogenic γ-secretase substrate. As almost all γ-secretase research focus on the qualitative activity, I provided the first specific γ-secretase activity from the PS1-PEN-2 tetramer complex in *E.coli*, which could be the reference of further γ-secretase research on enzymology. Furthermore, the obtained tetramer complex would be the first choice to investigate the assembly of full γ-secretase complex either *in vivo* or *in vitro*. At the same time, the PS1-PEN-2 tetramer complex, which is lack of the complete substrate docking site, could be a great initial model to evaluate the mechanism of the substrate processing by γ-secretase and the effect on Alzheimer's disease.

Another important sub-unit of γ-secretase is APH-1, which contains 7 transmembrane domains and is extremely unstable. Since APH-1 protein is required to stabilize the entire γ-secretase complex,

stable expression and purification of APH-1 protein is crucial to explore the assembly of the complex. Here I successfully expressed and purified the stable APH-1 protein in *E.coli* by introducing the solubility tag FleBt into APH-1 protein. This is the first isolated individual stable APH-1 protein in *E.coli* and could be the best choice to investigate the mechanism that how APH-1 stabilize the γ-secretase complex.

At last, I propose a model for the assembly of intact γ-secretase complex based on the binding constant of PS1-PEN-2 tetrameric complex and other two sub-units. Higher binding constant was found in PS1-PEN-2-APH-1 complex than PS1-PEN-2-NCT complex, which indicates that APH-1 is closer to the tetrameric complex than NCT. Therefore, APH-1 protein will be the 3rd sub-unit to be incorporated into the complex and NCT protein will be the last one. This provides new sight for the assembly of intact γ-secretase complex starting from the minimal catalytic units and could be the new model to investigate the assembly of intact γ-secretase complex.

Summary

The γ-secretase complex, consisting of Presenilin, PEN-2, Nicastrin (NCT) and APH-1, is a multi-transmembrane protein which processes over 90 type I membrane protein substrates. It had been identified as an aspartyl-protease with a central role in cellular regulation. The abnormal cleavage of the well-known γ-secretase substrate amyloid precursor proteins (APP) into neurotoxic peptides leads to Alzheimer's disease. Despite the extensive implementation of structural and functional studies on the γ-secretase complex in the past decades, the mechanism of cleavage and the role of assembly of the γ-secretase complex are unclear.

In this work, the PS1-PEN-2 protein complex was obtained by reconstitution into liposomes or co-expression in *E.coli* cells. No Presnilinase activity was observed in reconstitution experiments into liposomes due to the influence of detergent and the MBP-tag. Both the Presenilinase and the γ-secretase activities were not detected in DIBMA solubilized co-expressed PS1-PEN-2-lipid complexes because of effects of the *E.coli* lipids. DDM-solubilized PS1-PEN-2 protein complexes displayed an oligomer and a tetramer complex with approximately molecular weight of 600 kDa and 167 kDa, respectively. The tetrameric complex showed PS1-NTF and PS1-CTF fragments, representing the presence of Presenilinase activity, therefore for the first time a functional γ-secretase subcomplex has been characterized.

The biophysical characterization of the PS1-PEN-2 tetrameric complex was conducted by circular dichroism and fluorescence spectroscopy. The WT complex and the DDAA mutant complex without the catalytic aspartic acid residues exhibited similar secondary structures but different tertiary structures: The WT complex and the DDAA complex showed similar thermal stability of approximately 62 °C (CD). Additionally, FleBt-APH-1 showed higher binding constant to the DDAA complex (~33 nM) than to the WT complex (~83 nM). Whereas, NCT showed the dissociation constant of ~783 nM to the WT complex but ~272 nM to the DDAA complex by microscale thermophoresis (MST). These binding constants indicate that the assembly of intact γ-secretase from the minimal catalytic subcomplex PS1-PEN-2 should proceed in the order APH-1, NCT.

The activity of the PS1-PEN-2 protein complex with 2:2 stoichiometry from *E.coli* was detected by using a fluorogenic γ-secretase substrate. This sample allowed for the first time detecting a

specific activity of the γ-secretase type and analyze the effects of inhibitors. The WT complex showed the specific γ-secretase activity of 1.2E-4 U/mg with an initial velocity of 6 µM/min. Meanwhile the DDAA complex exhibited the specific γ-secretase activity of 8.3 E-5 U/mg with an initial velocity of 3.5 µM/min. The difference between the WT complex and the DDAA mutant would be the lower estimate of the γ-secretase activity, which is 3.9E-5 U/mg.

Based on the obtained complex, it is now possible to study the molecular mechanism of the production of the neurotoxic peptides which are the root cause Alzheimer's disease using the minimal complexes with FAD mutations.

Zusammenfassung

Der γ-Sekretase-Komplex, bestehend aus Presenilin, PEN-2, Nicastrin (NCT) und APH-1, ist ein Multitransmembranprotein, der über 90 Typ-I-Membranproteinsubstrate verarbeitet. Der Komplex wurde als Aspartyl-Protease identifiziert, die eine zentrale Rolle bei der zellulären Regulation spielt. Die abnorme Spaltung des bekannten γ-Sekretase-Substrats Amyloid-Vorläuferproteine (APP) in neurotoxische Peptide führt zur Alzheimer-Krankheit. Trotz umfangreicher struktureller und funktioneller Untersuchungen des γ-Sekretase-Komplexes in den letzten Jahrzehnten sind der Mechanismus der Spaltung und die Rolle des Zusammenbaus des γ-Sekretase-Komplexes unklar.

In dieser Arbeit wurde der PS1-PEN-2-Proteinkomplex durch Rekonstitution in Liposomen oder Koexpression in E.coli-Zellen gewonnen. Bei Rekonstitutionsversuchen in Liposomen wurde aufgrund des Einflusses des Detergens und des MBP-Tags keine Presnilinase-Aktivität beobachtet. Sowohl die Presenilinase- als auch die γ-Sekretase-Aktivitäten wurden in DIBMA-solubilisierten koexprimierten PS1-PEN-2-Lipid-Komplexen aufgrund der Auswirkungen der E.coli-Lipide nicht nachgewiesen. DDM-solubilisierte PS1-PEN-2-Proteinkomplexe wiesen ein hochmolekulares Oligomer und einen Tetramerkomplex mit einem Molekulargewicht von etwa 600 kDa bzw. 167 kDa auf. Der tetramerische Komplex wies PS1-NTF- und PS1-CTF-Fragmente auf, was das Vorhandensein von Presenilinase-Aktivität zeigt, so dass zum ersten Mal ein funktioneller γ-Sekretase-Subkomplex charakterisiert wurde.

Die biophysikalische Charakterisierung des tetrameren PS1-PEN-2-Komplexes wurde mittels Zirkulardichroismus und Fluoreszenzspektroskopie durchgeführt. Der WT-Komplex und der mutierte DDAA-Komplex ohne die katalytischen Asparaginsäurereste wiesen ähnliche Sekundärstrukturen, aber unterschiedliche Tertiärstrukturen auf: Der WT-Komplex und der DDAA-Komplex zeigten eine ähnliche thermische Stabilität von etwa 62 °C (CD). Weiterhin zeigte FleBt-APH-1 eine höhere Bindungskonstante an den DDAA-Komplex (~33 nM) als an den WT-Komplex (~83 nM). NCT hingegen zeigte eine Dissoziationskonstante von ~783 nM für den WT-Komplex, aber ~272 nM für den DDAA-Komplex bei der *Microscale Thermophoresis* (MST). Diese Bindungskonstanten weisen darauf hin, dass der Aufbau der intakten γ-Sekretase aus dem minimalen katalytischen Subkomplex PS1-PEN-2 in der Reihenfolge APH-1, NCT erfolgen sollte.

Die Aktivität des PS1-PEN-2-Proteinkomplexes mit 2:2-Stöchiometrie aus E.coli wurde mit einem fluorogenen γ-Sekretase-Substrat nachgewiesen. Mit dieser Probe konnte zum ersten Mal eine spezifische Aktivität des γ-Sekretase-Typs nachgewiesen und die Auswirkungen von Inhibitoren analysiert werden. Der WT-Komplex zeigte eine spezifische γ-Sekretase-Aktivität von 1,2E-4 U/mg mit einer Anfangsgeschwindigkeit von 6 µM/min. Der DDAA-Komplex hingegen wies eine spezifische γ-Sekretase-Aktivität von 8,3 E-5 U/mg bei einer Anfangsgeschwindigkeit von 3,5 µM/min auf. Der Differenz zwischen dem WT-Komplex und der DDAA-Mutante stellt die untere Grenze für γ-Sekretaseaktivität dar, die 3,9 E-5 U/mg beträgt.

Auf der Grundlage des erhaltenen Komplexes ist es nun möglich, den molekularen Mechanismus der Produktion der neurotoxischen Peptide, die die Ursache der Alzheimer-Krankheit sind, anhand der Minimalkomplexe mit FAD-Mutationen zu untersuchen.

Abbreviations

AD	Alzheimer's disease
AEBSF	4-(2-Aminoethyl)benzenesulfonyl fluoride
APH-1	Anterior Pharynx Defective 1
APP	Amyloid Precursor Protein
CD	Circular dichroism
CHAPSO	3-[(3-Cholamidopropyl)dimethylammonio]-2-hydroxy-1-propanesulfonate
CHS	cholesteryl hemisuccinate
CMC	Critical micelle concentration
CTF	C-terminal fragment
DDAA	D275A D385A mutant
DDM	n-Dodecyl-B-D-Maltoside
DIBMA	di-isobutylene maleic acid
DIBMALP	DIBMA lipids protein complex
DMPC	Dimyristoylphosphatidylcholine
EDTA	Ethylenediaminetetraacetic acid
EggPC	Egg phosphatidylcholine
EM	electron microscopy
FL	full-length
Fos-14	Fos-choline 14
GFP	Green fluorescent protein

IPTG	Isopropyl β- d-1-thiogalactopyranoside
kDa	kilodalton
LB	lysogeny broth
LC	Liquid chromatography
MBP	Maltose-binding protein
MS	Mass spectrometry
MSP	membrane scaffolding proteins
MST	Microscale thermophoresis
MW	Molecular Weight
NCT	Nicastrin
NTA	Nitriloacetic acid
NTF	N-terminal fragment
PCR	polymerase chain reaction
PE	Phosphatidylethanolamine
PEN-2	Presenilin Enhancer 2
PMSF	phenylmethylsulfonyl fluoride
PS	Presenilin
SDS-PAGE	Sodium dodecyl-sulfate polyacrylamide gel electrophoresis
SEC	size exclusion chromatography
SMA	styrene maleic acid
TB	Terrific Broth

TM   transmembrane

Tm   melting temperature

TMD   transmembrane domain

WT   Wild type

Bibliography

1. Adav, S. S. & Sze, S. K. Insight of brain degenerative protein modifications in the pathology of neurodegeneration and dementia by proteomic profiling. *Mol. Brain* **9**, 92 (2016).

2. Leandro, P. & Gomes, C. M. Protein misfolding in conformational disorders: rescue of folding defects and chemical chaperoning. *Mini Rev. Med. Chem.* **8**, 901–911 (2008).

3. Faiyaz, M. *et al.* Nanomaterials in Alzheimer's disease treatment: a comprehensive review. *Front. Biosci. Landmark Ed.* **26**, 851–865 (2021).

4. Schachter, A. S. & Davis, K. L. Alzheimer's disease. *Dialogues Clin. Neurosci.* **2**, 91–100 (2000).

5. Bertram, L. & Tanzi, R. E. Thirty years of Alzheimer's disease genetics: the implications of systematic meta-analyses. *Nat. Rev. Neurosci.* **9**, 768–778 (2008).

6. Castanho, I. & Lunnon, K. Chapter 8 - Epigenetic processes in Alzheimer's disease. in *Chromatin Signaling and Neurological Disorders* (ed. Binda, O.) vol. 12 153–180 (Academic Press, 2019).

7. Hippius, H. & Neundörfer, G. The discovery of Alzheimer's disease. *Dialogues Clin. Neurosci.* **5**, 101–108 (2003).

8. Amieva, H. *et al.* Prodromal Alzheimer's disease: successive emergence of the clinical symptoms. *Ann. Neurol.* **64**, 492–498 (2008).

9. Chu, L. W. Alzheimer's disease: early diagnosis and treatment. *Hong Kong Med. J. Xianggang Yi Xue Za Zhi* **18**, 228–237 (2012).

10. Galvin, J. E. *et al.* Early Stages of Alzheimer's Disease: Evolving the Care Team for Optimal Patient Management. *Front. Neurol.* **11**, 592302 (2021).

11. Förstl, H. & Kurz, A. Clinical features of Alzheimer's disease. *Eur. Arch. Psychiatry Clin. Neurosci.* **249**, 288–290 (1999).

12. Frank, E. M. Effect of Alzheimer's disease on communication function. *J. S. C. Med. Assoc. 1975* **90**, 417–423 (1994).

13. O'Shaughnessy, N. J. *et al.* Awareness in severe Alzheimer's disease: a systematic review. *Aging Ment. Health* **25**, 602–612 (2021).

14. Voisin, T. & Vellas, B. Diagnosis and treatment of patients with severe Alzheimer's disease. *Drugs Aging* **26**, 135–144 (2009).

15. Singh, S. K., Srivastav, S., Yadav, A. K., Srikrishna, S. & Perry, G. Overview of Alzheimer's Disease and Some Therapeutic Approaches Targeting Aβ by Using Several Synthetic and Herbal Compounds. *Oxid. Med. Cell. Longev.* **2016**, 7361613 (2016).

16. Brown, M. R., Radford, S. E. & Hewitt, E. W. Modulation of β-Amyloid Fibril Formation in Alzheimer's Disease by Microglia and Infection. *Front. Mol. Neurosci.* **13**, 228 (2020).

17. Gouras, G. K., Olsson, T. T. & Hansson, O. β-Amyloid peptides and amyloid plaques in Alzheimer's disease. *Neurother. J. Am. Soc. Exp. Neurother.* **12**, 3–11 (2015).

18. Butterfield, D. A., Swomley, A. M. & Sultana, R. Amyloid β-Peptide (1–42)-Induced Oxidative Stress in Alzheimer Disease: Importance in Disease Pathogenesis and Progression. *Antioxid. Redox Signal.* **19**, 823–835 (2013).

19. Ferreiro, E. *et al.* Mitochondrial- and endoplasmic reticulum-associated oxidative stress in Alzheimer's disease: from pathogenesis to biomarkers. *Int. J. Cell Biol.* **2012**, 735206 (2012).

20. Guo, C., Sun, L., Chen, X. & Zhang, D. Oxidative stress, mitochondrial damage and neurodegenerative diseases. *Neural Regen. Res.* **8**, 2003–2014 (2013).

21. Schilling, T. & Eder, C. Amyloid-β-induced reactive oxygen species production and priming are differentially regulated by ion channels in microglia. *J. Cell. Physiol.* **226**, 3295–3302 (2011).

22. Binder, L. I., Guillozet-Bongaarts, A. L., Garcia-Sierra, F. & Berry, R. W. Tau, tangles, and Alzheimer's disease. *Biochim. Biophys. Acta* **1739**, 216–223 (2005).

23. Hardy, J. & Selkoe, D. J. The amyloid hypothesis of Alzheimer's disease: progress and problems on the road to therapeutics. *Science* **297**, 353–356 (2002).

24. Smith, M. J. *et al.* Variable phenotype of Alzheimer's disease with spastic paraparesis. *Ann. Neurol.* **49**, 125–129 (2001).

25. Shin, R. W., Iwaki, T., Kitamoto, T. & Tateishi, J. Hydrated autoclave pretreatment enhances tau immunoreactivity in formalin-fixed normal and Alzheimer's disease brain tissues. *Lab. Investig. J. Tech. Methods Pathol.* **64**, 693–702 (1991).

26. Grundke-Iqbal, I. *et al.* Microtubule-associated protein tau. A component of Alzheimer paired helical filaments. *J. Biol. Chem.* **261**, 6084–6089 (1986).

27. Iqbal, K. *et al.* Defective brain microtubule assembly in Alzheimer's disease. *Lancet Lond. Engl.* **2**, 421–426 (1986).

28. Kuchibhotla, K. V. *et al.* Neurofibrillary tangle-bearing neurons are functionally integrated in cortical circuits in vivo. *Proc. Natl. Acad. Sci. U. S. A.* **111**, 510–514 (2014).

29. Hardy, J. A. & Higgins, G. A. Alzheimer's disease: the amyloid cascade hypothesis. *Science* **256**, 184–185 (1992).

30. Hardy, J. & Allsop, D. Amyloid deposition as the central event in the aetiology of Alzheimer's disease. *Trends Pharmacol. Sci.* **12**, 383–388 (1991).

31. Selkoe, D. J. The molecular pathology of Alzheimer's disease. *Neuron* **6**, 487–498 (1991).

32. Mullard, A. Alzheimer amyloid hypothesis lives on. *Nat. Rev. Drug Discov.* **16**, 3–5 (2016).

33. Gu, L. & Guo, Z. Alzheimer's Aβ42 and Aβ40 peptides form interlaced amyloid fibrils. *J. Neurochem.* **126**, 305–311 (2013).

34. Hellstrand, E., Sparr, E. & Linse, S. Retardation of Aβ Fibril Formation by Phospholipid Vesicles Depends on Membrane Phase Behavior. *Biophys. J.* **98**, 2206–2214 (2010).

35. Reiss, A. B., Arain, H. A., Stecker, M. M., Siegart, N. M. & Kasselman, L. J. Amyloid toxicity in Alzheimer's disease. *Rev. Neurosci.* **29**, 613–627 (2018).

36. Shin, R. W. *et al.* Amyloid beta-protein (Abeta) 1-40 but not Abeta1-42 contributes to the experimental formation of Alzheimer disease amyloid fibrils in rat brain. *J. Neurosci. Off. J. Soc. Neurosci.* **17**, 8187–8193 (1997).

37. Zhang, X., Li, Y., Xu, H. & Zhang, Y. The γ-secretase complex: from structure to function. *Front. Cell. Neurosci.* **8**, 427 (2014).

38. Panza, F., Lozupone, M., Logroscino, G. & Imbimbo, B. P. A critical appraisal of amyloid-β-targeting therapies for Alzheimer disease. *Nat. Rev. Neurol.* **15**, 73–88 (2019).

39. Edbauer, D. *et al.* Reconstitution of gamma-secretase activity. *Nat. Cell Biol.* **5**, 486–488 (2003).

40. Fraering, P. C. *et al.* Purification and characterization of the human gamma-secretase complex. *Biochemistry* **43**, 9774–9789 (2004).

41. Hayashi, I. *et al.* Selective reconstitution and recovery of functional gamma-secretase complex on budded baculovirus particles. *J. Biol. Chem.* **279**, 38040–38046 (2004).

42. Haapasalo, A. & Kovacs, D. M. The many substrates of presenilin/γ-secretase. *J. Alzheimers Dis. JAD* **25**, 3–28 (2011).

43. Zhang, S., Zhang, M., Cai, F. & Song, W. Biological function of Presenilin and its role in AD pathogenesis. *Transl. Neurodegener.* **2**, 15 (2013).

44. Laudon, H. *et al.* A nine-transmembrane domain topology for presenilin 1. *J. Biol. Chem.* **280**, 35352–35360 (2005).

45. Lu, S. H.-J. *et al.* Vigilin interacts with signal peptide peptidase. *Proteome Sci.* **10**, 33 (2012).

46. Steiner, H. *et al.* A loss of function mutation of presenilin-2 interferes with amyloid beta-peptide production and notch signaling. *J. Biol. Chem.* **274**, 28669–28673 (1999).

47. Wolfe, M. S. *et al.* Two transmembrane aspartates in presenilin-1 required for presenilin endoproteolysis and gamma-secretase activity. *Nature* **398**, 513–517 (1999).

48. De Strooper, B. & Annaert, W. Novel research horizons for presenilins and γ-secretases in cell biology and disease. *Annu. Rev. Cell Dev. Biol.* **26**, 235–260 (2010).

49. Li, Y. M. *et al.* Photoactivated gamma-secretase inhibitors directed to the active site covalently label presenilin 1. *Nature* **405**, 689–694 (2000).

50. Steiner, H., Fluhrer, R. & Haass, C. Intramembrane proteolysis by gamma-secretase. *J. Biol. Chem.* **283**, 29627–29631 (2008).

51. Chávez-Gutiérrez, L. *et al.* The mechanism of γ-Secretase dysfunction in familial Alzheimer disease. *EMBO J.* **31**, 2261–2274 (2012).

52. Chen, G.-F. *et al.* Amyloid beta: structure, biology and structure-based therapeutic development. *Acta Pharmacol. Sin.* **38**, 1205–1235 (2017).

53. Duggan, S. P. & McCarthy, J. V. Beyond γ-secretase activity: The multifunctional nature of presenilins in cell signalling pathways. *Cell. Signal.* **28**, 1–11 (2016).

54. Otto, G. P., Sharma, D. & Williams, R. S. B. Non-Catalytic Roles of Presenilin Throughout Evolution. *J. Alzheimers Dis. JAD* **52**, 1177–1187 (2016).

55. Peric, A. & Annaert, W. Early etiology of Alzheimer's disease: tipping the balance toward autophagy or endosomal dysfunction? *Acta Neuropathol. (Berl.)* **129**, 363–381 (2015).

56. Crystal, A. S. *et al.* Membrane topology of gamma-secretase component PEN-2. *J. Biol. Chem.* **278**, 20117–20123 (2003).

57. Francis, R. *et al.* aph-1 and pen-2 are required for Notch pathway signaling, gamma-secretase cleavage of betaAPP, and presenilin protein accumulation. *Dev. Cell* **3**, 85–97 (2002).

58. Gertsik, N., Chiu, D. & Li, Y.-M. Complex regulation of γ-secretase: from obligatory to modulatory subunits. *Front. Aging Neurosci.* **6**, 342 (2014).

59. Lessard, C. B., Wagner, S. L. & Koo, E. H. And four equals one: presenilin takes the gamma-secretase role by itself. *Proc. Natl. Acad. Sci. U. S. A.* **107**, 21236–21237 (2010).

60. Takasugi, N. *et al.* The role of presenilin cofactors in the gamma-secretase complex. *Nature* **422**, 438–441 (2003).

61. Ahn, K. *et al.* Activation and intrinsic gamma-secretase activity of presenilin 1. *Proc. Natl. Acad. Sci. U. S. A.* **107**, 21435–21440 (2010).

62. Bammens, L., Chávez-Gutiérrez, L., Tolia, A., Zwijsen, A. & De Strooper, B. Functional and topological analysis of Pen-2, the fourth subunit of the gamma-secretase complex. *J. Biol. Chem.* **286**, 12271–12282 (2011).

63. Holmes, O., Paturi, S., Selkoe, D. J. & Wolfe, M. S. Pen-2 is essential for γ-secretase complex stability and trafficking but partially dispensable for endoproteolysis. *Biochemistry* **53**, 4393–4406 (2014).

64. Mao, G., Cui, M.-Z., Li, T., Jin, Y. & Xu, X. Pen-2 is dispensable for endoproteolysis of presenilin 1, and nicastrin-Aph subcomplex is important for both γ-secretase assembly and substrate recruitment. *J. Neurochem.* **123**, 837–844 (2012).

65. Prokop, S., Shirotani, K., Edbauer, D., Haass, C. & Steiner, H. Requirement of PEN-2 for stabilization of the presenilin N-/C-terminal fragment heterodimer within the gamma-secretase complex. *J. Biol. Chem.* **279**, 23255–23261 (2004).

66. Kim, S.-H. & Sisodia, S. S. A sequence within the first transmembrane domain of PEN-2 is critical for PEN-2-mediated endoproteolysis of presenilin 1. *J. Biol. Chem.* **280**, 1992–2001 (2005).

67. Watanabe, N. *et al.* Pen-2 is incorporated into the gamma-secretase complex through binding to transmembrane domain 4 of presenilin 1. *J. Biol. Chem.* **280**, 41967–41975 (2005).

68. Campbell, W. A. *et al.* Zebrafish lacking Alzheimer presenilin enhancer 2 (Pen-2) demonstrate excessive p53-dependent apoptosis and neuronal loss. *J. Neurochem.* **96**, 1423–1440 (2006).

69. Dunys, J. *et al.* p53-Dependent Aph-1 and Pen-2 anti-apoptotic phenotype requires the integrity of the gamma-secretase complex but is independent of its activity. *J. Biol. Chem.* **282**, 10516–10525 (2007).

70. Niimura, M. *et al.* Aph-1 contributes to the stabilization and trafficking of the gamma-secretase complex through mechanisms involving intermolecular and intramolecular interactions. *J. Biol. Chem.* **280**, 12967–12975 (2005).

71. Gu, Y. *et al.* APH-1 interacts with mature and immature forms of presenilins and nicastrin and may play a role in maturation of presenilin.nicastrin complexes. *J. Biol. Chem.* **278**, 7374–7380 (2003).

72. Hu, Y. & Fortini, M. E. Different cofactor activities in gamma-secretase assembly: evidence for a nicastrin-Aph-1 subcomplex. *J. Cell Biol.* **161**, 685–690 (2003).

73. LaVoie, M. J. *et al.* Assembly of the gamma-secretase complex involves early formation of an intermediate subcomplex of Aph-1 and nicastrin. *J. Biol. Chem.* **278**, 37213–37222 (2003).

74. Hébert, S. S. *et al.* Coordinated and widespread expression of gamma-secretase in vivo: evidence for size and molecular heterogeneity. *Neurobiol. Dis.* **17**, 260–272 (2004).

75. Ma, G., Li, T., Price, D. L. & Wong, P. C. APH-1a is the principal mammalian APH-1 isoform present in gamma-secretase complexes during embryonic development. *J. Neurosci. Off. J. Soc. Neurosci.* **25**, 192–198 (2005).

76. Serneels, L. *et al.* Differential contribution of the three Aph1 genes to gamma-secretase activity in vivo. *Proc. Natl. Acad. Sci. U. S. A.* **102**, 1719–1724 (2005).

77. Shirotani, K., Edbauer, D., Prokop, S., Haass, C. & Steiner, H. Identification of distinct gamma-secretase complexes with different APH-1 variants. *J. Biol. Chem.* **279**, 41340–41345 (2004).

78. Araki, W. *et al.* Characterization of APH-1 mutants with a disrupted transmembrane GxxxG motif. *J. Mol. Neurosci. MN* **29**, 35–43 (2006).

79. Lee, S.-F. *et al.* A conserved GXXXG motif in APH-1 is critical for assembly and activity of the gamma-secretase complex. *J. Biol. Chem.* **279**, 4144–4152 (2004).

80. Li, Y., Liew, L. S. Y., Li, Q. & Kang, C. Structure of the transmembrane domain of human nicastrin-a component of γ-secretase. *Sci. Rep.* **6**, 19522 (2016).

81. Dries, D. R. *et al.* Glu-333 of nicastrin directly participates in gamma-secretase activity. *J. Biol. Chem.* **284**, 29714–29724 (2009).

82. Shah, S. *et al.* Nicastrin functions as a gamma-secretase-substrate receptor. *Cell* **122**, 435–447 (2005).

83. Yu, K., Yang, G. & Labahn, J. High-efficient production and biophysical characterisation of nicastrin and its interaction with APPC100. *Sci. Rep.* **7**, 44297 (2017).

84. Chávez-Gutiérrez, L. *et al.* Glu(332) in the Nicastrin ectodomain is essential for gamma-secretase complex maturation but not for its activity. *J. Biol. Chem.* **283**, 20096–20105 (2008).

85. Zhao, G., Liu, Z., Ilagan, M. X. G. & Kopan, R. Gamma-secretase composed of PS1/Pen2/Aph1a can cleave notch and amyloid precursor protein in the absence of nicastrin. *J. Neurosci. Off. J. Soc. Neurosci.* **30**, 1648–1656 (2010).

86. Hsu, C.-H., Liou, G.-G. & Jiang, Y.-J. Nicastrin Deficiency Induces Tyrosinase-Dependent Depigmentation and Skin Inflammation. *J. Invest. Dermatol.* **140**, 404-414.e13 (2020).

87. Dries, D. R. *et al.* Loss of Nicastrin from Oligodendrocytes Results in Hypomyelination and Schizophrenia with Compulsive Behavior. *J. Biol. Chem.* **291**, 11647–11656 (2016).

88. Wong, L.-W., Tae, H.-S. & Cromer, B. A. Assembly, trafficking and function of α1β2γ2 GABAA receptors are regulated by N-terminal regions, in a subunit-specific manner. *J. Neurochem.* **134**, 819–832 (2015).

89. Edbauer, D., Winkler, E., Haass, C. & Steiner, H. Presenilin and nicastrin regulate each other and determine amyloid beta-peptide production via complex formation. *Proc. Natl. Acad. Sci. U. S. A.* **99**, 8666–8671 (2002).

90. Kimberly, W. T. *et al.* Complex N-linked glycosylated nicastrin associates with active gamma-secretase and undergoes tight cellular regulation. *J. Biol. Chem.* **277**, 35113–35117 (2002).

91. Prokop, S., Haass, C. & Steiner, H. Length and overall sequence of the PEN-2 C-terminal domain determines its function in the stabilization of presenilin fragments. *J. Neurochem.* **94**, 57–62 (2005).

92. Yang, D.-S. *et al.* Mature glycosylation and trafficking of nicastrin modulate its binding to presenilins. *J. Biol. Chem.* **277**, 28135–28142 (2002).

93. Capell, A. *et al.* Gamma-secretase complex assembly within the early secretory pathway. *J. Biol. Chem.* **280**, 6471–6478 (2005).

94. Kim, S.-H., Yin, Y. I., Li, Y.-M. & Sisodia, S. S. Evidence that assembly of an active gamma-secretase complex occurs in the early compartments of the secretory pathway. *J. Biol. Chem.* **279**, 48615–48619 (2004).

95. Dries, D. R. & Yu, G. Assembly, maturation, and trafficking of the gamma-secretase complex in Alzheimer's disease. *Curr. Alzheimer Res.* **5**, 132–146 (2008).

96. Kaether, C., Haass, C. & Steiner, H. Assembly, trafficking and function of gamma-secretase. *Neurodegener. Dis.* **3**, 275–283 (2006).

97. Verdile, G., Gandy, S. E. & Martins, R. N. The role of presenilin and its interacting proteins in the biogenesis of Alzheimer's beta amyloid. *Neurochem. Res.* **32**, 609–623 (2007).

98. Yang, G., Zhou, R. & Shi, Y. Cryo-EM structures of human γ-secretase. *Curr. Opin. Struct. Biol.* **46**, 55–64 (2017).

99. Lazarov, V. K. *et al.* Electron microscopic structure of purified, active gamma-secretase reveals an aqueous intramembrane chamber and two pores. *Proc. Natl. Acad. Sci. U. S. A.* **103**, 6889–6894 (2006).

100. Li, Y. *et al.* Structural interactions between inhibitor and substrate docking sites give insight into mechanisms of human PS1 complexes. *Struct. Lond. Engl. 1993* **22**, 125–135 (2014).

101. Ogura, T. *et al.* Three-dimensional structure of the gamma-secretase complex. *Biochem. Biophys. Res. Commun.* **343**, 525–534 (2006).

102. Osenkowski, P. *et al.* Cryoelectron microscopy structure of purified gamma-secretase at 12 A resolution. *J. Mol. Biol.* **385**, 642–652 (2009).

103. Renzi, F. *et al.* Structure of gamma-secretase and its trimeric pre-activation intermediate by single-particle electron microscopy. *J. Biol. Chem.* **286**, 21440–21449 (2011).

104. Sobhanifar, S. *et al.* Structural investigation of the C-terminal catalytic fragment of presenilin 1. *Proc. Natl. Acad. Sci. U. S. A.* **107**, 9644–9649 (2010).

105. Lu, P. *et al.* Three-dimensional structure of human γ-secretase. *Nature* **512**, 166–170 (2014).

106. Zhang, X., Li, Y., Xu, H. & Zhang, Y.-W. The γ-secretase complex: from structure to function. *Front. Cell. Neurosci.* **8**, 427 (2014).

107. Wolfe, M. S. Structure and Function of the γ-Secretase Complex. *Biochemistry* **58**, 2953–2966 (2019).

108. Wolfe, M. S. & Selkoe, D. J. γ-Secretase: a horseshoe structure brings good luck. *Cell* **158**, 247–249 (2014).

109. Xie, T. *et al.* Crystal structure of the γ-secretase component nicastrin. *Proc. Natl. Acad. Sci. U. S. A.* **111**, 13349–13354 (2014).

110. Li, X. *et al.* Structure of a presenilin family intramembrane aspartate protease. *Nature* **493**, 56–61 (2013).

111. Bolduc, D. M. & Wolfe, M. S. Structure of nicastrin unveils secrets of γ-secretase. *Proc. Natl. Acad. Sci. U. S. A.* **111**, 14643–14644 (2014).

112. Sun, L. *et al.* Structural basis of human γ-secretase assembly. *Proc. Natl. Acad. Sci. U. S. A.* **112**, 6003–6008 (2015).

113. Bai, X.-C. *et al.* An atomic structure of human γ-secretase. *Nature* **525**, 212–217 (2015).

114. Bai, X., Rajendra, E., Yang, G., Shi, Y. & Scheres, S. H. W. Sampling the conformational space of the catalytic subunit of human γ-secretase. *eLife* **4**, e11182 (2015).

115. Zhou, R., Yang, G. & Shi, Y. Macromolecular complex in recognition and proteolysis of amyloid precursor protein in Alzheimer's disease. *Curr. Opin. Struct. Biol.* **61**, 1–8 (2020).

116. Yang, G. *et al.* Structural basis of Notch recognition by human γ-secretase. *Nature* **565**, 192–197 (2019).

117. Zhou, R. *et al.* Recognition of the amyloid precursor protein by human γ-secretase. *Science* **363**, eaaw0930 (2019).

118. Saiki, R. K. *et al.* Primer-directed enzymatic amplification of DNA with a thermostable DNA polymerase. *Science* **239**, 487–491 (1988).

119. Saiki, R. K. *et al.* Enzymatic amplification of beta-globin genomic sequences and restriction site analysis for diagnosis of sickle cell anemia. *Science* **230**, 1350–1354 (1985).

120. Li, M. Z. & Elledge, S. J. Harnessing homologous recombination in vitro to generate recombinant DNA via SLIC. *Nat. Methods* **4**, 251–256 (2007).

121. Doyle, S. A. High-throughput cloning for proteomics research. *Methods Mol. Biol. Clifton NJ* **310**, 107–113 (2005).

122. Hsu, P. D., Lander, E. S. & Zhang, F. Development and applications of CRISPR-Cas9 for genome engineering. *Cell* **157**, 1262–1278 (2014).

123. Berkner, K. L. & Folk, W. R. Polynucleotide kinase exchange reaction: quantitave assay for restriction endonuclease-generated 5'-phosphoroyl termini in DNA. *J. Biol. Chem.* **252**, 3176–3184 (1977).

124. MAHMOUDI, S. *et al.* Optimizing of Nutrients for High Level Expression of Recombinant Streptokinase Using pET32a Expression System. *Mædica* **7**, 241–246 (2012).

125. Magnusdottir, A., Johansson, I., Dahlgren, L.-G., Nordlund, P. & Berglund, H. Enabling IMAC purification of low abundance recombinant proteins from E. coli lysates. *Nat. Methods* **6**, 477–478 (2009).

126. Neilands, J. B. Siderophores: structure and function of microbial iron transport compounds. *J. Biol. Chem.* **270**, 26723–26726 (1995).

127. Hochuli, E., Bannwarth, W., Döbeli, H., Gentz, R. & Stüber, D. Genetic Approach to Facilitate Purification of Recombinant Proteins with a Novel Metal Chelate Adsorbent. *Bio/Technology* **6**, 1321–1325 (1988).

128. Bolanos-Garcia, V. M. & Davies, O. R. Structural analysis and classification of native proteins from E. coli commonly co-purified by immobilised metal affinity chromatography. *Biochim. Biophys. Acta* **1760**, 1304–1313 (2006).

129. Chen, Y., Li, Y., Liu, P., Sun, Q. & Liu, Z. Optimized expression in Pichia pastoris eliminates common protein contaminants from subsequent His-tag purification. *Biotechnol. Lett.* **36**, 711–718 (2014).

130. Locatelli-Hoops, S. C., Gorshkova, I., Gawrisch, K. & Yeliseev, A. A. Expression, surface immobilization, and characterization of functional recombinant cannabinoid receptor CB2. *Biochim. Biophys. Acta* **1834**, 2045–2056 (2013).

131. Hodges, R. S., Heaton, R. J., Parker, J. M., Molday, L. & Molday, R. S. Antigen-antibody interaction. Synthetic peptides define linear antigenic determinants recognized by monoclonal antibodies directed to the cytoplasmic carboxyl terminus of rhodopsin. *J. Biol. Chem.* **263**, 11768–11775 (1988).

132. Majeed, S. A., Sekhosana, K. E. & Tuhl, A. Progress on phthalocyanine-conjugated Ag and Au nanoparticles: Synthesis, characterization, and photo-physicochemical properties. *Arab. J. Chem.* **13**, 8848–8887 (2020).

133. Paul-Dauphin, S. *et al.* Probing Size Exclusion Mechanisms of Complex Hydrocarbon Mixtures: The Effect of Altering Eluent Compositions. *Energy Fuels* **21**, 3484–3489 (2007).

134. Fekete, S., Beck, A., Veuthey, J.-L. & Guillarme, D. Theory and practice of size exclusion chromatography for the analysis of protein aggregates. *J. Pharm. Biomed. Anal.* **101**, 161–173 (2014).

135. Hong, P., Koza, S. & Bouvier, E. S. P. Size-Exclusion Chromatography for the Analysis of Protein Biotherapeutics and their Aggregates. *J. Liq. Chromatogr. Relat. Technol.* **35**, 2923–2950 (2012).

136. Lee, J. *et al.* Principles and applications of steric exclusion chromatography. *J. Chromatogr. A* **1270**, 162–170 (2012).

137. Anandan, A. & Vrielink, A. Detergents in Membrane Protein Purification and Crystallisation. *Adv. Exp. Med. Biol.* **922**, 13–28 (2016).

138. Frenkel, E. J., Roelofsen, B., Brodbeck, U., van Deenen, L. L. & Ott, P. Lipid-protein interactions in human erythrocyte-membrane acetylcholinesterase. Modulation of enzyme activity by lipids. *Eur. J. Biochem.* **109**, 377–382 (1980).

139. Liao, Y., Yuan, Q., Torres, J., Tam, J. P. & Liu, D. X. Biochemical and functional characterization of the membrane association and membrane permeabilizing activity of the severe acute respiratory syndrome coronavirus envelope protein. *Virology* **349**, 264–275 (2006).

140. Aroca, J. D. *et al.* Correlation between the effect of the anti-neoplastic ether lipid 1-O-octadecyl-2-O-methyl-glycero-3-phosphocholine on the membrane and the activity of protein kinase Calpha. *Eur. J. Biochem.* **268**, 6369–6378 (2001).

141. Zoonens, M. & Popot, J.-L. Amphipols for each season. *J. Membr. Biol.* **247**, 759–796 (2014).

142. Ritchie, T. K. *et al.* Chapter 11 - Reconstitution of membrane proteins in phospholipid bilayer nanodiscs. *Methods Enzymol.* **464**, 211–231 (2009).

143. Rigaud, J.-L. & Lévy, D. Reconstitution of membrane proteins into liposomes. *Methods Enzymol.* **372**, 65–86 (2003).

144. Tribet, C., Audebert, R. & Popot, J.-L. Amphipols: Polymers that keep membrane proteins soluble in aqueous solutions. *Proc. Natl. Acad. Sci.* **93**, 15047–15050 (1996).

145. Bayburt, T. H., Grinkova, Y. V. & Sligar, S. G. Self-Assembly of Discoidal Phospholipid Bilayer Nanoparticles with Membrane Scaffold Proteins. *Nano Lett.* **2**, 853–856 (2002).

146. Shih, A. Y., Arkhipov, A., Freddolino, P. L., Sligar, S. G. & Schulten, K. Assembly of Lipids and Proteins into Lipoprotein Particles. *J. Phys. Chem. B* **111**, 11095–11104 (2007).

147. Shih, A. Y., Freddolino, P. L., Sligar, S. G. & Schulten, K. Disassembly of nanodiscs with cholate. *Nano Lett.* **7**, 1692–1696 (2007).

148. Denisov, I. G. & Sligar, S. G. NANODISCS IN MEMBRANE BIOCHEMISTRY AND BIOPHYSICS. *Chem. Rev.* **117**, 4669–4713 (2017).

149. Bayburt, T. H. & Sligar, S. G. Membrane protein assembly into Nanodiscs. *FEBS Lett.* **584**, 1721–1727 (2010).

150. Nisini, R., Poerio, N., Mariotti, S., De Santis, F. & Fraziano, M. The Multirole of Liposomes in Therapy and Prevention of Infectious Diseases. *Front. Immunol.* **9**, (2018).

151. Abu Lila, A. S. & Ishida, T. Liposomal Delivery Systems: Design Optimization and Current Applications. *Biol. Pharm. Bull.* **40**, 1–10 (2017).

152. Eytan, G. D. Use of liposomes for reconstitution of biological functions. *Biochim. Biophys. Acta* **694**, 185–202 (1982).

153. Goddard, A. D., Dijkman, P. M., Adamson, R. J., dos Reis, R. I. & Watts, A. Reconstitution of membrane proteins: a GPCR as an example. *Methods Enzymol.* **556**, 405–424 (2015).

154. Rigaud, J.-L. Membrane proteins: functional and structural studies using reconstituted proteoliposomes and 2-D crystals. *Braz. J. Med. Biol. Res. Rev. Bras. Pesqui. Medicas E Biol.* **35**, 753–766 (2002).

155. Edelhoch, H. Spectroscopic determination of tryptophan and tyrosine in proteins. *Biochemistry* **6**, 1948–1954 (1967).

156. Gill, S. C. & von Hippel, P. H. Calculation of protein extinction coefficients from amino acid sequence data. *Anal. Biochem.* **182**, 319–326 (1989).

157. Gasteiger, E. *et al.* Protein Identification and Analysis Tools on the ExPASy Server. in *The Proteomics Protocols Handbook* (ed. Walker, J. M.) 571–607 (Humana Press, 2005). doi:10.1385/1-59259-890-0:571.

158. Bradford, M. M. A rapid and sensitive method for the quantitation of microgram quantities of protein utilizing the principle of protein-dye binding. *Anal. Biochem.* **72**, 248–254 (1976).

159. Kielkopf, C. L., Bauer, W. & Urbatsch, I. L. Bradford Assay for Determining Protein Concentration. *Cold Spring Harb. Protoc.* **2020**, 102269 (2020).

160. Kielkopf, C. L., Bauer, W. & Urbatsch, I. L. Methods for Measuring the Concentrations of Proteins. *Cold Spring Harb. Protoc.* **2020**, 102277 (2020).

161. Olson, B. J. S. C. & Markwell, J. Assays for determination of protein concentration. *Curr. Protoc. Protein Sci.* **Chapter 3**, Unit 3.4 (2007).

162. Smith, P. K. *et al.* Measurement of protein using bicinchoninic acid. *Anal. Biochem.* **150**, 76–85 (1985).

163. Laemmli, U. K. Cleavage of structural proteins during the assembly of the head of bacteriophage T4. *Nature* **227**, 680–685 (1970).

164. Studier, F. W. Slab-gel electrophoresis. *Trends Biochem. Sci.* **25**, 588–590 (2000).

165. Ladner, C. L., Yang, J., Turner, R. J. & Edwards, R. A. Visible fluorescent detection of proteins in polyacrylamide gels without staining. *Anal. Biochem.* **326**, 13–20 (2004).

166. Bay, D. C. & Turner, R. J. Spectroscopic analysis of the intrinsic chromophores within small multidrug resistance protein SugE. *Biochim. Biophys. Acta* **1808**, 2233–2244 (2011).

167. Mahmood, T. & Yang, P.-C. Western blot: technique, theory, and trouble shooting. *North Am. J. Med. Sci.* **4**, 429–434 (2012).

168. Alegria-Schaffer, A. Western blotting using chemiluminescent substrates. *Methods Enzymol.* **541**, 251–259 (2014).

169. Johnson, W. C. Protein secondary structure and circular dichroism: a practical guide. *Proteins* **7**, 205–214 (1990).

170. Rogers, D. M. *et al.* Electronic Circular Dichroism Spectroscopy of Proteins. *Chem* **5**, 2751–2774 (2019).

171. Woody, R. W. Circular dichroism. *Methods Enzymol.* **246**, 34–71 (1995).

172. Kelly, S. M., Jess, T. J. & Price, N. C. How to study proteins by circular dichroism. *Biochim. Biophys. Acta* **1751**, 119–139 (2005).

173. Greenfield, N. J. Using circular dichroism spectra to estimate protein secondary structure. *Nat. Protoc.* **1**, 2876–2890 (2006).

174. Kelly, S. M. & Price, N. C. The use of circular dichroism in the investigation of protein structure and function. *Curr. Protein Pept. Sci.* **1**, 349–384 (2000).

175. Johnson, W. C. Analyzing protein circular dichroism spectra for accurate secondary structures. *Proteins* **35**, 307–312 (1999).

176. Whitmore, L. & Wallace, B. A. Protein secondary structure analyses from circular dichroism spectroscopy: methods and reference databases. *Biopolymers* **89**, 392–400 (2008).

177. Abdul-Gader, A., Miles, A. J. & Wallace, B. A. A reference dataset for the analyses of membrane protein secondary structures and transmembrane residues using circular dichroism spectroscopy. *Bioinforma. Oxf. Engl.* **27**, 1630–1636 (2011).

178. Ghisaidoobe, A. B. T. & Chung, S. J. Intrinsic tryptophan fluorescence in the detection and analysis of proteins: a focus on Förster resonance energy transfer techniques. *Int. J. Mol. Sci.* **15**, 22518–22538 (2014).

179. Jablonski diagram. *Wikipedia* (2021).

180. Masters, B. R. Book Review: Principles of Fluorescence Spectroscopy, Third Edition. *J. Biomed. Opt.* **13**, 029901 (2008).

181. Jerabek-Willemsen, M., Wienken, C. J., Braun, D., Baaske, P. & Duhr, S. Molecular interaction studies using microscale thermophoresis. *Assay Drug Dev. Technol.* **9**, 342–353 (2011).

182. Jerabek-Willemsen, M. *et al.* MicroScale Thermophoresis: Interaction analysis and beyond. *J. Mol. Struct.* **1077**, 101–113 (2014).

183. Wienken, C. J., Baaske, P., Rothbauer, U., Braun, D. & Duhr, S. Protein-binding assays in biological liquids using microscale thermophoresis. *Nat. Commun.* **1**, 100 (2010).

184. Shao, W., Sharma, R., Clausen, M. H. & Scheller, H. V. Microscale thermophoresis as a powerful tool for screening glycosyltransferases involved in cell wall biosynthesis. *Plant Methods* **16**, 99 (2020).

185. Corbeski, I. *et al.* Microscale Thermophoresis Analysis of Chromatin Interactions. *Methods Mol. Biol. Clifton NJ* **1837**, 177–197 (2018).

186. Petersen, K. J. *et al.* Fluorescence lifetime plate reader: Resolution and precision meet high-throughput. *Rev. Sci. Instrum.* **85**, 113101 (2014).

187. Gruber, S. J. *et al.* Discovery of enzyme modulators via high-throughput time-resolved FRET in living cells. *J. Biomol. Screen.* **19**, 215–222 (2014).

188. Cornea, R. L. *et al.* High-throughput FRET assay yields allosteric SERCA activators. *J. Biomol. Screen.* **18**, 97–107 (2013).

189. Farmery, M. R. *et al.* Partial purification and characterization of gamma-secretase from post-mortem human brain. *J. Biol. Chem.* **278**, 24277–24284 (2003).

190. Dang, S. *et al.* Cleavage of amyloid precursor protein by an archaeal presenilin homologue PSH. *Proc. Natl. Acad. Sci. U. S. A.* **112**, 3344–3349 (2015).

191. Blakeley, B. D., Chapman, A. M. & McNaughton, B. R. Split-superpositive GFP reassembly is a fast, efficient, and robust method for detecting protein-protein interactions in vivo. *Mol. Biosyst.* **8**, 2036–2040 (2012).

192. Mahapatra, A., Mandal, N. & Chattopadhyay, K. Cholesterol in Synaptic Vesicle Membranes Regulates the Vesicle-Binding, Function, and Aggregation of α-Synuclein. *J. Phys. Chem. B* **125**, 11099–11111 (2021).

193. Bergman, A. *et al.* Pen-2 is sequestered in the endoplasmic reticulum and subjected to ubiquitylation and proteasome-mediated degradation in the absence of presenilin. *J. Biol. Chem.* **279**, 16744–16753 (2004).

194. Hasegawa, H. *et al.* Both the sequence and length of the C terminus of PEN-2 are critical for intermolecular interactions and function of presenilin complexes. *J. Biol. Chem.* **279**, 46455–46463 (2004).

195. Oluwole, A. O. *et al.* Solubilization of Membrane Proteins into Functional Lipid-Bilayer Nanodiscs Using a Diisobutylene/Maleic Acid Copolymer. *Angew. Chem. Int. Ed Engl.* **56**, 1919–1924 (2017).

196. Autzen, H. E., Julius, D. & Cheng, Y. Membrane mimetic systems in CryoEM: keeping membrane proteins in their native environment. *Curr. Opin. Struct. Biol.* **58**, 259–268 (2019).

197. Oluwole, A. O. *et al.* Formation of Lipid-Bilayer Nanodiscs by Diisobutylene/Maleic Acid (DIBMA) Copolymer. *Langmuir ACS J. Surf. Colloids* **33**, 14378–14388 (2017).

198. Barniol-Xicota, M. & Verhelst, S. H. L. Stable and Functional Rhomboid Proteases in Lipid Nanodiscs by Using Diisobutylene/Maleic Acid Copolymers. *J. Am. Chem. Soc.* **140**, 14557–14561 (2018).

199. Dilworth, M. V., Findlay, H. E. & Booth, P. J. Detergent-free purification and reconstitution of functional human serotonin transporter (SERT) using diisobutylene maleic acid (DIBMA) copolymer. *Biochim. Biophys. Acta Biomembr.* **1863**, 183602 (2021).

200. Voskoboynikova, N. *et al.* Evaluation of DIBMA nanoparticles of variable size and anionic lipid content as tools for the structural and functional study of membrane proteins. *Biochim. Biophys. Acta Biomembr.* **1863**, 183588 (2021).

201. Yu, K. Characterization of the subunits of the γ-secretase complex. (Universität Düsseldorf, 2016).

202. Zhou, H., Zhou, S., Walian, P. J. & Jap, B. K. Dependency of γ-secretase complex activity on the structural integrity of the bilayer. *Biochem. Biophys. Res. Commun.* **402**, 291–296 (2010).

203. Osenkowski, P., Ye, W., Wang, R., Wolfe, M. S. & Selkoe, D. J. Direct and potent regulation of gamma-secretase by its lipid microenvironment. *J. Biol. Chem.* **283**, 22529–22540 (2008).

204. Hagn, F., Nasr, M. L. & Wagner, G. Assembly of phospholipid nanodiscs of controlled size for structural studies of membrane proteins by NMR. *Nat. Protoc.* **13**, 79–98 (2018).

205. Deshpande, S., Spoelstra, W. K., van Doorn, M., Kerssemakers, J. & Dekker, C. Mechanical Division of Cell-Sized Liposomes. *ACS Nano* **12**, 2560–2568 (2018).

206. Ayciriex, S. *et al.* The lipidome associated with the γ-secretase complex is required for its integrity and activity. *Biochem. J.* **473**, 321–334 (2016).

207. Holmes, O., Paturi, S., Wolfe, M. S. & Selkoe, D. J. Functional Analysis and purification of a Pen-2 Fusion Protein for γ-Secretase Structural Studies. *J. Neurochem.* **131**, 94–100 (2014).

208. Bokhove, M. *et al.* Easy mammalian expression and crystallography of maltose-binding protein-fused human proteins. *J. Struct. Biol.* **194**, 1–7 (2016).

209. Goutte, C., Tsunozaki, M., Hale, V. A. & Priess, J. R. APH-1 is a multipass membrane protein essential for the Notch signaling pathway in Caenorhabditis elegans embryos. *Proc. Natl. Acad. Sci. U. S. A.* **99**, 775–779 (2002).

210. Wang, C. *et al.* Flagellin lysine methyltransferase FliB catalyzes a [4Fe-4S] mediated methyl transfer reaction. *PLoS Pathog.* **17**, e1010052 (2021).

211. Yang, G. *et al.* Structural basis of Notch recognition by human γ-secretase. *Nature* **565**, 192–197 (2019).

212. Zhou, R. *et al.* Recognition of the amyloid precursor protein by human γ-secretase. *Science* **363**, eaaw0930 (2019).

213. Yang, G., Yu, K., Kaitatzi, C.-S., Singh, A. & Labahn, J. Influence of solubilization and AD-mutations on stability and structure of human presenilins. *Sci. Rep.* **7**, 17970 (2017).

214. Sandermann, H. Regulation of membrane enzymes by lipids. *Biochim. Biophys. Acta BBA - Rev. Biomembr.* **515**, 209–237 (1978).

215. Fukumori, A. & Steiner, H. Substrate recruitment of γ-secretase and mechanism of clinical presenilin mutations revealed by photoaffinity mapping. *EMBO J.* **35**, 1628–1643 (2016).

216. Sato, C., Takagi, S., Tomita, T. & Iwatsubo, T. The C-terminal PAL motif and transmembrane domain 9 of presenilin 1 are involved in the formation of the catalytic pore of the gamma-secretase. *J. Neurosci. Off. J. Soc. Neurosci.* **28**, 6264–6271 (2008).

217. Wang, J., Brunkan, A. L., Hecimovic, S., Walker, E. & Goate, A. Conserved 'PAL' sequence in presenilins is essential for gamma-secretase activity, but not required for formation or stabilization of gamma-secretase complexes. *Neurobiol. Dis.* **15**, 654–666 (2004).

218. Wang, J. *et al.* C-terminal PAL motif of presenilin and presenilin homologues required for normal active site conformation. *J. Neurochem.* **96**, 218–227 (2006).

219. Kornilova, A. Y., Bihel, F., Das, C. & Wolfe, M. S. The initial substrate-binding site of gamma-secretase is located on presenilin near the active site. *Proc. Natl. Acad. Sci. U. S. A.* **102**, 3230–3235 (2005).

220. Tian, G. *et al.* Linear non-competitive inhibition of solubilized human gamma-secretase by pepstatin A methylester, L685458, sulfonamides, and benzodiazepines. *J. Biol. Chem.* **277**, 31499–31505 (2002).

221. Yang, G. *et al.* Structural basis of γ-secretase inhibition and modulation by small molecule drugs. *Cell* **184**, 521-533.e14 (2021).

222. Barthet, G. *et al.* Inhibitors of γ-secretase stabilize the complex and differentially affect processing of amyloid precursor protein and other substrates. *FASEB J. Off. Publ. Fed. Am. Soc. Exp. Biol.* **25**, 2937–2946 (2011).

223. Ho, M. *et al.* Effect of Metal Chelators on γ-Secretase Indicates That Calcium and Magnesium Ions Facilitate Cleavage of Alzheimer Amyloid Precursor Substrate. *Int. J. Alzheimers Dis.* **2011**, 950932 (2010).

224. De Strooper, B. Aph-1, Pen-2, and Nicastrin with Presenilin generate an active gamma-Secretase complex. *Neuron* **38**, 9–12 (2003).

225. Xia, W. From presenilinase to gamma-secretase, cleave to capacitate. *Curr. Alzheimer Res.* **5**, 172–178 (2008).

226. Cacquevel, M., Aeschbach, L., Houacine, J. & Fraering, P. C. Alzheimer's disease-linked mutations in presenilin-1 result in a drastic loss of activity in purified γ-secretase complexes. *PloS One* **7**, e35133 (2012).

227. Nyabi, O. *et al.* Presenilins mutated at Asp-257 or Asp-385 restore Pen-2 expression and Nicastrin glycosylation but remain catalytically inactive in the absence of wild type Presenilin. *J. Biol. Chem.* **278**, 43430–43436 (2003).

228. Figueiredo-Pereira, M. E. *et al.* Distinct secretases, a cysteine protease and a serine protease, generate the C termini of amyloid beta-proteins Abeta1-40 and Abeta1-42, respectively. *J. Neurochem.* **72**, 1417–1422 (1999).

229. Petit, A. *et al.* New protease inhibitors prevent gamma-secretase-mediated production of Abeta40/42 without affecting Notch cleavage. *Nat. Cell Biol.* **3**, 507–511 (2001).

230. Peuchmaur, M. *et al.* Further characterization of a putative serine protease contributing to the γ-secretase cleavage of β-amyloid precursor protein. *Bioorg. Med. Chem.* **21**, 1018–1029 (2013).

231. Campbell, W. A., Iskandar, M.-K., Reed, M. L. O. & Xia, W. Endoproteolysis of presenilin in vitro: inhibition by gamma-secretase inhibitors. *Biochemistry* **41**, 3372–3379 (2002).

232. Campbell, W. A., Reed, M. L. O., Strahle, J., Wolfe, M. S. & Xia, W. Presenilin endoproteolysis mediated by an aspartyl protease activity pharmacologically distinct from gamma-secretase. *J. Neurochem.* **85**, 1563–1574 (2003).

233. Xia, W. Relationship between presenilinase and gamma-secretase. *Drug News Perspect.* **16**, 69–74 (2003).

234. Shinoda, T. *et al.* Cell-free methods to produce structurally intact mammalian membrane proteins. *Sci. Rep.* **6**, 30442 (2016).

235. Takeo, K. *et al.* Allosteric regulation of γ-secretase activity by a phenylimidazole-type γ-secretase modulator. *Proc. Natl. Acad. Sci. U. S. A.* **111**, 10544–10549 (2014).

236. Naing, S.-H. *et al.* Both positional and chemical variables control in vitro proteolytic cleavage of a presenilin ortholog. *J. Biol. Chem.* **293**, 4653–4663 (2018).

237. Phillips, J. C. Why Aβ42 Is Much More Toxic than Aβ40. *ACS Chem. Neurosci.* **10**, 2843–2847 (2019).

238. He, G. *et al.* Gamma-secretase activating protein is a therapeutic target for Alzheimer's disease. *Nature* **467**, 95–98 (2010).

239. Watanabe, H. *et al.* Specific Mutations in Aph1 Cause γ-Secretase Activation. *Int. J. Mol. Sci.* **23**, 507 (2022).

240. Morais, V. A. *et al.* The transmembrane domain region of nicastrin mediates direct interactions with APH-1 and the gamma-secretase complex. *J. Biol. Chem.* **278**, 43284–43291 (2003).

Appendix I: DNA and protein sequences

>Presenilin1_WT_nucl

ATGGGCAGCAGCCATCATCATCATCATCACAGCAGCGGCCTGGTGCCGCGCGGCAGC
CATATGACCGAACTGCCTGCACCGCTGAGCTATTTTCAGAATGCACAGATGAGCGAA
GATAACCATCTGAGCAATACCGTTCGTAGCCAGAATGATAATCGTGAACGTCAAGAA
CACAATGATCGTCGTAGCCTGGGTCATCCGGAACCGCTGAGTAATGGTCGTCCGCAG
GGTAATAGCCGTCAGGTTGTTGAACAGGATGAAGAGGAAGATGAAGAACTGACCCT
GAAATATGGTGCCAAACATGTGATTATGCTGTTTGTTCCGGTTACCCTGTGTATGGTT
GTTGTTGTGGCAACCATTAAAAGCGTGAGCTTTTATACCCGTAAAGATGGCCAGCTG
ATTTATACCCCGTTTACCGAAGATACCGAAACCGTTGGTCAGCGTGCACTGCATAGT
ATTCTGAATGCAGCAATTATGATTAGCGTGATTGTGGTGATGACCATTCTGCTGGTTG
TTCTGTATAAATACCGCTGCTATAAAGTGATTCATGCCTGGCTGATTATTAGCAGCCT
GCTGCTGCTGTTTTTCTTCAGCTTTATCTATCTGGGCGAAGTGTTCAAAACCTATAAT
GTTGCCGTTGATTATATCACCGTTGCACTGCTGATTTGGAATTTTGGTGTTGTTGGCA
TGATTAGCATCCATTGGAAAGGTCCGCTGCGTCTGCAGCAGGCATATCTGATTATGA
TTTCAGCACTGATGGCCCTGGTGTTCATCAAATATCTGCCGGAATGGACCGCATGGC
TGATTCTGGCAGTTATTAGCGTTTATGATCTGGTTGCAGTTCTGTGTCCGAAAGGCCC
TCTGCGTATGCTGGTTGAAACCGCACAAGAACGTAATGAAACCCTGTTTCCGGCACT
GATTTATTCAAGCACCATGGTTTGGCTGGTTAATATGGCAGAAGGTGATCCGGAAGC
ACAGCGTCGTGTTAGCAAAAATAGCAAATACAATGCAGAAAGCACCGAACGTGAAA
GCCAGGATACCGTTGCAGAAAATGATGATGGTGGTTTTAGCGAAGAATGGGAAGCC
CAGCGTGATAGCCATCTGGGTCCGCATCGTAGCACACCGGAAAGCCGTGCAGCAGTT
CAAGAACTGAGCAGCTCAATCCTGGCAGGCGAAGATCCTGAAGAACGTGGTGTTAA
ACTGGGTCTGGGTGATTTTATCTTTTATAGCGTTCTGGTTGGTAAAGCAAGCGCAACC
GCAAGCGGTGATTGGAATACCACCATTGCATGTTTTGTTGCCATTCTGATTGGTCTGT
GTCTGACATTACTGCTGCTGGCCATTTTCAAAAAAGCACTGCCTGCCCTGCCGATTAG
CATTACCTTTGGTCTGGTTTTTTACTTCGCAACCGATTATCTGGTTCAGCCGTTTATGG
ATCAACTGGCATTTCACCAGTTTTACATCTAA

>Presenilin1_WT_Prot

MGSSHHHHHHSSGLVPRGSHMTELPAPLSYFQNAQMSEDNHLSNTVRSQNDNRERQEH
NDRRSLGHPEPLSNGRPQGNSRQVVEQDEEEDEELTLKYGAKHVIMLFVPVTLCMVVV
VATIKSVSFYTRKDGQLIYTPFTEDTETVGQRALHSILNAAIMISVIVVMTILLVVLYKYR
CYKVIHAWLIISSLLLLFFFSFIYLGEVFKTYNVAVDYITVALLIWNFGVVGMISIHWKGP
LRLQQAYLIMISALMALVFIKYLPEWTAWLILAVISVYDLVAVLCPKGPLRMLVETAQE
RNETLFPALIYSSTMVWLVNMAEGDPEAQRRVSKNSKYNAESTERESQDTVAENDDGG
FSEEWEAQRDSHLGPHRSTPESRAAVQELSSSILAGEDPEERGVKLGLGDFIFYSVLVGK
ASATASGDWNTTIACFVAILIGLCLTLLLLAIFKKALPALPISITFGLVFYFATDYLVQPFM
DQLAFHQFYI

>Presenilin2_WT_nucl

ATGAAGCACCATCATCACCATCACCATATGCTGACCTTTATGGCGAGCGATAGCGAG
GAAGAAGTGTGCGACGAACGTACCAGCCTGATGAGCGCGGAAAGCCCGACCCCGCG
TAGCTGTCAGGAAGGCCGTCAGGGCCCGGAAGATGGCGAAAACACCGCCCAGTGGC
GTAGCCAAGAAAACGAAGAGGATGGCGAAGAAGATCCGGATCGTTACGTGTGTAGC
GGCGTGCCGGGTCGTCCGCCGGGTCTGGAAGAAGAACTGACCCTGAAATATGGCGC
GAAACATGTGATTATGCTGTTTGTGCCGGTGACCCTGTGCATGATTGTGGTGGTGGC
GACCATTAAAAGCGTGCGCTTCTACACCGAAAAAAACGGCCAGCTGATCTATACCAC
CTTTACCGAAGATACCCCGAGCGTGGGCCAGCGTCTGCTGAACAGCGTGCTGAACAC
CCTGATTATGATTAGCGTGATTGTGGTGATGACCATTTTTCTGGTGGTGCTGTATAAA
TATCGCTGTTATAAATTTATTCACGGCTGGCTGATTATGAGCAGCCTGATGCTGCTGT
TTCTGTTCACCTATATCTATCTGGGCGAAGTGCTGAAAACCTATAACGTGGCAATGG
ATTATCCGACCCTGCTGCTGACCGTGTGGAACTTTGGCGCGGTGGGCATGGTGTGCA
TTCATTGGAAAGGCCCGCTGGTGCTGCAGCAGGCGTATCTGATCATGATCTCTGCCC
TGATGGCGCTGGTGTTTATTAAATATCTGCCGGAATGGTCTGCGTGGGTGATTCTGG
GCGCGATTAGCGTGTATGATCTGGTGGCGGTGCTGTGCCCGAAAGGTCCGCTGCGTA
TGCTGGTTGAAACCGCGCAGGAACGTAACGAACCGATTTTTCCGGCGCTGATTTATT
CTAGCGCAATGGTGTGGACCGTGGGCATGGCGAAACTGGACCCGAGCAGCCAGGGT
GCGCTGCAGCTGCCGTATGATCCGGAAATGGAAGAAGATAGCTACGATAGCTTTGGC
GAACCGAGCTATCCGGAAGTGTTTGAACCGCCGCTGACCGGCTATCCGGGCGAAGA

ACTGGAAGAAGAAGAAGAACGCGGCGTTAAACTGGGCCTGGGCGATTTTATTTTTTA
TAGCGTGCTGGTTGGCAAAGCGGCGGCGACCGGTAGCGGCGATTGGAACACCACCC
TGGCCTGCTTTGTGGCGATTCTGATTGGCCTGTGCCTGACCCTGCTGCTGCTGGCCGT
GTTTAAAAAAGCGCTGCCGGCCCTGCCGATTAGCATTACCTTTGGCCTGATCTTTTAT
TTCAGCACCGATAACCTGGTGCGTCCGTTTATGGATACCCTGGCCAGCCATCAGCTG
TATATTTAA

>Presenilin2_WT_prot

MKHHHHHHHMLTFMASDSEEEVCDERTSLMSAESPTPRSCQEGRQGPEDGENTAQWRS
QENEEDGEEDPDRYVCSGVPGRPPGLEEELTLKYGAKHVIMLFVPVTLCMIVVVATIKSV
RFYTEKNGQLIYTTFTEDTPSVGQRLLNSVLNTLIMISVIVVMTIFLVVLYKYRCYKFIHG
WLIMSSLMLLFLFTYIYLGEVLKTYNVAMDYPTLLLTVWNFGAVGMVCIHWKGPLVLQ
QAYLIMISALMALVFIKYLPEWSAWVILGAISVYDLVAVLCPKGPLRMLVETAQERNEPI
FPALIYSSAMVWTVGMAKLDPSSQGALQLPYDPEMEEDSYDSFGEPSYPEVFEPPLTGYP
GEELEEEEERGVKLGLGDFIFYSVLVGKAAATGSGDWNTTLACFVAILIGLCLTLLLLAV
FKKALPALPISITFGLIFYFSTDNLVRPFMDTLASHQLYI

>Nicastrin_nucl

ATGCATCATCACCACCATCACCATCATCATCACGCAATTGAAGGTCGTAATAGCGTT
GAACGCAAAATCTATATTCCGCTGAATAAAACCGCACCGTGTGTTCGTCTGCTGAAT
GCAACCCATCAGATTGGTTGTCAGAGCAGCATTAGCGGTGATACCGGTGTTATTCAT
GTTGTGGAAAAAGAAGAGGATCTGCAGTGGGTTCTGACCGATGGTCCGAATCCGCCT
TATATGGTTCTGCTGGAAAGCAAACATTTTACCCGTGATCTGATGGAAAAACTGAAA
GGTCGTACCAGCCGTATTGCAGGTCTGGCAGTTAGCCTGACCAAACCGAGTCCGGCA
AGCGGTTTTAGCCCGAGCGTTCAGTGTCCGAATGATGGTTTTGGTGTTTATAGCAATA
GCTACGGTCCGGAATTTGCACATTGTCGTGAAATTCAGTGGAATAGCCTGGGTAATG
GTCTGGCCTATGAAGATTTTAGCTTTCCGATTTTCCTGCTGGAAGATGAGAATGAAA
CCAAAGTGATCAAACAGTGCTATCAGGATCATAATCTGAGCCAGAATGGTAGCGCA
CCGACCTTTCCGCTGTGTGCAATGCAGCTGTTTAGCCACATGCATGCAGTTATTAGCA
CCGCAACCTGTATGCGTCGTAGCAGCATTCAGAGCACCTTTAGCATTAATCCGGAAA

TTGTTTGTGATCCGCTGAGCGATTATAATGTTTGGAGCATGCTGAAACCGATTAATAC
CACCGGCACCCTGAAACCGGATGATCGTGTTGTTGTTGCAGCAACCCGTCTGGATAG
CCGTAGCTTTTTTTGGAATGTTGCACCGGGTGCAGAAAGCGCAGTTGCAAGCTTTGTT
ACCCAGCTGGCAGCAGCAGAAGCACTGCAAAAAGCACCGGATGTTACCACCCTGCC
TCGTAATGTGATGTTTGTTTTTTTTCAGGGCGAAACCTTCGATTATATTGGTAGCAGC
CGTATGGTGTACGATATGGAAAAAGGTAAATTTCCGGTGCAGCTGGAAAATGTTGAT
AGCTTTGTTGAACTGGGTCAGGTTGCACTGCGTACCAGTCTGGAACTGTGGATGCAT
ACCGATCCGGTTAGCCAGAAAAATGAAAGCGTTCGTAATCAGGTTGAAGATCTGCTG
GCAACCCTGGAAAAAGCGGTGCGGGTGTTCCGGCAGTTATTCTGCGTCGTCCGAAT
CAGAGCCAGCCGCTGCCTCCGAGCAGCCTGCAGCGTTTTCTGCGTGCACGTAATATT
AGTGGTGTTGTTCTGGCAGATCATAGCGGTGCATTTCACAATAAATACTACCAGAGC
ATCTATGACACCGCAGAAAATATCAATGTTAGCTATCCGGAATGGCTGAGTCCGGAA
GAAGATCTGAATTTTGTTACCGATACCGCAAAAGCACTGGCAGATGTTGCAACCGTT
CTGGGTCGTGCACTGTATGAACTGGCAGGCGGTACAAATTTTAGCGATACCGTTCAG
GCAGATCCGCAGACCGTTACCCGTCTGCTGTATGGTTTTCTGATTAAAGCAAATAAC
AGCTGGTTCCAGAGCATTCTGCGCCAGGATCTGCGTAGCTATCTGGGTGATGGTCCG
CTGCAGCACTATATTGCAGTTAGCAGCCCGACCAATACCACCTATGTTGTTCAGTAT
GCACTGGCAAATCTGACCGGCACCGTTGTTAATCTGACCCGTGAACAGTGTCAGGAT
CCGAGCAAAGTTCCGAGCGAAAATAAAGATCTGTATGAGTATAGCTGGGTTCAGGG
TCCTCTGCATAGCAATGAAACGGATCGTCTGCCTCGTTGTGTTCGTAGTACCGCACGT
CTGGCACGTGCGCTGTCACCGGCATTTGAACTGAGCCAGTGGTCAAGCACCGAATAT
AGCACCTGGACCGAAAGCCGTTGGAAAGATATTCGTGCCCGTATTTTTCTGATCGCA
AGCAAAGAACTGGAACTGATTACCCTGACCGTGGGTTTTGGTATTCTGATTTTTAGCC
TGATTGTGACCTATTGCATTAACGCAAAAGCCGATGTTCTGTTTATTGCACCGCGTGA
ACCGGGTGCCGTTAGCTATTAA

>Nicastrin_prot

MHHHHHHHHHHHAIEGRNSVERKIYIPLNKTAPCVRLLNATHQIGCQSSISGDTGVIHVVE
KEEDLQWVLTDGPNPPYMVLLESKHFTRDLMEKLKGRTSRIAGLAVSLTKPSPASGFSPS
VQCPNDGFGVYSNSYGPEFAHCREIQWNSLGNGLAYEDFSFPIFLLEDENETKVIKQCYQ
DHNLSQNGSAPTFPLCAMQLFSHMHAVISTATCMRRSSIQSTFSINPEIVCDPLSDYNVWS
MLKPINTTGTLKPDDRVVVAATRLDSRSFFWNVAPGAESAVASFVTQLAAAEALQKAP

DVTTLPRNVMFVFFQGETFDYIGSSRMVYDMEKGKFPVQLENVDSFVELGQVALRTSLE
LWMHTDPVSQKNESVRNQVEDLLATLEKSGAGVPAVILRRPNQSQPLPPSSLQRFLRAR
NISGVVLADHSGAFHNKYYQSIYDTAENINVSYPEWLSPEEDLNFVTDTAKALADVATV
LGRALYELAGGTNFSDTVQADPQTVTRLLYGFLIKANNSWFQSILRQDLRSYLGDGPLQ
HYIAVSSPTNTTYVVQYALANLTGTVVNLTREQCQDPSKVPSENKDLYEYSWVQGPLHS
NETDRLPRCVRSTARLARALSPAFELSQWSSTEYSTWTESRWKDIRARIFLIASKELELITL
TVGFGILIFSLIVTYCINAKADVLFIAPREPGAVSY

>PEN2_nucl_histag

ATGCATCATCACCACCATCACCATCATCATCACGCAATTGAAGGTCGTAATCTGGAA
CGTGTTAGCAACGAAGAAAAACTGAATCTGTGCCGCAAATATTACCTGGGTGGTTTT
GCATTTCTGCCGTTTCTGTGGCTGGTTAACATCTTTTGGTTTTTTCGTGAAGCATTTCT
GGTTCCGGCATATACCGAACAGAGCCAGATTAAAGGTTATGTTTGGCGTAGCGCAGT
TGGTTTTCTGTTTTGGGTTATTGTTCTGACCAGCTGGATTACCATCTTTCAGATTTATC
GTCCGCGTTGGGGTGCACTGGGTGATTATCTGAGCTTTACCATTCCGCTGGGCACCCC
GTAA

>PEN2_prot_histag

MHHHHHHHHHHAIEGRNLERVSNEEKLNLCRKYYLGGFAFLPFLWLVNIFWFFREAFL
VPAYTEQSQIKGYVWRSAVGFLFWVIVLTSWITIFQIYRPRWGALGDYLSFTIPLGTP

>PEN2_nucl_rhotag

ATGAATCTGGAACGTGTTAGCAACGAAGAAAAACTGAATCTGTGCCGCAAATATTAC
CTGGGTGGTTTTGCATTTCTGCCGTTTCTGTGGCTGGTTAACATCTTTTGGTTTTTTCG
TGAAGCATTTCTGGTTCCGGCATATACCGAACAGAGCCAGATTAAAGGTTATGTTTG
GCGTAGCGCAGTTGGTTTTCTGTTTTGGGTTATTGTTCTGACCAGCTGGATTACCATC
TTTCAGATTTATCGTCCGCGTTGGGGTGCACTGGGTGATTATCTGAGCTTTACCATTC
CGCTGGGCACCCCGGGCTCCTCCGGCACCGAGACTTCCCAGGTGGCGCCAGCTTAAT
AG

>PEN2_prot_rhotag

MNLERVSNEEKLNLCRKYYLGGFAFLPFLWLVNIFWFFREAFLVPAYTEQSQIKGYVWR
SAVGFLFWVIVLTSWITIFQIYRPRWGALGDYLSFTIPLGTPGSSGTETSQVAPA

>APPC100_nucl_flagtag

ATGGATGCAGAATTCCGACATGACTCAGGATATGAAGTTCATCATCAAAAATTGGTG
TTCTTTGCAGAAGATGTGGGTTCAAACAAAGGTGCAATCATTGGACTCATGGTGGGC
GGTGTTGTCATAGCGACAGTGATCGTCATCACCTTGGTGATGCTGAAGAAGAAACAG
TACACATCCATTCATCATGGTGTGGTGGAGGTTGACGCCGCTGTCACCCCAGAGGAG
CGCCACCTGTCCAAGATGCAGCAGAACGGCTACGAAAATCCAACCTACAAGTTCTTT
GAGCAGATGCAGAACGATTACAAGGACGATGACGATAAGTAG

>APPC100_prot_flagtag

MDAEFRHDSGYEVHHQKLVFFAEDVGSNKGAIIGLMVGGVVIATVIVITLVMLKKKQYT
SIHHGVVEVDAAVTPEERHLSKMQQNGYENPTYKFFEQMQNDYKDDDDK

>MBP_tag_nucl

ATGGGTGTACACAGCAGCCATCACCATCATCATCATAGCAGCGAAAATCTGTATTTT
CAGAGCCGTACGAAAATCGAAGAAGGCAAACTGGTTATTTGGATCAATGGCGATAA
AGGCTATAATGGTCTGGCAGAAGTTGGCAAAAAATTCGAAAAAGATACCGGCATTA
AAGTGACCGTTGAACATCCGGATAAACTGGAAGAAAATTTCCGCAGGTTGCAGCA
ACCGGTGATGGTCCGGATATTATCTTTGGGCACATGATCGTTTTGGTGGTTATGCAC
AGAGCGGTCTGCTGGCAGAAATTACACCGGCAGCAGCATTTCAGGACAAACTGTATC
CGTTTACCTGGGATGCAGTTCGCTATAACGGTAAACTGATTGCATATCCGATTGCAG
TTGAAGCACTGAGCCTGATCTATAACAAAGATCTGCTGCCGAATCCGCCTAAAACCT
GGGAAGAAATTCCGGCACTGGATAAGAACTGAAAGCAAAAGGTAAAAGCGCACTG
ATGTTTAATCTGCAAGAACCGTATTTTACCTGGCCTCTGATTGCAGCAGATGGTGGCT
ATGCATTCAAATATGCAGCAGGCAAATATGACATTAAAGATGTTGGTGTTGATAATG

162

CGGGTGCAAAAGCCGGTCTGACCTTTCTGGTTGATCTGATTAAAAACAAACACATGA
ACGCCGATACCGATTATAGCATTGCAGAACATGCATTTAATCATGGTGAAACCGCCA
TGACAATTAATGGTCCGTGGGCATGGTCAAATATTGATACCAGCGCAGTTAATTATG
GTGTTACCGTTCTGCCGACATTTAAAGGTCAGCCGAGCAAACCGTTTGTTGGTGTGCT
GAGCGCAGGTATTAATGCAGCAAGCCCGAACAAAGAACTGGCAAAAGAATTTCTGG
AAAACTATCTGCTGACCGATGAAGGTCTGGAAGCAGTGAATAAAGATAAACCGCTG
GGTGCAGTTGCACTGAAAAGCTATGAAGAAGAACTGGTTAAAGATCCGCGTGTTGC
AGCCACAATGGAAAATGCACAGAAGGTGAAATTATGCCGAATATTCCGCAGATGA
GCGCATTTTGGTATGCCGTTCGTACCGCAGTGATTAATGCCGCATCAGGTCGTCAGA
CCGTTGATGCAGCACTGGCAGCAGCCCAGACCAATCAT

>MBP_tag_prot

MGVHSSHHHHHHSSENLYFQSRTKIEEGKLVIWINGDKGYNGLAEVGKKFEKDTGIKVT
VEHPDKLEEKFPQVAATGDGPDIIFWAHDRFGGYAQSGLLAEITPAAAFQDKLYPFTWD
AVRYNGKLIAYPIAVEALSLIYNKDLLPNPPKTWEEIPALDKELKAKGKSALMFNLQEPY
FTWPLIAADGGYAFKYAAGKYDIKDVGVDNAGAKAGLTFLVDLIKNKHMNADTDYSIA
EHAFNHGETAMTINGPWAWSNIDTSAVNYGVTVLPTFKGQPSKPFVGVLSAGINAASPN
KELAKEFLENYLLTDEGLEAVNKDKPLGAVALKSYEEELVKDPRVAATMENAQKGEIM
PNIPQMSAFWYAVRTAVINAASGRQTVDAALAAAQTNHMGGGSGGGSASLEVLFQ

>FleBt_tag_nucl(unpublished)

ATGACTTCTAACATCAACGGTTTGACTGTGGCAGCACGTAATGCCAACGACGGTATC
TCACTGTCACAGACTGCTGAAGGCGCGTTGGGCGAAATCAACAACAACTTGCAACGT
GTGCGTGACCTGACTGTTCAGGCGCAAAACAGCTCTAACTCAGCATCTGATATCGAC
TCCATCCAGTCTGAAGTTAACCAGCGCATGGAAGAAATCAACCGCGTGACCAAGCA
AACTGATTTCAACGGCATCAAAGTATTGGATAACCGTACCAAGACAGACTCAAGCTA
CGATTTCCAGGTCGGTTCGAAAGATAATGAACAAATCAGCATTGCGATTGGTGCAAG
TTCTGGCTGGAATCTGGCGACAGCCAATGCTGATGGTACTTCATCAGATACTGTAAA
TACTTATGCTTTCACCAAGAAAGCTGCACTTGATACTGCGCAAACTGACTATGATAC
TGCGAATACTGCGTATTTGGCTGCGGTTAAAAGCGGTGTTGCTGGTGATATTACGAC

163

TACCAAAGCCACACTGGATGGTAAAAACACCGCATTAGCTACCGCAGTTAAAGATG

CAACTGCCGTTAATGAAGCGGTAAATGGCAAGGTGCGTACAGTTGCCGCCAAAGGTT

TTGACGTGTTGAATGGCACCGTCGCTGCTGATGGTAAAGCAACCGGTACCACGCCGT

TGGCTGATATCGATAAAGCGCTGAAAGCGGTTGATACACAGCGCAGCGTATTGGGTG

CGTCTCAGAACCGTTTTGAGTCAACCATCACTAACCTGAACAATACCGTGAACAACC

TGACTTCAGCCCGT

>FleBt_tag_prot(unpublished)

MTSNINGLTVAARNANDGISLSQTAEGALGEINNNLQRVRDLTVQAQNSSNSASDIDSIQ

SEVNQRMEEINRVTKQTDFNGIKVLDNRTKTDSSYDFQVGSKDNEQISIAIGASSGWNLA

TANADGTSSDTVNTYAFTKKAALDTAQTDYDTANTAYLAAVKSGVAGDITTTKATLDG

KNTALATAVKDATAVNEAVNGKVRTVAAKGFDVLNGTVAADGKATGTTPLADIDKAL

KAVDTQRSVLGASQNRFESTITNLNNTVNNLTSAR

Appendix II: Primers

Table II.1 Primers used for cloning

Primer names	sequences	nucleotides	CG (%)	Tm (°C)
Presenilin-1 thrombin insertion -F	CGCGGCAGCGCAGAAGGTGATCCGGAA	27	66.7	85.7
Presenilin-1 thrombin insertion -R	CGGCACCAGCATATTAACCAGCCAAACCATG	31	51.6	79.4
Presenilin-1 thrombin insertion after E321 -F	GCGCGGCAGCCGTGAAAGCCAGGATACC	28	67.9	84.3
Presenilin-1 thrombin insertion after E321 -R	GGCACCAGTTCGGTGCTTTCTGCATTG	27	55.6	78.3
MBP-PS1-F	TCTTATGGGCCCATGACCGAACTGCCTG	28	57.1	79.5
MBP-PS1-R	GGGCTCGAGAATTCTTAGATGTAAAACTGGTG	32	43.8	72.2
MBP-PEN2-F	TCTTATGGGCCCATGCATCATCACCACCA	29	51.7	80.5
MBP-PEN2-R	GGGCTCGAGTTACGGGGTGCCCA	23	69.6	78.9

MBP-APH-1-F	TCTTATGGGCCCATGCATCATCACCAC CATC	31	51.6	80.7
MBP-APH-1-R	GGGCTCGAGTTAATCTTCAGGCGGAAT ACG	30	53.3	76.6
MBP-NCT-F	CCGGAATTCATGCATCATCACCACCAT CAC	30	50.0	77.7
MBP-NCT-R	GCTCTAGATTAATAGCTAACGGCACCC GG	29	51.7	70.5
MBP-PS2-F	CCGGAATTCATGAAGCACCATCATCAC C	28	50.0	75.0
MBP-PS2-R	GCTCTAGATTAAATATACAGCTGATGG CTGG	31	41.9	66.9
FleBt-APH-1-F	AAAGCTAGCATGCATCATCACCACCAT C	28	46.4	71.7
FleBt-APH-1-R	AAAGGATCCTTAATCTTCAGGCGGAAT ACG	30	43.3	70.7
PS1-spGFP-F	AAAGCTAGCATGGGCAGCAGCCATC	25	56.0	73.1
PS1-spGFP-R	AAAGGATCCTTAGATGTAAAACTGGTG AAATGCC	34	38.2	70.9
PEN2-spGFP-F	AAACCATGGATGCATCATCACCACCAT CAC	30	46.7	75.9
PEN2-spGFP-R	AAAGACGTCCCCGGGGTGCCCAGC	34	70.8	79.4
APPC-spGFP-F	AAACCATGGATGCAGAATTCCGACAT G	27	44.4	72.3

APPC-spGFP-R	AAAGACGTCCCCTTATCGTCATCGTCC TTGTAATCGTTC	39	46.2	77.9
pETDuet-PS1-F	AAAGAGCTCGCTGGTGCCGCGC	22	68.2	76.6
pETDuet-PS1-R	CCCAAGCTTCGTTAGATGTAAAACTGG TGAAATGC	35	42.9	74.3
pETDuet-PEN2- F	AAACATATGAATCTGGAACGTGTTAGC AACG	31	38.7	70.0
pETDuet-PEN2- R	AAACTCGAGCTATTAAGCTGGCGCCAC CTG	30	53.3	75.3

Acknowledgements

The work presented in the thesis was performed at the Center for Structural Systems Biology in Hamburg. I was supported by my family for the first year, a scholarship from the China Scholarship Council (CSC) for the next 3 years and a working contract from Forschungszentrum Jülich for the last half a year.

First and foremost, I would like to express my deep gratitude to my supervisor Prof. Dr. Jörg Labahn, for offering me this awesome opportunity to carry out my doctoral study at CSSB. Thanks to Labahn being so patient with me on my project and teaching me for everything in both science life and daily life. I thank him for being so patient with my project and for teaching me everything in scientific life and in my daily life. I am very grateful to him for his kind guidance during my last year of doctoral studies when I wanted to give up. I appreciate his strong support in enriching my thesis. In particular, I want to thank him for offering me the working contract so that I can continue my PhD work.

Besides my superviosr, I sincerely thank our postdocs, Dr. Udaya Kumar Tiruttani Subhramanyam and Dr. Ge Yang, for guiding my experiments when I joined the group and giving me various suggestions when I faced difficulties in my research. I am thankful to my colleagues, Abhilasha Kerkmann, Nishika Sabharwal, Aziz Tumeh, Yajing Xiao and Dr. Weihou Guo for every help. It was a lot of fun to work with them.

In addition, I would like to thank the people from Prof. Dr. Michael Kolbe's group for their kind help when my experiment was in trouble, especially Dr. Chu Wang for providing me with FleBt tags, which were very important for my research.

My sincere thank also goes to Dr. Stephan Niebling and Angelica Struve Garcia from EMBL for their patient instruction for Microscale Thermophoresis. Special thanks to Prof. Dr. Oliver H. Weiergraeber for offering me the MBP vector for my research.

I am very happy to be a member of the football team BuffTreff, which allows me the possibility to save Chinese football in the future. I would also like to thanks my friends for every basketball game, badminton game and every meal we had together, which made my life in Germany so much fun. I

want to give a special thanks to my best friend in Hamburg Dr. Lanhai He who gives me a lot of suggestions for my further life.

Last but not least, I owe a special debt of gratitude to my parents, for their unconditional love and support. Thanks, my wife, Yanlin Li, for her strong support and understanding of my studies in Germany for over four years. Thank my parents in law for taking care of YanLin when I am not in China. I would like to say thank to all my family members, because of you, I am able to complete my studies without any worries.

Erklärung

Ich erkläre, dass ich die vorliegende Arbeit selbständig und ohne unerlaubte Hilfe verfasst habe. Die vorliegende Arbeit wurde weder in der jetzigen oder in ähnlicher Form bei einer anderen Institution eingereicht. Es wurden zuvor keine Promotionsversuche unternommen

Hamburg

_____

Chengcheng Tao